

FATIGUE DAMAGE ANALYSIS OF REINFORCED  
CONCRETE STRUCTURAL ELEMENTS

By

BENARD ISOJEH

A thesis submitted in conformity with the requirements

For the degree of Doctor of Philosophy

Graduate Department of Civil Engineering

University of Toronto

© Copyright by Benard Isojeh (2017)

# Fatigue Damage Analysis of Reinforced Concrete Structural Elements

Benard Isojeh

Doctor of Philosophy

Graduate Department of Civil Engineering

University of Toronto

2017

## ABSTRACT

The design of fatigue-prone structural elements such as wind turbine foundations requires adequate verification of the constituent materials to ascertain their resistance capacity under fatigue loading. Hence, the number of loading cycles that can be sustained in service using stress-life models, or the level of structural damage relative to a given limit, are required from the fatigue analysis of the structural components.

The presence of cracks in these structural components often renders them vulnerable to damage propagation because increased stresses in the steel reinforcing bars traversing cracked concrete planes may result in reinforcement crack initiation, and possibly propagation. As such, mediums involving the use of steel-fibre reinforced concrete have been adopted in designs to prevent or inhibit concrete crack evolution and reinforcement crack propagation under fatigue loading.

Investigations reported in the literature have shown that current fatigue resistance analysis approaches for concrete composites are insufficient, lack significant levels of reliance, and do not appropriately account for fatigue-governing mechanisms within a cracked concrete plane with intersecting reinforcement that exhibits progressive crack propagation. The effects of irreversible damage accumulation of concrete composites are often neglected, and damage models ignore important influencing factors; hence, they are limited to the analysis of structures

with similar loading conditions as the test specimens used for developing such models.

An experimental campaign was conducted to develop robust damage models which account for relevant fatigue loading parameters. Various assumptions incorporated into fatigue analysis constitutive models were further verified to ascertain their conservative level and reliance. Based on the obtained results, a new analysis and design approach which accounts for irreversible damage accumulation of concrete composites (including steel fibres) is proposed. In addition, the complex behaviour at a concrete crack plane is considered by incorporating fracture mechanics and residual capacity models into the corresponding equilibrium equation, hence accounting for steel reinforcement crack propagation.

The proposed models were further incorporated into algorithms for strut and tie analysis and into the Disturbed Stress Field Model (finite element framework) for fatigue life and damage evolution predictions. Corroborated results of the experimental investigation conducted with the modified analysis approaches exhibited good correlation. From the verified improved analysis concepts and the unambiguity of the results interpretation, the proposed approach can be used for the fatigue resistance design and analysis of fatigue-prone structures in order to ascertain the required fatigue resistance capacity during service life.

## ACKNOWLEDGEMENTS

First, I will like to express my profound appreciation to my advisor, Professor Frank J. Vecchio, for his guidance and encouragement throughout the period of actualising this thesis. His supervision within the period of my studies has reoriented my solution-finding abilities.

I thank Professors Shamim Sheikh, Karl Peterson, Paul Gauvreau, and Bruno Massicotte for their thorough reviews, invaluable comments, and suggestions in ensuring a prolific thesis was produced.

The invaluable contributions and financial support provided by NSERC, the University of Toronto School of Graduate Studies, HATCH Ltd, Professor F.J. Vecchio, the Department of Civil Engineering of the University of Toronto, NDDC, and Delta State Government of Nigeria are highly appreciated.

The success in the experimental investigation reported in this thesis was achieved with the assistance of the the Structures Laboratory staff: Renzo Bassett, Giovanni Buzzeo (retired), John MacDonald (retired), Xiaming Sun, Alan McClenaghan, Bryant Cook, and Michel Fiss.

I wish to thank my friends and colleagues Vahid Sadeghian, Anca Ferche, Stamatina Chasioti, Mark Hunter, Raymond Ma, Simon Liu, Saif Shaban, Siavash Habibi, Fady ElMohandes, and Trevor Hrynyk for their support throughout my course of study.

Lastly, I want to thank my wife Yvonne for her encouragement and care, my family, my mother and my father for their prayers, support and motivation in ensuirng I persevere despite daunting challenges.

## TABLE OF CONTENTS

|   |       |
|---|-------|
| ABSTRACT.....   | ii    |
| LIST OF FIGURES.....  | xi    |
| LIST OF TABLES.....   | xviii |
| <br>  |       |
| CHAPTER 1: INTRODUCTION.....  | 1     |
| 1.1 General Background .....  | 1     |
| 1.2 Types of Structures Affected by Fatigue.....                                      | 1     |
| 1.2.1 Onshore Wind Turbine Foundation.....  | 1     |
| 1.2.2 Other Fatigue-Prone Structures.....   | 4     |
| 1.3 Approaches for Fatigue Analysis.....  | 5     |
| 1.3.1 Fatigue Life of Steel Reinforcement.....  | 6     |
| 1.3.2 Fatigue Life of Concrete.....   | 9     |
| 1.3.3 Fatigue Life of Steel-Fibre Reinforced Concrete.....                            | 14    |
| 1.4 Loading History and Cumulative Damage under Fatigue Load.....                     | 14    |
| 1.5 Outstanding Questions in the Fatigue Resistance Analysis and Design Approach..... | 15    |
| 1.6 Research Motivation.....  | 16    |
| 1.7 Study Scope and Objectives.....   | 18    |
| 1.8 Thesis Contents.....  | 19    |
| 1.9 References.....   | 20    |
| <br>  |       |
| CHAPTER 2: CONCRETE DAMAGE UNDER FATIGUE LOADING IN UNIAXIAL<br>COMPRESSION.....      | 25    |
| 2.1 Abstract.....   | 25    |
| 2.2 Introduction.....   | 25    |

|   |    |
|---|----|
| 2.3 Research Significance.....  | 29 |
| 2.4 Experimental Investigation.....   | 30 |
| 2.4.1 Test Specimens.....   | 32 |
| 2.4.2 Results.....  | 33 |
| 2.4.3 Maximum Strain Evolution.....   | 34 |
| 2.5 Model Formulation.....  | 35 |
| 2.5.1 Relationship between Secondary Strain Rate and Number of Cycles to Failure.....             | 35 |
| 2.5.2 Strength and Stiffness Degradation under Fatigue Loading.....                               | 37 |
| 2.5.3 Damage Evolution Model for Concrete Strength and Fatigue Secant Modulus.....                | 40 |
| 2.5.4 Influence of Loading Parameters on the Fatigue Damage of Concrete.....                      | 44 |
| 2.6 Variable-Amplitude Fatigue Loading.....   | 45 |
| 2.7 Conclusions.....  | 48 |
| 2.8 Notations.....  | 49 |
| 2.9 References.....   | 51 |
| <br>  |    |
| CHAPTER 3: SIMPLIFIED CONSTITUTIVE MODEL FOR FATIGUE BEHAVIOUR OF<br>CONCRETE IN COMPRESSION..... | 57 |
| 3.1 Abstract.....   | 57 |
| 3.2 Introduction.....   | 58 |
| 3.3 Experimental Study.....   | 61 |
| 3.3.1 Test Specimens.....   | 62 |
| 3.3.2 Failure Modes.....  | 64 |
| 3.3.3 Experimental Results and Verification.....  | 65 |
| 3.3.3.1 Fatigue Degradation.....  | 65 |

|  |     |
|--|-----|
| 3.3.3.2 Irreversible Strain under Fatigue Loading.....                         | 68  |
| 3.3.3.3 Strength Degradation.....  | 70  |
| 3.4 Damaged Constitutive Models for Residual Strength of Concrete.....         | 75  |
| 3.4.1 Normal Strength Concrete.....  | 75  |
| 3.4.2 High Strength Concrete.....  | 77  |
| 3.5 Verification of Proposed Model for Irreversible Strain.....                | 79  |
| 3.6 Conclusions.....   | 80  |
| 3.7 Notations.....   | 82  |
| 3.8 References.....  | 84  |
| <br>   |     |
| CHAPTER 4: FATIUE BEHAVIOUR OF STEEL-FIBRE CONCRETE IN DIRECT TENSION          |     |
| .....  | 89  |
| 4.1 Abstract.....  | 89  |
| 4.2 Introduction.....  | 90  |
| 4.3 Material Parameter in Aas-Jakobsen's S-N Model.....                        | 91  |
| 4.4 Experimental Program.....  | 94  |
| 4.5 Fatigue Test Results.....  | 97  |
| 4.5.1 Failure Mode.....  | 97  |
| 4.5.2 Progressive Deformation.....   | 98  |
| 4.6 Material Parameters for Concrete and Steel-Fibre.....                      | 101 |
| 4.7 Damage Evolution for Steel-Fibre Residual Strength and Secant Modulus..... | 107 |
| 4.8 Conclusions.....   | 110 |
| 4.9 References.....  | 111 |

|  |         |
|--|---------|
| CHAPTER 5: FATIGUE RESISTANCE OF STEEL-FIBRE REINFORCED CONCRETE DEEP BEAMS.....         | 115     |
| 5.1 Abstract.....  | 115     |
| 5.2 Introduction.....  | 116     |
| 5.3 Research Significance.....   | 118     |
| 5.4 Experimental Investigation.....  | 119     |
| 5.4.1 Test Specimens.....  | 119     |
| 5.4.2 Materials.....   | 121     |
| 5.4.3 Test Procedure.....  | 122     |
| 5.4.4 Instrumentation.....   | 124     |
| 5.5 Test Results and Discussions.....  | 125     |
| 5.5.1 Failure Mode.....  | 125     |
| 5.5.2 Crack Pattern.....   | 132     |
| 5.5.3 Shear Strain Evolution/Mid-Span Deflection.....                                    | 134     |
| 5.5.4 Average Principal Strain Evolution.....  | 135     |
| 5.5.5 Bond Behaviour.....  | 136     |
| 5.6 Conclusion.....  | 137     |
| 5.7 References.....  | 138     |
| <br>CHAPTER 6: HIGH-CYCLE FATIGUE LIFE PREDICTION OF REINFORCED CONCRETE DEEP BEAMS..... | <br>142 |
| 6.1 Abstract.....  | 142     |
| 6.2 Introduction.....  | 143     |
| 6.2.1 Mechanism of Fatigue Failure.....  | 143     |

|   |     |
|---|-----|
| 6.2.2 Design for Fatigue Resistance.....  | 145 |
| 6.3 Experimental Program.....   | 147 |
| 6.3.1 Test Specimens.....   | 147 |
| 6.3.2 Materials.....  | 148 |
| 6.3.3 Test Setup.....   | 149 |
| 6.3.4 Test Procedure.....   | 150 |
| 6.3.5 Instrumentation.....  | 152 |
| 6.4 Test Results.....   | 154 |
| 6.4.1 Mid-Span Deflection/Stiffness Degradation.....  | 155 |
| 6.4.2 Shear-Span Deformation.....   | 158 |
| 6.5 Fatigue Life Verification using Strut and Tie Model.....  | 159 |
| 6.5.1 Fatigue Equilibrium Equation.....   | 163 |
| 6.5.2 Fatigue Constitutive Models.....  | 164 |
| 6.5.3 Reinforcement Crack Growth.....   | 167 |
| 6.5.4 Compatibility Equation.....   | 168 |
| 6.6 Conclusions.....  | 173 |
| 6.7 References.....   | 173 |
| <br>  |     |
| CHAPTER 7: REINFORCED CONCRETE AND STEEL-FIBRE CONCRETE ELEMENTS<br>UNDER FATIGUE LOADING: MODEL FORMULATION..... | 178 |
| 7.1 Abstract.....   | 179 |
| 7.2 Introduction.....   | 179 |
| 7.3 Disturbed Stress Field Model.....   | 181 |
| 7.3.1 Equilibrium Condition.....  | 182 |

|   |     |
|---|-----|
| 7.3.2 Equilibrium of Average Stresses.....  | 182 |
| 7.3.3 Equilibrium of Stresses at a Crack.....   | 184 |
| 7.3.4 Reinforcement Crack Growth Factor ( $Z_0$ ).....  | 185 |
| 7.4 Compatibility Condition.....  | 188 |
| 7.5 Constitutive Relation.....  | 189 |
| 7.5.1 Conventional Reinforcement.....   | 195 |
| 7.6 Finite Element Implement.....   | 196 |
| 7.7 Failure Criterion for Reinforced Concrete and Steel-Fibre Concrete under Fatigue Loading.....               | 199 |
| 7.8 Conclusions.....  | 208 |
| 7.9 Notations.....  | 209 |
| 7.10 References.....  | 212 |
| <br>  |     |
| CHAPTER 8: REINFORCED CONCRETE AND STEEL-FIBRE CONCRETE ELEMENTS UNDER FATIGUE LOADING: MODEL VERIFICATION..... | 218 |
| 8.1 Abstract.....   | 218 |
| 8.2 Introduction.....   | 218 |
| 8.3 Experiment Details.....   | 220 |
| 8.4 Finite Element Modelling.....   | 223 |
| 8.4.1 Material Properties.....  | 223 |
| 8.4.2 Finite Element Mesh.....  | 225 |
| 8.4.3 Constitutive Model.....   | 225 |
| 8.4.4 Loading Condition.....  | 226 |
| 8.5 Finite Element Fatigue Damage Analysis Results.....   | 226 |

|   |         |
|---|---------|
| 8.5.1 Fatigue Life and Deformation Evolution Predictions..... | 228     |
| 8.5.2 Fatigue Residual Capacity.....                          | 229     |
| 8.5.3 Mid-Span Deflection Evolution.....                      | 233     |
| 8.5.4 Variation in Loading and Material Parameters.....       | 235     |
| 8.5.5 Reinforcement Stresses under Fatigue Loading.....       | 237     |
| 8.6 Variable Fatigue Loading.....                             | 238     |
| 8.7 Conclusions.....  | 241     |
| 8.8 References.....   | 242     |
| <br>CHAPTER 9: CONCLUSIONS AND RECOMMENDATIONS .....          | <br>244 |
| 9.1 Summary.....  | 244     |
| 9.2 Conclusions.....  | 245     |
| 9.3 Recommendations for Future Work.....                      | 247     |
| <br>APPENDIX A.....   | <br>249 |
| APPENDIX B.....   | 250     |
| APPENDIX C.....   | 252     |
| APPENDIX D.....   | 254     |
| APPENDIX E.....   | 255     |
| APPENDIX F.....   | 256     |
| APPENDIX G.....   | 257     |

## LIST OF FIGURES

### CHAPTER 1: INTRODUCTION

|  |    |
|--|----|
| Fig. 1.1 - Collapsed wind turbine structures.....                            | 3  |
| Fig. 1.2 - Stress-life relations for reinforcing and prestressing steel..... | 8  |
| Fig. 1.3 – S-N curve based on equations above (FIB Model code 2010).....     | 10 |
| Fig. 1.4 – Linear damage accumulation.....                                   | 15 |
| Fig. 1.5 – Nonlinear damage accumulation.....                                | 15 |
| Fig. 1.6 – Double linear damage rule for two step load levels.....           | 15 |

### CHAPTER 2: CONCRETE DAMAGE UNDER FATIGUE LOADING IN UNIAXIAL COMPRESSION

|  |    |
|--|----|
| Fig. 2.1 – Fatigue loading setup.....  | 30 |
| Fig. 2.2 – Concrete specimen in undamaged and damaged states.....                                  | 33 |
| Fig. 2.3 – Maximum strain evolution.....   | 34 |
| Fig. 2.4 – Plot of maximum strain against number of cycles.....                                    | 36 |
| Fig. 2.5 – Logarithm of number of cycles to failure against the secondary strain rate.....         | 37 |
| Fig. 2.6 – Verification of strain rate model for high number of cycles.....                        | 37 |
| Fig. 2.7 – Normalised residual strength against normalised cycles (sec. strain rate approach)..... | 38 |
| Fig. 2.8 – Normalised residual strength against normalised cycles (S-N model).....                 | 38 |
| Fig. 2.9 – Static and fatigue secant moduli.....   | 39 |
| Fig. 2.10 – Degradation of residual fatigue secant modulus.....                                    | 39 |
| Fig. 2.11 – Estimation of damage parameter $s$ .....   | 42 |
| Fig. 2.12 – Normalised concrete strength degradation model.....                                    | 43 |
| Fig. 2.13 – Normalised fatigue secant modulus degradation.....                                     | 43 |

|  |    |
|--|----|
| Fig. 2.14 - Effect of stress level on the fatigue damage of concrete compressive strength..... | 44 |
| Fig. 2.15 - Effect of frequency on the fatigue damage of concrete compressive strength.....    | 45 |
| Fig. 2.16- Effect of stress ratio on the fatigue damage of concrete compressive strength.....  | 45 |
| Fig. 2.17 - Stress-cycle diagram for variable amplitude loading.....                           | 47 |
| Fig. 2.18 - Damage evolution for variable loading.....   | 47 |

### CHAPTER 3: SIMPLIFIED CONSTITUTIVE MODEL FOR FATIGUE BEHAVIOUR OF CONCRETE IN COMPRESSION

|  |    |
|--|----|
| Fig. 3.1. Relationship between monotonic stress-strain curve and fatigue hysteresis loops..... | 59 |
| Fig. 3.2. Fatigue loading set-up.....  | 62 |
| Fig. 3.3. Specimens in damaged states.....   | 64 |
| Fig. 3.4. Fatigue degradation ST3: ( $f'_c = 52.8$ MPa) & H16: ( $f'_c = 55.8$ MPa).....       | 65 |
| Fig. 3.5. Fatigue degradation E5: ( $f'_c = 52.8$ MPa) & E10: ( $f'_c = 52.8$ MPa).....        | 65 |
| Fig. 3.6. Fatigue degradation I1 & I6 ( $f'_c = 23.1$ MPa) at 5 Hz.....                        | 66 |
| Fig. 3.7. Fatigue degradation (I6) & (I5) ( $f'_c = 23.1$ MPa) at 1 Hz.....                    | 66 |
| Fig. 3.8. Fatigue degradation (high frequency).....  | 68 |
| Fig. 3.9. Fatigue degradation (low frequency).....   | 68 |
| Fig. 3.10. Residual strength (Batch 1).....  | 71 |
| Fig. 3.11. Strain evolution corresponding to residual strength for Batch 1.....                | 71 |
| Fig. 3.12. Residual strength (Batch 2).....  | 72 |
| Fig. 3.13. Strain evolution corresponding to residual strength for Batch 2.....                | 72 |
| Fig. 3.14. Residual strength (Batch 3).....  | 73 |
| Fig. 3.15. Strain evolution corresponding to residual strength for Batch 3.....                | 73 |
| Fig. 3.16. Static and fatigue secant moduli.....   | 75 |

|   |     |
|---|-----|
| Fig. 3.17. Plot of the ratio of the fatigue secant modulus ( $\epsilon$ ) to the static secant modulus against normalized number of cycles..... | 75  |
| Fig. 3.18. Modified Hognestad's stress-strain curve for damaged concrete.....   | 77  |
| Fig. 3.19. Modified Popovic's stress-strain curve for damaged concrete.....   | 78  |
| Fig. 3.20. Irreversible fatigue strain for high strength concrete (stress level: 0.74).....   | 79  |
| Fig. 3.21. Irreversible fatigue strain for normal strength concrete.....  | 79  |
| Fig. 3.22. Steps for estimating the irreversible strain of concrete under fatigue loading in compression.....                                   | 81  |
| <br>  |     |
| <b>CHAPTER 4: FATIGUE BEHAVIOUR OF STEEL-FIBRE CONCRETE IN DIRECT TENSION</b>   |     |
| Fig. 4.1- Test set-up.....  | 95  |
| Fig. 4.2 - Test specimen.....   | 96  |
| Fig. 4.3 - Test specimens after failure (plain concrete (a); steel fibre (b)).....  | 98  |
| Fig. 4.4 - Fatigue maximum strain evolution for plain and steel fibre concrete.....   | 99  |
| Fig. 4.5 - Fatigue hysteresis loops for plain and steel fibre concrete.....   | 100 |
| Fig. 4.6 - Maximum strain versus number of fatigue loading cycles.....  | 102 |
| Fig. 4.7 - Secondary strain rate for plain and steel fiber concrete.....  | 103 |
| Fig. 4.8 - Plot of number of cycles to failure against secondary strain rate.....   | 104 |
| Fig. 4.9 - Plot of $\text{Log}(\text{Log } N_f)$ versus $\text{Log } \epsilon_{sec}$ .....  | 105 |
| Fig. 4.10 - Plot of $\text{Log}(\text{Log } N_f)$ versus $\text{Log } \epsilon_{sec}$ .....   | 106 |
| Fig. 4.11 – (a) Damage parameter $s$ for secant modulus of steel fibre; (b) residual strength of steel fibre.....                               | 108 |
| Fig. 4.12 - Residual strength (a) and fatigue secant modulus (b) damage evolution for steel fibre concrete.....                                 | 109 |

## CHAPTER 5: FATIGUE RESISTANCE OF STEEL-FIBRE

|  |     |
|--|-----|
| Fig. 5.1 - Details of deep beam specimen.....  | 120 |
| Fig. 5.2 - Load versus deflection under monotonic loading (Beams C'S and CS).....                        | 123 |
| Fig. 5.3 - LVDTs strain transformation.....  | 124 |
| Fig. 5.4 - Longitudinal reinforcement strain versus number of cycles at maximum load (2-10M rebars)..... | 127 |
| Fig. 5.5 - Load versus deformation plot after fatigue loading.....                                       | 127 |
| Fig. 5.6 - Crack pattern and inclination of principal tensile strain (15M-70%Pu).....                    | 128 |
| Fig. 5.7 - Crack pattern and inclination of principal tensile strain (10M-80%Pu).....                    | 128 |
| Fig. 5.8 - Crack pattern and inclination of principal tensile strain (10M-70%Pu).....                    | 129 |
| Fig. 5.9 - Crack pattern and inclination of principal tensile strain (15M-80%Pu).....                    | 129 |
| Fig. 5.10 - Average shear strain evolution (2-15M).....  | 130 |
| Fig. 5.11 - Mid-span deflection for (2-15M).....   | 131 |
| Fig. 5.12 - Mid-span deflection for (2-10M).....   | 131 |
| Fig. 5.13 - Average shear strain evolution (2-10M).....  | 131 |
| Fig. 5.14 - Average principal compressive strain evolution (2-15M).....                                  | 132 |
| Fig. 5.15 - Average principal compressive strain evolution (2-15M).....                                  | 132 |
| Fig. 5.16 - Evolution of concrete and reinforcement strain variation.....                                | 137 |

## CHAPTER 6: HIGH-CYCLE FATIGUE LIFE PREDICTION OF TREINFORCED CONCRETE

### DEEP BEAMS

|  |     |
|--|-----|
| Fig. 6.1 - Beam specimen setup.....                    | 150 |
| Fig. 6.2 – Details of deep beam specimen.....          | 152 |
| Fig. 6.3 – Load versus deformation (strain) plots..... | 154 |

|   |     |
|---|-----|
| Fig. 6.4 – LVDTs strain transformation.....   | 155 |
| Fig. 6.5 – Evolution of mid-span deflection.....                                    | 156 |
| Fig. 6.6 – Crack pattern and shear-span fatigue degradation.....                    | 157 |
| Fig. 6.7 – Fatigue hysteresis loops.....  | 159 |
| Fig. 6.8 – Strain evolution in reinforcing bars.....                                | 160 |
| Fig. 6.9 – Average principal strain and shear strain evolution.....                 | 161 |
| Fig. 6.10 – Strut and tie model for a deep beam under fatigue loading.....          | 163 |
| Fig. 6.11 – Crack growth on a reinforcing bar surface.....                          | 166 |
| Fig. 6.12 – Algorithm for predicting the fatigue life of a deep beam.....           | 169 |
| Fig. 6.13 – Fatigue life prediction from strut and tie model (C80-0 and C75-0)..... | 171 |
| Fig. 6.14 – Fatigue life prediction from strut and tie (C70-0 and C80-20).....      | 171 |

## CHAPTER 7: REINFORCED CONCRETE AND STEEL-FIBRE CONCRETE ELEMENTS

### UNDER FATIGUE LOADING: MODEL FORMULATION

|  |     |
|--|-----|
| Fig. 7.1 – Steel fibre reinforced concrete element (a) Loading conditions; (b) Mohr’s circle for average stresses in concrete..... | 183 |
| Fig. 7.2 – Equilibrium conditions: (a) Parallel to crack direction; (b) Along crack surface.....                                   | 184 |
| Fig. 7.3 – Equilibrium conditions along crack surface after reinforcement crack propagation.....                                   | 184 |
| Fig. 7.4 – Crack growth on a reinforcing bar cross-section.....  | 190 |
| Fig. 7.5 – Damage parameter $s$ for steel fibre secant modulus (A) and residual strength (B).....                                  | 193 |
| Fig. 7.6 – Flow chart for the modified solution algorithm for DSFM.....  | 200 |
| Fig. 7.7 – Shear panel (PV19).....   | 201 |
| Fig. 7.8 – Crack slip evolution.....   | 206 |
| Fig. 7.9 – Shear stress evolution at crack.....  | 206 |

|  |     |
|--|-----|
| Fig. 7.10 – Reinforcement (Y-direction) crack growth depth.....                | 207 |
| Fig 7.11 – Reinforcement (X-direction) strain evolution at crack location..... | 207 |
| Fig 7.12 – Reinforcement (X-direction) average stress evolution.....           | 207 |
| Fig. 7.13 – Localised reinforcement strain evolution (Y-direection).....       | 208 |

**CHAPTER 8: REINFORCED CONCRETE AND STEEL-FIBRE CONCRETE ELEMENTS  
UNDER FATIGUE LOADING: MODEL VERIFFICATION**

|   |     |
|---|-----|
| Fig. 8.1 – Details of deep beam specimen.....   | 220 |
| Fig. 8.2 – Experimental setup.....  | 221 |
| Fig. 8.3 – Load-deformation plot for beams CS and C’S.....                                    | 222 |
| Fig. 8.4 – Bean specimen.....   | 224 |
| Fig. 8.5 – Mesh structure layout.....   | 228 |
| Fig 8.6 – Load-deformation plot for beams CS and C’S with crack patterns.....                 | 227 |
| Fig. 8.7 – Calculated fatigue residual capacity for beam: (a) C-80-0-0 (B) C-70-0.....        | 230 |
| Fig. 8.8 – Calculated fatigue residual capacity for beam: (a) C’-80-0 (b) C’-70-0.....        | 230 |
| Fig. 8.9 – Calculated fatigue residual capacity evolution for beam A70-0F1.5.....             | 231 |
| Fig. 8.10 – Calculated fatigue residual capacity for beam: (a) A70-0F1.5 (b) A80-0F1.5.....   | 231 |
| Fig. 8.11 – Calculated fatigue residual capacity for beam: (a) A80-0F0.75 (b) A70-0F0.75..... | 232 |
| Fig. 8.12 – Calculated fatigue residual capacity for beam: (a) A70-0N0.75 (b) B80-0N1.5.....  | 232 |
| Fig. 8.13 - Mid-span deflection evolution for (a) C-80-0 and (b) C-70-0.....                  | 234 |
| Fig. 8.14 - Mid-span deflection evolution for (a) C’-80-0 and (b) C’-70-0.....                | 234 |
| Fig. 8.15 - Mid-span deflection evolution for (a) A70-0.75 and (b) A80-0F0.75.....            | 234 |
| Fig. 8. 16 - Mid-span deflection evolution for (a) A70-0F1.5 and (b) A80-0F1.5.....           | 235 |
| Fig. 8.17 - Mid-span deflection evolution for (a) A70-0N0.75 and (b) B80-0N1.5.....           | 235 |

|   |     |
|---|-----|
| Fig. 8.18 - Mid-span deflection evolution (effect of stress level) (a) 10M bars (b) 15M bars.....       | 236 |
| Fig. 8.19 - Mid-span deflection evolution (effect of stress level) (a) 1.5% $V_f$ (b) 0.75% $V_f$ ..... | 236 |
| Fig. 8.20 - Mid-span deflection evolution (effect of steel fibres) (a) 70% (b) 80%.....                 | 237 |
| Fig. 8.21 - Mid-span deflection evolution (effect of steel fibres) (a) 70% (b) 80%.....                 | 237 |
| Fig. 8.22 - Evolution of stresses in reinforcing bars for beam C-80-0.....                              | 239 |
| Fig. 8.23 - Evolution of stresses in reinforcing bars for beam A70-0F0.75.....                          | 240 |
| Fig. 8.24 - Variable fatigue loading of reinforced concrete.....  | 241 |

## LIST OF TABLES

### CHAPTER 1: INTRODUCTION

|   |   |
|---|---|
| Table 1.1- Fatigue cycles spectrum with corresponding structures..... | 2 |
|---|---|

### CHAPTER 2: CONCRETE DAMAGE UNDER FATIGUE LOADING IN UNIAXIAL COMPRESSION

|   |    |
|---|----|
| Table 2.1- Average compressive strength and corresponding strain..... | 31 |
|---|----|

|  |    |
|--|----|
| Table 2.2 - Specimen fatigue parameters and test failure data..... | 32 |
|--|----|

### CHAPTER 3: SIMPLIFIED CONSTITUTIVE MODEL FOR FATIGUE BEHAVIOUR OF CONCRETE IN COMPRESSION

|  |    |
|--|----|
| Table 3.1 - Average Compressive Strength and Corresponding Strain..... | 63 |
|--|----|

|   |    |
|---|----|
| Table 3.2 - Percentage of Average Compressive Strength for Fatigue Loading..... | 63 |
|---|----|

|  |    |
|--|----|
| Table 3.3 - Strength and Secant Modulus Degradation Test Data..... | 74 |
|--|----|

### CHAPTER 4: FATIGUE BEHAVIOUR OF STEEL-FIBRE CONCRETE IN DIRECT TENSION

|  |    |
|--|----|
| Table 4.1- Compressive Strength of Plain and Steel Fibre Concrete..... | 94 |
|--|----|

|  |    |
|--|----|
| Table 4.2 - Direct Tension Fatigue Test Results..... | 97 |
|--|----|

|   |     |
|---|-----|
| Table 4.3 - Material parameter for plain and steel fibre reinforced concrete..... | 107 |
|---|-----|

### CHAPTER 5: FATIGUE RESISTANCE OF STEEL-FIBRE REINFORCED CONCRETE DEEP BEAMS

|  |     |
|--|-----|
| Table 5.1- Average compressive strength of concrete..... | 121 |
|--|-----|

|                                      |     |
|--------------------------------------|-----|
| Table 5.2: Specimen description..... | 121 |
|--------------------------------------|-----|

CHAPTER 6: HIGH-CYCLE FATIGUE LIFE PREDICTION OF REINFORCEMENT  
CONCRETE DEEP BEAMS

Table 6.1- Specimens Description.....149  
Table 6.2 - Fatigue test results and predictions.....155

CHAPTER 8: REINFORCED CONCRETE AND STEEL-FIBRE CONCRETE ELEMENTS  
UNDER FATIGUE LOADING: MODEL VERIFICATION

Table 8.1 - Specimens description..... 223  
Table 8.2 – Finite element material description.....224  
Table 8.3 - Fatigue life for beam specimens (experimental and predicted).....233

# CHAPTER 1

## 1.0 INTRODUCTION

### 1.1 General Background

The damage effects of fatigue loading on many types of structures, such as wind turbine foundations, have been investigated and reported by various researchers in the literature. As such, appropriate designs now require verification to ensure the invulnerability of fatigue-prone structural elements to collapse while in service (Holmen, 1982).

Generally, a combination of an empirical stress-life model and a damage rule (e.g., Palmgren-Miner rule) is used for such verifications. However, due to the effects of progressive deformation, damage accumulation, and material crack initiation and propagation associated with fatigue loading on a global structure, the implementation of time/cycle-dependent models in the fatigue analysis of structural elements is considered invaluable. Various types of structures prone to fatigue damage are discussed subsequently.

### 1.2 Types of Structures Affected by Fatigue

Depending on the range of the number of cycles to which a structure is subjected during service life, fatigue-prone structures may be grouped into three main classes. These are low-cycle, high-cycle, and super-high cycle fatigue structures. The characteristic cyclic loads to which these structures are subjected include vibrations, traffic loads, wind, and water waves. Examples of some common structures in these groups are shown in Table 1.1 (Hsu, 1981).

#### 1.2.1 Onshore Wind Turbine Foundations

In recent years, increases in the size of wind turbine structures have been seen due to higher demands for energy generation. In line with this development, notable fatigue failures of foundations have been reported in the wind energy industry in various parts of the world. Some of

these failures were linked to concrete damage or to fracture of the embedded reinforcing bolts connecting the wind turbine super-structure to its foundation.

Table 1.1- Fatigue cycles spectrum with corresponding structures

| Low-Cycle Fatigue<br>( $0 - 10^3$ cycles)  | High-Cycle Fatigue<br>( $10^3 - 10^7$ cycles)  | Super-High-Cycle Fatigue<br>( $10^7 - 5 \times 10^8$ cycles)   |
|--|--|--|
| <ul style="list-style-type: none"> <li>• Structures subjected to earthquakes</li> <li>• Structures subjected to storm</li> </ul> | <ul style="list-style-type: none"> <li>• Bridges</li> <li>• Airport pavement</li> <li>• Wind power plants</li> <li>• Highway pavement</li> <li>• Concrete railroad ties</li> </ul> | <ul style="list-style-type: none"> <li>• Mass rapid transit structures</li> <li>• Sea structures</li> <li>• Machine foundations</li> </ul> |

On the 27<sup>th</sup> and 30<sup>th</sup> of January, 2013, two wind turbine structures were observed to have collapsed in Devon and Cornwall, United Kingdom, respectively, due to embedded bolt fatigue fracture (Figure 1.1(a) and Figure 1.1 (b)). The investigation reports revealed that the exposure of the bolts due to loss of grout at the intersection between the tower structure and the foundation intensified the crack propagation in the connecting bolts under tensile forces. In each case, the lack of resilience to the fatigue load within the structure resulted in poor fatigue resistance.

On the 24<sup>th</sup> of December, 2015, a wind turbine structure was observed to have fallen at the Lemnhult wind farm in Sweden. Similarly, the investigation conducted by the government accident investigation authority revealed that the wind turbine failure was attributable to fatigue of the bolts at the joint between the foundation and the tower structure (Figure 1.1(c)).

Figure 1.1(d) shows the collapsed wind turbine structure at Fenner, New York that occurred on the 27<sup>th</sup> of January, 2009. The wind turbine superstructure was observed to have been detached from its base with an attached mass of concrete. This observation gave an indication of concrete degradation within the foundation (see Figure 1.1(e)) leading to a concrete shear failure. In the case of a 1.5 Megawatt wind turbine structure in Pennsylvania that failed on the 14<sup>th</sup> of January,

2014 (Figure 1.1 (f)), a large mass of damaged concrete was also observed at the base of the fallen turbine structure. Although an electrical fault indication was assumed, the observed mode of failure was attributable to the fatigue damage of concrete within the foundation.

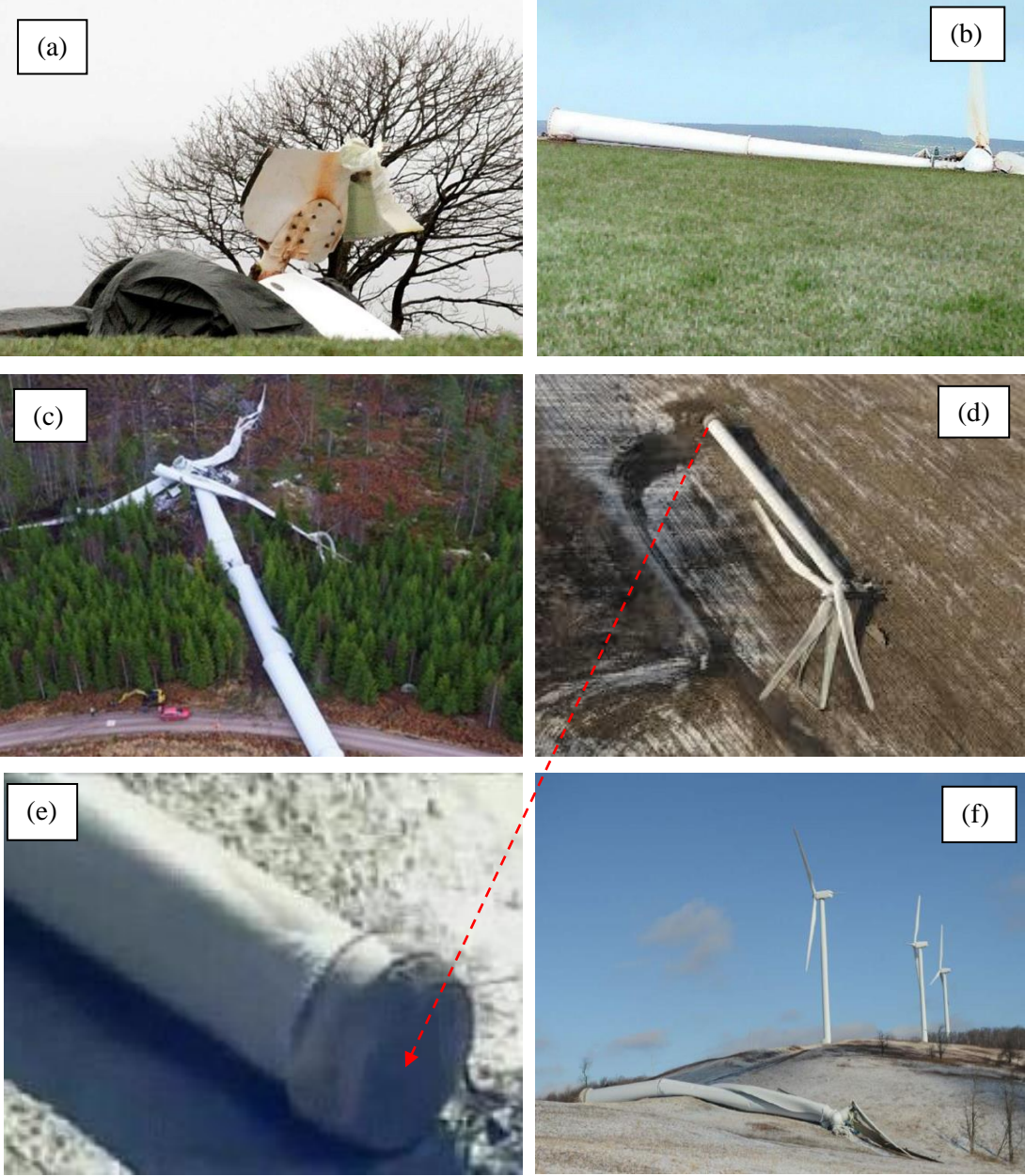


Fig. 1.1- Collapsed wind turbine structures.

Inferred results from investigations conducted by Structural Integrity Associates and ANATECH on the causes of wind turbine foundation failures, considering the turbine failures observed at Fenner and Pennsylvania in the United States of America, led to a recommendation quoted thus:

*“Given the aging fleet of wind turbines and the substantial adverse effects of fatigue on reinforced concrete foundations, wind turbine owners should carefully evaluate their foundation designs given the potential for collapse”.*

### **1.2.2 Other Fatigue-Prone Structures**

Structures subjected to dynamic stresses are generally prone to fatigue damage. Some of these structures are identified in Table 1.1; however, the type of fatigue loading giving rise to the dynamic stresses in each structure may differ from one another. For example, machine foundations are subjected to oscillations of machine components in service, while bridge decks are subjected to fatigue loading cycles resulting from traffic load (moving wheels). Railways are subjected to high numbers of transiting axles that flex the sleepers and ballasts, rendering them susceptible to fatigue damage. Offshore platforms and offshore wind turbines are normally exposed to environments different from those on land. In these cases, fatigue loading results from the effects of wind forces and water waves or current conditions. The rate of degradation of concrete and steel reinforcement may be aggravated depending on the salt level of the ocean and moisture in the air. In addition, the dynamic stresses induced in airport runways from aircraft wheels in motion also subject them to fatigue damage.

Learning from the reported cases, the constituent materials of a reinforced concrete structure are susceptible to fatigue degradation, and, as such, the resistance of the structural component to fatigue degradation should be appropriately verified. In codes of practice, each constituent material is independently verified for fatigue damage using the critical stresses in the constituent materials.

Fatigue analysis approaches and independent behaviour of embedded steel reinforcing bars, concrete, and steel-fibre reinforced concrete under fatigue loading are considered in Sections 1.3.1 to 1.3.3.

### **1.3 Approaches for Fatigue Analysis**

The fatigue behaviour of a structural component can be analysed using the stress-life approach, the strain-life approach, the fatigue crack growth (fracture mechanics) approach (Halford et al, 2001; Lee et al, 2005), and non-destructive test approaches (Shah et al, 1984; Yuyama et al, 2001).

The stress approach involves a plot of various stress ranges for a particular material against the corresponding number of cycles leading to failure. This is the most common approach for fatigue analysis both in research literature and in codes of practice. In this approach, several specimens of a specific material are tested using different stress ranges. The tests are conducted using maximum stresses between 0 and 100 % of the static strength of the material either in tension, compression or shear. A negative-gradient linear equation is obtained from a plot of stress levels against the logarithms of the number of cycles resulting in failure. A plot from the equation is known as the finite life region from which the number of cycles resulting in failure at a known stress level can be obtained. However, a single stress-life plot has limitations in the prediction of local plasticity or crack initiation life, deformation evolution, and mean-stress effects (Halford et al, 2001; Lee et al, 2005).

The strain-based approach involves a plot of strain against the number of cycles to failure. A cyclic stress-strain curve is also required to complement the strain-life curve. This approach basically considers plasticity nucleation within a structural component (crack initiation life). Equations from the aforementioned curves contain elastic and plastic strain terms (Dowling and Thangjitham,

2000); hence, the approach has the advantage of indicating the transition life between the plastic region and the elastic region under fatigue loading. Using stress concentration factors, the local amplitude of the stress and strain required for analysis are obtained from Neuber's rule or simply from a finite element analysis. However, this approach is only significant in reinforced concrete structures when the crack initiation life in a reinforcing bar is required.

The crack growth approach can also be used to predict the fatigue life of reinforced concrete structures. This approach adopts the use of a fatigue crack growth law (e.g. Paris law) and a stress intensity factor concept as functions of crack depth, shape factor, and stress range. The number of load cycles it takes for an initial crack length to increase to a final crack length in a region of high stress concentration is calculated (Lee et al., 2005). Although fracture mechanics models have been used in fatigue-crack prediction, they are unable to predict the number of cycles required to initiate a crack. Secondly, in concrete structures with numerous smeared cracks, models from fracture mechanics are inappropriate for predicting fatigue life.

Non-destructive tests have also been employed in the study of fatigue damage evolution of reinforced concrete elements using the inherent properties (Shah et al, 1984; Yuyama et al, 2001). For example, the fatigue damage of concrete is associated with increased cracks, higher temperature, lower strength, and degraded stiffness. Progressive measurement and plotting of the values of these properties for a fatigue-damaged concrete element give indications of the fatigue deformation profiles.

### **1.3.1 Fatigue Life of Steel Reinforcement**

The fatigue life of steel reinforcing bars are commonly estimated using stress-life models. As previously discussed, this involves a plot of the stress range against the numbers of cycles resulting

in failure. Various models have been proposed and used in different codes for estimating the number of cycles to failure for steel reinforcing bars under fatigue loading (Tilly, 1979; JSCE, 1986; Chinese Code, GB 50010-2002; CEB-FIP Model Code 1990; AASHTO (Specified in ACI-217R-74); EN 1992-1-1: 6.8). The model proposed by AASHTO considers the influence of the stress range, the diameter of the bar, and the ratio of the radius at the root and the height of the reinforcement rib (r/h) (Equation 1.1 and Equation 1.2).

$$f_r = 145 - 0.133\sigma_{min} + 55 (r/h) \quad (1.1)$$

$$\begin{aligned} \text{Log } N = & 6.1044 - 591 \times 10^{-5} f_r - 200 \times 10^{-5} \sigma_{min} + \\ & 103 \times 10^{-3} f_b - 8.77 \times 10^{-5} A_s + 0.0127 d (r/h) \end{aligned} \quad (1.2)$$

where  $f_r$  is equal to  $\sigma_{max} - \sigma_{min}$ ,  $d$  is the diameter of the reinforcing bar in mm,  $\sigma_{max}$  is the maximum stress in the steel reinforcing bar,  $\sigma_{min}$  is the minimum stress in the steel reinforcing bar,  $f_b$  is the tensile strength of the reinforcement, and  $A_s$  is the sectional area of the reinforcement in  $mm^2$ .

Two basic approaches are specified in Eurocode (EN 1992-1-1: 6.8). The first approach is used under constant fatigue loading. In this approach, the damage of a single stress amplitude is determined using the corresponding S-N curves (Figure 1.2) for reinforcing and prestressing steel. It is expected that Equation 1.3 is satisfied for an appropriate fatigue resistance capacity.

$$\gamma_{F,fat} \cdot \Delta\sigma_{s,max} \leq \frac{\Delta\sigma_{Rsk}(N^*)}{\gamma_{s,fat}} \quad (1.3)$$

where  $\gamma_{F,fat}$  is a partial factor for fatigue loading (recommended value of 1.0), EN 1992-1-1:2005-2.4.2.3 (1),  $\Delta\sigma_{s,max}$  is the maximum steel stress range,  $\Delta\sigma_{Rsk}(N^*)$  is the reference resisting fatigue stress range at  $N^*$  cycles, and  $\gamma_{s,fat}$  is a partial factor for fatigue that takes the material uncertainties into account (Table 2.1N in EN 1992-1-1:2005-2.4.2.4).

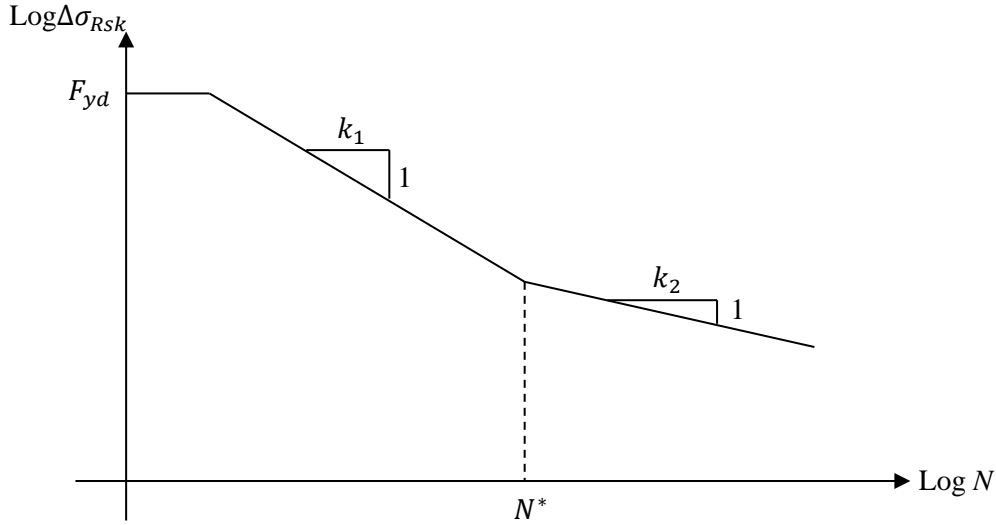


Fig. 1.2- Stress-life relations for reinforcing and prestressing steel.

$k_1$  is the exponent that defines the slope of the first part of the stress-life curve (Table 6.3N in EN 1992-1-1:2005),  $k_2$  is the exponent that defines the slope of the second part of the stress-life curve (Table 6.3N in EN 1992-1-1:2005), and  $F_{yd}$  is the yield strength of the reinforcement.

In reality, the fatigue loading on a structural component is variable in nature; hence, the second approach for estimating the fatigue life of steel reinforcement involves the use of the Palmgren-Miner variable damage accumulation rule. The total damage ( $D_{Ed}$ ) can be estimated thus:

$$D_{Ed} = \sum_i \frac{n(\Delta\sigma_i)}{N(\Delta\sigma_i)} < 1 \quad (1.4)$$

where  $n(\Delta\sigma_i)$  is the number of cycles for the stress range  $\Delta\sigma_i$ , and  $N(\Delta\sigma_i)$  is the ultimate number of cycles for the stress range  $\Delta\sigma_i$ . From the stress-life curve of reinforcing and prestressing steel, the corresponding ultimate number of cycles  $N(\Delta\sigma_i)$  can be estimated thus:

$$N(\Delta\sigma_i) = N^* \left( \frac{\left( \frac{\Delta\sigma_{Rsk}}{\gamma_{s,fat}} \right)}{\gamma_{F,fat} \cdot \Delta\sigma_i} \right)^{k_1} \quad \text{if } \gamma_{F,fat} \cdot \Delta\sigma_i \geq \frac{\Delta\sigma_{Rsk}}{\gamma_{s,fat}} \quad (1.5)$$

$$N(\Delta\sigma_i) = N^* \left( \frac{\left( \frac{\Delta\sigma_{Rsk}}{\gamma_{s,fat}} \right)}{\gamma_{F,fat} \cdot \Delta\sigma_i} \right)^{k_2} \quad \text{if } \gamma_{F,fat} \cdot \Delta\sigma_i < \frac{\Delta\sigma_{Rsk}}{\gamma_{s,fat}} \quad (1.6)$$

$k_1$  and  $k_2$  are given in EN 1992-1-1:2004 (Table 6.3N).

The methods described above are used for straight reinforcing bars; however, for bent bars, the reinforcing bar strength is modified. First, the strength of the reinforcing bars may be reduced by half (Hawkins, 1974; Okamura et al., 1981). Second, from EN 1992-1-1: 2004, the value of the resisting fatigue stress range  $\Delta\sigma_{Rsk}(N^*)$  at  $N^*$  may be reduced by a reduction factor  $\xi$  for bent bars.

$$\xi = 0.35 + 0.026 \frac{D}{\phi} \quad (1.7)$$

where  $D$  is the diameter of the reinforcing bar, and  $\phi$  is the bending diameter of the bent bar.

### 1.3.2 Fatigue Life of Concrete

The fatigue life of concrete can be estimated using stress-life models similar to steel reinforcement. From investigations conducted in the past, the fatigue behaviour of concrete is influenced by various factors such as stress level, stress ratio, eccentricity of loading, frequency, shape of the waveform, and stress reversals amongst others. Many such models are available in the literature; however, those with insufficient fatigue-influencing factors are seldom used. Stress-life models used for estimating the fatigue life of concrete are usually given as plots of normalized concrete stress levels against the logarithm of the number of cycles resulting in failure (Aas-Jakobsen, 1970; Hsu, 1981, Zhang et al., 1996; Zhang et al., 1998; Fib, 2010).

FIB Model Code 2010 considers uniaxial compression, tension, or reversed loads. Stress-life curves are developed for normalized maximum compressive stresses for various concrete compressive strengths. The curves produced correspond to normalized minimum effective compressive stress levels with the compressive strength ( $f'_c$ ) from 0 to 0.8. According to FIB Model Code 2010, the equations presented are valid for concrete under a constant environment with approximate conditions of 20°C and 65% relative humidity; however, the effect of creep is not accounted for (Figure 1.3).

For pure compression where  $0 \leq S_{c,min} \leq 0.8$ , then

$$\text{Log } N_1 = \frac{8}{(Y-1)} \cdot (S_{c,max}-1) \quad (1.8)$$

$$\text{Log } N_2 = 8 + \frac{8 \cdot \ln(10)}{(Y-1)} \cdot (Y - S_{c,min}) \cdot \log\left(\frac{S_{c,max}-S_{c,min}}{Y-S_{c,min}}\right) \quad (1.9)$$

$$Y = \frac{0.45+1.8 \cdot S_{c,min}}{1+1.8 \cdot S_{c,min} - 0.3 S_{c,min}^2} \quad (1.10)$$

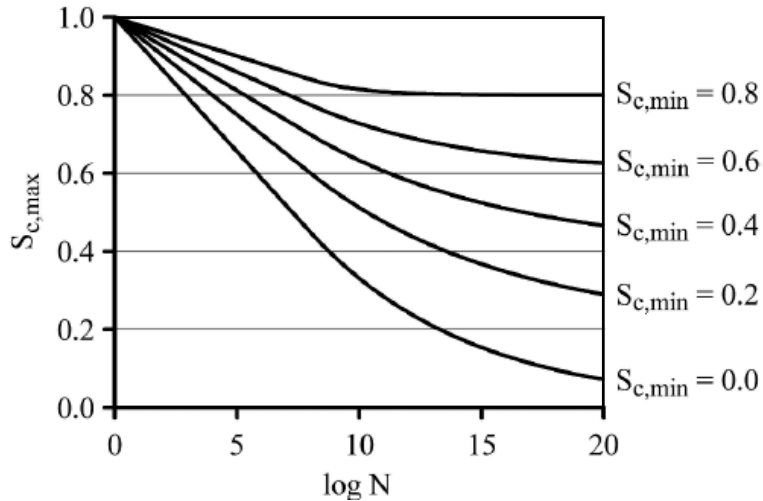


Fig. 1.3- S-N curve based on equations above (FIB Model code 2010).

where

$\text{Log } N = \text{Log } N_1$  if  $\text{Log } N_1 \leq 8$

$\text{Log}N = \text{Log} N_2$ , if  $\text{Log} N_1 > 8$

$$S_{c,max} = |\sigma_{c,max}| / f_{ck,fat} \quad (1.11)$$

$$S_{c,min} = |\sigma_{c,min}| / f_{ck,fat} \quad (1.12)$$

$$\Delta S_c = S_{c,max} - S_{c,min} \quad (1.13)$$

$$f_{ck,fat} = \beta_{cc}(t) \cdot \beta_{c,sus}(t, t_0) \cdot f_{ck} \cdot (1 - f_{ck}/400) \quad (1.14)$$

For concrete in compression-tension with  $\sigma_{ct,max} \leq 0.026 |\sigma_{c,max}|$

$$\text{Log}N = 9 \cdot (1 - S_{c,max}) \quad (1.15)$$

For plain concrete in tension, and compression-tension  $> 0.026 |\sigma_{c,max}|$

$$\text{Log}N = 12 \cdot (1 - S_{ct,max}) \quad (1.16)$$

$$S_{ct,max} = \sigma_{ct,max} / f_{ctk,min}$$

where

N: number of cycles

$S_{c,max}$ : maximum compressive stress level (normalized with  $f'_c$ )

$S_{c,min}$ : minimum compressive stress level (normalized with  $f'_c$ )

$S_{ct,max}$ : maximum tensile stress level (normalized with  $f'_c$ )

$\Delta S_c$ : stress range

$\sigma_{c,max}$ : maximum compressive stress in MPa

$\sigma_{c,min}$ : minimum compressive stress in MPa

$\sigma_{ct,max}$ : maximum tensile stress in MPa

$f_{ck}$ : characteristic compressive strength (MPa)

$f_{ck,fat}$ : fatigue reference compressive strength (MPa)

$f_{ctk,min}$ : minimum characteristic tensile strength (MPa)

$\beta_{cc}(t)$ : coefficient depending on the age of the concrete at the beginning of fatigue loading

$\beta_{c,sus}(t,t_0)$ : coefficient which considers the mean stresses at loading; taken as 0.85 for fatigue loading.

In the case of variable fatigue loading, FIB Model Code 2010 also proposes the use of the Palmgren-Miner cumulative damage rule as considered in steel reinforcement. As such, the cumulative damage (D) can be estimated thus:

$$D = \sum_i \frac{n_{si}}{n_{Ri}} < 1 \quad (1.17)$$

where  $n_{si}$  is the number of fatigue loading cycles at a given stress level, and  $n_{Ri}$  is the corresponding number of cycles resulting in failure at the given stress level.

In the literature, other approaches which consider a comparison between the induced concrete stresses and a limiting value for appropriate fatigue resistance capacity are available. In EN 1992-1-1 2004, two approaches exist. In the first approach (EN 1992-1-1 2004 (6.8.6)), a satisfactory fatigue resistance capacity may be assumed for concrete under compression, if the following condition is fulfilled:

$$E_{cd,max,equ} + 0.43 \sqrt{1 - R_{equ}} \leq 1 \quad (1.18)$$

where

$$R_{equ} = \frac{E_{cd,min,equ}}{E_{cd,max,equ}}$$

$$E_{cd,min,equ} = \frac{\sigma_{cd,min,equ}}{f_{cd,fat}}$$

$$E_{cd,max,equ} = \frac{\sigma_{cd,max,equ}}{f_{cd,fat}}$$

$R_{equ}$ : stress ratio

$E_{cd,min,equ}$ : minimum compressive stress level

$E_{cd.max.equ}$  : maximum compressive stress level

$f_{cd.fat}$  : design fatigue strength of concrete

$\sigma_{cd.max.equ}$ : upper stress of the ultimate amplitude for N cycles

$\sigma_{cd.min.equ}$ : lower stress of the ultimate amplitude for N cycles.

From the code, a recommended value for N is  $10^6$  cycles.

$$f_{cd.fat} = k_1 \beta_{cc}(t_0) f_{cd} \left(1 - \frac{f_{ck}}{250}\right) \quad (1.19)$$

$\beta_{cc}(t_0)$  is a coefficient for concrete strength at first load application, and  $t_0$  is the time of the start of the cyclic loading on concrete in days. The recommended value of  $k_1$  for N equal to  $10^6$  cycles is 0.85.

In the second approach, the fatigue verification for concrete under compression may be assumed if the following condition is satisfied:

$$\frac{\sigma_{c.max}}{f_{cd.fat}} \leq 0.5 + 0.45 \frac{\sigma_{c.min}}{f_{cd.fat}} \quad (1.20)$$

$$\leq 0.9 \text{ for } f_{ck} \leq 50 \text{ MPa}$$

$$\leq 0.8 \text{ for } f_{ck} > 50 \text{ MPa}$$

where

$\sigma_{c.max}$  is the maximum compressive stress at a fibre under the frequent load combination (compression stress measured positive), and  $\sigma_{c.min}$  is the minimum compressive stress at the same fibre where  $\sigma_{c.max}$  occurs. If  $\sigma_{c.min}$  is a tensile stress, then  $\sigma_{c.min}$  should be taken as 0.

Equation 1.20 also applies to the compression struts of members subjected to shear. In this case the concrete strength  $f_{cd.fat}$  should be reduced. Other similar approaches for the fatigue analysis of concrete are available in DNV RISØ (Guidelines for Fatigue Design of Wind Turbines) and DIBt (Wind Turbine Guideline for Design).

### **1.3.3 Fatigue Life of Steel-Fibre Reinforced Concrete**

In the literature, tests have been conducted on steel-fibre reinforced concrete in order to verify its performance under fatigue loading. Results reported on tests conducted on flexural fatigue strength, endurance limit, and compressive fatigue strength have shown that concrete fatigue resistance can be improved using steel fibre. As such, the use of smaller cross sections or increases in the life-span of structural components such as pavements, bridge deck overlays, offshore structures, machine foundations etc. are obtainable. Despite the well-documented qualitative attributes of steel fibre in enhancing fatigue life, no appropriate model has been proposed for quantifying or estimating the fatigue life of steel fibre concrete. This has obviously impeded its wide-spread use.

### **1.4 Loading History and Cumulative Damage under Fatigue Load**

As previously indicated, reinforced concrete structures are generally subjected to variable amplitude fatigue load. The Palmgren-Miner's linear cumulative damage rule is often used to calculate the total damage value due to each number of load cycles corresponding to a given load level (Figure 1.4). Fatigue analysis reports from Hilsdorf et al. (1960), Wirshig et al., (1995), and Lee et al. (2005) have shown that the linear Palmgren-Miner rule gives inconsistent results, and hence may result in unsafe designs.

In order to show the inconsistency of the Palmgren-Miner rule, other damage rules such as the nonlinear damage rule and the double linear damage rule for two or more load steps have been used to illustrate the damage value per fatigue load (Figure 1.5 and Figure 1.6). As an illustration, consider equal damage values ( $A$  and  $A'$ ) on damage profiles  $OB$  and  $OB'$  for a high and a low stress level, respectively. The number of cycles required for failure on profile  $OB'$  after an initial fatigue loading of the high stress level ( $n_1$ ) on  $OB$  (intersection of  $A$ ) can be observed to be less

than the number of cycles required for failure after the initial application of the lower stress level ( $n_2$ ).

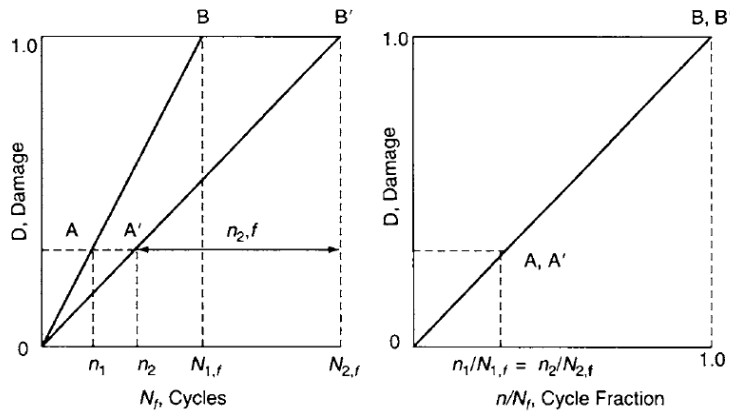


Fig. 1.4- Linear damage accumulation (Lee et al, 2005).

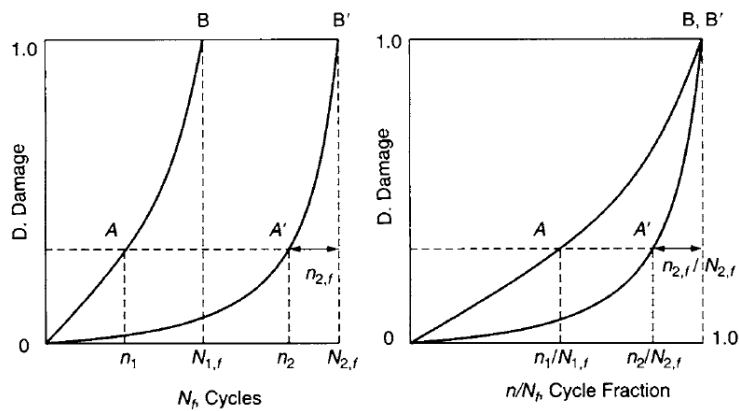


Figure 1.5: Nonlinear damage accumulation (Lee et al, 2005).

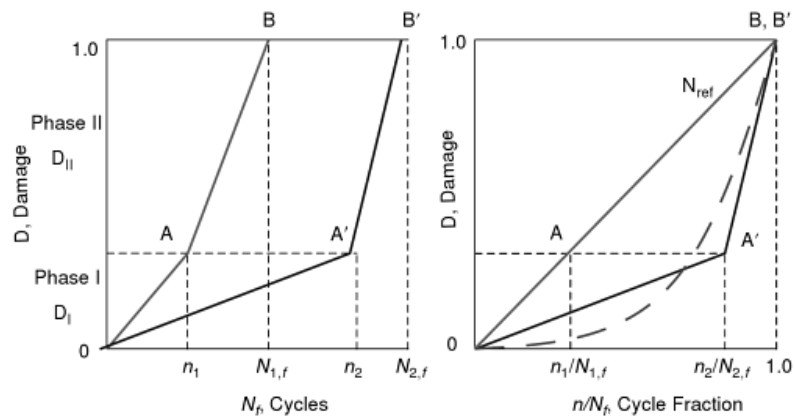


Fig. 1.6 - Double linear damage rule for two step load levels (Lee et al, 2005).

## **1.5 Outstanding Questions in the Fatigue Resistance Analysis and Design Approach**

A number of outstanding questions remain; these include:

- Can damage evolution models which account for various controlling factors be developed for residual concrete strength and modulus degradation, since these models are required to develop fatigue constitutive equations for time-dependent numerical analysis?
- Certain assumptions have been made regarding the behaviour of concrete under fatigue loading; hence, resulting in the simplification of fatigue analysis. In addition, experimental results indicate that irreversible fatigue strains accumulate in concrete under fatigue loading; however, this is neglected in analysis. As such, can the reliability of these assumptions be verified and can irreversible fatigue strain be accounted for in fatigue analysis?
- A majority of fatigue-prone structural elements are designed as deep beams. How viable is the use of steel fibre in enhancing their fatigue life? Further, can appropriate stress-life models be developed for steel-fibre concrete?
- Stress-life models are generally used in the progressive damage analysis of steel reinforcing bars. However, progressive crack growth up to fracture in reinforcing bars traversing cracked concrete planes has been observed in reinforced concrete structures, apparent in the progressive increase in the width of a traversed cracked concrete plane and the increase in deformation. Hence, can crack growth be taken into account in the equilibrium equations for a cracked concrete plane?

## **1.6 Research Motivation**

The behaviour of concrete under fatigue loading is well known to be nonlinear. As such, the cumulative damage predictions using the Palmgren-Miner rule do not give values corresponding

to the deformed state of a structural element at any instant (Hilsdorf et al., 1966; Hawkins, 1974; Holmen, 1982; Shah, 1984; Oh, 1991; Vega et al., 1995; Lee et al., 2005; Lloyd et al., 2007). Although the Palmgren-Miner rule has been reported in the literature to be suitable for steel reinforcement (Byers et al., 1997; Petryna et al., 2002; Maekawa et al., 2006; Teng et al., 2000), crack propagation in reinforcing bars is characterised by a nonlinear profile, thus supporting evidence of nonlinearity in the behaviour of reinforced concrete structures under fatigue loading (Paris et al., 1961; Dowling, 1993; Hirt and Nussbaumer, 2006; Herwig, 2008; Rocha and Bruhwiler, 2012).

Irreversible deformation accumulates in concrete structures as fatigue loads progress (Maekawa et al., 2006; Zanuy et al., 2009). In addition, once concrete cracking initiates due to the degradation of its tensile strength, concrete cracking propagates within a plane while the stresses in the reinforcing bars intersecting the plane increase (Isojeh and Vecchio, 2016). Provided the induced reinforcement stresses are higher than the threshold values required for crack initiation, reinforcement crack propagation may also occur and result in a progressive increase in the deformation within the cracked concrete planes. The stability and deformation of the global structure may be influenced by these local deformations in addition to the irreversible deformation accumulation in concrete. As such, rather than estimating the number of cycles at which a material may fail at a locality, the progressive stability in terms of residual strength and the corresponding deformation evolution is of more importance, considering the fact that the residual strength of the global structure or the serviceability limits may be surpassed even before a local material failure occurs under fatigue loading.

In design, the volumes of materials (concrete and steel reinforcement) are usually increased once the estimated cumulative damage exceeds the proposed limit. In the case of a wind turbine

foundation with a restricted size, the increase in reinforcement may result in bulkiness or congestion within the foundation. Hence, a means of reducing reinforcement congestion (especially shear reinforcement), optimising the structural size, and preventing or mitigating concrete crack growth under fatigue loading is required.

As an improvement over the rudimentary use of stress-life models and the Palmgren-Miner rule, fatigue constitutive models and damage models for concrete which account for progressive damage and irreversible deformation accumulation are available in the literature. However, these models are typically void of the salient factors affecting fatigue loading. A majority of such models are limited in use to structural components having the same parameters as the experimental tests conducted for deriving the models.

The implementation of fatigue damage models, which account for the aforementioned deficiencies, into the governing equations (constitutive, compatibility, and equilibrium) of a nonlinear finite element algorithm will enhance the fatigue damage analysis of complex structures such as wind turbine foundations. Further, it will provide for appropriate design verification, rather than having to rely on the use of rudimentary approaches. The development of a residual capacity-based and deformation evolution-based analysis approach will lead to a new fatigue life theorem.

Although various reports, analyses, inferences, and so on have been provided in the past for the design of structural elements susceptible to fatigue damage, the actual mechanisms governing behaviour while in service are quite complex and at present are not well understood. Hence, further investigation is imperative.

### **1.7 Study Scope and Objectives**

The main focus of this research program is aimed towards the development and implementation

of plain concrete damage models, steel fibre concrete damage models, and steel reinforcement crack propagation models into the governing equations of strut and tie models and the Disturbed Stress Field Model algorithm for fatigue analysis of reinforced concrete structures.

In order to develop such an approach for the fatigue analysis and resistance design of conventional reinforced concrete and steel-fibre reinforced concrete elements, an experimental campaign is described at the structural and materials levels.

Damage models are implemented into the monotonic stress-strain equations for concrete and steel fibre concrete for fatigue analysis. A modified localised reinforcement crack growth model is also used to account for the reinforcement area reduction at its intersection with a concrete crack. The accumulation of irreversible compressive strain in concrete or steel fibre is accounted for, using a fatigue offset strain model.

The research program presented in this thesis can be subdivided into the following objectives:

- 1) Development of robust fatigue damage models, building on previously existing models, to account for controlling factors under fatigue loading such as stress ratio, frequency of fatigue loading and fatigue waveform.
- 2) Development of a constitutive model and damage parameters for plain and steel-fibre reinforced concrete under fatigue loading in addition to an irreversible strain accumulation model.
- 3) Investigation of the behaviour of reinforced concrete and steel fibre reinforced concrete beams under fatigue loading.
- 4) Implementation of the proposed models into the analysis algorithm of strut and tie models and the Disturbed Stress Field Model (Vecchio, 2000) for the analysis of fatigue-damaged

structures. Further, results from the experiments conducted will be corroborated with results obtained using nonlinear finite element analysis (VecTor2).

## **1.8 Thesis Contents**

In the second chapter, the behaviour of concrete under fatigue loading in uniaxial compression is presented. Tests methodology and specimens details used in developing a secondary strain rate model and damage parameters are also presented (published in ACI Materials Journal).

In addition to the proposed irreversible strain accumulation model, simplified constitutive models for normal and high strength concrete are developed and discussed in Chapter 3 (published in ASCE Materials Journal).

Chapter 4 presents an overview of the behaviour of steel fibre concrete under fatigue loading. Damage parameters and corresponding evolution models are developed (published in ASCE Materials Journal).

Small-scale deep beams were tested by varying the fatigue loading parameters, including the steel fibre volume ratio and the reinforcement ratio. The test procedures and results are presented in Chapter 5. In addition, the enhancing influence of steel fibre in reinforced concrete beams is discussed (ACI Structural Journal (in-press)).

The proposed models are further implemented into the constitutive, compatibility and equilibrium equations of strut and tie (stress-path) models and the DSFM algorithm for finite element analysis. These are presented in Chapters 6 and 7, respectively (Engineering Structures (in-press) and ASCE Structural Journal (submitted), respectively).

In Chapter 8, the experimental results obtained from the tested beams are corroborated with finite element analysis results obtained using VecTor2 (submitted to ASCE Structural Journal).

Lastly, the conclusions from the experimental and analytical studies are presented in Chapter 9. In addition, considerations for future investigations are given.

## 1.9 References

1. Byers W.G., Marley M. J., Mohammadi J., Nielsen R.J., and Sarkani S. (1997). "Fatigue Reliability Reassessment Applications: State-of-the-Art Paper." *Journal of Structural Engineering*, Vol. 123, pp. 277-285.
2. Dowling N.E. (1993). "Mechanical Behaviour of Materials." Prentice Hall, New Jersey.
3. Goransson F., and Nordenmark A. (2011). "Fatigue Assessment of Concrete Foundations for Wind Power Plants." Department of Civil and Environmental Engineering (Master's thesis), Chalmers University of Technology, Goteborg, Sweden 2011.
4. Grunberg J., and Gohlmann J. (2013). "Concrete Structures for Wind Turbines." Wilhelm Ernst & Sohn, Verlag fur Architektur und technische Wissenschaften GmbH & Co. KG, Rotherstrae, 21, 10245 Berlin, Germany.
5. Hassanzadeh M. (2012). "Cracks in Onshore Wind Power Foundations." *Elforsk rapport* 11:56.
6. Hawkins N. M. (1974). "Fatigue Characteristics in Bond and Shear of Reinforced Concrete Beams." *Abeles Symposium*, ACI Pub. SP41-10, pp.203-236.
7. Herwig A. (2008). "Reinforced Concrete Bridges under Increased Railway Traffic Loads- Fatigue Behaviour and Safety Measures." Ph. D Thesis No. 4010, Ecole Polytechnique Federale de Lausanne.

8. Hilsdorf H.K., and Kesler C.E. (1966). "Fatigue Strength of Concrete under Varying Flexural Stresses." *ACI Journal*, Vol. 63, No. 1. pp. 1059-1076.
9. Hirt M.A., and Nussbaumer A. (2006). "Construction Metallique: Notions Fondamentales et Methods de Dimensionnement, Nouvelle Edition Revue et Adaptee aux Nouvelles Norms de Structures." *Traite de Genie Civil de l'Ecole Polytechnique Federale*, Vol. 10. Lausanne, Switzerland.
10. Holmen J.O. (1982). "Fatigue of Concrete by Constant and Variable Amplitude Loading." *ACISP 75-4*, pp. 71-110.
11. Isojeh M.B., and Vecchio F.J. (2016). "Parametric Damage of Concrete under High-Cycle Fatigue Loading in Compression." *Proc., 9<sup>th</sup> International Conference on Fracture mechanics of Concrete and Concrete Structures. FraMCoS-9*, 10.21012/FC9.009.
12. JSCE (1986). "Standard Specification for Design of Concrete Structures." Japan Society of Civil Engineers.
13. Landen N., and Lilljegen J. (2012). "Three-Dimensional Strut and Tie Modelling of Wind Power Plant Foundations." Master's Thesis, Chalmers University of Technology, Goteborg, Sweden.
14. Lee Y., Pan J., Hathaway R., and Barkey M. (2005). "Fatigue Testing and Analysis: Theory and Practice." Elsevier Butterworth-Heinemann.
15. Lloyd J.P., Lott J. L., Kesler C. E. (2007). "Fatigue of Concrete." University of Illinois, Urbana- Champaign, Large-Scale Digitization Project.

16. Maekawa K., Toongoenthong K., Gebreyouhannes E., Kishi T. (2006). "Direct Path-Integral Scheme for Fatigue Simulation of Reinforced Concrete in Shear." *Journal of Advanced Concrete Technology*, Vol. 4, No. 1, pp. 159-177.
17. Nicholson J.C. (2012). "Design of Wind Turbine Tower and Foundation Systems: Optimization Approach." Master's Thesis, University of Iowa.
18. Oh B.H. (1991). "Cumulative Damage Theory of Concrete under Variable-Amplitude Fatigue Loadings." *ACI Materials Journal*, Vol. 88, No. 2, pp. 122-128.
19. Paris P., Gomez M.P., Anderson W.E. (1961). "A Rational Analytical Theory of Fatigue." *The Trend in Engineering* Vol.13, pp. 9-14.
20. Petryna, Y.S., Pfanner, D., Stangenberg, F., and Kratzig, W.B. (2002). "Reliability of Reinforced Concrete Structures under Fatigue." *Reliability Engineering and System Safety*, Vol. 77, pp. 253-261.
21. Rocha M, and Bruhwiler E. (2012). "Prediction of Fatigue Life of Reinforced Concrete Bridges." In Biondini and Frangopol (Eds) *Bridge Maintenance, Safety, Management, Resilience and Sustainability*, pp. 3755-3760.
22. Shah S.P. (1984). "Predictions of Cumulative Damage for Concrete and Reinforced Concrete." *Materiaux et Construction*, Vol. 17 No.1, 1984, pp. 65-68.
23. Sheng J., and Chen S. (2010). "Fatigue Load Simulation for Foundation Design of Offshore Wind Turbines Due to Combined Wind and Wave Loading." *Institute of Electrical and Electronic Engineers*.

24. Spera D.A. (2009). "Wind Turbine Technology: Fundamental Concepts of Wind Turbine Engineering." ASME Press, New York, NY.
25. Teng S., and Wang F. (2000). "Finite Element Analysis of Reinforced Concrete Deep Beams under Fatigue Loading." ACI Structural Journal, Vol. 98, No.3, pp. 315-323.
26. Vecchio F.J. (2000). "Disturbed Stress Field Model for Reinforced Concrete: Formulation." Journal of Structural Engineering, Vol. 126, No. 8, pp. 1070-1077.
27. Vega I.M., Bhatti M.A., and Nixon W.A. (1995). "A Nonlinear Fatigue Damage Model for Concrete in Tension." International of Journal of Damage Mechanics, Vol. 4, pp. 362-379.
28. Wirshing P.H., Paez T.L., and Ortiz H. (1995). "Random Vibrations: Theory and Practice." Wiley, New York.
29. Yuyama S., Li Z.W., Yoshizawa M., Tomokiyo T., Uomoto T. (2001). "Evaluation of Fatigue Damage in Reinforced Concrete Slab by Acoustic Emission." NDT & E International, Vol. 34, pp. 381-387.
30. Zanuy C., Fuente P., and Albajar L. (2009). "Effect of Fatigue Degradation of the Compression Zone of Concrete in Reinforced Concrete Sections." Eng. Structures, Vol. 29, pp. 2908-2920.

## CHAPTER 2

### CONCRETE DAMAGE UNDER FATIGUE LOADING IN UNIAXIAL COMPRESSION

The material in this chapter was previously published as follows:

*Isojeh B., El-Zeghayar M., and Vecchio F.J (2017). "Concrete Damage under Fatigue Loading in Uniaxial Compression." ACI Materials Journal, Vol. 114, No. 2, pp. 225-35.*

#### 2.1 Abstract

Despite rigorous efforts in the derivation of various fatigue damage models for concrete, damage predictions of sufficient accuracy are still limited to loading conditions similar to those of the experiments used for developing the models. Most models are void of important factors affecting the fatigue behaviour of concrete such as frequency, stress ratio, and loading waveform, and the approaches used in developing such models tend to be rudimentary. Therefore, further investigation is required.

In this study, damage models are developed for residual concrete strength and fatigue secant modulus using experimental data from tested cylindrical specimens, a damage function, and a stress-life model in the literature. The number of cycles leading to failure, required for normalising the fatigue cycles for each specimen, is obtained using a proposed secondary strain rate model. The aforementioned influencing factors incorporated into the damage function result in robust models that account for variations in loading parameters.

#### 2.2 Introduction

During fatigue loading, the properties of concrete undergo alterations which result in damage. The progressive damage of a concrete element can be observed from the evolution of various deformation parameters, such as total strain, residual strain, stiffness degradation, strength

degradation, heat dissipation due to micro-cracking, crack growth, and speed of sound in concrete (Shah, 1984; Torrenti et al., 2010). Based on previous investigations on the fatigue behaviour of concrete, the damage evolution for each parameter is nonlinear (Papa and Taliercio, 1993; Vega et al., 1995; Taliercio and Gobbit, 1996; Song et al., 2005; Tamulenas et al., 2014).

The fatigue behaviour of concrete is influenced by various factors, unlike the fatigue behaviour of steel reinforcing bars. Investigations conducted by Aas-Jakobsen (1970), Murdock et al. (1955), Hilsdorf and Kesler (1966), Awad (1971), and Oh (1991) have shown that the increase in maximum fatigue stress results in a decrease in the number of cycles to failure, while a higher minimum stress level corresponds to an increase in the number of cycles to failure. According to Ople et al. (1966) on the matter of stress gradient (eccentricity in fatigue loading), the number of cycles to failure increases as the eccentricity of loading increases.

As reported in previous investigations, an overestimation of the fatigue life will occur if a fatigue model developed using a higher frequency of loading compared to that of the real structure is used in an analysis or design. Investigations conducted on the influence of frequency by Graf et al. (1936), Spark et al. (1973), Raithby and Galloway (1974), Holmen (1982), Naik (1993), and Zhang et al. (1996) all indicate that the number of cycles leading to failure decrease as the frequency of loading decreases. This behaviour has been observed to be more pronounced as the maximum fatigue stress level increases. For higher fatigue stress levels, the behaviour of concrete depends on the fatigue cycles and on the duration of loading where creep effects become significant, leading to a reduction in the fatigue life (Hilsdorf and Kesler, 1966). To the contrary, Takhar et al. (1974), based on statistical analysis, concluded that there was no significant difference between tests conducted at a loading frequency of 20 cycles per minute and 60 cycles per minute for stress levels of 0.8 and 0.9 (fractions of average compressive strength).

It has also been reported in the literature that the shape of the waveform used in fatigue loading influences the fatigue life. However, the influence is more prominent at maximum stress levels equal to or greater than 0.8, or at maximum stress levels that result in failure at cycles less than or equal to 1000. From observations, the number of cycles leading to failure with a sinusoidal waveform will be about half of the number of failure cycles for a triangular waveform, while the number of cycles to failure for a rectangular waveform will be about one-sixth of the number of cycles to failure for a sinusoidal waveform under the same stress level (Torrenti et al., 2010; RILEM, 1984).

The impact of stress reversal under fatigue loading was investigated by Zhang et al. (1996) on 171 beams with seven stress ratios, including negative stress ratios. The ratios were combined with 13 stress levels. The stress-life curves (S-N), obtained by plotting the stress level against the number of cycles to failure for each specimen, portrayed a reduction in the fatigue life of the concrete specimens as the stress ratio reduced.

The effects of other factors such as shape of the specimen, water-cement ratio, aggregate type and gradation, concrete strength, curing conditions, age at loading, and moisture conditions, that affect concrete, can be removed by normalizing the stress levels with the ultimate capacity of concrete under static load (Raithby and Galloway, 1974; Hsu, 1984; Hooi, 2000; Lee and Barr, 2002; Grebreyouhannes et al., 2008). This concept reduces the number of factors considered in analytical models for predicting the behaviour of concrete elements under fatigue load to the loading parameters alone (Torrenti et al., 2010).

The perception of damage evolution of a material provides a conceptual basis by which the degradation of the mechanical properties of concrete and the corresponding physical deformation

can be correlated. Obtaining the damage evolution for parameters such as residual strength and secant stiffness may require discrete test points from a number of tested specimens (Cook and Chindaprasirt, 1980; Cook and Chindaprasirt, 1981; Cornelissen and Reinhardt, 1987; Zhang and Wu, 1997). To obtain the discrete test points, specimens are loaded cyclically to different numbers of cycles before failure; thereafter, the observed deformation parameter at given cycles are plotted against the normalised number of cycles.

Due to the stochastic nature of concrete (CEB Bull 188, 198; FIB Model Code, 2000; Lohaus et al., 2012), the actual number of cycles to failure for each specimen is different even under the same magnitude of fatigue load. Hence, the use of S-N models in estimating the number of cycles to failure for normalising the specified tests cycles is inappropriate, and the corresponding models developed do not portray the actual parametric damage evolution (Schaff and Davidson, 1997; Zhu and Li, 2011; Paepegem and Degrieck, 2002).

According to Sparks and Menzies (1973), Cornelissen et al. (1987), and Taliercio et al. (1996), a correlation exists between the secondary strain rate and the number of cycles leading to failure. As such, provided the secondary strain rate can be obtained for each specimen tested, the number of cycles to failure can be estimated.

At the final damage states of concrete specimens, the fatigue secant modulus at failure has been reported to converge to about 60% of the initial fatigue secant moduli (Torrenti et al., 2010; Holmen, 1982). In a similar manner to the fatigue secant modulus, the strength of composite materials also deteriorates under fatigue loading. Hence, it has been reported that the same damage evolution model can be used for residual strength and stiffness (Paepegem and Degrieck, 2002). However, the initial stage of fatigue loading of concrete is characterised by a slight increase in strength (Talierco and Gobbit, 1996; Cook and Chindaprasit, 1981). This phenomenon is attributed

to the consolidation or the closing up of micro-voids in concrete at the initial stage of fatigue loading (Zhang and Wu, 1997). The increase in strength may also be attributed to the stochastic nature of concrete (CEB Bull 188., 1988; FIB Model Code, 2010; Lohaus et al., 2012).

Once strength damage initiates, an increase in damage will be observed in subsequent cyclic loading; thereafter, loading a concrete specimen monotonically to failure will result in a lower compressive strength.

In this investigation, the stress ratios for the experiments conducted are either equal to or greater than zero; hence, no fatigue stress reversal is considered. In addition, a sinusoidal waveform is used for all fatigue tests conducted.

To obtain normalised fatigue cycles, the numbers of cycles to failure of tested specimens were estimated using the secondary strain rate concept. Building on a damage function formulated by Gao and Hsu (1998), modified robust damage models which incorporate influencing fatigue factors from an S-N model (Zhang et al., 1996; Zhang et al., 1998) are developed for concrete strength and residual fatigue secant modulus using data from tested specimens.

### **2.3 Research Significance**

This investigation incorporates the concept of secondary strain rate for obtaining fatigue life in the formulation of improved damage models for concrete in compression. Further, key fatigue factors from an existing S-N model (frequency, stress ratio, loading waveform) are incorporated; hence, the combined models are suitable for a wide variety of fatigue loading conditions for concrete structures. The models proposed can be implemented into general concrete constitutive models for predicting strength and stiffness deterioration and improved fatigue analysis of concrete structures.

## 2.4 Experimental Investigation

Experiments were conducted on concrete cylinders to develop a secondary strain rate model and to observe subsequent residual strengths and fatigue secant moduli as the number of fatigue loading cycles increased. The secondary strain rate is defined as the rate of change in maximum fatigue strain per unit cycle within the linear portion of the strain evolution profile (secondary stage). For the residual strength and fatigue modulus, each specimen was tested to a different number of cycles less than the actual number of cycles leading to failure.

The tests were conducted using servohydraulic testing equipment having a loading capacity of 1000 kN. The loading equipment was programmed to generate a pulsating load of a continuous sinusoidal waveform throughout the test duration. Each specimen was mounted with attached displacement transducers (LVDTs) as shown in Figure 2.1. The LVDTs were used to measure average strains in the specimens throughout the duration of the fatigue tests.

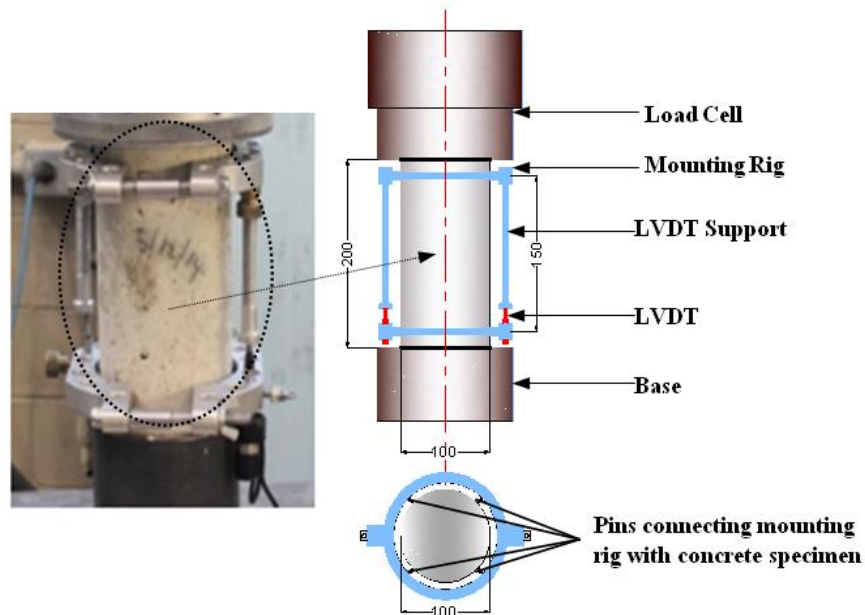


Fig. 2.1 – Fatigue loading setup.

Table 2.1- Average compressive strength and corresponding strain.

| Batch (# of Specimens) | Average Compressive Strength (MPa) | Average Corresponding Strain (x 0.001) | Mix ratio | Wct-ratio |
|------------------------|------------------------------------|--|-----------|-----------|
| 1(5)                   | 52.8                               | 2.01                                   | 1:2:2*    | 0.5       |
| 2(3)                   | 55.8                               | 2.00                                   | 1:2:2*    | 0.5       |
| 3(3)                   | 46.2                               | 1.95                                   | 1:2:3*    | 0.5       |
| 4(3)                   | 23.1                               | 1.52                                   | 1:2:4*    | 0.6       |

\*represents cement: sand: coarse aggregate by weight

Concrete cylinders (38 specimens) with dimensions of 100 mm diameter x 200 mm height were subjected to uniaxial fatigue loading in compression. Prior to the fatigue tests, concrete specimens (at least three per batch) were tested statically to obtain the average compressive strength, as shown in Table 2.1. The stress levels (maximum and minimum stresses) for the fatigue tests were taken as percentages of the average compressive strength.

The maximum stress level, the concrete strength, and the loading frequency were variables in this experimental investigation. Maximum stress levels of 0.69 to 0.80, as fractions of the average compressive strength, were used as the fatigue loads. Sixteen specimens were loaded to failure to observe the evolution of the maximum strain as indicated in Table 2.2, while 22 specimens, as indicated in Table A-1 (Appendix A), were loaded to different numbers of cycles which were less than the number of cycles to failure at a constant maximum stress level of 0.74.

The 22 specimens tested were used to observe the evolution of the strength and fatigue secant modulus of concrete. Although the value of 0.74 was chosen arbitrarily, it falls within the range for high-cycle fatigue. The 22 specimens tested under fatigue loading were subsequently loaded monotonically to failure. For the specified load levels, a frequency of 5 Hz was used for all batches. A frequency of 1 Hz was used for testing three specimens from the fourth batch. For all fatigue tests conducted, a constant minimum load of 5 kN was used.

Table 2.2 - Specimen fatigue parameters and test failure data.

| Specimen | Compressive Strength<br>( $f'_c$ ) MPa | Stress Level<br>(% of $f'_c$ ) | Frequency<br>(Hz) | Number of Cycles<br>to failure ( $N_f$ ) | Log $N_f$ |
|----------|--|--------------------------------|-------------------|--|-----------|
| E5       | 52.8                                   | 74                             | 5                 | 12210                                    | 4.09      |
| E8       | 52.8                                   | 74                             | 5                 | 10180                                    | 4.01      |
| E13      | 52.8                                   | 74                             | 5                 | 8720                                     | 3.94      |
| E21      | 52.8                                   | 74                             | 5                 | 8460                                     | 3.93      |
| E3       | 52.8                                   | 74                             | 5                 | 5640                                     | 3.75      |
| G4       | 46.2                                   | 74                             | 5                 | 4690                                     | 3.67      |
| G11      | 46.2                                   | 74                             | 5                 | 4600                                     | 3.66      |
| E10      | 52.8                                   | 69                             | 5                 | 25200                                    | 4.40      |
| E15      | 52.8                                   | 69                             | 5                 | 20500                                    | 4.31      |
| H16      | 55.8                                   | 80                             | 5                 | 747                                      | 2.87      |
| H17      | 55.8                                   | 80                             | 5                 | 3530                                     | 3.55      |
| I1       | 23.1                                   | 75                             | 5                 | 3220                                     | 3.51      |
| I5       | 23.1                                   | 75                             | 1                 | 4910                                     | 3.69      |
| I6       | 23.1                                   | 75                             | 5                 | 1560                                     | 3.19      |
| I8       | 23.1                                   | 75                             | 1                 | 3030                                     | 3.48      |
| I10      | 23.1                                   | 75                             | 1                 | 5010                                     | 3.70      |

### 2.6.1 Test Specimens

The concrete specimens were made from Portland cement (general use, GU), sand, and limestone aggregates (10 mm maximum size) with three different mixture proportions. The concrete for the first two batches, as indicated in Table 2.1, was cast using a mixture proportion of 1: 2: 2, (cement:sand:coarse aggregate by weight) with a water-cement ratio (w/c) of 0.5. For the third and fourth batches, mix proportion ratios of 1:2:3 with a w/c of 0.5 and 1:2:4 with a w/c of 0.6 were used, respectively. The fineness modulus of the sand used was estimated to be 2.6. The slumps observed from the fresh concrete from all batches were 100 to 150 mm. The static strengths of concrete after curing for 28 days were obtained from each batch, while the fatigue tests were conducted 30 to 40 days after casting. The first, second, third and fourth batches were denoted as E, H, G, and I, respectively, as indicated in Table 2.1. The number added to each alphabet in the table indicates the number assigned to the specimen before testing.

## 2.4.2 Results

At the initial stage of fatigue loading, an increase in strain at a decreasing rate was observed due to the closing up of concrete pores and micro-cracks between aggregates and cement mortar. Subsequently, the rate of strain evolution was constant while micro-cracks within the cement mortar increased. Within the last stage of fatigue damage evolution, the micro-cracks merged to form macro-cracks. Similar to static loading, these cracks (hairlines) were obvious on the surfaces of the concrete specimens and were approximately parallel to the direction of loading. Further, the ends of these macro-cracks merged and developed a failure plane which resembled a fault (Figure 2.2). The numbers of cycles leading to failure were recorded for the 16 specimens tested and are given in Table 2.2. The standard deviations (in terms of the logarithm of the number of cycles to failure,  $N_f$ ) observed for the four different stress levels (74%, 75%, 69% and 80%) are 0.17, 0.21, 0.06, and 0.48, respectively. The respective mean values are 3.86, 3.51, 4.36, and 3.21. However, the standard deviation of the error ( $\text{Log } N_f$ ) between the experimental data and the model by Zhang et al. (1998) is 0.26 and the model prediction (in logarithm) is 3.80 for a 74% stress level.

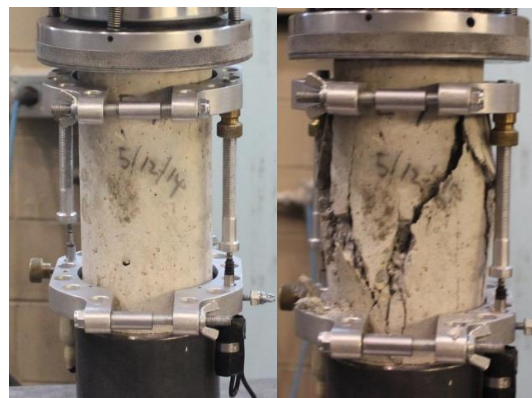


Fig. 2.2 - Concrete specimen in undamaged and damaged states.

### 2.4.3 Maximum Strain Evolution

The strain evolutions for the 16 specimens tested to failure under fatigue loading were plotted against the normalised number of cycles, as shown in Figure 2.3. The shapes or profiles of the strain evolutions were similar, irrespective of the concrete strength and stress level. The three stages of the strain evolution shown in Figure 2.3 for the stress levels used are also in agreement with previously reported observations (Torrenti et al., 2010; Papa and Taliercio, 1993; Vega et al., 1995; Taliercio and Gobbit, 1996; Song et al., 2005). The first stage, within 10% of the total number of cycles to failure, indicates a nonlinear deformation of concrete at a decreasing rate. The second stage is characterized with a constant rate of deformation within a range of approximately 70% of the fatigue life, while the last stage is characterized with an increasing rate of damage leading to failure. This was observed to be within the last 30% of the fatigue life.

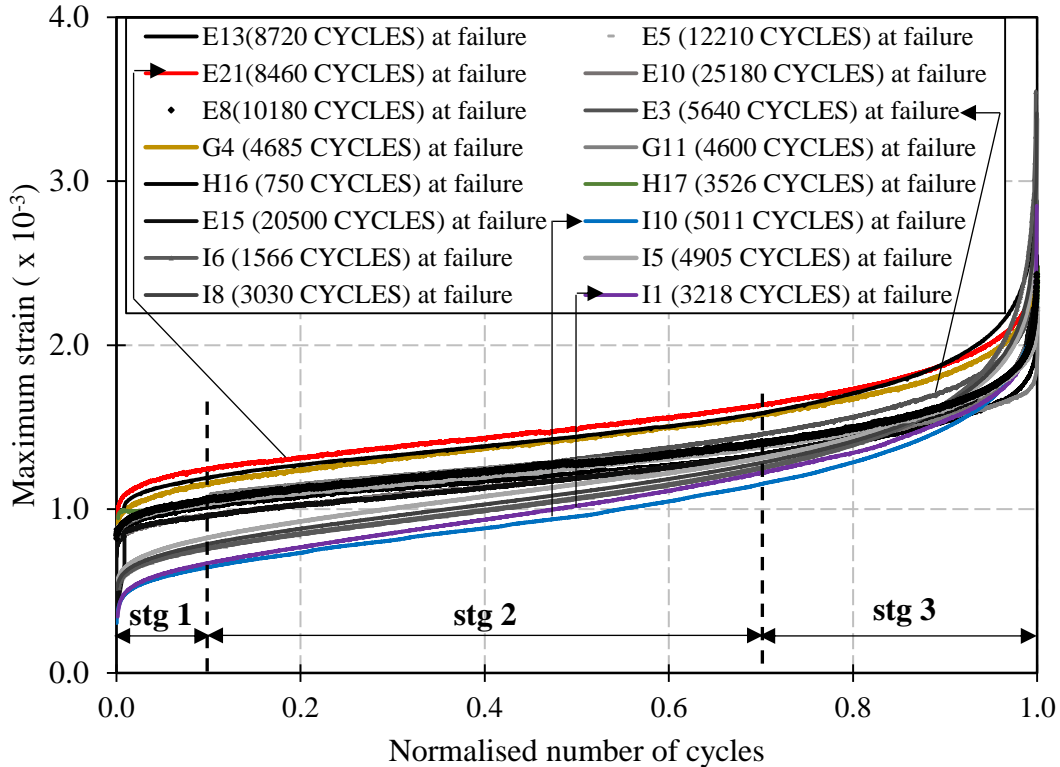


Fig. 2.3 – Maximum strain evolution.

## 2.5 Model Formulation

A major challenge in the development of residual strength and fatigue modulus models involves the estimation of the expected fatigue life for each specimen, because the applied fatigue load is usually stopped after a given number of cycles before failure occurs. In the literature, S-N models are generally used to normalise the tests cycles. As such, the plot of the residual strength against the number of cycles to failure obtained is often not appropriate. This is due to the fact that the actual number of cycles to failure of some of the specimens may be higher or lower than the value estimated using an S-N model. As such, an approach for estimating the number of cycles to failure for each specimen is required.

### 2.5.1 Relationship between Secondary Strain Rate and Number of Cycles to Failure

The secondary strain rates ( $\epsilon_{SEC}$ ) for 11 specimens (high strength concrete) out of the 16 specimens tested to failure were all estimated, as illustrated in Figure 2.4 (the values for each specimen are given in Appendix B). The logarithms of the fatigue life ( $N_f$ ) were plotted against the secondary strain rates ( $\epsilon_{SEC}$ ) as indicated in Figure 2.5. Using the experimental data, a model was proposed (Equation 2.1). Figure 2.5 also shows a comparison of the model with other models in the literature. The coefficients in the models were obtained based on best fit curves. To show the predictability of the model, data from fatigue tests at different loading parameters from different researchers were obtained and included in the plot, as shown in Figure 2.6 (Taliencio and Gobbit, 1996; Sparks and Menzies, 1973; Oneschkow, 2012). In addition, a prediction interval (using 95% confidence interval) is also shown in Figure 2.6 (Log-Log plot). However, due to scarce data for very high cycles to failure in the literature, fatigue strain evolution tests involving very high fatigue life are also required for corroboration.

$$N_f = 0.0009 (\epsilon_{SEC})^{-0.972} \quad (2.1)$$

The proposed model was used to estimate the failure cycles for the 22 specimens to obtain a plot of the residual concrete strength against the corresponding normalised number of cycles for each specimen. The plot of the normalised residual strength against the normalised number of cycles in Figures 2.7 and 2.8 were obtained using the proposed model (Equation 2.1) and the Aas-Jakobsen's (1970) model (Equation 2.2), respectively. It can be observed from the figures that the actual degradation path is well represented using the proposed model.

$$\frac{\Delta f}{f'_c} = 1 - \beta (1 - R) \text{Log } N_f \quad (2.2)$$

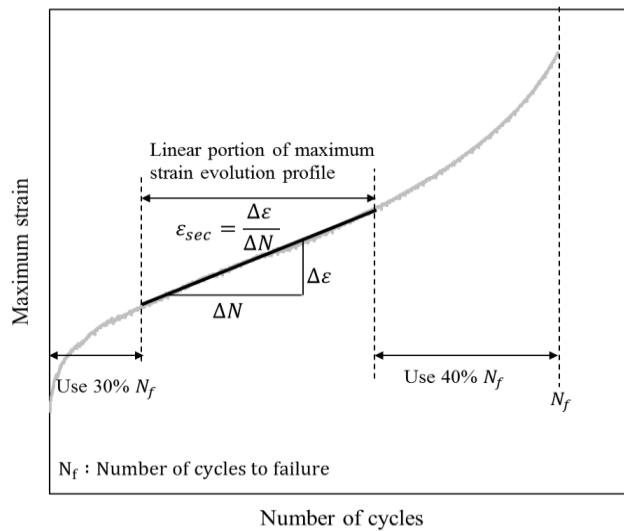


Fig. 2.4 – Plot of maximum strain against number of cycles.

In Equation 2.2,  $\beta$  is a material parameter and R is the ratio of the minimum stress level to the maximum stress level. The ratio of  $\Delta f$  to  $f'_c$  is the stress level which is the applied loading stress divided by the average compressive strength of the concrete considered. On the other hand, the residual strength of concrete corresponds to the actual stress at which a fatigue-damaged specimen will fail when loaded monotonically under static condition. After considerable damage of concrete due to fatigue loading, the residual strength of concrete is usually lower than the actual compressive strength in its undamaged state.

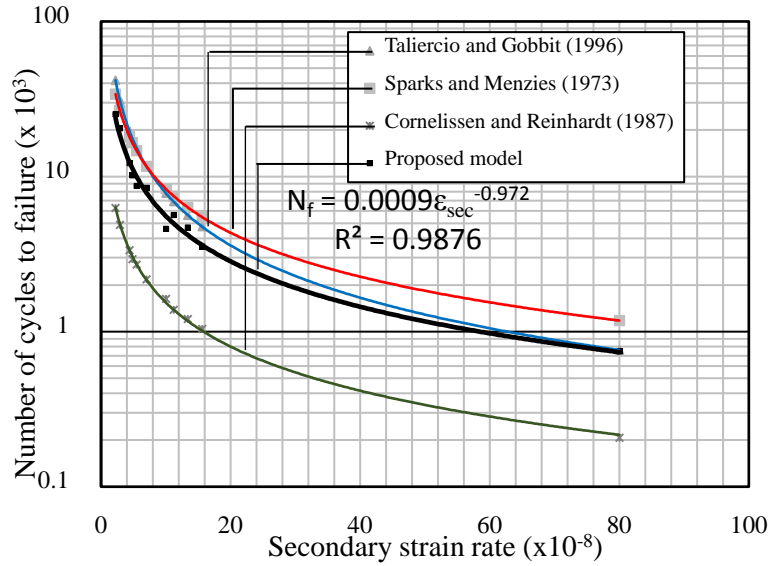


Fig. 2.5 – Logarithm of number of cycles to failure against the secondary strain rate.

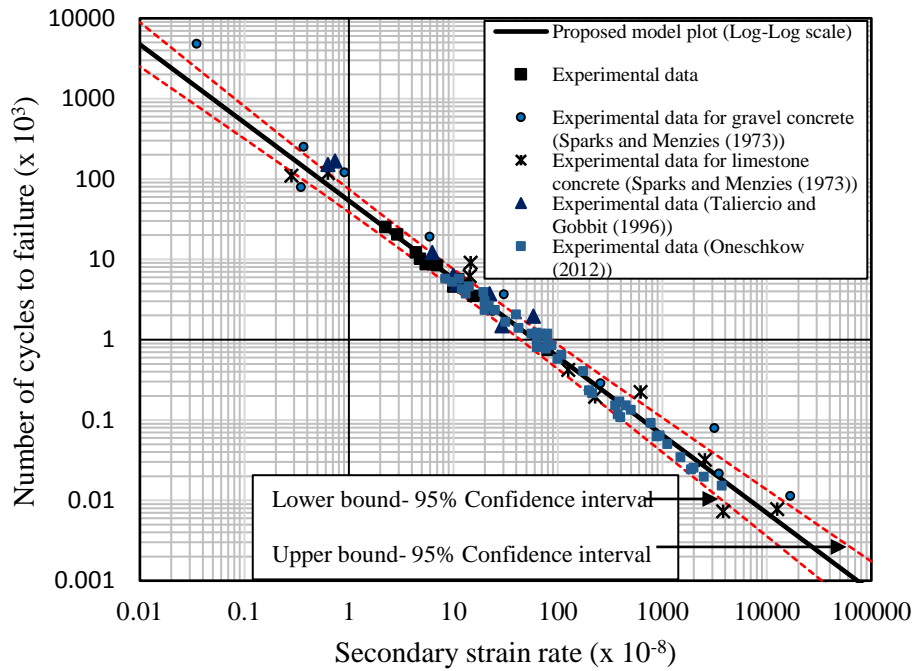


Fig. 2.6 – Verification of strain rate model for high number of cycles.

### 2.5.2 Strength and Stiffness Degradation under Fatigue Loading

During the initial stage of the fatigue loading, the residual strengths of the concrete specimens were observed to increase. This observation has also been reported in the literature on fatigue tests

of concrete specimens in compression. However, based on the damage path depicted by the experimental data points, obvious strength degradation began within the secondary stage of the damage evolution (Figure 2.7). Figure 2.9 and Equations 2.3 and 2.4 describe the approach taken for estimating the static and fatigue secant moduli of concrete ( $E$  and  $E_{SEC}$ , respectively) for each of the 22 specimens tested (Appendix A).

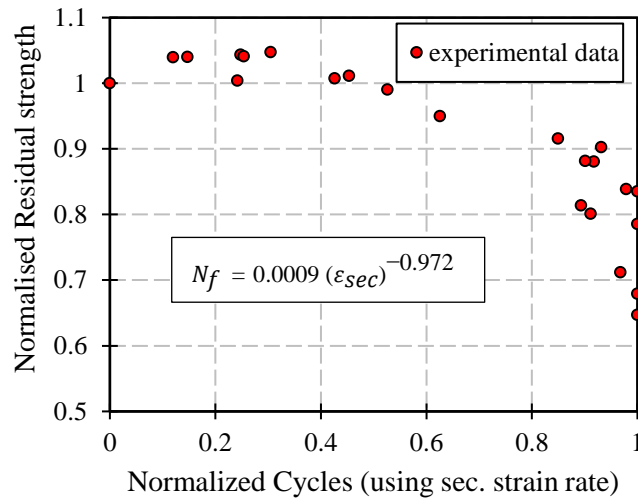


Fig. 2.7 – Normalized residual strength against normalized cycles (secondary strain rate approach).

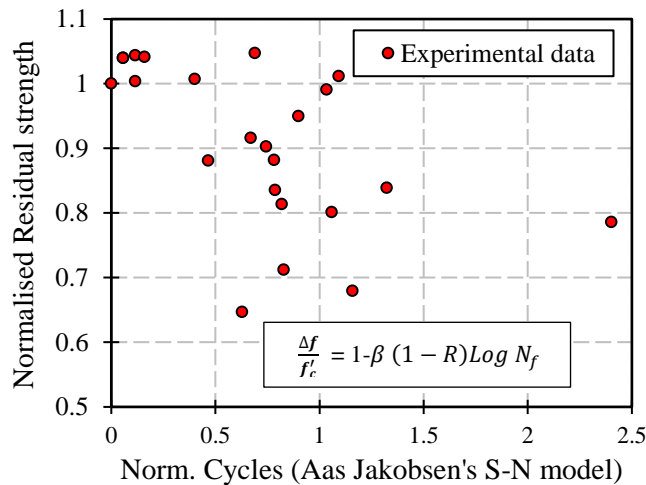


Fig. 2.8 – Normalized residual strength against normalized cycles (S-N model).

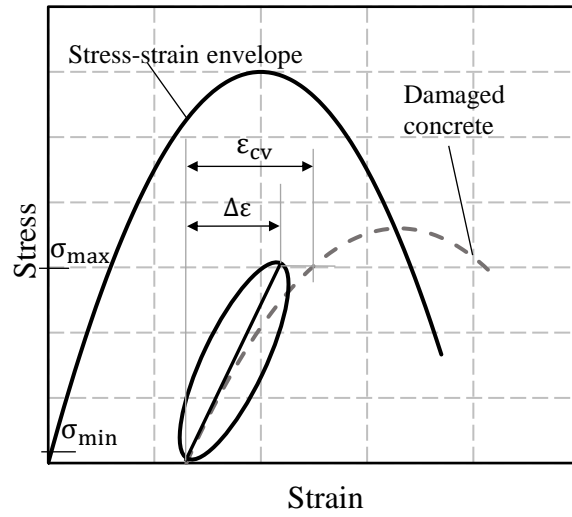


Fig. 2.9 – Static and fatigue secant moduli.

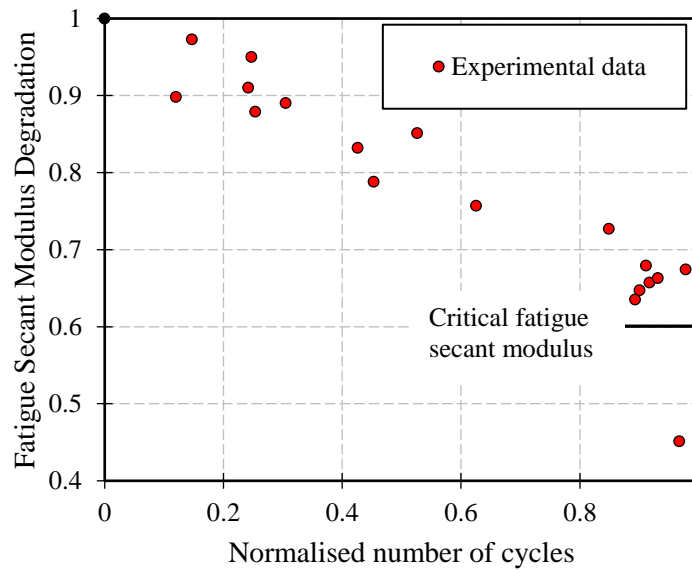


Fig. 2.10 – Degradation of residual fatigue secant modulus.

$$E = \frac{\sigma_{max} - \sigma_{min}}{\Delta\epsilon} \quad (2.3)$$

$$E_{sec} = \frac{\sigma_{max} - \sigma_{min}}{\epsilon_{cv}} \quad (2.4)$$

The fatigue secant modulus degradation began within the primary stage of damage and at a

faster rate compared to the residual strength degradation. The degradation of the normalised fatigue secant moduli is also shown in Figure 2.10. Towards failure, an abrupt drop was observed in the residual fatigue moduli data points.

### 2.5.3 Damage Evolution Model for Concrete Strength and Fatigue Secant Modulus

From the fundamentals of damage mechanics, the rate of fatigue damage per cycle is a function of the number of cycles, stress level, and a damage variable. From Gao and Hsu (1998), the rate of change of damage per fatigue cycle is expressed as:

$$\frac{\delta D}{\delta N} = F(N, \Delta f, D) = k_1 \exp\left(\frac{s \Delta f}{f'_c}\right) N^K \quad (2.5)$$

By integrating Equation 2.5 with respect to N,

$$D = k_1 \exp\left(\frac{s \Delta f}{f'_c}\right) \frac{N^{K+1}}{(K+1)} \quad (2.6)$$

At failure, damage (D) =  $D_{cr}$ .

$$D_{cr} = k_1 \exp\left(\frac{s \Delta f}{f'_c}\right) \frac{(N_f)^{K+1}}{(K+1)} \quad (2.7)$$

Rearranging Equation 2.7,

$$\frac{\Delta f}{f'_c} = \frac{1}{s} \ln \frac{D_{cr}(K+1)}{k_1} - \frac{K+1}{s} \ln N_f \quad (2.8)$$

To account for the influence of loading parameters such as frequency, waveform and stress ratio, a modified Aas-Jacobsen S-N model (Aas-Jacobsen, 1970; Zhang et al., 1998), (Equation 2.9), which considers various factors affecting the fatigue behaviour of concrete, was implemented.

$$\Delta f / f'_c = C_f [1 - \beta_2 (1 - R) \text{Log } N_f - \gamma_2 \text{Log}(\zeta N_f T)] \quad (2.9)$$

where

$$\beta_2 = 0.0661 - 0.0226R \quad (2.10)$$

and

$$\gamma_2 = 2.47 \times 10^{-2}$$

$\zeta$  is a dimensionless coefficient which is taken as 0.15 for a sinusoidal cycle (Torrenti et al., 2010;

Zhang et al., 1998),  $C_f$  accounts for the loading frequency, and  $\gamma_2$  is a constant which accounts for high stress level.

The modified S-N model for predicting failure cycles is expressed in a form similar to Equation 2.8; hence:

$$\Delta f / f'_c = C_f [1 - \gamma_2 \log(\zeta N_f T)] - 0.434 C_f (\beta_2 (1 - R)) \ln N_f \quad (2.11)$$

where  $\log N_f = 0.434 \ln N_f$

Comparing Equations 2.8 and 2.11,

$$\frac{(K+1)}{s} = 0.434 C_f (\beta_2 (1 - R)) \quad (2.12)$$

$$K + 1 = 0.434 s C_f (\beta_2 (1 - R)) \quad (2.13)$$

$$C_f (1 - \gamma_2 \log(\zeta N_f T)) = \frac{1}{s} \ln \frac{D_{cr} (K+1)}{k_1} \quad (2.14)$$

$$D_{cr} \text{Exp}(-s C_f (1 - \gamma_2 \log(\zeta N_f T))) = \frac{k_1}{K+1} \quad (2.15)$$

By substituting Equations 2.13 and 2.15 into Equation 2.6, and expressing the modified damage model in a form similar to the initially proposed model by Gao and Hsu (1998), then:

$$D = D_{cr} \text{Exp} \left[ s \left( \frac{\Delta f}{f'_c} - u \right) \right] N^v \quad (2.16)$$

$$u = C_f (1 - \gamma_2 \log(\zeta N_f T)) \quad (2.17)$$

$$v = 0.434 s C_f (\beta_2 (1 - R)) \quad (2.18)$$

From Zhang et al. (1996) on influence of loading frequency,

$$C_f = ab^{-\log f} + c \quad (2.19)$$

where a, b and c are 0.249, 0.920 and 0.796 respectively, and f is the frequency of the fatigue loading. The residual strength of concrete and modulus damage at a given stress level can be obtained using the damage model. As observed, the damage model does not require the values of

the constants  $K$  and  $k_1$ .

Using the damage model (Equation 2.16), parameters in the constitutive equations can be modified to account for fatigue damage. From calibration using the test data, the values of the parameter  $s$  (stress ratios between 0 and 0.5) for concrete strength and modulus damage can be obtained from Figure 2.11. From the experiments conducted, the degraded fatigue modulus tends towards 60% of the initial modulus (Torrenti et al., 2010; Holmen, 1982) (Figure 2.10). As such, the critical damage value  $D_{Cr}$  for the concrete fatigue secant modulus is taken as 0.4. As observed from the experimental data in Figure 2.12, the residual strength of concrete at failure tends towards 0.65; hence, the critical damage value for the residual strength of concrete is taken as 0.35.

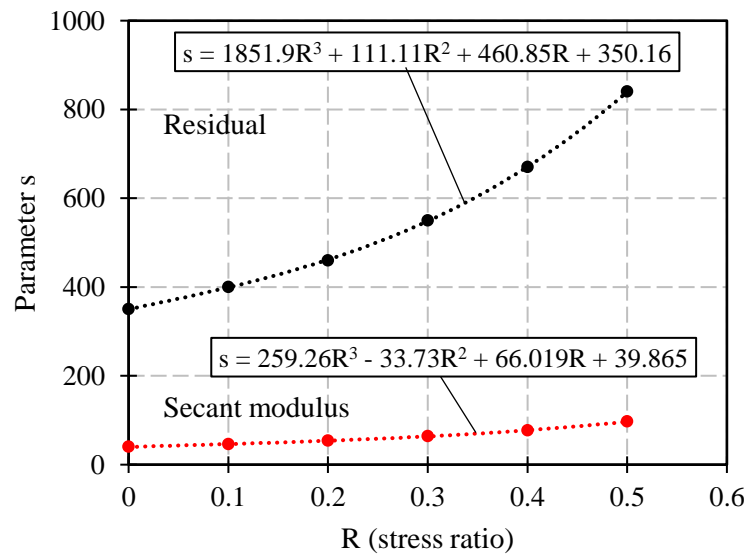


Fig. 2.11 – Estimation of damage parameter  $s$ .

Using the loading conditions for the experiments conducted and the modified damage model (Equation 2.16), the damage profiles for normalised residual strength and fatigue modulus alongside other residual concrete strength models in the literature (Zhang and Wu, 1997; Schaff

and Davidson, 1997; Zhu and Li, 2010; Edalatmanesh and Newhook, 2013) were plotted. The residual strength models are shown in Figure 2.12.

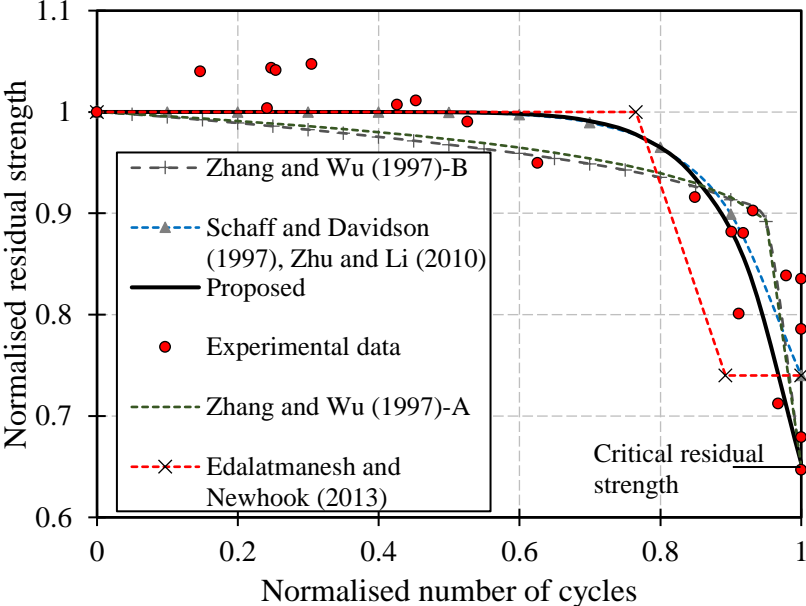


Fig. 2.12 – Normalized concrete strength degradation model.

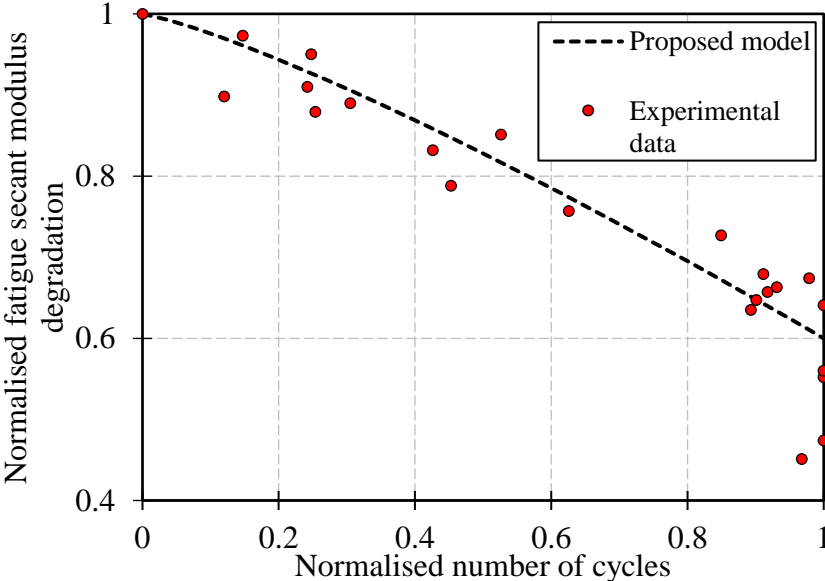


Fig. 2.13 – Normalized fatigue secant modulus degradation.

The proposed damage evolution model plot matches well with the Schaff et al. (1997) residual strength damage plot. However, towards failure, there is an obvious deviation. This is due to

the fact that it is assumed by Schaff et al. (1997) that failure will occur at the point where the concrete strength degrades to the maximum fatigue stress applied. On the other hand, the proposed model assumes that failure will occur at a critical damage value based on the experimental observations. Figure 2.13 also shows the fatigue modulus damage evolution superimposed on the experimental data.

### 2.5.4 Influence of Loading Parameters on the Fatigue Damage of Concrete

The loading parameters (maximum stress level, frequency and stress ratio) were varied in order to observe their effects on the damage evolution of concrete strength using the proposed damage model. The fatigue life that corresponds to the critical damage was estimated using Equation 2.9. Figure 2.14 portrays a delay in damage as the maximum stress level decreases; hence, an increase is seen in the number of cycles to failure. Figures 2.15 and 2.16 indicate delays in damage as the frequency and stress ratio increase, respectively. Using the appropriate damage parameter for fatigue modulus (Figure 2.11), a similar trend as seen in the residual strength can also be observed.

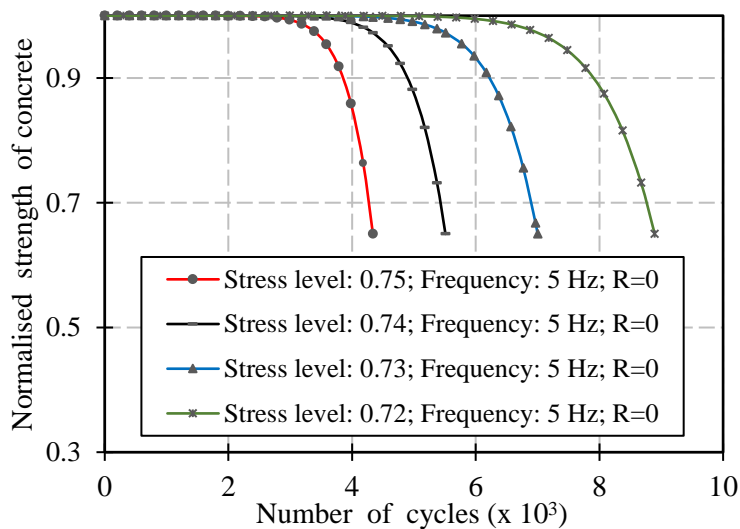


Fig. 2.14 – Effect of stress level on fatigue damage of concrete compressive strength.

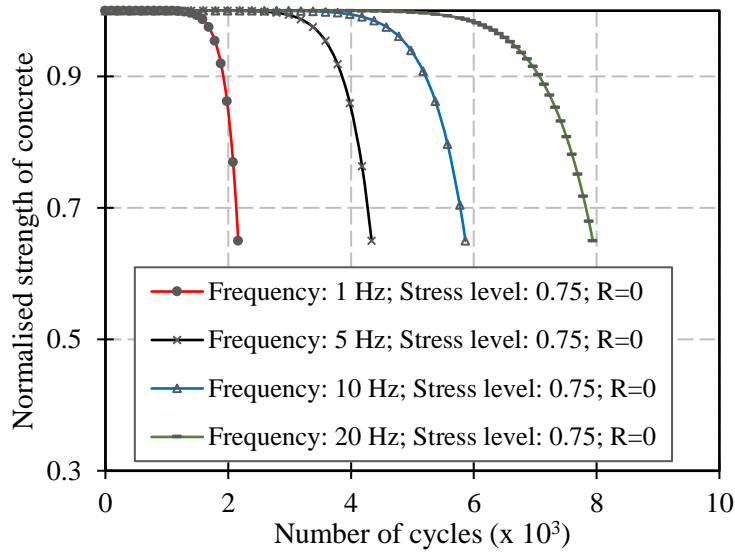


Fig. 2.15 – Effect of frequency on fatigue damage of concrete compressive strength.

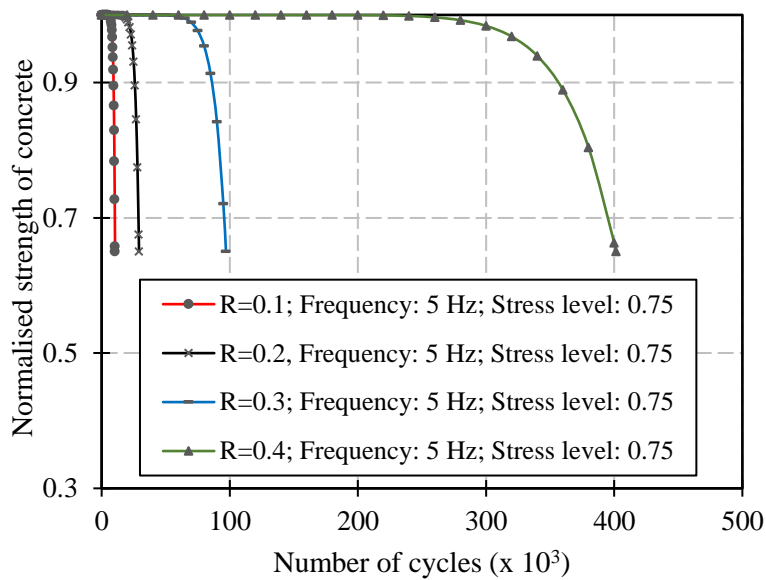


Fig. 2.16 – Effect of stress ratio on fatigue damage of concrete compressive strength.

## 2.6 Variable-Amplitude Fatigue Loading

Generally, the fatigue loading of concrete structures are variable in nature. Hence, it is imperative that the proposed damage model account for the variability of the fatigue loading in a simple and explicit manner.

The Palmgren-Miner rule (Palmgren, 1924; Miner, 1945) is commonly used for fatigue damage accumulation when considering variable fatigue loading. The damage per stress level is estimated as the ratio of the number of cycles to the estimated fatigue life. The summation of all estimated damage values gives the total damage. As a criterion for failure, the summation should be equal to 1.0 or a given critical value.

Typically, the rate of damage accumulation is assumed to be linear; however, a majority of the tests conducted and reported in the literature show that the fatigue behaviour of concrete is nonlinear. In addition, it has been observed that the Palmgren-Miner rule does not account for loading sequence; hence, overly-conservative or unconservative predictions have been obtained using the Palmgren- Miner rule (Papa and Taliercio, 1996; Vega and Bhatti, 1995; Taliercio and Gobbit, 1996, Song et al., 2005).

A procedure similar to that proposed by Schaff et al. (1997) is described below and is illustrated in Figures 2.17 and 2.18. However, experiments on variable fatigue loading of plain concrete specimens are required to verify the results obtained from this approach. As an alternative to the estimation of the number of cycles leading to failure using the proposed strain-rate approach or stress-life (Zhang et al., 1998) approach, a method described by Thun et al. (2011) can also be used.

Irrespective of the magnitude of the current stress level ( $S_i$ ), the number of cycles (equivalent number of cycles) that will induce damage equal to a previous damage value can be obtained using the damage model (Equation 2.16). In Figures 2.17 and 2.18, the stresses  $S_1$ ,  $S_2$ , and  $S_3$  are applied for  $N_1$ ,  $N_2$ , and  $N_3$  cycles respectively. The final damage after the application of  $S_3$  for  $N_3$  cycles can be estimated thus:

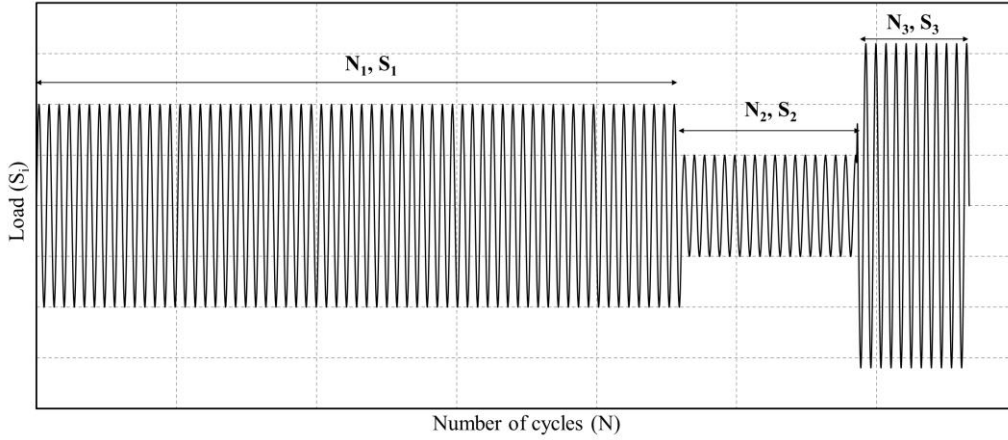


Fig. 2.17 - Stress-cycle diagram for variable amplitude loading.

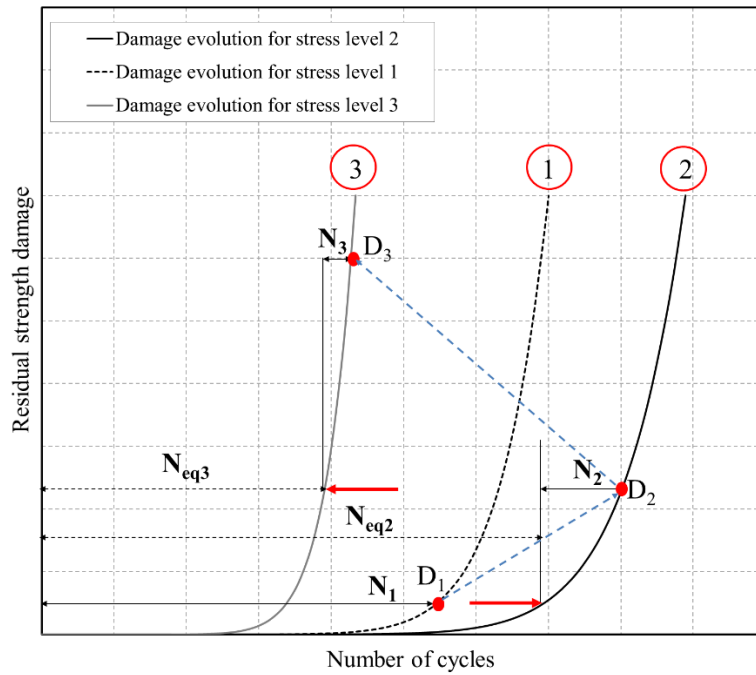


Figure 2.18 - Damage evolution for variable loading.

**Step 1:** Initially, the damage ( $D_1$ ) due to the first stress level ( $S_1$ ) and the corresponding number of cycles ( $N_1$ ) is estimated using the proposed damage model (Equation 2.16).

**Step 2:**  $N$  is calculated by substituting  $D_1$  and the second stress level ( $S_2$ ) into the damage model

(Equation 2.16). The value of  $N$  obtained is equal to the equivalent cycles  $N_{eqv2}$  for the second load stage. This step converts the previous damage into equivalent cycles.

**Step 3:** To calculate the damage ( $D_2$ ) after the second stress level ( $S_2$ ) fatigue loading, the number of cycles ( $N_2$ ) for the second stress level is added to  $N_{eqv2}$  (equivalent cycles). By substituting the summed cycles ( $N_2 + N_{eqv2}$ ) into the damage model and using the second stress level,  $D_2$  for the residual strength is estimated.

**Step 4:** The third stress level ( $S_3$ ) is substituted into the damage model in order to obtain the equivalent cycles  $N_{eqv3}$ . Subsequently, the value of  $N$  in the damage model is replaced by the summation of  $N_{eqv3}$  and  $N_3$  as described for  $D_2$  in Step 3.

**Step 5:** By substituting the summed number of cycles ( $N_3 + N_{eqv3}$ ) and the third stress level ( $S_3$ ) in the damage model,  $D_3$  can be estimated.

Based on this concept, the value of the estimated damage takes into account the previous damage. For more variable fatigue loading, this procedure continues until the last variable load is reached. The procedure described for concrete strength under variable fatigue loading can also be used for the residual fatigue secant modulus; hence, similar to residual strength of concrete, the degradation of the concrete fatigue secant modulus can also be predicted appropriately under different loading conditions.

## 2.7 Conclusions

Based on the results of the experimental and analytical work conducted, the following conclusions were derived:

1. The behaviour of concrete elements under fatigue loading can vary greatly, and depends on various factors which should be incorporated in the fatigue analysis of concrete for meaningful predictions and results.

2. In the development of damage models, the use of secondary strain rates to estimate failure cycles is a reasonable alternative to the use of S-N models.

3. The residual strength and fatigue secant modulus of concrete do not deteriorate to zero as expected in theory; hence, the use of critical damage values is appropriate as observed from experimental results.

4. The evolution of the maximum strain is phased into three stages (normalized profiles in Figure 2.3). The three stages were observed in all specimens tested, although the gradients of the evolutions were influenced by the loading parameters (e.g., stress level, frequency).

5. The proposed damage models for concrete residual strength and fatigue modulus give reasonable correlations to the observed experimental data and represent an improvement on previously available models as shown in Figure 2.12.

6. Although an approach which accounts for the sequence effect of loading has been proposed for variable fatigue loading, the predictability of this approach requires verification using variable fatigue loading tests of concrete.

7. Further experiments and verifications, especially for a very high number of cycles to failure, are required in order to more fully establish the validity of the proposed models.

## **2.8 Notation**

*The following symbols are used in this chapter:*

a: material parameter

b: material parameter

c: material constant

$C_f$  : frequency factor

$D$  : damage

$D_{cr}$  : critical damage

$E$ : fatigue secant modulus

$E_{sec}$  : static secant modulus

f : frequency

$f'_c$  : compressive strength

K: constant

$k_1$ : constant

$N$  : number of load cycles

$N_{eqv}$ : equivalent cycles

$N_f$  : numbers of cycles at failure

$s$  : constant parameter

$S_{max}$ : maximum stress level

R: stress ratio

$T$  : period of fatigue cycle

u: damage parameter

v : damage parameter

$\beta$  : material constant

$\beta_2$  : material constant

$\gamma_2$ : material constants

$\Delta\varepsilon$  : fatigue strain range

$\Delta f$  : maximum stress level

$\varepsilon_{cv}$  : strain corresponding to the stress range ( $\sigma_{max}-\sigma_{min}$ ) using the monotonic stress-strain curve

$\varepsilon_{sec}$  : secondary strain rate

$\zeta$  : dimensionless coefficient

$\sigma_{max}$ : maximum stress level

$\sigma_{min}$  : minimum stress level

## 2.7 References

1. Lausanne: International Federation for Structural Concrete (fib), 312 pp.
2. Cook D.J., and Chindaprasirt P. (1980). "Influence of Loading History upon the Compressive Properties of Concrete." Magazine of Concrete Research, Vol. 32, No. 111, 1980, pp. 89-100.
3. Cook D.J., and Chindaprasirt P. (1981). "Influence of Loading History upon the Tensile Properties of Concrete." Magazine of Concrete Research, Vol. 33, No. 116, pp. 154-160.
4. Cornelissen H.A.W., and Reinhardt H.W. (1987). "Effect of Static and Fatigue Preloading on Residual Strength and Stiffness of Plain Concrete." Fracture Control of Engineering Structures- ECF 6.
5. Edalatmanesh R., and Newhook J.P. (2013). "Residual Strength of Precast Steel-Free Panels." ACI Structural Journal, Vol.110, pp. 715-722.
6. Fib Model Code 2010. (2013). "FIB Model Code for Concrete Structures – FIB- Federation

- Internationale du Beton.” John Wiley & Sons, 434 pp.
7. Gao L., and Hsu T.T.C. (1998). “Fatigue of Concrete under Uniaxial Compression Cyclic Loading.” *ACI Materials Journal*, Vol. 95, No. 5, pp. 575-580.
  8. Graf O., and Brenner E. (1936). “Experiments for Investigating the Resistance of Concrete under Often Repeated Compressive Loads.” *Bulletin No. 83, Deutscher Ausschuss für Eisenbeton*.
  9. Grebreyouhannes E., Kishi T., and Maekawa, K. (2008). “Shear Fatigue of Cracked Concrete Interface.” *Journal of Advanced Concrete Technology*, Vol. 6, No. 2, pp. 365-376.
  10. Hilsdorf H.K., and Kesler C.E. (1966). “Fatigue Strength of Concrete under Varying Flexural Stresses.” *Journal Proceedings*, Vol. 63, No. 10, pp. 1059-1076.
  11. Holmen J.O. (1982). “Fatigue of Concrete by Constant and Variable Amplitude Loading.” *ACI SP 75-4*, pp. 71-110.
  12. Hooi T. (2000). “Effects of Passive Confinement on Fatigue Behaviour of Concrete.” *Magazine of Concrete Research*, Vol.52, No.1, pp. 7-15.
  13. Hsu T.C. (1984). “Fatigue and Micro-Cracking of Concrete.” *Mater. Constr.*, Vol. 17, pp. 51-54.
  14. Lee M.K., and Barr B.I.G. (2004). “An Overview of the Fatigue Behaviour of Plain and Fibre Reinforced Concrete.” *Cement & Concrete Composites*, Vol. 26, pp. 299-305.
  15. Lohaus L., Oneschkow N., and Wefer M. (2012). “Design Model for the Fatigue Behaviour of Normal-Strength, High-Strength and Ultra-High-Strength Concrete.” *Structural Concrete*,

- E 3, pp. 182-192.
16. Miner M.A. (1945). "Cumulative Damage in Fatigue." *Journal of Applied Mechanics*, Vol 12, No 1, Transactions of the American Society of Mechanical Engineers, Vol 67, 1945, pp. A159-A164.
  17. Murdock J.W., and Kesler C.E. (1955). "Effects of Range of Stress on Fatigue Strength of Plain Concrete Beams." *ACI Journal* Vol. 55, No. 2, pp. 221-231.
  18. Naik T.R., Singh S.S., and Ye C. (1993). "Fatigue Behaviour of Plain Concrete Made With or Without Fly Ash." Centre for By-Products Utilization, Department of Civil Engineering & Mechanics, University of Wisconsin-Milwaukee.
  19. Oh B.H. (1991). "Cumulative Damage Theory of Concrete under Variable-Amplitude Fatigue Loadings." *ACI Materials Journal*, Vol. 88, No. 2, pp. 122-128.
  20. Oneschkow N. (2012). "Influence of Loading Frequency on the Fatigue Behaviour of High-Strength Concrete." Proceedings of the 9<sup>th</sup> fib International Phd Symposium in Civil Engineering, Karlsruhe, Germany.
  21. Ople F.S., and Hulsbos C.L. (1966). "Probable Fatigue Life of Plain Concrete with Stress Gradient." *ACI Proceedings*, Vol. 63, pp. 59-81.
  22. Paepegem W.V., and Degrieck J. (2002). "A New Coupled Approach of Residual Stiffness and Strength for Fatigue of Fibre-Reinforced Composites." *International Journal of Fatigue*, Vol. 24, No. 7, pp. 747-762.
  23. Palmgren A. (1924). "Die Lebensdauer von Kugellagern." *Zeitschrift des Vereines Deutcher*

- Ingenieure (VDI Zeitschrift), ISSN 0341-7258, Vol 68, pp.339-341.
24. Papa E., and Taliercio A. (1993). "Anisotropic Damage Model for the Multiaxial Static and Fatigue Behaviour of Plain Concrete." *Eng. Fract. Mech.*, Vol. 55, pp. 163-179.
  25. Raithby K.D., and Galloway J.W. (1974). "Effect of Moisture Condition, Age, and Rate of Loading on Fatigue of Plain Concrete." *ABELES Symposium, Fatigue of Concrete*, ACI Publication SP-41, pp. 15-34.
  26. RILEM COMMITTEE 36-RDL. (1984). "Long Term Random Dynamic Loading of Concrete Structures," *Mat. Struct.* Vol. 17, pp. 1-28.
  27. Schaff J.R., and Davidson B.D. (1997). "Life Prediction Methodology for Composite Structures. Part 1- Constant Amplitude and Two-Stress Level Fatigue." *Journal of Composite Materials*, Vol. 31, No. 2, pp. 128-157.
  28. Shah S.P. (1984). "Predictions of Cumulative Damage for Concrete and Reinforced Concrete." *Materiaux et Construction*, Vol. 17, No.1, pp. 65-68.
  29. Shah S.P., and Chandra S. (1970). "Fracture of Concrete Subjected to Cyclic and Sustained Loading." *ACI Journal* , No. 67-49, pp. 816-827.
  30. Sparks P.R., and Menzies J.B. (1973). "The Effect of Rate of Loading upon the Static and Fatigue Strength of Plain Concrete in Compression." Department of the Environment, Building Research Establishment.
  31. Song Y., Cao W., and Meng X.J. (2005). "Fatigue Properties of Plain Concrete under Triaxial Constant-Amplitude Tension-Compression Cyclic Loading." *Journal of Shanghai*

- University, Vol.9, No.2, pp. 127-133.
32. Takhar S.S., Jordaan I.J., and Gamble B.R. (1974). "Fatigue of Concrete under Lateral Confining Pressure." ACI Special Publication Journal, Vol. 41, No. 4, pp. 59-70.
  33. Taliercio A.L.F., and Gobbit E. (1996). "Experimental Investiagtion on the Triaxial Fatigue Behaviour of Plain Concrete." Magazine of Concrete Research, Vol. 48, No. 176, pp. 157-172.
  34. Tamulenas V., Gelazius V., and Ramanauskas R. (2014). "Calculation Technique for Stress-Strain Analysis of RC Elements Subjected to High-Cyclic Compression." Civil and Transport Engineering, Aviation Technologies, Vol. 6, No. 5, pp. 468-473.
  35. Torrenti J.M., Pijaudier-Cabot G., and Reynouard J. (2010). "Mechanical Behaviour of Concrete." John Wiley & Sons, Inc., pp. 185-223.
  36. Thun H., Ohlsson U., and Elfgren L. (2011). "A Deformation Criterion for Fatigue of Concrete in Tension." Structural Concrete, Journal of fib, Vol.12, No. 3, pp. 187-197.
  37. Vega I.M., Bhatti M.A., and Nixon W.A. (1995). "A Nonlinear Fatigue Damage Model for Concrete in Tension." International of Journal of Damage Mechanics, Vol. 4, pp. 362-379.
  38. Zhang B., Phillips D.V., and Green D.R. (1998). "Sustained Loading Effect on the Fatigue Life of Plain Concrete." Mag. of Concrete Res., Vol. 50, pp. 263-278.
  39. Zhang B., Phillips D.V., and Wu K. (1996). "Effects of Loading Frequency and Stress Reversal on Fatigue Life of Plain Concrete." Magazine of Concrete Research, Vol. 48, pp. 361-375.

40. Zhang B., and Wu K. (1997). "Residual Fatigue Strength and Stiffness of Ordinary Concrete under Bending." *Cement and Concrete Research*, Vol. 27, No. 1, pp. 115-126.
41. Zhu H., and Li X. (2011). "Experimental Research on Residual Strength of Recycled Aggregate Concrete under Compressive Fatigue Loading." *Advanced Materials Research*, Vol. 150-151, pp. 1379-1382.

## CHAPTER 3

### SIMPLIFIED CONSTITUTIVE MODEL FOR FATIGUE BEHAVIOUR OF CONCRETE IN COMPRESSION

The material in this chapter was previously published as follows:

*Isojeh B., El-Zeghayar M., and Vecchio F.J (2017). "Simplified Constitutive Model for Fatigue Behaviour of Concrete in Compression." ASCE Journal of Materials in Civil Engineering, DOI: 10.1061/(ASCE)MT.1943-5533.0001863.*

#### **3.1 Abstract**

In the literature, three basic assumptions are used to modify monotonic constitutive models in order to simplify the fatigue analysis of concrete. First, the fatigue hysteresis loop at failure is assumed to intersect the monotonic stress-strain envelope. Second, it is assumed that the peak stress of a fatigue-damaged concrete element intersects the monotonic stress-strain envelope. Third, the centerlines of the fatigue hysteresis loops are assumed to converge at a common point. Although the modifications supposedly lead to improved predictions, experimental verifications of these assumptions are currently insufficient to justify their implementation in the fatigue analysis of complex and large concrete structures where considerations of safety and cost effectiveness are paramount. From experimental verifications conducted to ascertain the conservative level of these assumptions, it was found that the first and second assumptions seem reasonable, while the third assumption is inaccurate and thus is in need of improvement. As such, a new convergence point is proposed. The constitutive models for high and normal strength concrete in compression are also modified as functions of the irreversible strain and residual strength. Further, a model is proposed for the irreversible strain accumulation, and its corroboration with experimental results shows good agreement.

### **3.2 Introduction**

In the design of fatigue-prone concrete structures, fatigue life models for concrete are used to verify the resistance of critical components. Basically, the verification ensures that fatigue failure will not occur during service life (Su and Hsu, 1998).

One such model used is the stress-life model (S-N curve). An S-N curve is a plot of normalized stresses (with material strength) against the corresponding numbers of cycles at which failure occurs. Provided that the induced stress in the concrete element, corresponding ultimate strength, and other influencing factors such as frequency are taken into consideration, the number of cycles to failure can be estimated.

Investigations conducted on the influence of frequency on the fatigue life of concrete by Sparks and Menzies (1973), Raithby and Galloway (1974), Holmen (1982), Zhang et al.(1996), and Medeiros et al. (2015) all indicate that the number of cycles leading to failure decreases as the frequency of loading decreases. This behaviour has been observed to be more pronounced as the maximum fatigue stress level increases (Torrenti et al., 2010).

Although the influence of loading parameters can be observed in the estimated number of cycles leading to failure, stress-life models do not account for the progressive degradation of concrete properties under fatigue loading. Hence, the corresponding influence of frequency in progressive damage cannot be observed (Zanuy et al., 2007; Tamulenas and Gelazius, 2014). In order to account for the progressive degradation of concrete, two alternative approaches have been used.

In the first approach, certain assumptions are made for the relationship between monotonic stress-strain envelopes and evolving fatigue hysteresis loops. One such assumption is that the failure of a concrete specimen occurs at the instant when a fatigue stress-strain hysteresis loop

intersects the softening portion of a monotonic stress-strain curve (Figure 3.1) (Karsan and Jirsa, 1969; Otter and Naaman, 1989; Cachim et al., 2002; Petryna et al., 2002; Torrenti et al., 2010). In subsequent sections, the monotonic stress-strain curve will be referred to as the stress-strain envelope.

The peak stress point from a fatigue-damaged stress-strain curve is also assumed to intersect the descending portion of the stress-strain envelope (Petryna et al, 2002; Xiang et al., 2007). From this assumption, a constitutive model which considers the damage evolution of concrete residual strength can be developed for concrete.

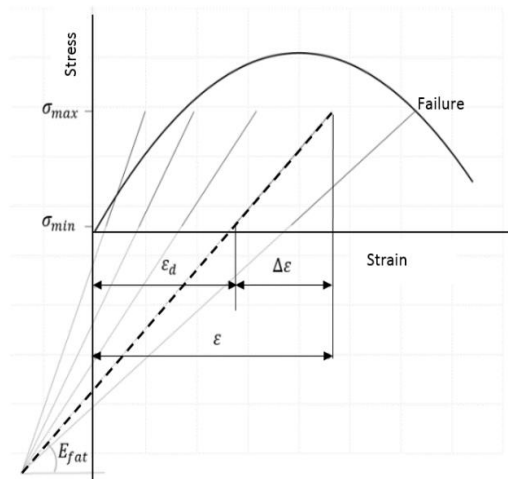


Fig. 3.1- Relationship between monotonic stress-strain curve and fatigue hysteresis loops.

According to Park (1990), the centerlines of the hysteresis loops always pass through a common point irrespective of the stress level or stress range. Similarly, Xiang et al. (2007) also assumed that the initial tangential moduli of a damaged concrete element meet at a common point, although different from the point assumed by Park (1990).

In Figure 3.1,  $\varepsilon$ ,  $\varepsilon_d$ , and  $E_{fat}$  are the total strain, irreversible strain, and fatigue secant modulus, respectively. Provided the damage evolution models for any two of the parameters (total strain,

irreversible strain and fatigue secant modulus) are known, the damage evolution of the unknown parameter can be developed using the assumptions (Park et al., 1990; Xiang et al., 2007; Torrenti et al., 2010).

Analytical results reported in the literature using the aforementioned approach and assumptions are acceptable (Park, 1990; Eligehausen et al., 1992; Petryna et al., 2002; Xiang and Zhao, 2007; Zuradzka, 2008). However, available experimental investigations on these assumptions are insufficient to ascertain their validity and to justify their conservative form in the fatigue analysis of concrete structures.

The second approach involves the use of damage mechanics based on the thermodynamics of irreversible processes. In this approach, a damage variable or matrix is used to represent microcracks and microvoids. The damage matrix may be assumed to depend on the orthotropic nature of fatigue microcracks (Chaboche, 1981; 1988a, Lemaitre, 1986; Chaboche, 1988, Lemaitre and Chaboche, 1990; Vega et al, 1995; Zhang and Cai, 2010).

The damage strain energy release rate required in this approach is derived from the strain energy with respect to the damage variable. In addition, the elastic strain is derived from the strain energy with respect to the applied stress.

A damage-evolution function can be developed based on an incremental theory of plasticity in which multiple surfaces in stress space or strain energy release space are defined (Dafalias and Popov, 1977; Suaris et al., 1990; Al-Gadhib et al., 2000). However, a simplified concept which involves experimental data and a phenomenological approach can also be implemented to obtain models for damage evolution (Vega et al., 1995).

Verification studies via experiments with models developed from the second approach have also shown acceptable predictions. However, the approach involves extensive analysis. Since concrete is not homogeneous, constant and sufficient accuracy using this approach cannot be guaranteed. Further, the implementation of other salient factors in the derived fatigue-damage-evolution models and the modification of the approach for variable fatigue loading will require more assumptions and further complexity in analysis.

In this chapter, the assumptions reported in the literature are verified experimentally and a constitutive model for concrete elements under fatigue loading in compression is developed. The irreversible strain accumulation required in the constitutive model is proposed to be a function of the residual strength and fatigue secant modulus damage. The damage models for concrete strength and secant modulus used in the irreversible strain and constitutive models were developed previously (Chapter 2).

### **3.3 Experimental Study**

Tests were conducted in order to verify the three basic assumptions used for simplifying the behaviour of concrete under fatigue loading. Monotonic tests were initially conducted on concrete cylindrical specimens in order to obtain the average compressive strength. Thereafter, percentages of the average strength were used as fatigue loads.

In the first group of fatigue tests, 22 specimens were tested to different numbers of cycles at a constant stress level and subsequently subjected to monotonic loading. The obtained stress-strain curves from monotonic loading were plotted alongside the stress-strain envelope to observe the intersection of the peak stress of the stress-strain curves with the softening portion of the stress-strain envelope. In the second group of fatigue tests, 16 specimens were tested to failure under

constant fatigue loading, and the hysteresis loops were plotted. The centerline of each loop was extended in order to observe a convergence point. The intersection of the hysteresis loop at failure with the stress-strain envelope was also verified. The test procedures, the specimen tested, and the test observations are discussed subsequently.

Servohydraulic testing equipment with a loading capacity of 1000 kN was used to conduct fatigue tests on concrete cylinders (100 mm diameter x 200 mm height). In all tests, the waveform of the applied fatigue loading was sinusoidal in nature. In order to measure the progressive average strains throughout the tests, LVDTs were mounted on opposite sides of each specimen. Figure 3.2 shows the test set-up and LVDTs attached to a concrete specimen.

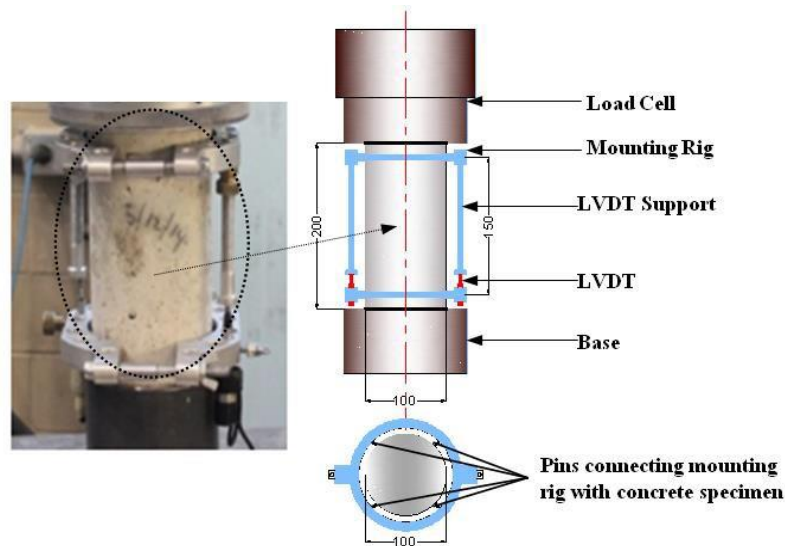


Fig. 3.2 - Fatigue loading set-up.

### 3.3.1 Test Specimens

The concrete specimens were made from Portland cement (general use, GU), sand, and limestone aggregates (10 mm maximum size) with three different mix ratios. The concrete from the first two batches (Table 3.1) were cast using a mix proportion of 1: 2: 2 with a water/cement ratio of 0.5, indicating cement, sand, and coarse aggregate by weight respectively. Mix

proportion ratios of 1:2:3 with a water/cement ratio of 0.5 and 1:2:4 with a water/cement ratio of 0.6 were used for the third and fourth batches respectively. The static strengths of concrete after curing for 28 days were obtained for each batch (Table 3.1), while the fatigue tests were conducted 30 to 40 days after casting.

Table 3.1 - Average Compressive Strength and Corresponding Strain.

| Batch (# of Specimens) | Average Compressive Strength (MPa) | Average Corresponding Strain (x 0.001) | Mix Ratio |
|------------------------|------------------------------------|--|-----------|
| 1(5)                   | 52.8                               | 2.01                                   | 1:2:2     |
| 2(3)                   | 55.8                               | 2.00                                   | 1:2:2     |
| 3(3)                   | 46.2                               | 1.95                                   | 1:2:3     |
| 4(3)                   | 23.1                               | 1.52                                   | 1.2.4     |

Percentages of the average compressive strengths of the four batches (69% to 80 %) were used as maximum stress levels for the fatigue tests conducted on 16 specimens to failure (Table 3.2). The 22 specimens loaded to different numbers of cycles less than the number of cycles leading to failure at a constant maximum stress level of 0.74 (Table 3.3) and a frequency of 5 Hz are given in Table 3.3. A constant minimum load of 5 kN was used for all the tests conducted. The approach for estimating the fatigue secant modulus will be discussed in a subsequent section.

Table 3.2 - Percentage of Average Compressive Strength for Fatigue Loading.

| Batch (# of Specimens) | % of Average Comp. Strength (MPa) | Average Compressive Strength (MPa) | Freq. (Hz) |
|------------------------|-----------------------------------|------------------------------------|------------|
| 1(5)                   | 74                                | 52.8                               | 5          |
| 1(2)                   | 69                                | 52.8                               | 5          |
| 2(2)                   | 80                                | 55.8                               | 5          |
| 3(2)                   | 74                                | 46.2                               | 5          |
| 4(2)                   | 75                                | 23.1                               | 5          |
| 4(3)                   | 75                                | 23.1                               | 1          |

The progressive strain readings of the concrete cylinders (100 mm diameter x 200 mm height) tested under uniaxial constant fatigue loading in compression were obtained using a data acquisition system. The specimens tested to failure were used to verify Park's (1990) assumption

and that of the intersection of the hysteresis loop with the stress-strain envelope at failure. The 22 specimens tested to different numbers of cycles before failure were used to verify the assumption of the intersection of the peak stress with the softening portions of the stress-strain envelope.

The servohydraulic testing equipment used was unable to properly capture the softening of concrete after attaining peak strength due to the insufficient stiffness of the MTS (Material Testing Systems) set-up used; hence, the average compressive strength and the corresponding average peak strain values obtained from monotonic tests were substituted into Popovics' (1973) and Hognestad's (1954) stress-strain equations for high and normal strength concrete, respectively. The stress-strain curves generated were used as the stress-strain envelopes required to verify the intersection of the peak stresses for the statically loaded fatigue-damaged specimens. However, the stress-strain curves obtained from the experiments were also included in the plots.

### 3.3.2 Failure Modes

Figure 3.3 shows specimens in various damaged states. In all, hairline cracks parallel to the applied loading direction were initially observed. Thereafter, the cracks widened and finally failed in the form of faults.



Fig. 3.3 - Specimens in damaged states.

### 3.3.3 Experimental Results and Verification

#### 3.3.3.1 Fatigue Degradation

The fatigue stress-strain hysteresis loops for the concrete cylinders tested are shown in Figures 3.4 to 3.7 for some of the tested specimens. The monotonic stress-strain curves obtained from the experiments conducted and from Popovics' equation for high strength concrete ( $\geq 40$  MPa) were plotted as envelopes for the hysteresis loops. In the case of normal strength concrete ( $< 40$  MPa), stress-strain curves generated from Hognestad's constitutive equation were used.

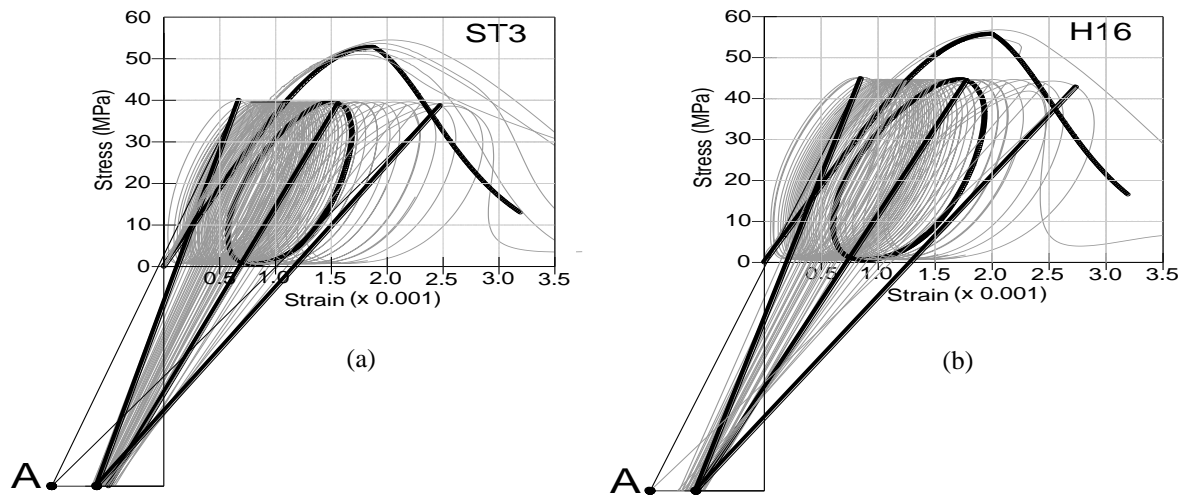


Fig. 3.4 - Fatigue degradation ST3 ( $f'_c = 52.8$  MPa) & H16 ( $f'_c = 55.8$  MPa).

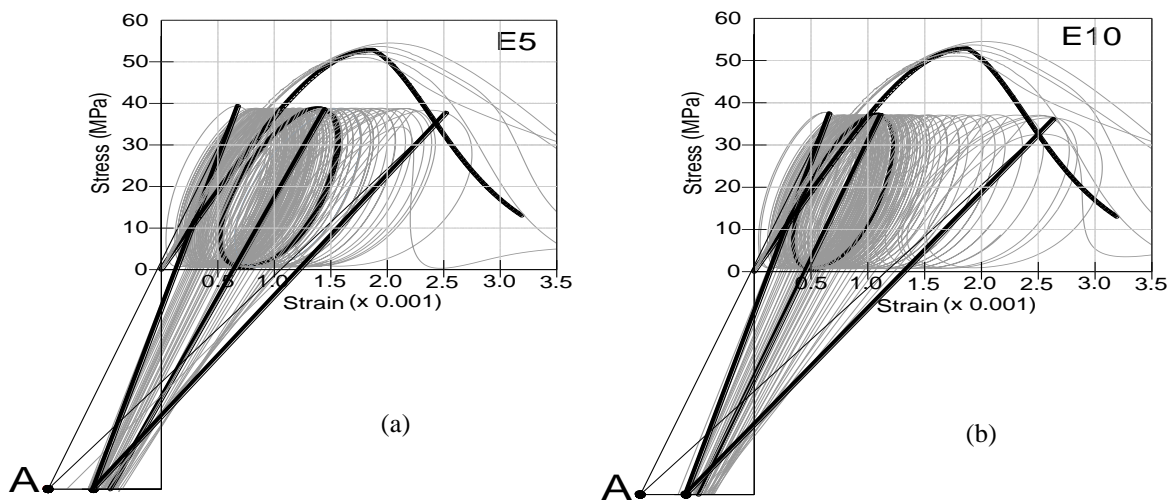


Fig. 3.5 - Fatigue degradation E5 ( $f'_c = 52.8$  MPa) & E10 ( $f'_c = 52.8$  MPa).

The fatigue hysteresis loops for each specimen tested were plotted using stress-strain values at intervals of cycles. As the specimen degradation became substantial, the intervals were reduced.

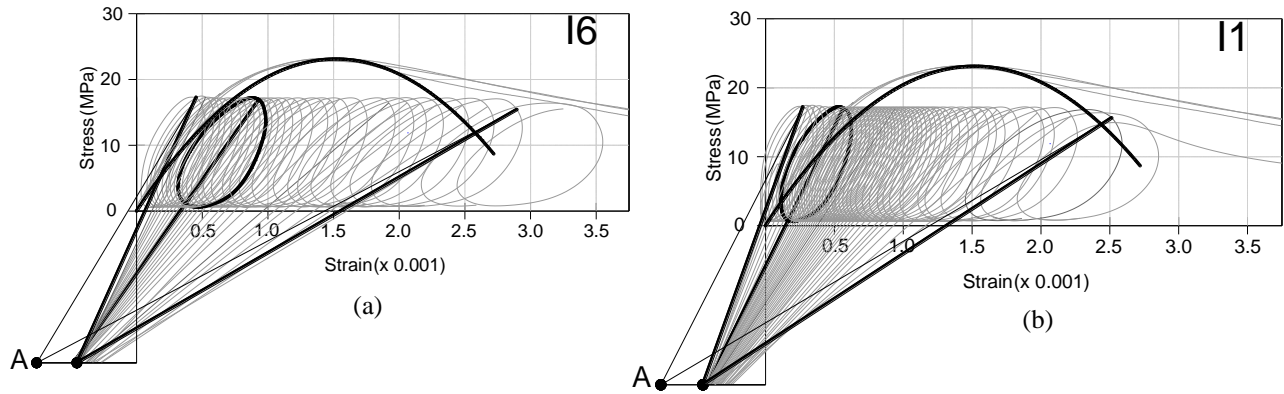


Fig. 3.6 - Fatigue degradation I1 & I6 ( $f'_c = 23.1$  MPa) at 5 Hz.

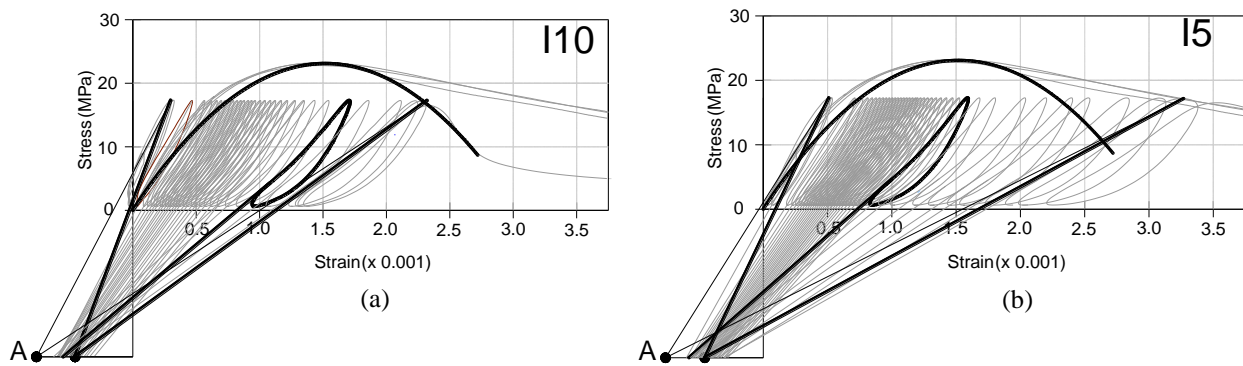


Fig. 3.7 - Fatigue degradation I6 & I5 ( $f'_c = 23.1$  MPa) at 1 Hz.

From the experiment plots, the shapes of the hysteresis loops at a loading frequency of 5 Hz were observed to be fully developed ellipses (Figures 3.4 to 3.7). The sizes increased progressively with a corresponding increase in the loading cycles. However, towards failure, the elliptical shapes became distorted. The centerline for each hysteresis loop was further extended along the approximate major axes (Figures 3.4 to 3.6). On the other hand, the shapes of the hysteresis loops obtained from tests conducted at a frequency of 1 Hz were initially elliptical with smaller minor axes. As the number of cycles increased, the reloading paths of the curves

were approximately linear and subsequently became concave with further increases in the number of cycles (Figure 3.7). This observation reveals the influence of the loading frequency on the shapes of the fatigue hysteresis loops for plain concrete in compression.

From Figures 3.4 to 3.7, the last hysteresis loop at failure approached or intersected the softening portion of the stress-strain envelope. Generally, each last loop evolved between the softening portion of the experimental stress-strain curve and the stress-strain models used (Popovics' and Hognestad's). Hence, the assumption of the intersection of the last loop with the softening portion of the stress-strain envelope can be considered realistic.

In order to verify the assumption proposed by Park (1990), the centerline of each hysteresis loop plotted was extended to cross a horizontal line drawn at an ordinate of  $-f'_c$  ( $f'_c$  is the compressive strength value) as shown in Figures 3.4 to 3.7 (others are given in Appendix C). The required slopes (fatigue secant moduli) for the hysteresis loops with concave reloading paths were obtained by extending centerlines drawn between ordinate points ( $0.25f'_c$ ) and tangents at lower points on the hysteresis loops.

The point A indicated in Figures 3.4 to 3.7, with a coordinate of  $(-0.5\varepsilon'_c, -f'_c)$  ( $\varepsilon'_c$  is the strain corresponding to the peak stress), corresponds to the convergence point proposed by Park (1990). As observed, Park's convergence point underestimates the fatigue modulus of degraded concrete. This is due to the assumption that the initial concrete fatigue secant modulus is equal to the static secant modulus. Based on the observed results, the fatigue secant modulus of concrete is generally higher than the static secant modulus. From the observed hysteresis loops (Figures 3.4 to 3.7), the initial centerline meets a coordinate point at approximately  $(-0.3\varepsilon'_c, -f'_c)$ . Subsequent centerlines deviate from the point as the irreversible strain accumulates. As the damage becomes

substantial (more inclined loops), the centerlines tend towards the initial convergence point. Hence, from the geometry of the stress-strain plots (Figures 3.8 and 3.9), an assumed convergence point of  $(-0.3\epsilon'_c, -f'_c)$  is proposed.

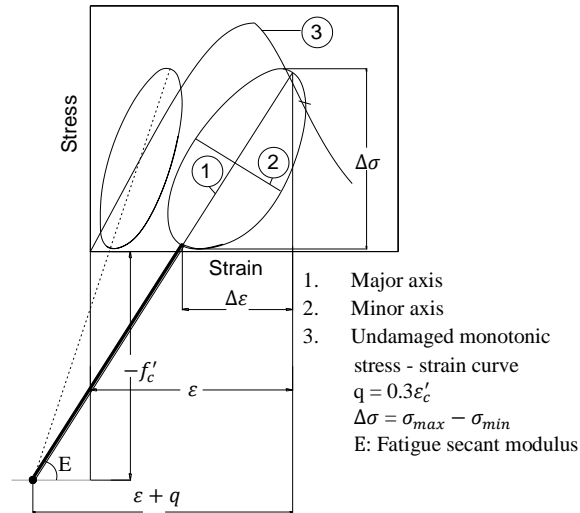


Fig. 3.8 - Fatigue degradation (high frequency).

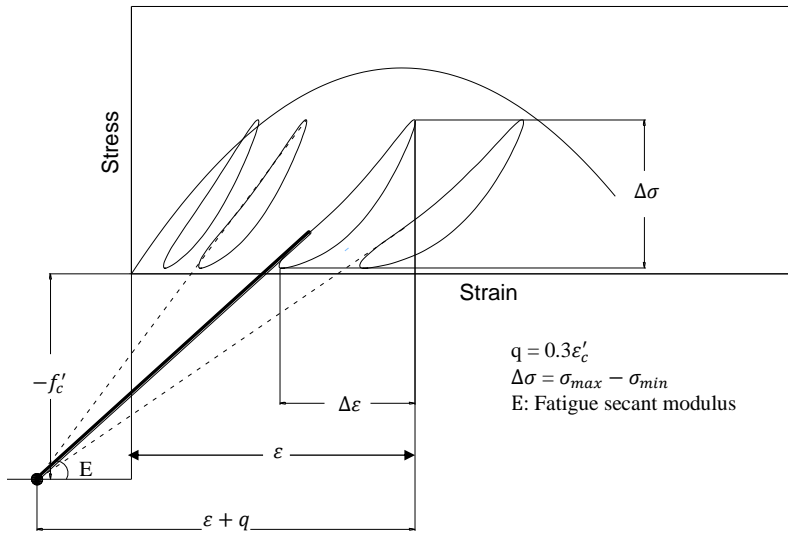


Fig. 3.9 - Fatigue degradation (low frequency).

### 3.3.3.2 Irreversible Strain under Fatigue Loading

The irreversible strain at a given cycle is equal to the strain corresponding to the minimum stress level at that cycle. Initially, the centerlines intersected the hysteresis loops at points corresponding

to the minimum stress point on each hysteresis loop (Figures 3.8 and 3.9).

As the cycles increased, the distance between each centerline and the point corresponding to the minimum stress level on the fatigue hysteresis loops increased progressively. This is attributed to the subsequent inclination of the loops and a strain evolution due to the minimum applied stress under static condition.

The strain due to the minimum stress level under static condition (i.e., at the lower turning point of the fatigue loading) is a function of the static secant modulus evolution. However, at zero minimum stress level, the value is null. Based on the proposed assumption and from the geometries in Figure 3.8 or Figure 3.9, a model was proposed for the irreversible fatigue strain ( $\varepsilon_d$ ) as follows:

For  $0.3N_f \leq N \leq N_f$  ( $N_f$  is the number of cycles to failure and  $N$  is the fatigue loading cycles)

$$\varepsilon_d = \varepsilon - \Delta\varepsilon \quad (3.1)$$

where

$$\varepsilon_d = \varepsilon_{do} + \varepsilon_{d1} + \varepsilon_{d2}$$

$\Delta\varepsilon$  is the fatigue strain range,  $\varepsilon_{do}$  is the strain due to loops centerlines convergence,  $\varepsilon_{d1}$  is the strain due to the hysteresis loop inclination, and  $\varepsilon_{d2}$  is the strain due to the minimum stress at the turning point of fatigue loading.

$$\varepsilon_{do} = - \left( \frac{f'_c + (\sigma_{max} R)}{E} \right) - 0.3 \varepsilon'_c \quad (3.2)$$

$$\varepsilon_{d1} = k_2 q \left( \frac{D_{fc}}{\sqrt{D_{ce}}} \right) \quad (3.3)$$

$$\varepsilon_{d2} = \frac{(\sigma_{max} R)}{E_{sec}} \quad (3.4)$$

$E$  is the fatigue secant modulus,  $k_2$  is 1.0 for high strength concrete and 2.0 for normal strength concrete,  $q$  in Figures 3.8 and 3.9 is equal to  $-0.3 \varepsilon'_c$ ,  $R$  is the stress ratio,  $\sigma_{max}$  is the maximum

stress level, and  $E_{sec}$  is the degraded static secant modulus. The models for  $D_{fc}$  (concrete strength damage) and  $D_{ce}$  (fatigue secant modulus damage) used were previously proposed by Isojeh et al. (2017) and are given in Section 2.5 (Chapter 2).

As reported in the literature, the first stage of deformation under fatigue loading is characterized by cyclic creep. As such, the irreversible strain for any number of cycles less than 30% of the cycles leading to failure ( $N_f$ ) is estimated as a function of the irreversible strain at 0.3, where the irreversible strain at 0.3 is estimated using Equations 3.1 to 3.4. Hence, for  $N < 0.3N_f$ ,

$$\varepsilon_d = \varepsilon_{d3} \left( \frac{N}{0.3N_f} \right)^\delta \quad (3.5)$$

$\varepsilon_{d3}$  is the irreversible strain ( $\varepsilon_d$ ) value at  $0.3N_f$ . The value of  $\delta$  (fatigue creep constant) can be taken as 0.3. The implementation of the irreversible strain model into constitutive models for normal and high strength concrete will be discussed in a subsequent section.

### 3.3.3.3 Strength Degradation

The results of the 22 cylindrical specimens tested for strength degradation are presented in Table 3.3. Figures 3.10 to 3.15 show the residual strengths and corresponding strain evolutions after loading each specimen to the number of cycles specified in Table 3.3. As observed from the stress-strain plots shown in Figure 3.10 and the maximum strain evolution plots shown in Figure 3.11, an obvious degradation of concrete strength began after a substantial number of cycles had been applied to a specimen, as in the case of specimen ST2.

From Figures 3.10 and 3.11, there was no obvious strength deterioration within the primary phase and within a large portion of the secondary phase of damage for the strain evolution. The obvious strength deterioration in specimen ST2 corresponds to the tertiary stage of damage. From Figures

3.10, 3.12 and 3.14, the assumption that the peak stress of the degraded stress-strain curve after fatigue loading intersects the stress-strain curve envelop at a point on the softening portion is considered reasonable.

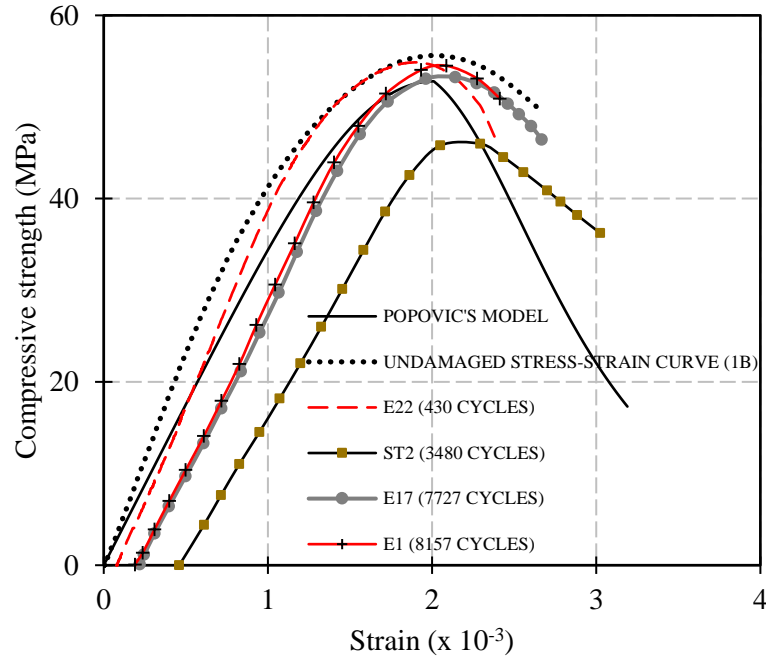


Fig. 3.10 - Residual strength (Batch 1).

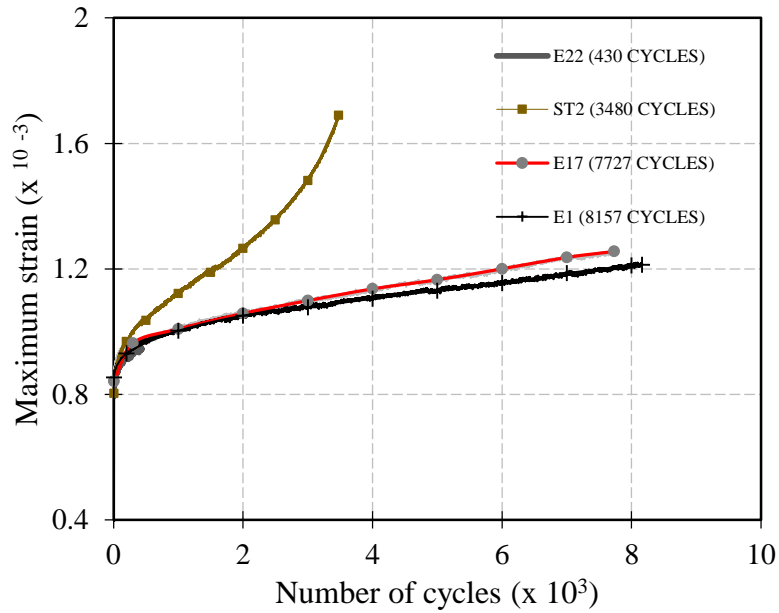


Fig. 3.11 - Strain evolution corresponding to residual strength for Batch 1.

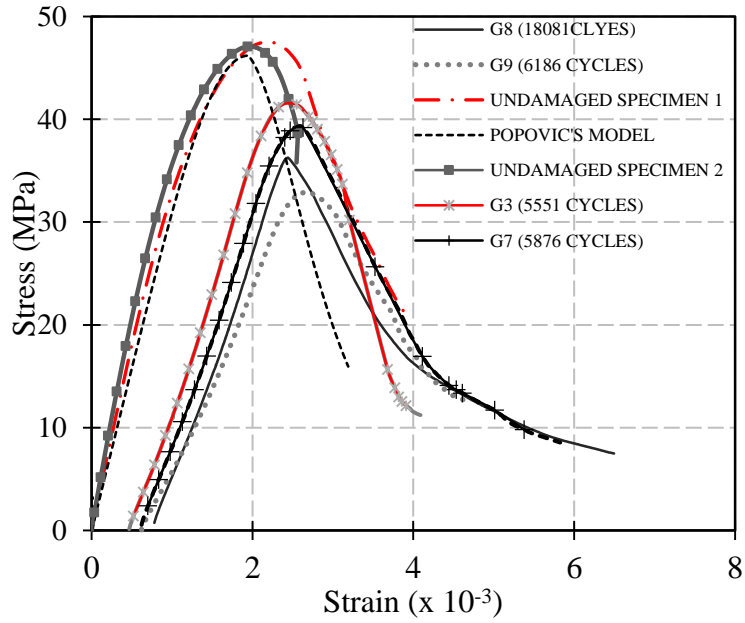


Fig. 3.12 - Residual strength (Batch 2).

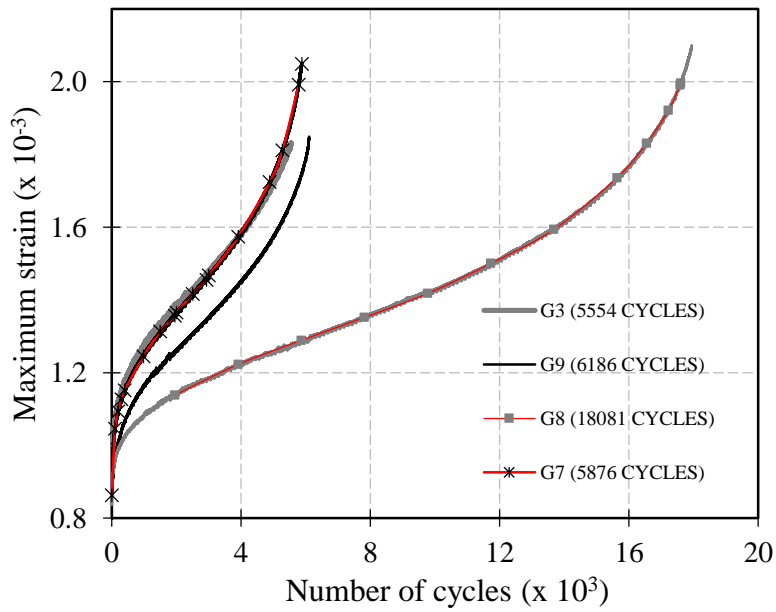


Fig. 3.13 - Strain evolution corresponding to residual strength for Batch 2.

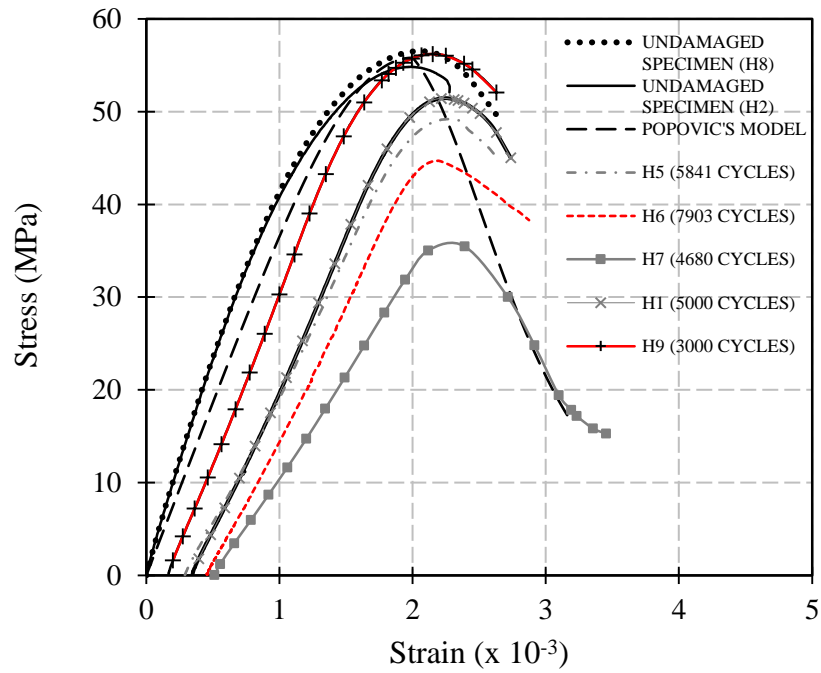


Fig. 3.14 - Residual strength (Batch 3).

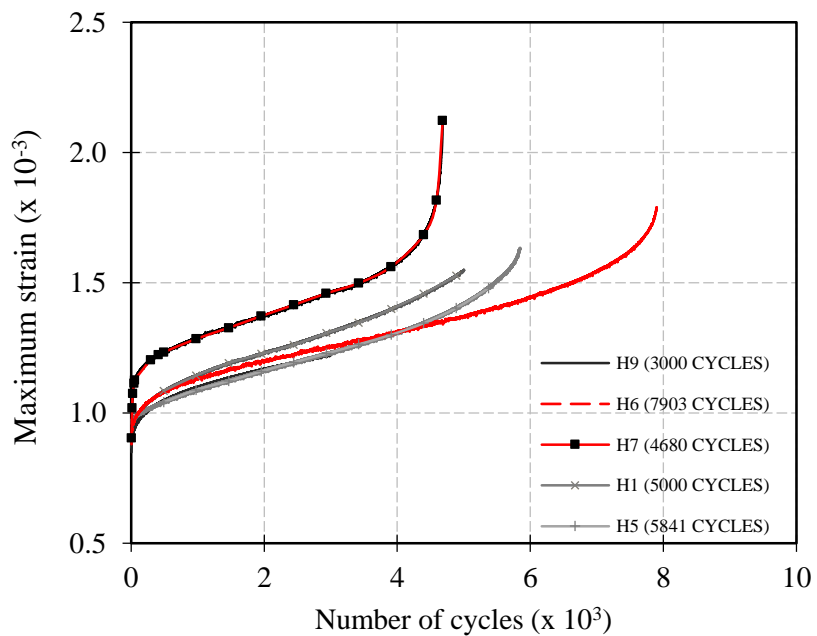


Fig. 3.15 - Strain evolution corresponding to residual strength for Batch 3.

Table 3.3 - Strength and Secant Modulus Degradation Test Data.

| Specime<br>n | Initial<br>compressive<br>strength $f'_c$ | Number of<br>cycles before<br>static loading | Residual<br>strength after<br>static loading<br>(MPa) | Residual<br>fatigue<br>modulus<br>(MPa) | Corresponding<br>static secant<br>modulus<br>(MPa) |
|--------------|---|--|---|---|--|
| E22          | 52.8                                      | 430  | 54.9  | 68900                                   | 41900  |
| E9           | 52.8                                      | 430  | 54.4  | 58100                                   | 38500  |
| E20          | 52.8                                      | 860  | 55.1  | 65100                                   | 40200  |
| E11          | 52.8                                      | 860  | 53  | 58800                                   | 37100  |
| E4           | 52.8                                      | 5150   | 55.3  | 62000                                   | 39000  |
| E17          | 52.8                                      | 7730   | 52.3  | 55200                                   | 35000  |
| E1           | 52.8                                      | 8160   | 53.4  | 53300                                   | 35500  |
| ST2          | 52.8                                      | 3480   | 46.5  | 44200                                   | 30500  |
| G3           | 46.2                                      | 5550   | 41.7  | 33400                                   | 23500  |
| G7           | 46.2                                      | 5880   | 38.6  | 30100                                   | 21600  |
| G8           | 46.2                                      | 18100  | 36.3  | 31400                                   | 21900  |
| G9           | 46.2                                      | 6180   | 32.9  | 25800                                   | 17600  |
| H1           | 55.8                                      | 5000   | 51.4  | 50200                                   | 31800  |
| H3           | 55.8                                      | 1200   | 58.1  | 61800                                   | 39700  |
| H9           | 55.8                                      | 3000   | 56.2  | 57600                                   | 36800  |
| H4           | 55.8                                      | 6120   | 45.6  | 45100                                   | 29200  |
| H5           | 55.8                                      | 5840   | 49.2  | 43900                                   | 28800  |
| H6           | 55.8                                      | 7900   | 44.7  | 42800                                   | 28300  |
| H7           | 55.8                                      | 4680   | 36.1  | 37200                                   | <sup>a</sup>                                       |
| H11          | 55.8                                      | 6710   | 52.5  | 54300                                   | 34600  |
| H14          | 55.8                                      | 9870   | 46.8  | 38800                                   | 26700  |
| H15          | 55.8                                      | 8660   | 37.9  | 33300                                   | <sup>a</sup>                                       |

<sup>a</sup>Failed before reaching maximum fatigue load applied

Figure 3.16 and Equations 3.6 and 3.7 describe the procedure for estimating the static and fatigue secant moduli of concrete,  $E$  and  $E_{SE}$ , respectively, for each of the 22 specimens tested. The results are shown in Figure 3.17. From Figure 3.17, it can be observed that the ratios are fairly constant throughout the evolution and the damage evolution for both are similar. Hence, the value of the ratio of the fatigue secant modulus to the static secant modulus can be assumed to be between 1.3 and 1.6. Based on this observation, and provided that the initial static secant modulus for concrete is known, the value of the fatigue secant modulus can be taken as 1.5 and 1.45 times the static secant modulus for high and normal-strength concrete, respectively. In Equations 3.6 and 3.7,  $\sigma_{min}$

= minimum stress level,  $\Delta\varepsilon$  = fatigue strain range, and  $\varepsilon_{cv}$  = strain corresponding to the stress range ( $\sigma_{max}-\sigma_{min}$ ) on the monotonic stress-strain curve.

$$E = \frac{\sigma_{max}-\sigma_{min}}{\Delta\varepsilon} \tag{3.6}$$

$$E_{sec} = \frac{\sigma_{max}-\sigma_{min}}{\varepsilon_{cv}} \tag{3.7}$$

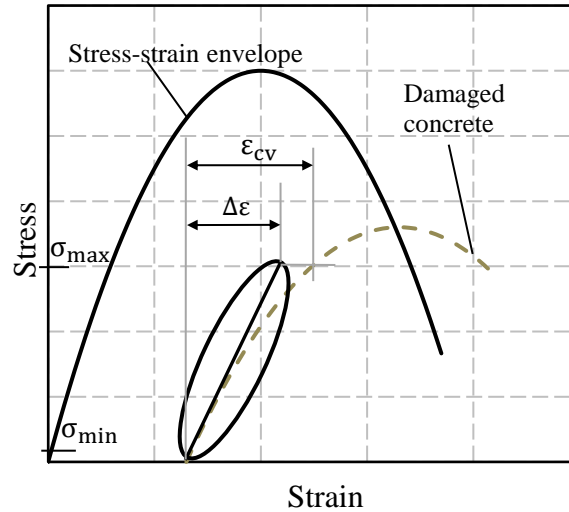


Fig. 3.16 - Static and fatigue secant moduli.

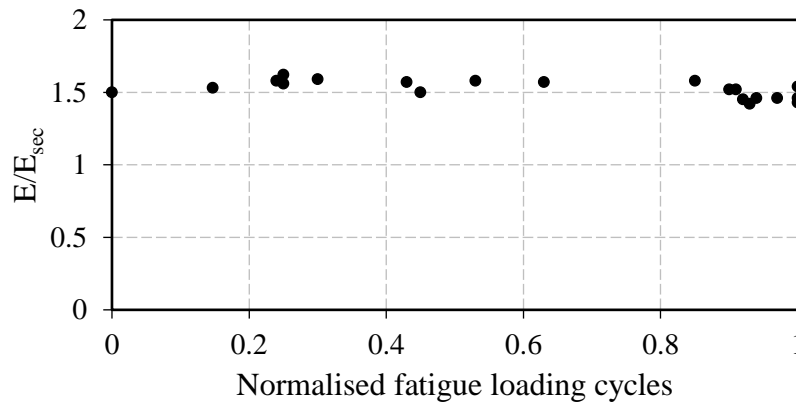


Fig. 3.17 - Plot of the ratio of the fatigue secant modulus (e) to the static secant modulus against normalized number of cycles.

### 3.4 Damaged Constitutive Models for Residual Strength of Concrete

#### 3.4.1 Normal Strength Concrete

The Hognestad stress-strain curve for normal strength is used for estimating the effective stress

of a concrete element under a monotonic loading, provided the concrete peak stress (or compressive strength), induced effective strain, and the strain corresponding to the peak stress are known. Based on the assumption of the intersection of the peak stress of a damaged concrete specimen with the softening portion of the stress-strain envelope, the Hognestad parabolic equation can be used to obtain the strain corresponding to the degraded strength and, as such, a damage constitutive model can be developed for concrete under fatigue loading by modifying the peak strength and the strain corresponding to the peak stress (Figure 3.18). The Hognestad's equation is modified thus

$$\left(\frac{\varepsilon_{c2}}{\varepsilon_p}\right)^2 - \frac{2\varepsilon_{c2}}{\varepsilon_p} + \frac{f_{c2}}{f_p} = 0 \quad (3.8)$$

$f_{c2}$  is the principal compressive stress,  $f_p$  is the peak concrete compressive stress (equal to  $f'_c$ ),  $\varepsilon_p$  (equal to  $\varepsilon'_c$ ) is the compressive strain corresponding to  $f_p$ , and  $\varepsilon_{c2}$  is the average net strain in the principal compressive direction.

Based on the assumption  $(1 - D_{fc}) f_p = f_c^*$ , and  $f_{c2} = f_c^*$

$$\left(\frac{\varepsilon_2^*}{\varepsilon_p}\right)^2 - \frac{2\varepsilon_2^*}{\varepsilon_p} + \frac{(1-D_{fc}) f_p}{f_p} = 0 \quad (3.9)$$

$$\left(\frac{\varepsilon_2^*}{\varepsilon_p}\right)^2 - \frac{2\varepsilon_2^*}{\varepsilon_p} + (1 - D_{fc}) = 0 \quad (3.10)$$

$\varepsilon_2^*$  is the total strain at peak stress intersection point with stress-strain envelope, and  $f_c^*$  is the degraded concrete strength.

Solving the equation for the total strain corresponding to the new degraded strength gives

$$\varepsilon_2^* = \varepsilon_p (1 + \sqrt{D_{fc}}) \quad (3.11)$$

From Figure 3.18, it can be observed that the value of  $\varepsilon_2^*$  also includes the strain offset ( $\varepsilon_d$ ), hence the strain corresponding to the peak stress of the degraded concrete strength  $\varepsilon_c^*$  is given as:

$$\varepsilon_c^* = \varepsilon_2^* - \varepsilon_d \quad (3.12)$$

$$\varepsilon_c^* = \varepsilon_p (1 + \sqrt{D_{fc}}) - \varepsilon_d \quad (3.13)$$

where  $\varepsilon_d$  can be obtained from Equations 3.2 to 3.4,  $\varepsilon_p$  is equal to the concrete compressive strain corresponding to the peak stress of undamaged concrete, and  $D_{fc}$  (concrete strength damage factor) can be estimated as described by Isojeh et al. (2017a) (also given in Chapter 2, Section 2.5).

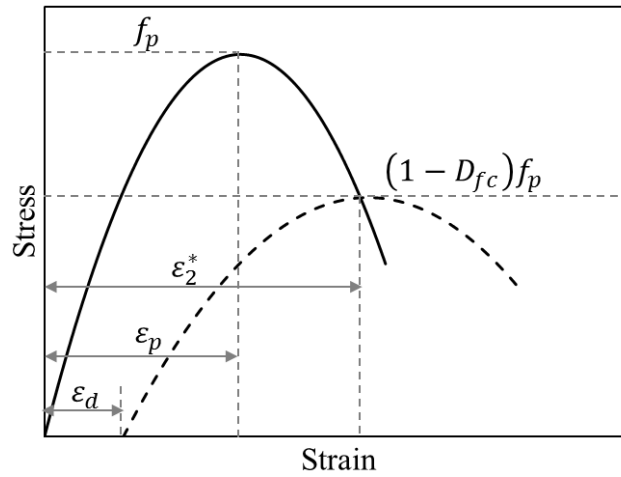


Fig. 3.18 - Modified Hognestad's stress-strain curve for damaged concrete.

### 3.4.2 High Strength Concrete

Popovics stress-strain model was modified for fatigue-damaged concrete for high strength concrete. The approach is similar to that for normal strength concrete (see Figure 3.19). However, to obtain the strain corresponding to the degraded strength, an iterative method is required such as the Newton-Raphson method; thus

$$f_{c2} = f_p \frac{n(\varepsilon_{c2}/\varepsilon_p)}{(n-1) + (\varepsilon_{c2}/\varepsilon_p)^{nk}} \quad (3.14)$$

where, according to Collins et al. (1997):

$$n = 0.80 - f_p/17 \text{ (in MPa)} \quad (3.15)$$

$$k = 0.6 - \frac{f_p}{62} \quad \text{for } \varepsilon_{c2} < \varepsilon_p < 0 \quad (3.16)$$

n is a curve fitting parameter for stress-strain response of concrete in compression, and k is a post-decay parameter for stress-strain response of concrete in compression.

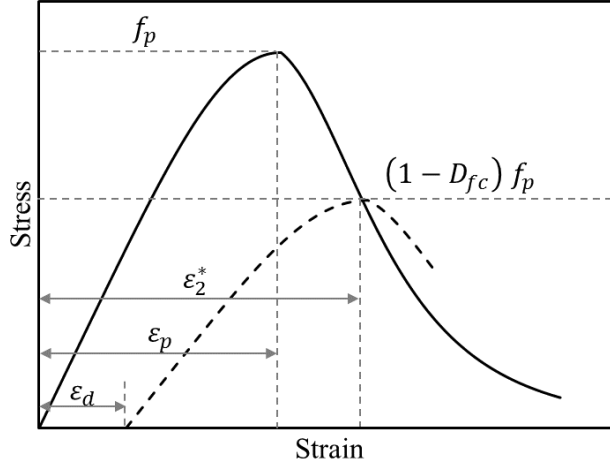


Fig. 3.19 - Modified Popovic's stress-strain curve for damaged concrete.

From Equation 3.14,  $\varepsilon_{c2}/\varepsilon_p$  can be assumed to be  $t$  and  $f_{c2} = (1 - D_{fc}) f_p$ ; hence:

$$(1 - D_{fc}) = \frac{nt}{(n-1)+t^{nk}} \quad (3.17)$$

Rearranging, 
$$f(t_i) = n-1+t^{nk} - \frac{nt}{(1-D_{fc})} = 0 \quad (3.18)$$

Using Newton-Raphson's method and differentiating Equation 3.18 with respect to  $t$ :

$$m' = nkt^{nk-1} - \frac{n}{(1-D_{fc})} \quad (3.19)$$

where  $m'$  is the differentiation of Equation 3.18.

$$t_{i+1} = t_i - \frac{f(t_i)}{m'} \quad (3.20)$$

$t_i$  is the initial value of  $t$  assumed and  $t_{i+1}$  is the value of the next step computed using Equation

3.20. Provided  $\left| \frac{t_{i+1}-t_i}{t_i} \right|$  is small enough, then the value of  $t = t_{i+1}$ . Hence,  $\varepsilon_2^*$  and  $\varepsilon_c^*$  can be obtained

as described for normal concrete and in Figure 3.19.

### 3.5 Verification of Proposed Model for Irreversible Strain

The model developed for fatigue irreversible strain was corroborated using the experiment results from Batches 1 and 4 for high and normal strength concrete, respectively. The irreversible strain

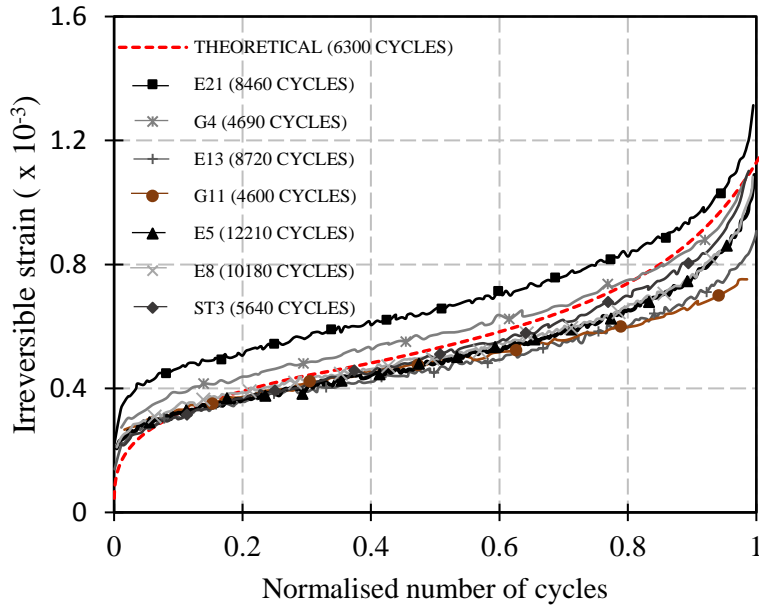


Fig. 3.20 - Irreversible fatigue strain for high strength concrete (stress level: 0.74).

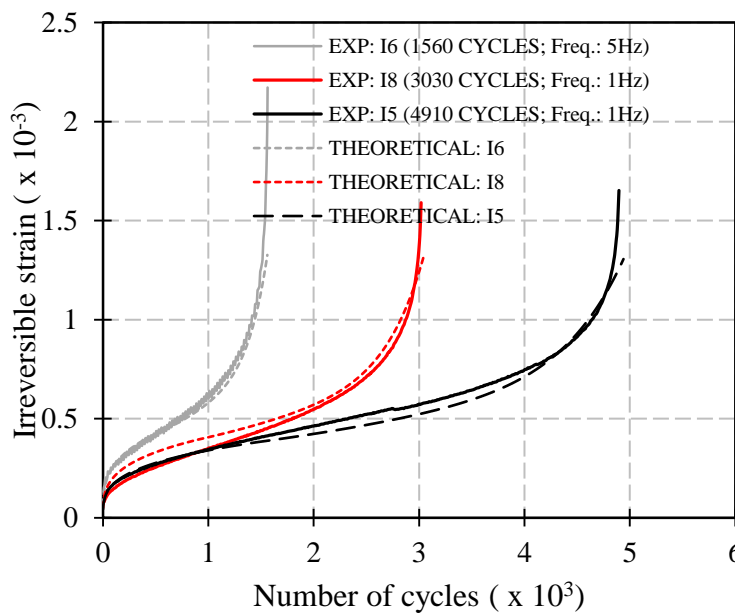


Fig. 3.21 - Irreversible fatigue strain for normal strength concrete.

evolution for seven high strength concrete specimens, tested under fatigue loading at a maximum stress level and minimum force of 0.74 and 5 kN, respectively, were plotted as shown in Figure 3.20. The specimens were all tested at a frequency of 5 Hz.

Figure 3.21 shows the irreversible strain plot for normal-strength concrete specimens. As previously indicated, the irreversible strain model incorporates residual strength and secant modulus damage models which, in turn, are functions of loading parameters such as frequency.

Specimen I5 and I8 were tested at a frequency of 1 Hz, while specimen I6 was tested at 5 Hz. Due to the stochastic nature of concrete observed in the number of cycles to failure at a stress level of 0.75, the maximum stress level corresponding to the number of cycles at failure was estimated for each specimen using a backward approach from Zhang et al.'s (1998) S-N model. The stress levels for Specimens I5, I8 and I6 were observed to be 0.73, 0.75, and 0.80 respectively. Each stress level was further used to estimate the progressive damage for residual strength and secant modulus per cycle and implemented into Equations 3.2 to 3.5 for each cycle. The procedure for estimating the irreversible strain is described subsequently in Figure 3.22. A program was written to generate the irreversible strain per loading cycle.

### **3.6 Conclusions**

From the investigations conducted, the following can be deduced:

- The intersections of the fatigue hysteresis at failure and the stress-strain curve of a fatigue-damaged concrete with the stress-strain envelope were found to be realistic, taking into account the well-known stochastic behaviour of concrete. However, the common point at which the centerlines of fatigue hysteresis loops converge required modification in order to enhance the simplified constitutive model;

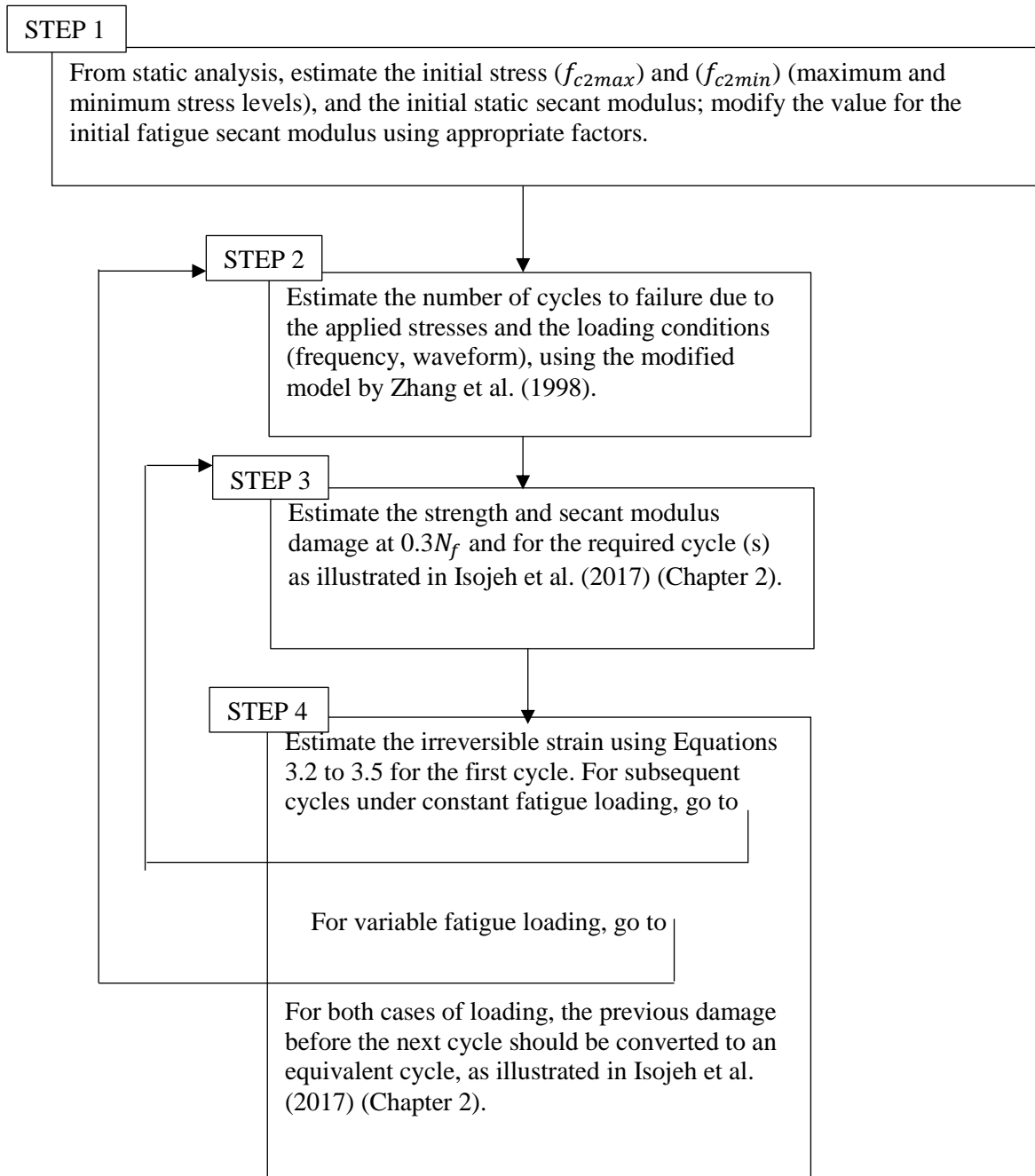


Fig. 3.22 - Steps for estimating the irreversible strain of concrete under fatigue loading in compression.

- Having observed the fact that the fatigue secant modulus is generally higher than the corresponding static secant modulus, a more accurate fatigue-deformation prediction can

be obtained using the modified convergence coordinate proposed;

- The conducted investigation shows the influence of the loading frequency on the shape of the fatigue hysteresis loops. This should be accounted for in any hysteresis loop model. However, since high-cycle fatigue loading involves a large number of hysteresis loops, expressing the fatigue behaviour of concrete using maximum deformation evolutions saves computation time;
- Using the proposed constitutive models for concrete under fatigue loading, the deformation evolution of a concrete element can be estimated per cycle since the progressive damage of concrete strength and stiffness, and the irreversible strain accumulation, are accounted for;
- There is a reasonable correlation between the theoretical and the experimental plots for the irreversible strains. As such, the proposed irreversible strain models can be used for estimating the required fatigue prestrain, provided the progressive variation in loading is taken into account;
- More investigation on the implementation of the proposed models into the fatigue analysis of reinforced concrete structures is required in order to study the interaction between fatigue-damaged concrete and other constituent materials.

### **3.7 Notations**

*The following symbols are used in this chapter:*

$D_{ce}$  : damage value for fatigue secant modulus

$D_{fc}$  : damage value for concrete strength

$E$ : fatigue secant modulus

$E_{sec}$  : static secant modulus

$f$  : frequency

$f_{c2}$  : principal compressive stress

$f_p$  : peak concrete compressive stress

$f'_c$  : compressive strength

$f_c^*$  : degraded compressive strength

$k$ : post-peak decay parameter for stress-strain response of concrete in compression

$k_2$  : strain factor (1.5 for high strength and 1.45 for normal strength concrete)

$n$ : curve fitting parameter for stress-strain response of concrete in compression

$N$  : number of cycles

$N_f$  : number of cycles at failure

$N_{eqv}$ : equivalent cycles

$q$ : abscissa of proposed convergence point

$R$ : stress ratio

$S_{max}$  : maximum stress level

$\Delta\varepsilon$  : fatigue strain range

$\Delta f$  : maximum stress level

$\delta$  : fatigue creep constant

$\varepsilon$  : total fatigue strain

$\varepsilon_{c2}$  : average net concrete axial strain, in the principal compressive direction

$\varepsilon_{cv}$  : strain corresponding to the stress range ( $\sigma_{max}-\sigma_{min}$ ) using the monotonic stress-strain curve

$\varepsilon_{do}$  : irreversible strain due to loop centerline convergence

$\varepsilon_{d1}$  : irreversible strain due to the hysteresis loop inclination

$\varepsilon_{d2}$  : irreversible strain due to the minimum stress level under static condition

$\varepsilon_{d3}$  : irreversible strain at  $0.3N_f$

$\varepsilon_d$  : irreversible fatigue strain

$\varepsilon'_c$  : strain corresponding to peak stress

$\varepsilon^*_2$  : total strain at peak stress intersection point with stress-strain envelope

$\varepsilon_p$  : concrete compressive strain corresponding to  $f_p$

$\sigma_{max}$  : maximum stress level

$\sigma_{min}$  : minimum stress level

### 3.8 References

1. Al-Gadhib A.H., Baluch M.H., Shaalan A., and Khan A.R. (2000). "Damage Model for Monotonic and Fatigue Response of High Strength Concrete." Intl. Journal of Damage Mech., Vol. , No. 1, pp. 57-58.
2. Cachim P.B., Figueiras J.A., and Pereira P.A.A. (2002). "Fatigue Behaviour of Fibre-Reinforced Concrete in Compression." Cement and Concrete Composites Vol. 24, pp. 211-217.
3. Chaboche J. (1981). "Continuum Damage Mechanics: A Tool to Describe the Phenomena before Crack Initiation." Nuclear Engineering and Design, Vol. 64, No. 2, pp. 233-247.
4. Chaboche J. (1988). "Continuum Damage Mechanics: Part I. General Concepts." Journal of Appl. Mech., Vol. 55, No. 1, pp. 59-72.
5. Chaboche J. (1988). "Continuum Damage Mechanics: Part II. Damage Growth, Crack Initiation, and Crack Growth." Journal of Appl. Mech., 55(1), pp. 59-72.
6. Collins M.P., and Mitchell D. (1997). "Prestressed Concrete Structures." Response

Publication, Canada.

7. Dafalias Y.F., and Popov E.P. (1977). "Cyclic Loading for Materials with a Vanishing Elastic Region." *Nuclear Engineering and Design*, Vol. 41, pp. 293-302.
8. Eligehausen R., Kazic M., and Sippel, T.M. (1992). "Creep and Fatigue Analysis of Reinforced Concrete Structures." *Proceedings, Riga, Latvia, International Conference bond in Concrete from Research to Practice. Bd. 3. Riga: Riga Technical University, S. 7-49-7-58.*
9. Gao L., and Hsu C.T.T. (1998). "Fatigue of Concrete under Uniaxial Compression Cyclic Loading." *ACI Materials Journal*, Vol. 95, No. 5, pp. 575-581.
10. Hognestad, E. (1954). "Confirmation of Inelastic Stress Distribution in Concrete." *Proceedings, ASCE 1954; Vol. 83, No. 2, pp. 1-17.*
11. Holmen J.O. (1982). "Fatigue of Concrete by Constant and Variable Amplitude Loading." *ACI SP Vol. 75, No. 4, pp. 71-110.*
12. Isojeh, B., El-Zeghayar, M., and Vecchio, F.J. (2017). "Concrete Damage under Fatigue Loading in Uniaxial Compression." *ACI Materials Journal*, Vol. 114, No. 2, 225-235.
13. Karsan I.D., and Jirsa J.O. (1969). "Behaviour of Concrete under Compressive Loadings." *J. Struct. Div., ASCE, Vol. 9, No. 12, pp. 2543-2563.*
14. Lemaitre J. (1986). "Local Approach of Fracture." *Journal of Eng. Fract. Mech., Vol. 25, No. 5-6, pp. 523-537.*
15. Lemaitre J., and Chaboche J.L. (1990). "Mechanics of Solid Materials." Cambridge. U.K.,

Cambridge Press University.

16. Medeiros A., Zhang X., Ruiz G., Yu R.C., and Velasco M. (2015). "Effect of the Loading Frequency on the Compressive Fatigue Behavior of Plain and Fiber Reinforced Concrete." *International Journal of Fatigue*, Vol. 70, pp. 342-350.
17. Otter D.E., and Naaman A.E. (1989). "Model for Response of Concrete to Random Compressive Loads." *Journal of Structural Engineering, ASCE*, Vol. 115, No. 11, pp. 2794- 2809.
18. Park Y.J. (1990). "Fatigue of Concrete under Random Loadings." *Journal of Structural Engineering, ASCE*, Vol. 116, No. 11, pp. 3228-3235.
19. Petryna Y.S., Pfanner D., Stangenberg F., and Kratzig W.B. (2002). "Reliability of Reinforced Concrete Structures under Fatigue." *Reliability Engineering and System Safety*, Vol. 77, pp. 253-261.
20. Popovics S. (1973). "A Numerical Approach to the Complete Stress Strain Curve for Concrete." *Cement and Concrete Research*, Vol. 3, No. 5, pp. 583-599.
21. Raithby K.D, and Galloway J.W. (1974). "Effect of Moisture Condition, Age, and Rate of Loading on Fatigue of Plain Concrete." *ABELES Symposium, Fatigue of Concrete*, ACI Publication SP-Vol. 41, pp. 15-34.
22. Sparks P.R., and Menzies J.B. (1973). "The Effect of Rate of Loading upon the Static and Fatigue Strength of Plain Concrete in Compression." *Department of the Environment, Building Research Establishment*.

23. Su E.C.M., and Hsu T.T.C. (1988). "Biaxial Compression Fatigue and Discontinuity of Concrete." *ACI Materials Journal*, Vol. 85, No. 3, pp. 178-188.
24. Suaris W., Ouyang C., and Fernando V. M. (1990). "Damage Model for Cyclic Loading of Concrete." *Journal of Engineering Mechanics*, ASCE, Vol. 116, No. 5, pp. 1020-1035.
25. Tamulenas V., Gelazius V., and Ramanauskas R. (2014). "Calculation Technique for Stress- Strain Analysis of RC Elements Subjected to High-Cycle Compression." *Civil and Transport Engineering, Aviation Technologies*, Vol. 6, No. 5, pp. 468-473.
26. Torrenti J.M., Pijaudier-Cabot G., and Reynouard J. (2010). "Mechanical Behaviour of Concrete: Cyclic and Dynamic Loading, Fatigue of Structural Concrete." ISTE Ltd and John Wiley & Sons, Inc. pp. 185-223.
27. Vega I.M., Bhatti M.A., and Nixon W.A. (1995). "A Nonlinear Fatigue Damage Model for Concrete in Tension." *International of Journal of Damage Mechanics*, Vol.4, pp. 362-379.
28. Xiang T., and Zhao R. (2007). "Reliability Evaluation of Chloride Diffusion in Fatigue Damaged Concrete." *Engineering Structures*, Vol. 29, pp. 1539-1547.
29. Zanuy C., Fuente P., and Albajar L. (2007). "Effect of Fatigue Degradation of the Compression Zone of Concrete in Reinforced Concrete Sections." *Engineering Structures*, Vol. 29, pp. 2908- 2920.
30. Zhang B., Phillips D.V., Wu K. (1996). "Effects of Loading Frequency and Stress Reversal on Fatigue Life of Plain Concrete." *Magazine of Concrete Research*, Vol. 48, pp. 361-375.

31. Zhang B., and Wu K. (1997). "Residual Fatigue Strength and Stiffness of Ordinary Concrete under Bending." *Cement and Concrete Research*, Vol. 27, No. 1, pp. 115-126.
32. Zhang W., and Cai Y. (2010). "Continuum Damage Mechanics and Numerical Applications." Zhejiang University Press, Hangzhou and Springer-Verlag Berlin Heidelberg.
33. Zuradzka S.S. (2008). "Fatigue Strength of Concrete under Sulphate Attack." Cracow University of Technology, Institute of Building Materials and Structures, ul. Warszawska 24, 31-155, Cracow, Poland.

## CHAPTER 4

### FATIGUE BEHAVIOUR OF STEEL-FIBRE CONCRETE IN DIRECT TENSION

The material in this chapter was previously published as follows:

*Isojeh B., El-Zeghayar M., and Vecchio F.J (2017). "Simplified Constitutive Model for Fatigue Behaviour of Concrete in Compression." ASCE Journal of Materials in Civil Engineering, DOI: 10.1061/(ASCE)MT.1943-5533.0001949.*

#### 4.1 Abstract

An investigation was conducted to study the behaviour of plain concrete and steel fibre reinforced concrete under direct tension fatigue loading. Tests were conducted on dogbone specimens with varying amounts of steel fibre volume content (0%, 0.75%, and 1.5%). A new concept was introduced in deriving material damage parameters for plain and steel fibre concrete. The parameters developed were implemented into a damage evolution function to enable the prediction of concrete strength and fatigue secant modulus deterioration of steel fibre reinforced concrete. As such, the damage evolution models developed for steel fibre concrete can be implemented into steel fibre reinforced concrete constitutive models for the analysis of fatigue-damaged concrete elements. From the experimental results, it was found that the deformation profiles for plain and steel fibre concrete were similar, and that the well-known relationship between the fatigue life and secondary strain rate of concrete in compression also exists for plain concrete and steel fibre concrete in tension. In addition, under the same loading parameters, the fatigue life of steel fibre concrete was found to increase as the steel fibre content increased from 0% to 1.5%.

#### 4.2 Introduction

The deterioration of a concrete element evolves as cracked planes emanate in concrete under

fatigue loading. In reinforced concrete elements, the initiation of macrocracks results in localized stress increments in the embedded reinforcement. Depending on the magnitude of the induced stress, a crack may initiate on a reinforcing bar at its intersection with the cracked concrete plane and subsequent fatigue loading cycles may result in widening of the concrete cracks. Ultimately, fracture of the reinforcement may occur as the reinforcing bar cracks propagate.

The presence of concrete cracks and excessive opening under fatigue loading may result in serious durability issues such as accelerated reinforcement crack growth (arising from a more corrosive environment) and reduced stiffness of the overall structural element. As such, a majority of fatigue-prone concrete structures such as highways, airport pavements, offshore structures, and wind turbine foundations are usually designed to ensure cracking of concrete is held to a minimum (Vega et al., 1995; Guo, 2014).

Because cracks are inevitable in some concrete structures, developing a means of ensuring that their evolution is prevented by crack-bridging is imperative. However, designs of fatigue-prone concrete structures against excessive cracking under tensile fatigue loading require adequate knowledge of the fatigue life of concrete in tension and its corresponding deformation evolutions.

Reports in the literature have shown that steel fibre possesses crack-bridging attributes which restrain the opening of cracks under fatigue loading. As such, its use has been employed in various structural elements such as concrete pavements, bridge decks, and machine foundations (Zhang et al., 1999). Experimental investigations on steel fibre concrete portraying crack-bridging and enhanced fatigue life attributes have been reported in the literature using flexural

fatigue tests on steel fibre concrete prisms. Test reported by Ramakrishnan et al. (1989), Chenkui and Guofan (1995), Nanni (1991), Chang and Chai (1995), and Naaman and Hammoud (1998) all indicate enhanced fatigue life through crack arrests.

To predict the fatigue life of plain concrete elements, stress-life models have been developed in the literature for concrete under tension and compression fatigue loading (Tepfers, 1979; Oh, 1986; Torrenti et al., 2010; FIB, 2010). Such models relate the ratio of the maximum stress level (ratio of applied stress to concrete strength) to the number of cycles resulting in fatigue failure. However, a concrete material parameter obtained from experiments and other known loading parameters such as the stress ratio (ratio of the minimum stress level to the maximum stress level) are required in such models for reasonable predictions.

#### **4.3 Material Parameter in Aas-Jakobsen's S-N Model**

It widely accepted that the Aas-Jakobsen and Lenshow linear model (Equation 4.1) can be used to estimate the fatigue life of plain concrete in tension, compression, and flexure. The model shows the relationship between the fatigue strength of concrete after a given number of cycles and the ratio of the minimum to maximum stress level. The material parameter ( $\beta$ ) required in the model proposed by Aas-Jakobsen and Lenshow was 0.064. Oh (1986), having conducted flexural tests on plain concrete, proposed a material parameter of 0.069. To account for other plain light-weight concrete, Tepfers and Kutti (1978) proposed a material parameter of 0.0685.

$$S_{\max} = 1 - \beta (1 - R) \text{Log } N_f \quad (4.1)$$

In Equation 4.1,  $S_{\max}$  is the ratio of the maximum stress level to the concrete compressive strength,  $N_f$  is the number of cycles to failure, and  $R$  is the stress ratio (minimum stress level ( $\sigma_{\min}$ ) to maximum stress level ( $\sigma_{\max}$ )).

As a means of predicting the fatigue life of steel fibre concrete using the Aas-Jakobsen stress-life model, Singh and Kaushik (2001) developed material parameters for steel fibre concrete with fibre volume contents of 0.5%, 1.0% and 1.5% using flexural fatigue tests, obtaining values of 0.0536, 0.0425, and 0.0615, respectively. Although the attempt seems reasonable, the material parameters obtained indicated a lower fatigue life as the steel fibre volume increases from 1.0% to 1.5%. The proposed material parameters also exhibited higher fatigue life for steel fibre concrete with a volume content of 0.5% compared with steel fibre concrete with a volume content of 1.5%. These contradict the trend reported by previous investigators (Chang and Chai, 1995; Chenkui and Guofan, 1995).

As an alternative to the estimation of fatigue life, strain evolution models have been used in the literature. According to Sparks and Menzies (1973), Cornelissen and Reinhardt (1987), and Taliercio and Gobbit (1996), the fatigue life of a concrete element can be predicted from its strain evolution because a correlation was found to exist between the secondary strain rate and the number of cycles to failure. From experimental investigations reported in the literature, this approach is not significantly affected by the stochastic nature of concrete. However, the use of such models still requires the fatigue stress levels.

Equation 4.1 can be expressed as:

$$\text{Log}(1-S_{\max}) = \text{Log } \beta + V \text{Log}(\text{Log } N_f) \quad (4.2)$$

where  $V = (1-R)k$ , and  $k$  is a constant.

From the correlation between the secondary strain rate and the number of cycles to failure,

$$\text{Log}(\text{Log } N_f) = A + B \text{Log } \varepsilon_{sec} \quad (4.3)$$

where  $\varepsilon_{sec}$  is the secondary strain rate, and  $A$  and  $B$  are constants to be obtained from experiments.

A power law correlation (nonlinear) was initially proposed by Sparks and Menzies (1973);

however, the correlation between the number of cycles resulting in fatigue failure and the secondary strain rate is expressed in a linear form (Equation 4.3) by the authors in order to simplify the analysis required for deriving the material parameter  $\beta$  for plain and steel fibre concrete. The corroboration of the model with experimental data is presented in a subsequent section.

A relationship between  $\text{Log}(1-S_{\max})$  and the secondary strain rate ( $\epsilon_{sec}$ ) can be given thus:

$$\text{Log}(1-S_{\max}) = C + D \text{Log} \epsilon_{sec} \quad (4.4)$$

C and D are constants obtained from experiments.

From Equations 4.3 and 4.4,

$$\text{Log} \epsilon_{sec} = \frac{\text{Log}(\text{Log}N_f) - A}{B} \quad (4.5)$$

$$\text{Log} \epsilon_{sec} = \frac{\text{Log}(1-S_{\max}) - C}{D} \quad (4.6)$$

From Equations 4.5 and 4.6,

$$\text{Log}(1-S_{\max}) = \frac{(C B) - (A D)}{B} + \frac{D}{B} \text{Log}(\text{Log}N_f) \quad (4.7)$$

$$T_0 = \frac{(C B) - (A D)}{B}$$

By comparing Equation 4.2 and Equation 4.7, the material parameter required in the S-N model can be obtained thus:

$$\beta = 10^{T_0} \quad (4.8)$$

In this investigation, direct tension fatigue tests are conducted using dogbone specimens. The dogbone specimens were initially developed by past researchers at the University of Toronto and elsewhere for direct tension tests under monotonic loading. Herein, the deformation evolution in terms of maximum strain evolution, strain rate, and hysteresis loops are plotted for the given steel fibre volume contents (0%, 0.75%, and 1.5%). The material constant  $\beta$  is estimated for plain concrete and compared with previous values in the literature. Parameter

values are then developed for steel fibre volume contents of 0%, 0.75% and 1.5%. In addition, conservative damage models are proposed for the residual strength and fatigue secant modulus of steel fibre concrete.

#### 4.4 Experimental Program

Experiments on the fatigue behaviour of plain and steel fibre reinforced concrete in direct tension were conducted using dogbone specimens with dimensions of 500 mm (length) x 200 mm x 70 mm. Eight plain concrete specimens and 10 specimens reinforced with 0.75% and 1.5% steel fibre volume content were tested under fatigue loading. Two batches of concrete were cast for each fibre volume content (0.75% and 1.5%), whereas three batches were cast for plain concrete. At least two dogbones from each cast were tested under monotonic loading before the fatigue tests in order to observe the average tensile strength per batch. Percentages of the observed tensile strengths were used for the fatigue tests conducted between one and two months after casting. The average tensile strengths are given in Table 4.1.

Table 4.1- Compressive Strength of Plain and Steel Fibre Concrete.

| Batch no. | Average compressive strength (MPa) | Standard deviation for compressive strength | Average tensile strength (MPa) | Steel fibre volume (%) | Days | Date of cast (day/month/year) | Date of test (day/month/year) |
|-----------|------------------------------------|---|--------------------------------|------------------------|------|-------------------------------|-------------------------------|
| 1         | 63.1                               | 1.34  | 3.5                            | 0                      | 34   | 12/11/2015                    | 16/12/2015                    |
| 2         | 65.6                               | 0.76  | 3.6                            | 0                      | 54   | 18/11/2015                    | 11/1/2016                     |
| 3         | 74.2                               | 2.4   | 3.7                            | 0                      | 40   | 18/3/2016                     | 27/4/2016                     |
| 4         | 59.6                               | 3.96  | 3.2                            | 0.75                   | 32   | 22/1/2016                     | 23/2/2016                     |
| 5         | 52.2                               | 4.91  | 3.5                            | 0.75                   | 34   | 26/2/2016                     | 31/3/2016                     |
| 6         | 51.4                               | 2.04  | 4.5                            | 1.5                    | 39   | 4/3/2016                      | 12/4/2016                     |
| 7         | 56.2                               | 3.88  | 4.1                            | 1.5                    | 46   | 11/3/2016                     | 26/4/2016                     |

A design compressive strength of 50 MPa, having a mix ratio of 1:2:2 and water-cement ratio of 0.5 was used for the cast. The mix ratio represents cement, fine aggregate (fineness modulus 2.6) and coarse aggregate (10 mm maximum size). High strength end-hooked steel fibres with volume contents of 0.75% and 1.5% (Dramix RC80/30BP) and an ultimate tensile stress capacity of 3070

MPa were used. The geometrical properties of the fibre included a 30 mm fibre length, a diameter of 0.37 mm, and an aspect ratio of 79. Table 4.1 also contains the compressive strengths and the corresponding standard deviation per batch of concrete cylinders tested under monotonic loading.

Figure 4.1 shows the test set-up for the fatigue test in tension. The specimen shown in Figure 4.2, specifically for fatigue loading in direct tension, is a modification of dogbone specimens used for direct tension monotonic tests at the University of Toronto. Under monotonic loading, some specimens have been observed to fail because of bond slip between concrete and the threaded bars.

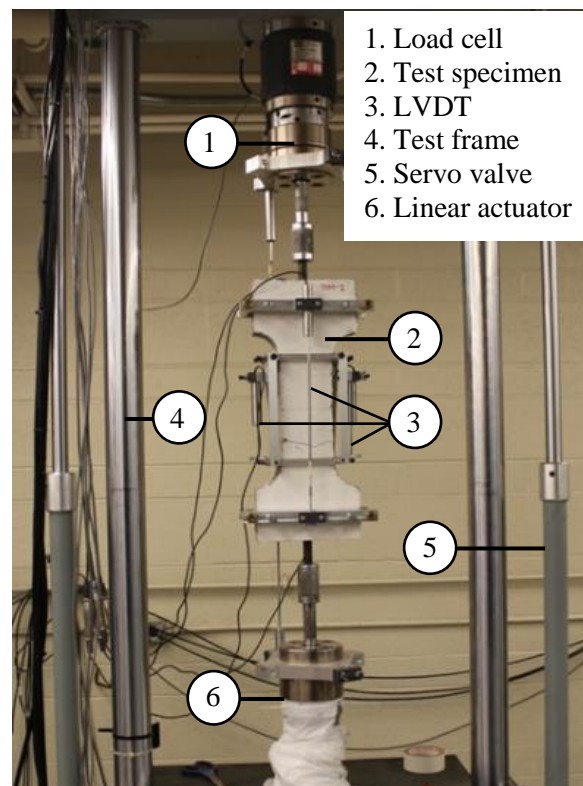


Fig. 4.1: Test set-up.

This was prevented by attaching crossbars or anchorage bars in order to enhance the bond between concrete and steel reinforcement (see Figure 4.2). Figure 4.2(a) shows the front elevation of the specimen (wider face), Figure 4.2(b) shows the side view of the specimen, and Figure 4.2(c) shows

one of the test specimens. LVDTs (Linear Variable Displacement Transducers) (attached on the four faces of each specimen) for measuring displacement and the attached mounting rigs are also indicated in Figure 4.2.

The tests were conducted using an MTS (Material Testing Systems) servo-hydraulic testing equipment with a loading capacity of 245 kN. The ends of the threaded rods of the dogbone specimens were connected to the testing equipment as shown in Figure 4.1. A pulsating load of a continuous sinusoidal waveform, which acted to induce tensile stresses in the vertical direction of the specimen, was used throughout the investigation. Each specimen was mounted with attached linear variable displacement transducers (LVDTs) as shown in Figure 4.2. The LVDTs were used to measure average strains in the specimens throughout the duration of the fatigue tests.

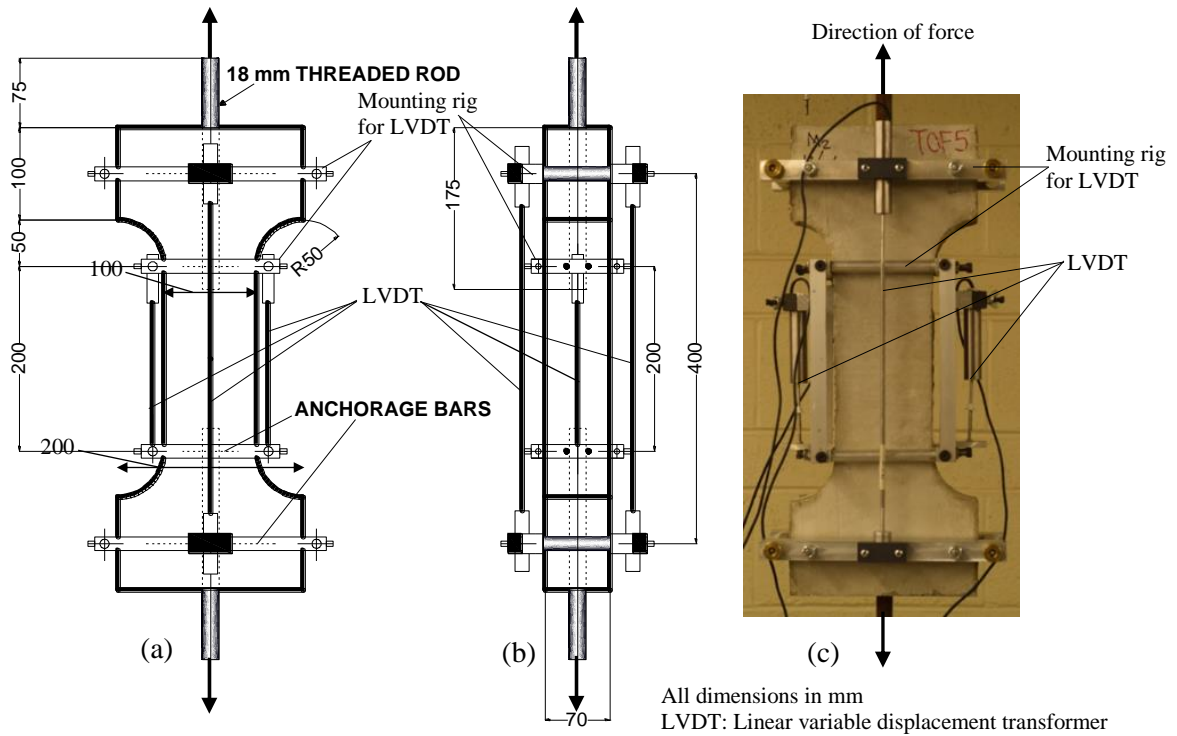


Fig. 4.2 – Test specimen.

Percentages of the average tensile strengths from the four batches (between 70% and 95%) were used as maximum stress levels for the fatigue tests conducted on plain and steel fibre reinforced

concrete dogbones. During fatigue loading, a frequency of 5 Hz (Hertz) and a minimum fatigue load of 2 kN were used for all specimens tested.

#### 4.5 Fatigue Test Results

The results obtained from the experiments are presented in Table 4.2. The results are subsequently discussed in terms of the failure modes, hysteresis loops, maximum strain evolution, and secondary strain rates.

Table 4.2 - Direct Tension Fatigue Test Results

| Specimen name     | Steel fibre volume (%) | Stress level | No. of cycles to failure | Secondary strain rate ( x 10 <sup>-8</sup> ) |
|-------------------|------------------------|--------------|--------------------------|--|
| TOF1              | 0                      | 0.79         | 1540                     | 1.32   |
| TOF2              | 0                      | 0.78         | 1900                     | 1.23   |
| TOF3              | 0                      | 0.81         | 450                      | 4.20   |
| TOF7              | 0                      | 0.80         | 641                      | -  |
| TOF9              | 0                      | 0.80         | 4052                     | 2.04   |
| TKF1              | 0                      | 0.77         | 29269                    | 0.15   |
| TKF3              | 0                      | 0.73         | 14566                    | 0.03   |
| TKF4 <sup>a</sup> | 0                      | 0.75         | 21244                    | 0.10   |
| TT2               | 0.75                   | 0.77         | 47182                    | 0.09   |
| TT4 <sup>b</sup>  | 0.75                   | 0.77         | -                        | -  |
| TT5               | 0.75                   | 0.90         | 64                       | 11.10  |
| TT6               | 0.75                   | 0.82         | 4664                     | 0.22   |
| CF1               | 0.75                   | 0.87         | 238                      | 8.90   |
| CF2               | 0.75                   | 0.79         | 18335                    | 0.12   |
| CF3               | 0.75                   | 0.88         | 302                      | 4.36   |
| CF4               | 0.75                   | 0.83         | 1528                     | 1.35   |
| CF5               | 0.75                   | 0.90         | 62                       | 38.90  |
| CF6               | 0.75                   | 0.81         | 5740                     | 0.21   |
| X2                | 1.5                    | 0.87         | 915                      | 1.67   |
| X3                | 1.5                    | 0.80         | 2998                     | 0.50   |
| X5                | 1.5                    | 0.83         | 4553                     | 0.19   |
| X6                | 1.5                    | 0.75         | 30391                    | 0.06   |
| X7                | 1.5                    | 0.78         | 9834                     | 0.08   |
| DAB1 <sup>c</sup> | 1.5                    | -            | 200                      | 6.37   |
| DAB2              | 1.5                    | 0.83         | 4326                     | 0.40   |
| DAB3              | 1.5                    | 0.91         | 42                       | 28.90  |
| DAB6              | 1.5                    | 0.86         | 1029                     | 1.54   |
| DAB7 <sup>c</sup> | 1.5                    | -            | 736                      | 2.11   |

a, b, c : unable to capture deformation data appropriately

##### 4.5.1 Failure mode

Under fatigue loading, failure in tension for plain concrete specimens was observed to be localized

(discrete). More cracks (smeared) were observed around the failure plane for specimens reinforced with steel fibre (see Figure 4.3). In all tests, fracture (separation of each specimen into two parts (Appendix D)) occurred at the necked region of each specimen. In some cases, the failure plane coincided with the end of the embedded threaded rod. The estimated applied loading stresses were modified by deducting the cross-sectional area of the threaded rod.

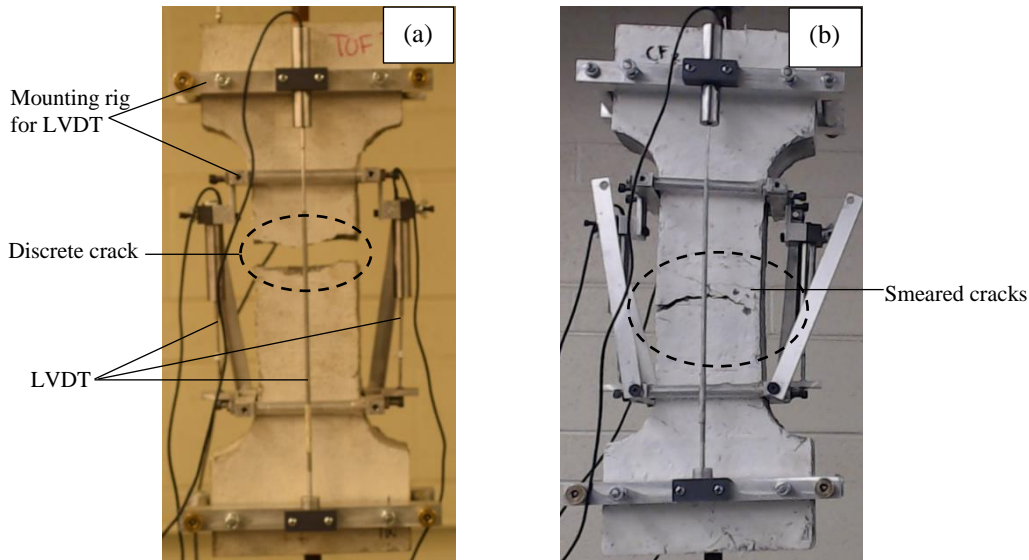


Fig. 4.3 - Test specimens after failure (a) plain concrete; (b) steel fibre.

#### 4.5.2 Progressive Deformation

The evolutions of the maximum strain were obtained by averaging the LVDT data from the two wide faces of each specimen. As in the case of the maximum strain evolutions obtained for concrete specimens tested under compression fatigue loading (Holmen, 1982), the evolution of the maximum strain of concrete tested under tension fatigue loading can also be phased into three stages as reported in the literature. Further, similar evolution profiles were observed for plain and steel fibre reinforced concrete under fatigue loading in direct tension. As shown in Figure 4.4, the initial phase portrayed a nonlinear evolution of strain at a decreasing rate (approximately 10% to 20% of fatigue life).

A constant rate of deformation within a range of approximately 70% of the fatigue life characterised the second phase, whereas the third phase (within 30% of fatigue life) exhibited an increasing rate of damage leading to failure. However, in some steel fibre reinforced concrete specimens, further resistance and increased cycles to failure were observed after sudden increases

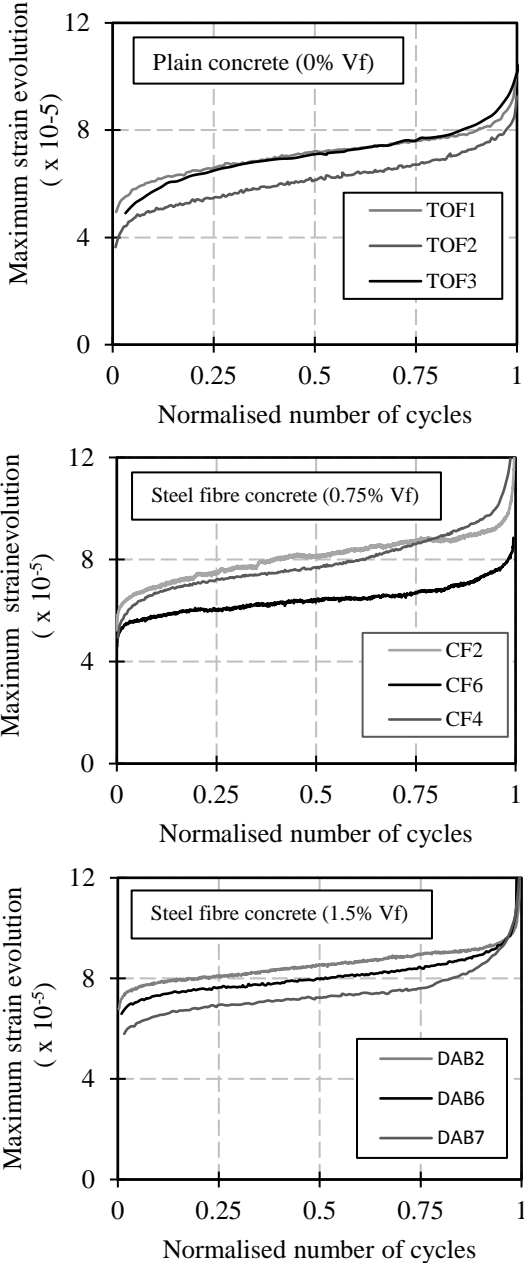


Fig. 4.4 - Fatigue maximum strain evolution for plain and steel fibre concrete.

in the deformation within the final phase of damage. This was attributed to crack-bridging ability of the steel fibres between the cracked concrete faces.

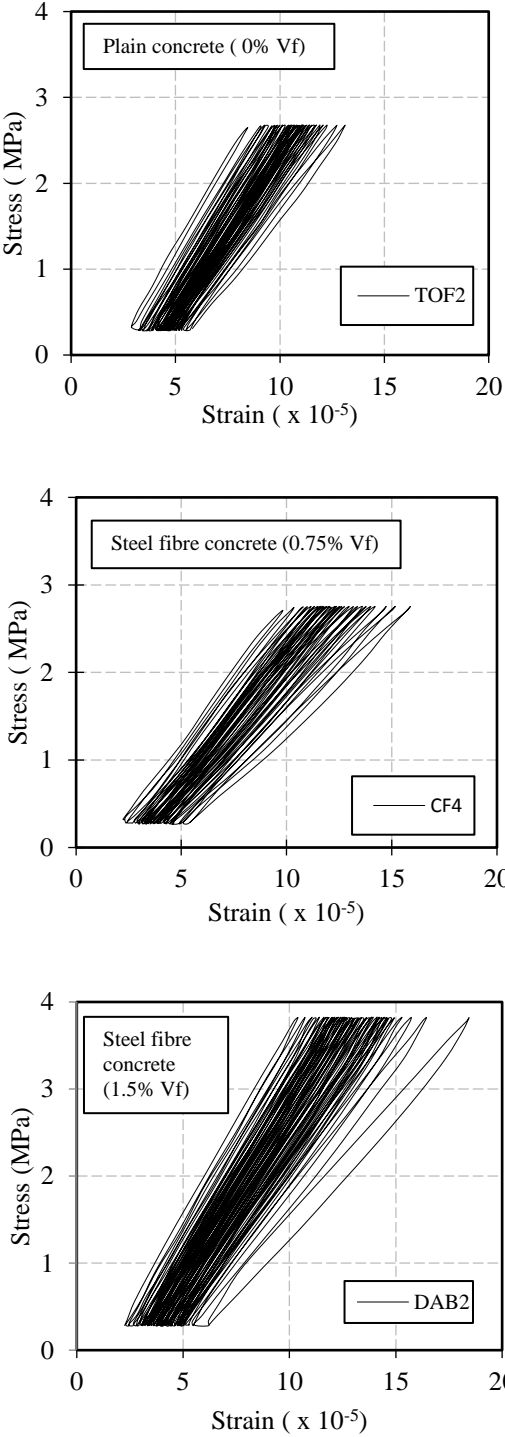


Fig. 4.5 - Fatigue hysteresis loops for plain and steel fibre concrete.

In the literature, constitutive models for concrete in tension are usually assumed to be elasto-damage models (Petryna et al, 2002, Maekawa et al., 2006). On the other hand, the behaviour of concrete in compression is assumed to be consistent with an elasto-plastic damage model. In Figure 4.5, the evolutions of the hysteresis loops of deformation indicate accumulation of irreversible strains from the onset of fatigue loading. The evolutions for plain and steel fibre reinforced concrete were also observed to be similar. These indicate that the fatigue damage constitutive model for concrete in tension is also elasto-plastic in nature; however, because of the insignificant value of the accumulated tensile strains and the computation time saved in analysis, the use of elasto- damage models for concrete in tension may be justified.

Although it is well known that the fatigue life of plain concrete in tension and compression are similar, this observation was ascertained to also extend to the profiles of corresponding damage evolutions. Further, the progressive deformations and the damage evolution profiles due to fatigue loading of steel fibre concrete specimens were also analogous to those of plain concrete.

#### **4.6 Material Parameters for Concrete and Steel-Fibre**

As previously indicated, the material parameters for plain and steel fibre concrete can be obtained using Equation 4.8 provided the coefficients (A, B, C, and D) can be obtained experimentally. To obtain A and B, the average maximum tensile strains (obtained from LVDTs) were plotted for each specimen as described in Figure 4.6. The secondary strain rates were obtained as the gradient of the plots (Figure 4.7).

The correlation between the number of cycles to failure and the secondary strain rates was verified using the data from the specimens tested (Figure 4.8(a)). Because the frequencies of loading used for plain and fibre reinforced concrete were similar, it was observed that all data

points tend to fall along a given curve. The 95% confidence and prediction intervals are also shown in Figure 4.8(b). Experiment data from previous investigations on the fatigue behaviour of concrete in compression were also plotted as shown in Figure 4.8(c) (Sparks and Menzies, 1973; Taliercio and Gobbit, 1996; Oneschkow, 2012; Isojeh et al., 2017). As observed, the profiles for the correlation between the number of cycles and the secondary strain rates are similar for concrete in tension and compression because both fit a power law curve.

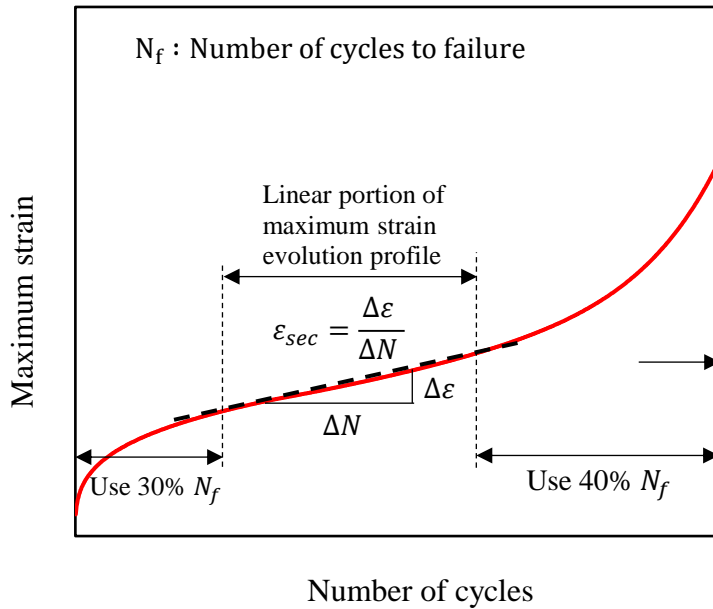


Fig. 4.6 - Maximum strain versus number of fatigue loading cycles.

Experiment data observed for the secondary strain rates and the number of cycles to failure for each specimen were plotted per steel fibre volume content in the form expressed in Equation 4.3 (Figure 4.9). From the plots, the value of A and B were obtained for plain and steel fibre reinforced concrete as the intercept and slope, respectively. To obtain the values for parameters C and D, the maximum stress level per specimen was also plotted against the observed secondary strain rate as in Equation 4.4 (Figure 4.10). By substituting the values of A, B, C, and D into Equation 4.8, the material parameters for plain and fibre reinforced concrete were obtained.

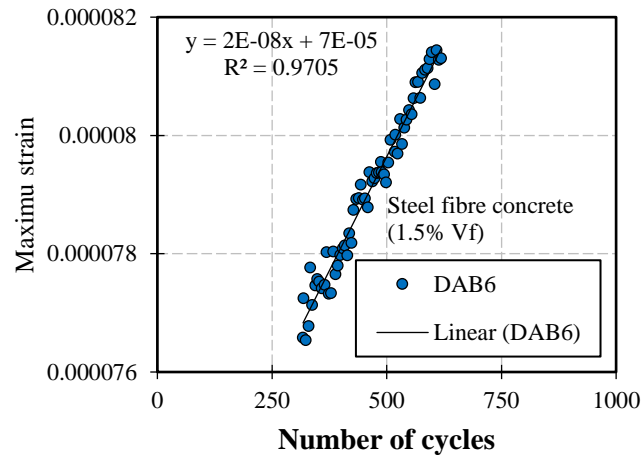
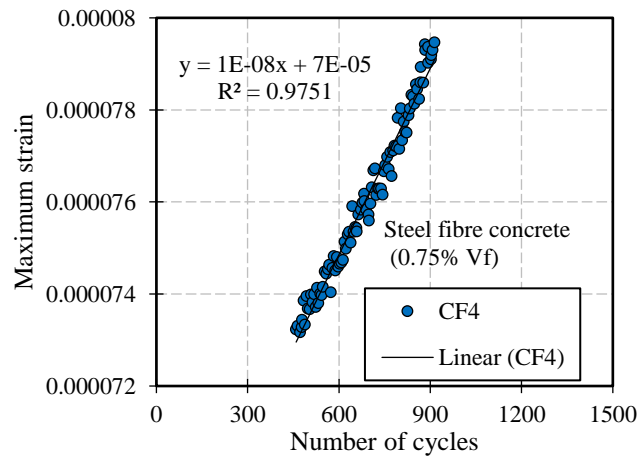
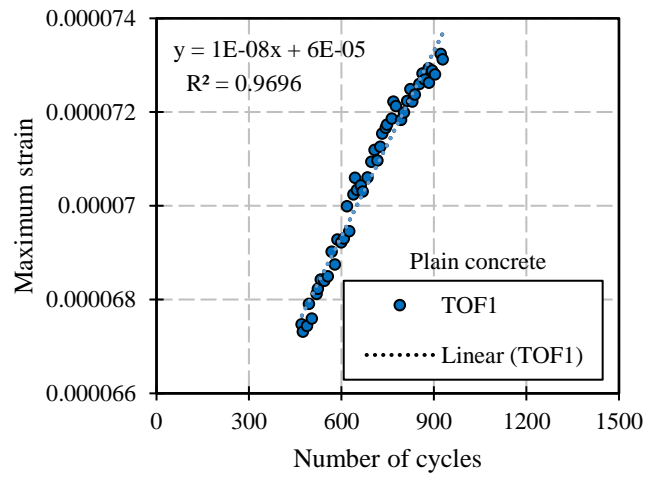


Fig. 4.7 - Secondary strain rate for plain and steel fiber concrete.

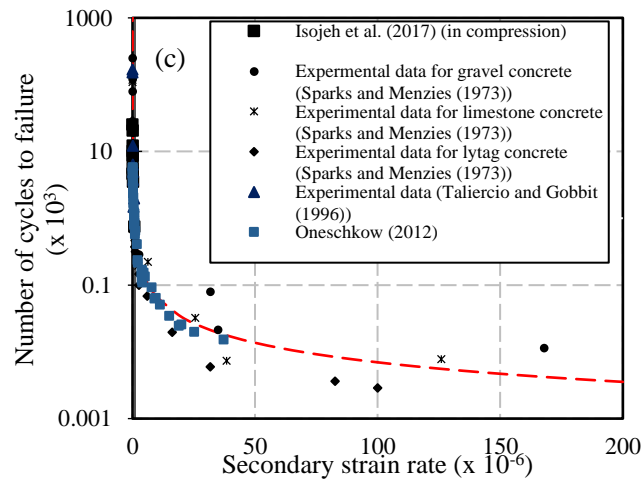
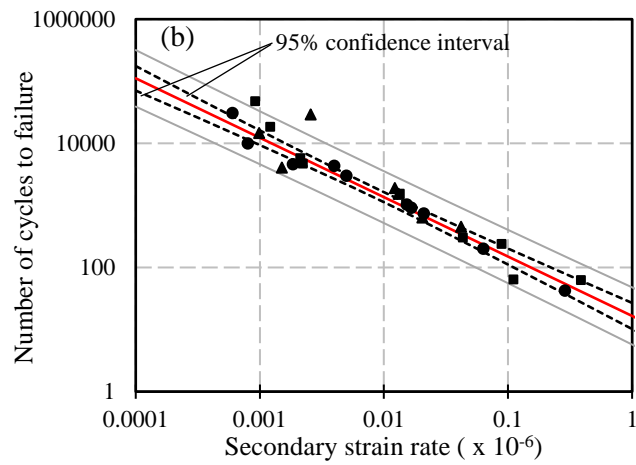
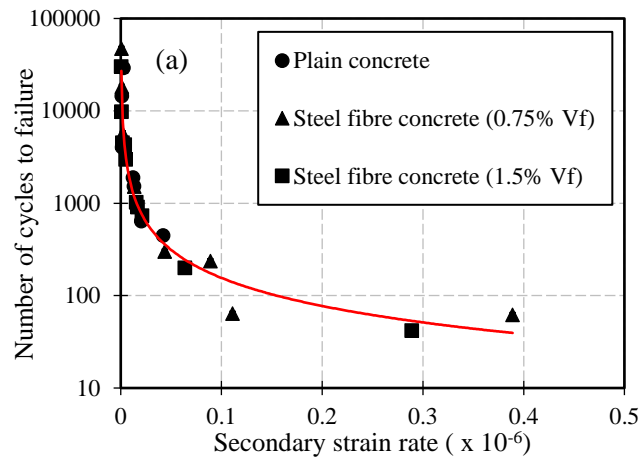


Fig. 4.8 - Plot of number of cycles to failure against secondary strain rate.

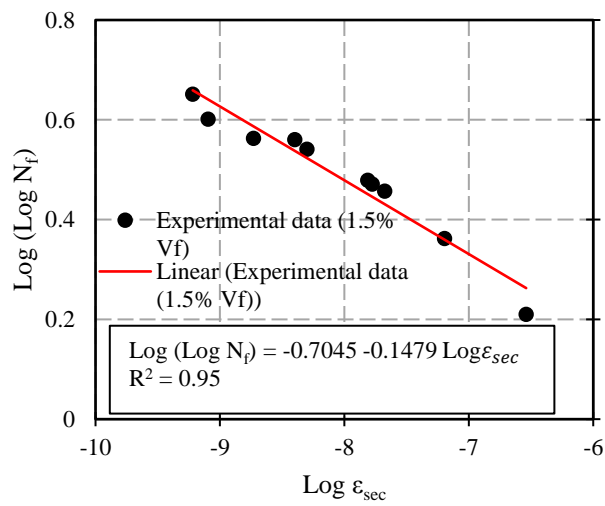
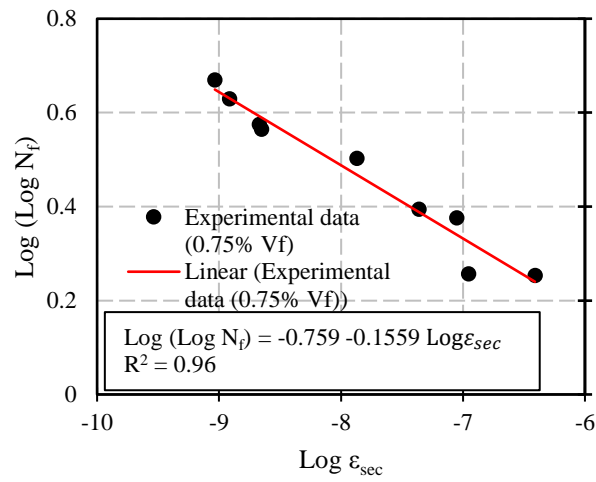
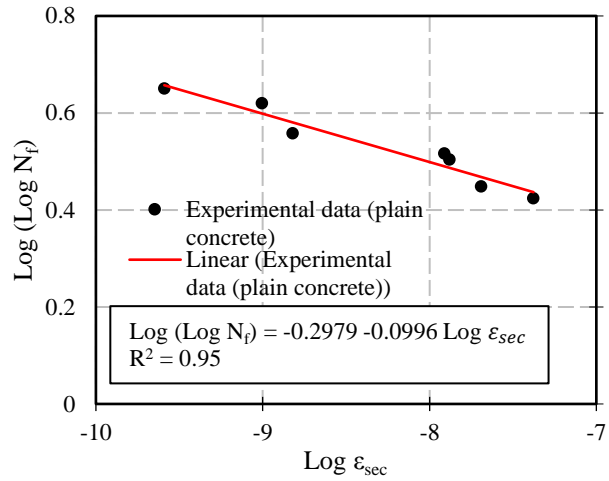


Fig. 4.9 - Plot of  $\text{Log (Log } N_f)$  versus  $\text{Log } \epsilon_{sec}$ .

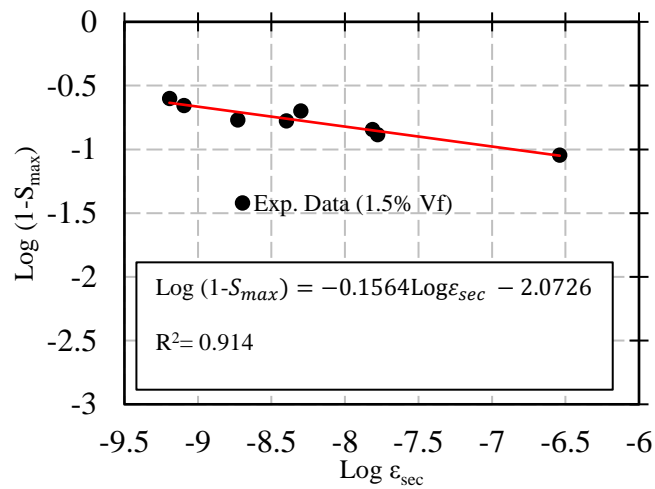
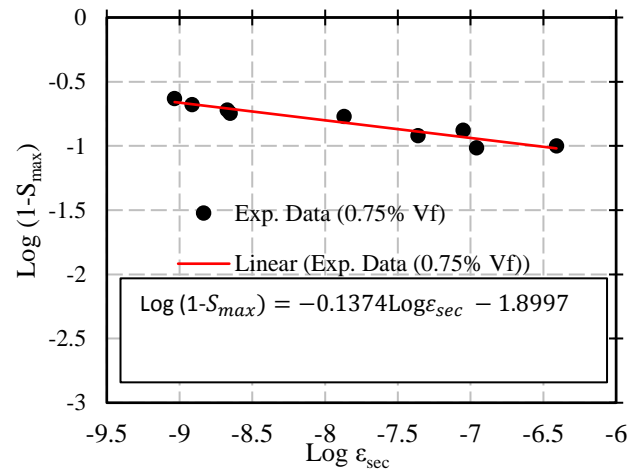
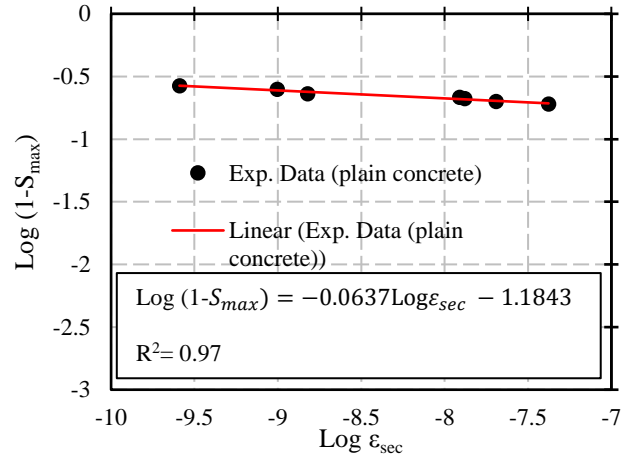


Fig. 4.10 - Plot of  $\text{Log}(\text{Log } N_f)$  versus  $\text{Log } \epsilon_{sec}$ .

The values for the material parameters are given in Table 4.3 for plain concrete, and for fibre

concrete with 0.75% and 1.50% fibre volume content. As observed, the material parameter obtained for plain concrete is similar to that observed in the literature; hence, the approach developed for the determination of the material parameter ( $\beta$ ) and the estimated parameters for steel fibre is reasonable.

Table 4.3 - Material parameter for plain and steel fibre reinforced concrete.

| Fibre volume content<br>% Vf | Coefficient<br>A | Coefficient<br>B | Coefficient<br>C | Coefficient<br>D | Material parameter<br>$\beta$ |
|------------------------------|------------------|------------------|------------------|------------------|-------------------------------|
| 0                            | -0.2979          | -0.0996          | -1.1843          | -0.0637          | 0.0968                        |
| 0.75                         | -0.759           | -0.1559          | -1.8997          | -0.1374          | 0.0588                        |
| 1.50                         | -0.7045          | -0.1479          | -2.0726          | -0.1564          | 0.0470                        |

The values of A, B, C, and D may vary depending on the loading parameters selected. However, for loading parameters different from those used in this investigation, the combination of the parameters (A, B, C, and D) used in obtaining the material constant ( $\beta$ ) in Equation 4.8 will result in a value similar to the actual material constant in the Aas-Jakobsen and Lenschow linear model.

#### 4.7 Damage Evolution for Steel Fibre Residual Strength and Secant Modulus

Modified damage evolution models have been proposed previously by the authors for concrete residual strength and fatigue secant modulus (Equation 4.9) (Isojeh et al., 2017) (Chapter 2). The models are functions of the maximum stress level, critical damage value, damage parameter  $s$ , and material parameter  $\beta$ . The critical damage is the percentage reduction in concrete strength or fatigue secant modulus at failure. The values were reported to be 0.35 and 0.40 for concrete strength and fatigue secant modulus, respectively. Using these values for steel fibre concrete will give reasonable and conservative models.

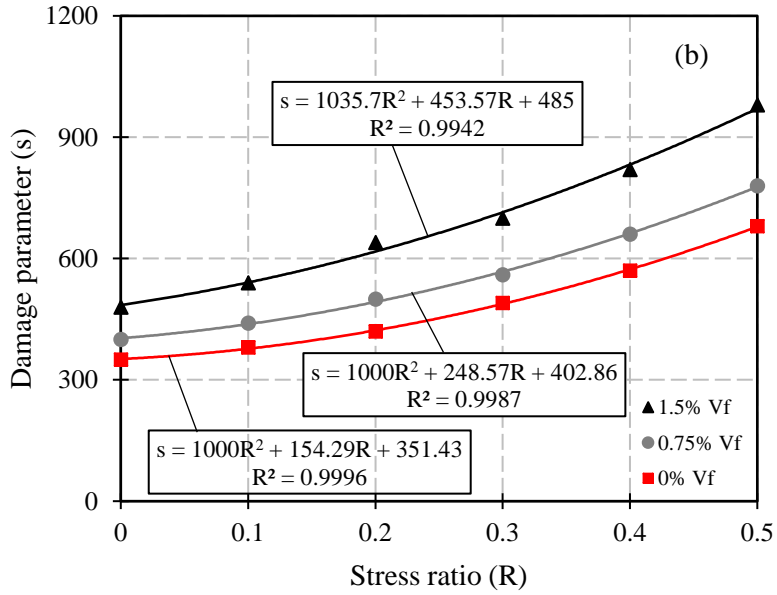
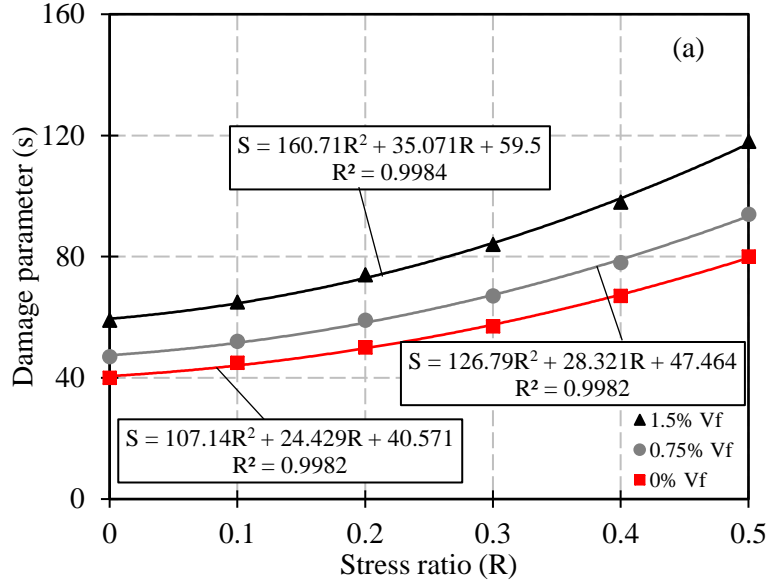


Fig. 4.11 – (a) Damage parameter  $s$  for secant modulus of steel fibre concrete; (b) residual strength of steel fibre concrete.

$$D = D_{cr} \text{Exp} \left[ s \left( \frac{\Delta f}{f_c} - C_f \right) \right] N^v \quad (4.9)$$

$$v = 0.434 s C_f (\beta(1 - R)) \quad (4.10)$$

From Zhang et al. (1996) on influence of loading frequency,

$$C_f = ab^{-\log f} + c \quad (4.11)$$

where  $N$  is the number of cycles,  $s$  is the damage parameter,  $D_{cr}$  is the critical damage value, and  $C_f$  accounts for fatigue frequency.

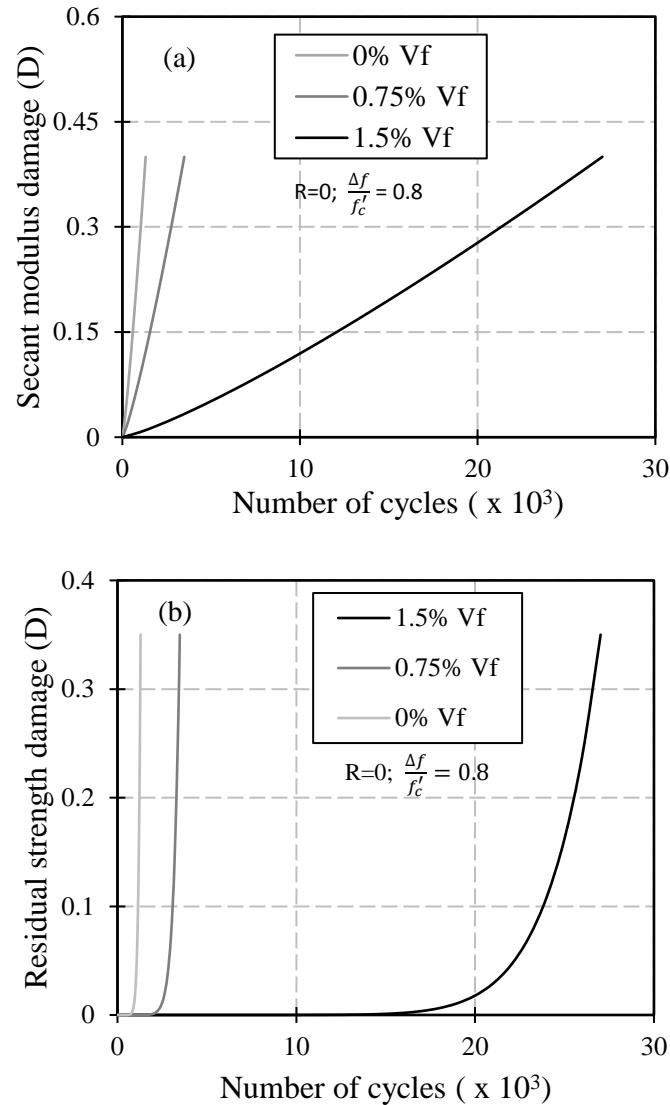


Fig. 4.12 - Damage evolution for steel fibre concrete: (a) residual strength; (b) fatigue secant modulus.

Test data from Zhang et al. (1996) were used to obtain optimized values of the parameters (a,b, and c) in Equation 4.11. These are given as 0.283, 0.941 and 0.715, respectively. The residual

strength and fatigue secant modulus degradation can be estimated by substituting the material parameter  $\beta$  for steel fibre concrete into the damage model.

The parameter  $s$  in the damage model depends on the stress ratio  $R$  and can be estimated from Figure 4.11 for stress ratio values between 0 and 0.5. The damage evolution of plain and steel fibre reinforced concrete strength and fatigue secant modulus (0%, 0.75%, and 1.5% Vf) under fatigue loading at a maximum stress level of 0.8, stress ratio of zero, and a frequency of 5 Hz, are given in Figure 4.12. As observed, as the steel fibre volume content increased from 0 to 1.5% Vf, the number of cycles leading to failure increased with corresponding delays in progressive damage.

#### **4.8 Conclusions**

Fatigue tests were conducted to study the progressive behaviour and to develop damage and material parameters for steel fibre concrete under fatigue loading. To achieve this, a new concept was used to develop the required material parameters for plain and steel fibre reinforced concrete. From a comparison of the deformation evolution profiles in this investigation with those from compression fatigue tests in the literature, similarities were observed for tension and compression fatigue loading. Further, fatigue life was found to increase as the steel fibre volume content in concrete increased from 0% to 1.5%. The concept used in deriving the material parameter seems appropriate since the value obtained for plain concrete agrees well with values in the literature. The damage models which incorporate the estimated material and damage parameters for steel fibre concrete can be implemented into constitutive models to enhance fatigue analyses of steel fibre concrete structures.

#### 4.9 References

1. Aas-Jacobsen K. (1970). "Fatigue of Concrete Beams and Columns." Trondheim: Institutt for Betonkonstruksjoner, Bulletin No 70-1, 148 pp.
2. Chang D., and Chai W. (1995). "Flexural Fracture and Fatigue Behaviour of Steel-Fibre Reinforced Concrete Structures." Nuclear Engineering and Design, Vol. 156, pp. 201-207.
3. Chenkui H., and Guofan Z. (1995). "Properties of Steel Fibre Reinforced Concrete Containing Larger Coarse Aggregate." Cement & Concrete Composites, Vol. 17, pp.199-206.
4. Cornelissen H.A.W., and Reinhardt H.W. (1984). "Uniaxial Tensile Fatigue Failure of Concrete under Constant-Amplitude and Programme Loading." Magazine of Concrete Research, Vol. 36, No. 129, pp.216-226.
5. Cornelissen H.A.W., and Reinhardt H.W. (1987). "Effect of Static and Fatigue Preloading on Residual Strength and Stiffness of Plain Concrete." Fracture Control of Engineering Structures- ECF 6.
6. Davies J.D., and Bose D.K. (1968). "Stress Distribution in Splitting Tests." ACI Journal, Proceeding Vol. 65, No. 8, pp. 662-669.
7. FIB (2010). "Model Code for Concrete Structures (First Edition)." Fib-Federation international du beton/International Federation for Structural Concrete, Ernst & Sohn GmbH & Co. KG.
8. Guo Z. (2014). "Principles of Reinforced Concrete: Fatigue Resistance." Tsinghua University Press.

9. Isojeh B., El-Zeghayar M., and Vecchio, F.J. (2016). "Concrete Damage under Fatigue Loading in Uniaxial Compression." *ACI Materials Journal*, Vol. 114, No. 2, pp. 225-235.
10. Maekawa K., Toongoenthong K., and Gebreyouhannes E., and Kishi T. (2006). "Direct Path-Integral Scheme for Fatigue Simulation of Reinforced Concrete in Shear." *Journal of Advanced Concrete Technology*, Vol. 4, No. 1, pp. 159-177.
11. Naaman A.E., and Hammoud H. (1998). "Fatigue Characteristics of High Performance Fibre- Reinforced Concrete." *Cement and Concrete Composites*, Vol. 20, pp. 353-363.
12. Nanni A. (1991). "Fatigue Behaviour of Steel Fibre Reinforced Concrete." *Cement & Concrete Composites*, Vol. 13, pp. 239-245.
13. Oh B.H. (1986). "Fatigue Analysis of Plain Concrete in Flexure." *ASCE Journal of Structural Engineering*, Vol. 112, No. 2, pp. 273-288.
14. Oneschkow N. (2012). "Influence of Loading Frequency on the Fatigue Behaviour of High-Strength Concrete." *Proceedings of the 9<sup>th</sup> fib International Phd Symposium in Civil Engineering, Karlsruhe, Germany.*
15. Petryna Y.S., Pfanner D., Stangenberg F., and Kratzig, W.B. (2002). "Reliability of Reinforced Concrete Structures under Fatigue." *Reliability Engineering and System Safety*, Vol. 77, pp. 253-261.
16. Ramakrishnan V., Wu Y.G., and Hossali G. (1989). "Flexural Fatigue Strength, Endurance Limit and Impact Strength of Fibre Reinforced Concretes." *Transport Research Board, Washington, D.C.*

17. Saito M., and Imai S. (1983). "Direct Tensile Fatigue of Concrete by the Use of Friction Grips." *ACI Journal*, Vol. 80, No. 5, pp. 431-438.
18. Singh S.P., and Kaushik S.K. (2001). "Flexural Fatigue Analysis of Steel Fibre-Reinforced Concrete." *ACI Materials Journal*, Vol. 98, No. 4, pp. 306-312.
19. Sparks P.R., and Menzies J.B. (1973). "The Effect of Rate of Loading upon the Static and Fatigue Strength of Plain Concrete in Compression." *Mag. Concrete Res.*, Vol. 25, pp. 73-80.
20. Taliercio A.L.F., and Gobbit E. (1996). "Experimental Investiagtion on the Triaxial Fatigue Behaviour of Plain Concrete." *Magazine of Concrete Research*, Vol. 48, No. 176, pp. 157-172.
21. Tepfers R. (1979). "Tensile Fatigue Strength of Plain Concrete." *ACI Journal*. Title no. 76-39, pp. 919-933.
22. Tepfers R., and Kutti T. (1979). "Fatigue Strength of Plain, Ordinary, and Lightweight Concrete." *ACI Journal*, Vol. 76, pp. 635-652.
23. Thun H., Ohlsson U., and Elfgrén L. (2011). "A Deformation Criterion for Fatigue of Concrete." *Structural Concrete*, Vol. 12, No. 3, pp. 187-197.
24. Torrenti J.M., Pijaudier-Cabot G., and Reynouard J. (2010). "Mechanical Behaviour of Concrete." *John Wiley& Sons, Inc.*, pp. 185-223.
25. Vega I.M., Bhatti M.A., and Nixon W.A. (1995). "A Nonlinear Fatigue Damage Model for Concrete in Tension." *International of Journal of Damage Mechanics*, Vol.4, pp. 362-379.

26. Zhang J., Stang H., and Li V.C. (1999). "Fatigue Life Prediction of Fibre Reinforced Concrete under Flexural Load." *International Journal of Fatigue*, Vol. 21, pp. 1033-1049.
27. Zhang B., Phillips D.V., and Wu K. (1996). "Effects of Loading Frequency and Stress Reversal on Fatigue Life of Plain Concrete." *Magazine of Concrete Research*, VI. 48, No. 177, pp. 361- 375.

## CHAPTER 5

### FATIGUE RESISTANCE OF STEEL-FIBRE REINFORCED CONCRETE DEEP BEAMS

*The material in this chapter was accepted for publication, as follows:*

*Isojeh B., El-Zeghayar M., Vecchio, F.J. "Fatigue Resistance of Steel-Fibre Reinforced Concrete Deep Beams." ACI Structural Journal (in-press).*

#### **5.1 Abstract**

An investigation into the fatigue resistance of small-scale steel-fibre reinforced concrete deep beams, with steel-fibre volume ratios of 0%, 0.75% and 1.5%, is reported. The behaviour of steel fibres in enhancing the fatigue life of deep beams and reducing the congestion of reinforcement in concrete structures is studied, and the possibility of obtaining optimised structural sections which are cost effective using steel-fibre reinforced concrete is verified. Evolutions and inclinations of average principal strains and bond strength between concrete and steel reinforcing bars within the shear spans are also examined. The use of steel fibres, especially with a volume ratio of 1.5%, was observed to reduce the progressive strain values in concrete and steel reinforcing bars, hence resulting in enhanced fatigue life. No significant evolution profile was observed for the inclination of the principal directions, while the use of adequate anchorage preserved the bond strength between concrete and steel reinforcement. In all specimens, fracture of the longitudinal reinforcing bars occurred at failure, and fibre pull-out was more prevalent than fibre breakage.

Keywords: deep beam, fatigue, steel fibre, strain evolution, strength, wind turbine foundations.

## 5.2 Introduction

In practice, some elements of fatigue-sensitive structures such as wind turbine foundations, offshore structures, transfer girders, and pile caps, are generally designed as deep beams. Due to the dynamic nature of loading while in service, these structures are susceptible to fatigue failure resulting from reinforcement fracture, crushing of concrete struts coupled with irreversible compressive strain accumulation, or excessive opening of concrete cracks. As such, it is expedient that designs guard against the occurrence of such failure modes during the service life of the structure (Teng et al., 1998; Teng et al., 2000; Isojeh and Vecchio, 2016).

In the literature, the fatigue failure resistance of deep beams has been shown to be enhanced using increased amounts of vertical or longitudinal reinforcement. The use of horizontal or inclined web reinforcement has also been reported to enhance the fatigue life of deep beams (Teng et al., 1998; Teng et al., 2000). Although the provision of more reinforcing bars and the use of inclined reinforcement have been shown to enhance fatigue performance, the congestion of reinforcement (ACI 318/ACI 346) during construction has prompted further investigation of other possible means. As well, the need for optimised designs involving cost-effective and reduced sizes of fatigue-prone structures necessitates the consideration of other enhanced concrete composites (Chenkui and Guofan, 1995; RILEM Proceeding 31).

Steel-fibre reinforced concrete exhibits improved properties such as increased toughness, ductility, and crack-bridging attributes which result in the increase of the load resistance capacity when compared to conventional reinforced concrete. The enhancing performance of steel fibres, especially after cracking of concrete, has been attributed to the ability of the fibres to delay crack growth by bridging the crack surfaces (Lee and Barr, 2004; ACI 544; ACI 506).

At the material level, flexural fatigue tests conducted on steel-fibre reinforced concrete prisms by Ramakrishnan et al. (1989), Nanni (1991), Chenkui and Guofan (1995), Chang and Chai (1995), and Naaman and Hammoud (1998) all indicate enhanced fatigue life and reduced progressive deformation when compared with plain concrete prisms. It has also been reported that steel-fibre reinforced concrete beams subjected to fatigue stresses below the observed endurance limit exhibited increases in strength when subsequently subjected to monotonic loading.

In steel-fibre reinforced concrete beams also containing conventional longitudinal reinforcement, the influence of steel-fibre crack-bridging reduces the induced stresses in the longitudinal reinforcing bars; hence, the number of cycles at which fracture will occur in the steel reinforcing bars is increased compared to conventional reinforced concrete without steel fibres (Ramakrishnan et al., 1989). Experimental investigations on the fatigue behaviour of steel-fibre reinforced concrete beams are scarce and, prior to the investigation reported in this paper, no fatigue tests conducted on steel-fibre reinforced concrete beams with shear-span to effective depth ratios less than 2.5 had been reported. However, tests conducted by Kormeling et al. (1980) on beams governed by flexure showed the enhancing effects of steel fibres on fatigue life, progressive deflection, and crack width growth.

The significant influence of steel fibres in reinforced concrete beams under fatigue loading has been reported by Kwak et al. (1991) through tests conducted on steel-fibre reinforced concrete beams with shear-span to effective depth ratio of 2.5. The fatigue failure mechanism of steel fibres using different volume ratios was observed to be a result of fibre fracture rather than pull-out.

Parvez and Foster (2013, 2015) investigated the influence of steel fibres on the fatigue behaviour of small-scale and large-scale reinforced concrete beams governed by flexure. The final failure mechanism in all beams was fracture of the longitudinal reinforcement. Generally, it was

reported that steel reinforcing bar fracture propagation governed the fatigue life of under-reinforced beams. Further, the fatigue life of beams with steel fibres was enhanced and the measured deformations and stresses were observed to decrease as the volume ratio increased from 0% to 0.8%.

Although Parvez and Foster (2015) reported that the reduction in steel reinforcing bars strain after some cycles was a result of debonding which led to the loss of tension stiffening, no practical results showing the strain variation or bond slip between concrete and a steel reinforcing bar were reported. The segmental protection of the strain gauges on the reinforcing bars may have resulted in debonding between concrete and steel reinforcement. However, further investigation is required in order to observe the bond behaviour under fatigue loading of well-anchored embedded reinforcement.

As part of a long-term research program on the improvement of the design and analysis of wind turbine foundations using steel-fibre reinforced concrete, this investigation considers the behaviour of shear-critical beams under fatigue loading by observing the principal strain and shear strain evolutions within the planes of the shear spans. Further, the inclination of the principal strains and the bond behaviour between concrete and steel reinforcement are considered.

### **5.3 Research Significance**

This investigation considers the influence of steel fibres in enhancing the fatigue life of shear-critical deep beams. A new approach is presented drawing on a comparison between conventional reinforced and steel-fibre reinforced concrete deep beams using the progressive average principal strain and shear strain evolutions within the shear-span. Tests have not been previously reported

for elements with a shear-span to effective depth ratio of less than 2.5. The observed results show that the fatigue life of deep beams can be enhanced using steel fibres, and optimized designs of steel fibre fatigue-prone structures can be extended to deep beams.

## **5.4 Experimental Investigation**

### **5.4.1 Test Specimens**

Deep beams with dimensions of 175 x 250 x 700 mm were used in this experimental investigation (Figure 5.1). The supports were prepared such that no lateral restraint was permitted. To achieve this, the roller between the two grooved plates (Figure 5.1) was made smaller than the groove size.

The properties of the beams tested are given in Tables 5.1 and 5.2. The reinforcement provisions used for the beams surpassed the minimum required in CSA (2004) A23.3-04 11.2.8.1 and 11.2.8.2 for shear, and 10.5.1.2 for flexure, Eurocode 2-1-1(2004) 9.2.1.1 and 9.2.1.1 for shear and flexure respectively, and ACI 318-14 to 346-09 Section R9.6.3.1 and R9.6.1.2 for shear and flexure respectively.

As a means of ensuring that bond fatigue failure was deliberately averted, adequate anchorage was provided based on code requirements CSA (2004) - N12.13.1, N12.13.2 (shear reinforcement anchorage), and N12.5.2 (flexural reinforcement anchorage). The bar bending detail used for anchorage also satisfied EC 2-1-1 (2004) clause 8.5(1) and (2) for shear reinforcement and 2-1-1 clause 8.4.1 (1) P for longitudinal reinforcement requirements. The anchorage also satisfied ACI 318-14 to 346-09 Table 25-3-1 and Table 25.3.2 for longitudinal and shear reinforcement respectively.

Two different steel-fibre volume ratios, 0.75% and 1.50%, were examined. High strength end-hooked steel fibres (Dramix RC80/30BP) were used. The geometrical properties of the fibres

included a 30 mm fibre length, a diameter of 0.37 mm, and an aspect ratio of 79. The ultimate tensile stress capacity of the steel fibres was 3070 MPa. Longitudinal reinforcement ratios of 0.45% and 0.90% and shear reinforcement ratios of either 0% or 0.20% were provided in beams having steel-fibre volume ratios of 0.75% and 1.50% in this investigation.

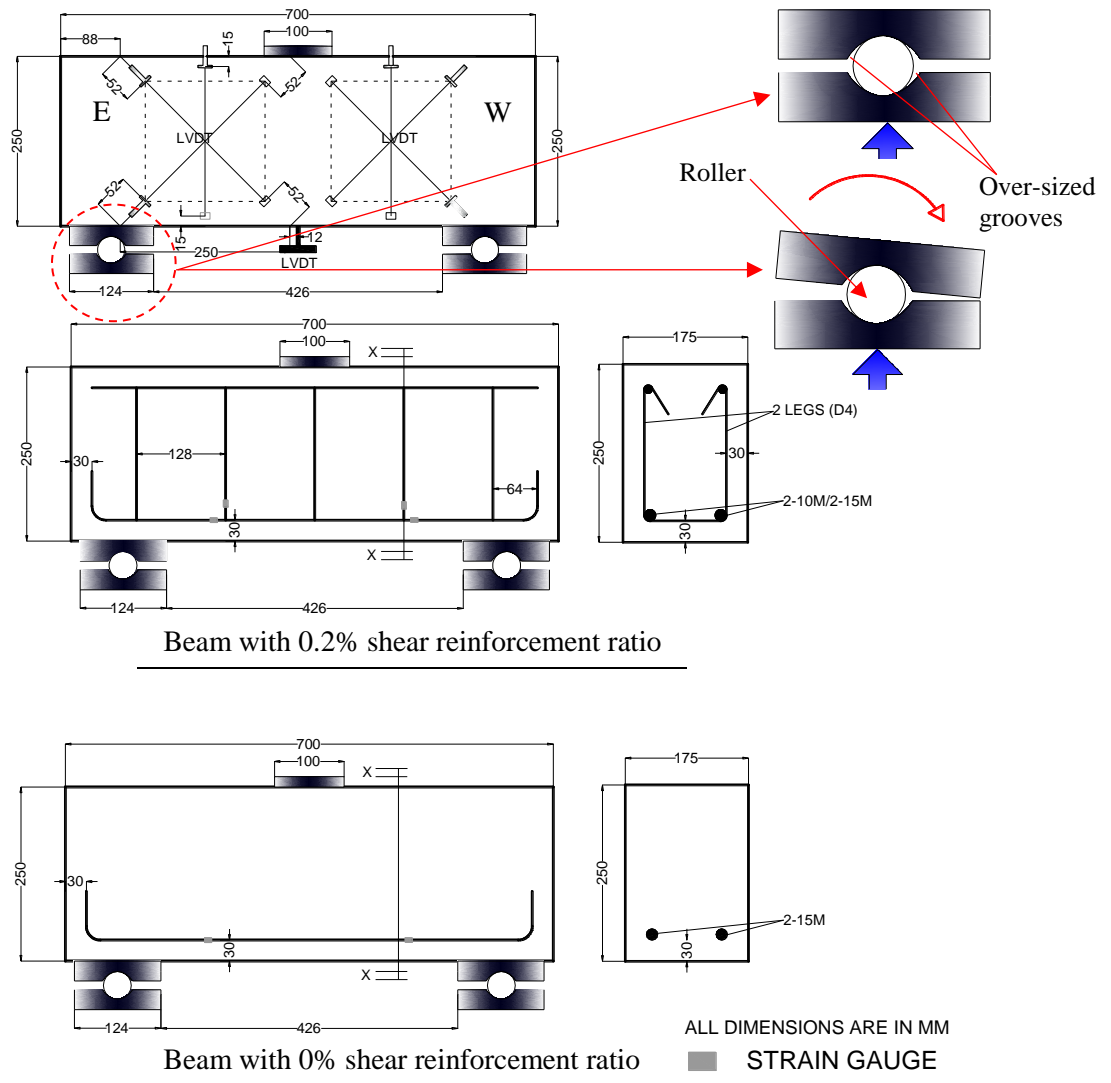


Fig. 5.1 - Details of deep beam specimen.

In Table 5.2, the names attached to each beam are given; C'S and CS are assigned to beams (monotonic tests) without steel fibres and reinforced with 2-10M and 2-15M reinforcing bars,

respectively. Similarly, C and C' are assigned to the control beams (beams without steel fibres) reinforced with 2-10M and 2-15M reinforcing bars, respectively.

Table 5.1- Average compressive strength of concrete.

| Concrete Batch | Volume of steel fibre ( $V_f$ %) | No. of Specimens | Average compressive Strength ( $f_c'$ ) MPa | Standard Deviation (compressive strength) | Coefficient of Variation (compressive strength) |
|----------------|----------------------------------|------------------|---|---|---|
| 1              | $0 V_f^1$                        | 13               | 62.6  | 6.0                                       | 8.5   |
| 2              | $0 V_f^2$                        | 18               | 55.1  | 2.5                                       | 4.6   |
| 3              | $0.75 V_f$                       | 23               | 55.3  | 5.2                                       | 9.5   |
| 4              | $1.5 V_f$                        | 24               | 55.8  | 5.1                                       | 9.1   |
| 5              | $1.5 V_f^*$                      | 8                | 55.6  | 2.1                                       | 3.7   |

where:

$V_f$  % = steel fibre volume content (in percentage)

$0 V_f^1$ : batch without steel fibre for control beam specimens tested under fatigue loading.

$0 V_f^2$ : batch without steel fibre for specimens tested under monotonic loading.

$V_f^*$  = steel fibre volume for B80-0N1.5 and A97-0F1.5

Table 5.2: Specimen description.

| Concrete Batch | Volume of Steel Fibre $V_f$ (%) | Specimen Identification Number | Design $f_c^d$ MPa | $\rho_l$ (%) | $\rho_v$ (%) | Maximum Fatigue Load (% Pu) kN | Minimum Fatigue Load (% Pu) kN | No. of cycles to Failure (N) |
|----------------|---------------------------------|--------------------------------|--------------------|--------------|--------------|--------------------------------|--------------------------------|------------------------------|
| 2              | 0                               | C'S                            | 50                 | 0.9          | 0.2          | Monotonic                      | -                              | -                            |
| 2              | 0                               | CS                             | 50                 | 0.45         | 0.2          | Monotonic                      | -                              | -                            |
| 1              | 0                               | C'-70-0                        | 50                 | 0.9          | 0.2          | 70                             | 1.3                            | 210,000                      |
| 3              | 0.75                            | B70-0F0.75                     | 50                 | 0.9          | 0.2          | 70                             | 1.3                            | 3,000,000 <sup>a</sup>       |
| 4              | 1.5                             | B70-0F1.5                      | 50                 | 0.9          | 0.2          | 70                             | 1.3                            | 3,000,000 <sup>a</sup>       |
| 1              | 0                               | C-80-0                         | 50                 | 0.45         | 0.2          | 80                             | 1.8                            | 47,000                       |
| 3              | 0.75                            | A80-0F0.75                     | 50                 | 0.45         | 0.2          | 80                             | 1.8                            | 66 000                       |
| 4              | 1.5                             | A80-0F1.5                      | 50                 | 0.45         | 0.2          | 80                             | 1.8                            | 320 000                      |
| 5              | 1.5                             | A97-0F1.5                      | 50                 | 0.45         | 0.2          | 97                             | 1.8                            | 81 000                       |
| 1              | 0                               | C-70-0                         | 50                 | 0.45         | 0.2          | 70                             | 1.8                            | 72 000                       |
| 3              | 0.75                            | A70-0F0.75                     | 50                 | 0.45         | 0.2          | 70                             | 1.8                            | 123 000                      |
| 3              | 0.75                            | A70-0N0.75                     | 50                 | 0.45         | 0            | 70                             | 1.8                            | 260 000                      |
| 4              | 1.5                             | A70-0F1.5                      | 50                 | 0.45         | 0.2          | 70                             | 1.8                            | 410 000                      |
| 1              | 0                               | C'-80-0                        | 50                 | 0.9          | 0.2          | 80                             | 1.3                            | 62 000                       |
| 5              | 1.5                             | B80-0N1.5                      | 50                 | 0.9          | 0            | 80                             | 1.3                            | 650 000                      |

where:

$V_f$  (%) = steel fibre volume content (in percentage)

$f_c^d$  = design compressive strength of concrete

$\rho_l$  (%) = longitudinal reinforcement ratio (in percentage)

$\rho_v$  (%) = shear reinforcement ratio (in percentage)

<sup>a</sup> = specimen did not fail at the specified number of cycles

A and B represent steel-fibre reinforced concrete beams with 2-10M and 2-15M reinforcing bars, respectively. The numbers 70-0, 80-0, 97-0 represent the maximum load level used for the fatigue tests. The letter N denotes no shear reinforcement, while F0.75 and F1.5 represent the steel fibre volume contents used.

### **5.4.2 Materials**

A design compressive strength of 50 MPa was selected, with a maximum aggregate size of 10 mm. The slump readings obtained during concrete casts were between 80 and 150 mm. After casting, the specimens were removed from the curing room at 28 days and placed in a dry compartment. The average compressive strengths of concrete cast for the tests are given in Table 5.1. The value given in the fourth column of Table 5.1, for the fatigue loading phase, is equivalent to the average compressive strength within the time frame for testing the beams.

Canadian standard 15M, 10M, and D4 bars were used as reinforcement. The D4 reinforcing bars were used for the shear reinforcement. In the beams with shear reinforcement, 2-10M reinforcing bars were also provided as the top (hanger) bars.

The average yield strength obtained for the 15M, 10M, and D4 reinforcing bars were 430 MPa, 480 MPa, and 610 MPa respectively. The yield strength of the cold-worked steel rebar corresponded to the 0.2% offset strains. Although the expected yield plateau was absent in the cold-worked D4 stress-strain curve, the stresses observed in the shear reinforcement were sufficiently low to justify their use.

### **5.4.3 Test Procedure**

Initially two beams, C'S and CS as indicated in Table 5.2, were tested under monotonic loading. The corresponding failure loads observed were 390 kN and 270 kN respectively (Figure 5.2). The

longitudinal reinforcement ratios were varied in order to observe different failure mechanisms. The failure mode of C'S was observed to be crushing of the compression strut. A combination of shear and flexure was observed in CS, as the fracture of the reinforcing bars occurred at the mid-span region. As indicated in the sixth and seventh column of Table 5.2, percentages of the failure load observed from the monotonic tests were used for the fatigue tests conducted. Each specimen was subjected to fatigue loading without an initial application of monotonic loading.

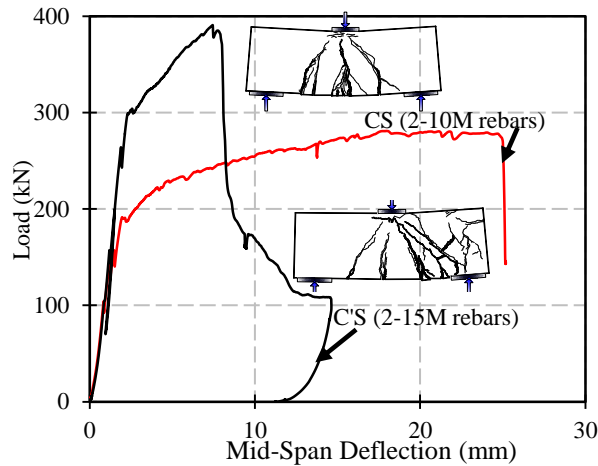


Fig. 5.2 - Load versus deflection under monotonic loading (Beams C'S and CS).

The fatigue tests were conducted using servo-hydraulic testing equipment having a loading capacity of 350 kN. The loading equipment was used to generate a pulsating load of a continuous sinusoidal waveform throughout the test duration. All fatigue tests were conducted at a frequency of 5 Hz, and a constant minimum load of 5 kN was used in order to prevent backlash due to inertia of the actuator under dynamic loading. The stress ratio resulting from this minimum load is considered to be insignificant (i.e., approximately equal to 0.0).

#### 5.4.4 Instrumentation

Figure 5.1 shows the details of the beam specimen dimensions and instrumentation. The attached LVDTs were used to measure the evolution of the average strains within the shear span. Using

a Mohr's circle of strain, the average shear strains, the average principal strains, and the inclination of the principal tensile strain relative to the x- and y-directions within the shear spans of each beam were obtained from strain transformations of the LVDT data (Figure 5.3). In Figure 5.3,  $\varepsilon_1$  is the principal tensile strain,  $\varepsilon_2$  is the principal compressive strain,  $e_a$ ,  $e_b$ , and  $e_c$  are the corresponding strains in the directions of the LVDTs,  $\gamma_{xy}$  is the average shear strain,  $\varepsilon_x$  and  $\varepsilon_y$  are the average strains in the horizontal and vertical directions, respectively, and  $\theta$  is the inclination of the average principal tensile strain. A program was developed to generate the deformation evolutions from the laboratory data.

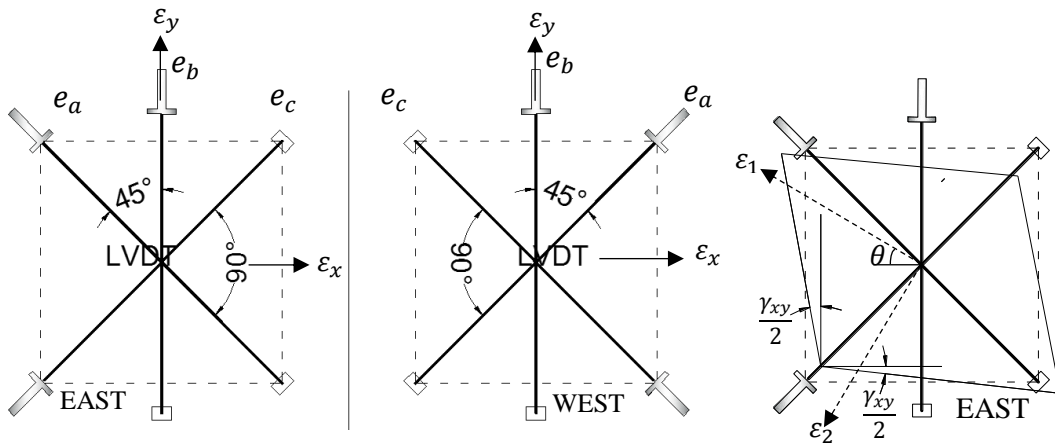


Fig. 5.3 - LVDTs strain transformation.

Considering the West LVDTs, ( $\gamma_{xy}$  is positive)

$$\varepsilon_x = e_c - e_b + e_a$$

where  $\varepsilon_y = e_b$

$$\gamma_{xy} = e_a - e_c \tag{5.1}$$

Considering the East LVDTs, ( $\gamma_{xy}$  is negative)

$$\varepsilon_x = e_c - e_b + e_a$$

where  $\varepsilon_y = e_b$

$$\gamma_{xy} = e_c - e_a \quad (5.2)$$

The average principal concrete strains were obtained thus:

$$\varepsilon_{1,2} = \frac{1}{2}(\varepsilon_x + \varepsilon_y) \pm \frac{1}{2} \left( \sqrt{(\varepsilon_x - \varepsilon_y)^2 + \gamma_{xy}^2} \right) \quad (5.3)$$

The averages of the strain values obtained from the East and West sets of LVDTs were used. The values for the evolution of  $\theta$ , the inclination of the principal tensile strain direction, was estimated using  $\gamma_{xy}$  (shear strain),  $\varepsilon_x$  (average strain in the horizontal direction) and  $\varepsilon_y$  (average strain in the vertical direction).

## 5.5 Test Results and Discussions

The number of cycles leading to failure for each specimen tested under fatigue loading is given in Table 5.1. The experimental results are expressed in terms of failure modes, principal strain evolutions, shear strain evolutions, mid-span deflections, and residual strengths of beams that did not fail after 3,000,000 cycles (see Figures 5.4 to 5.16). These are discussed subsequently.

### 5.5.1 Failure Mode

In all beam specimens tested, except specimens B70-0 F0.75 and B70-0 F1.5 which sustained 3,000,000 million cycles without failure, fracture of the longitudinal reinforcing bars was observed. An increase in the fatigue life was observed for the beams as the fibre volume content increased (as shown in columns 2 and 9, Table 5.2). In the steel-fibre reinforced concrete beams, a combination of pull-out and fracture of steel fibres were also observed. However, steel fibre pullout was more prevalent, especially in beams reinforced with 1.5% steel-fibre volume ratio compared to beams with 0.75% steel-fibre volume ratio. This is attributed to lower stresses

induced in steel fibres with 1.5% steel-fibre volume ratio at crack-bridges; hence bond resistance between steel fibres and concrete governed. On the other hand, fracture of steel fibre predominated due to high stresses. Throughout the tests conducted, no fracture of shear reinforcement was observed (see Appendix E and F). This observation is consistent with those reported in the literature for conventional reinforced concrete deep beams (Teng et al., 1998; Teng et al., 2000).

The strain induced in the longitudinal reinforcing bars was observed to reduce as the steel-fibre volume ratio increased from 0.75% to 1.5%. (e.g., see Figure 5.4 for beams with 2-10M rebars). The strain evolution for beam A70-0NF0.75 reinforced with 2-10M reinforcing bars was truncated after 10,000 cycles due to a malfunction of the strain gauge attached to the longitudinal reinforcement. The reinforcement strain evolutions shown in Figure 5.4 were obtained from the region at which fracture occurred, hence in close proximity to the maximum strain along the longitudinal reinforcement. As also reported in the literature on flexural beams (Parvez and Foster, 2013, 2015), the reduced strain or stress values (attributed to the addition of steel fibres) resulted in the enhanced fatigue life of the steel-fibre reinforced concrete beams.

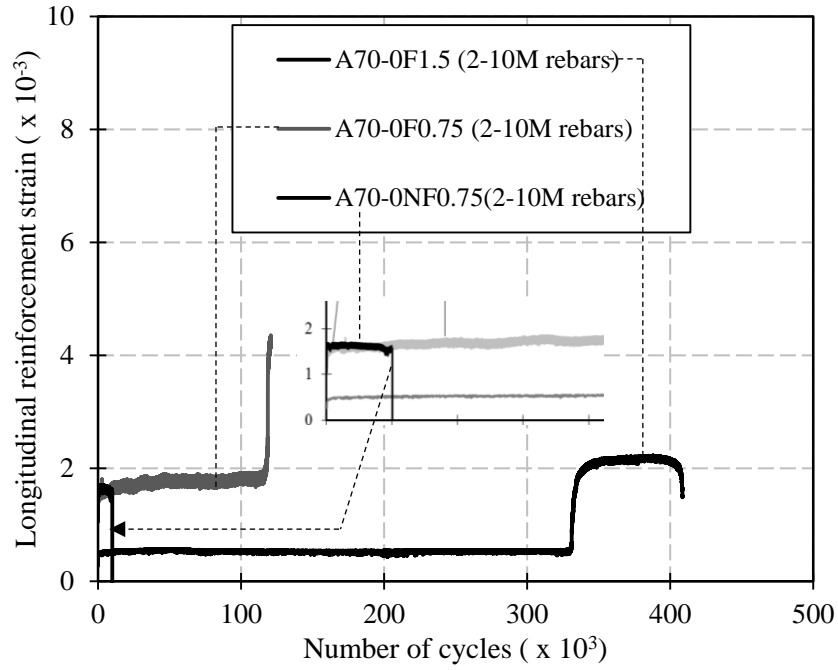


Fig. 5.4 - Longitudinal reinforcement strain versus number of cycles at maximum load (2-10M rebar).

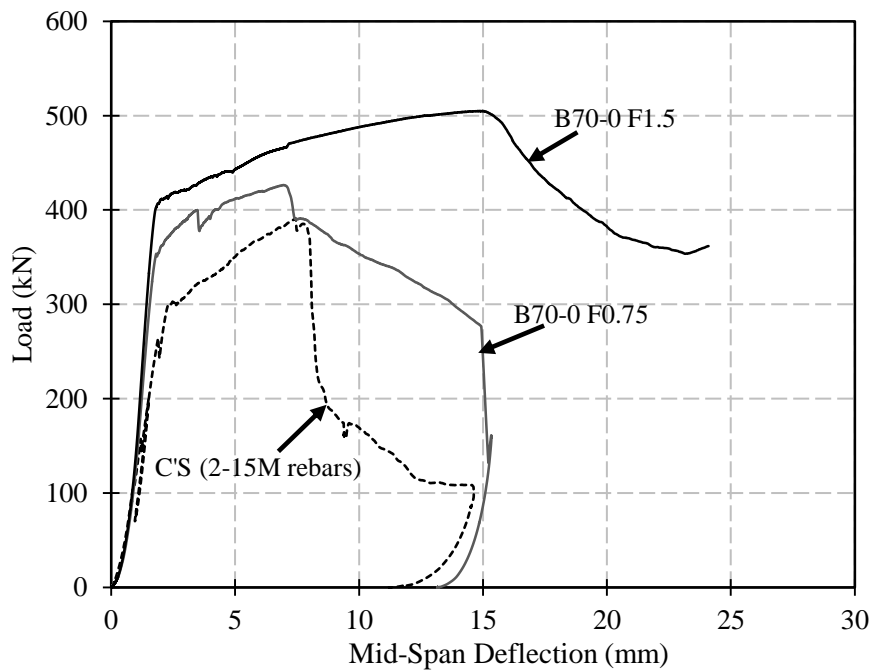


Fig. 5.5 - Load versus deformation plot after fatigue loading.

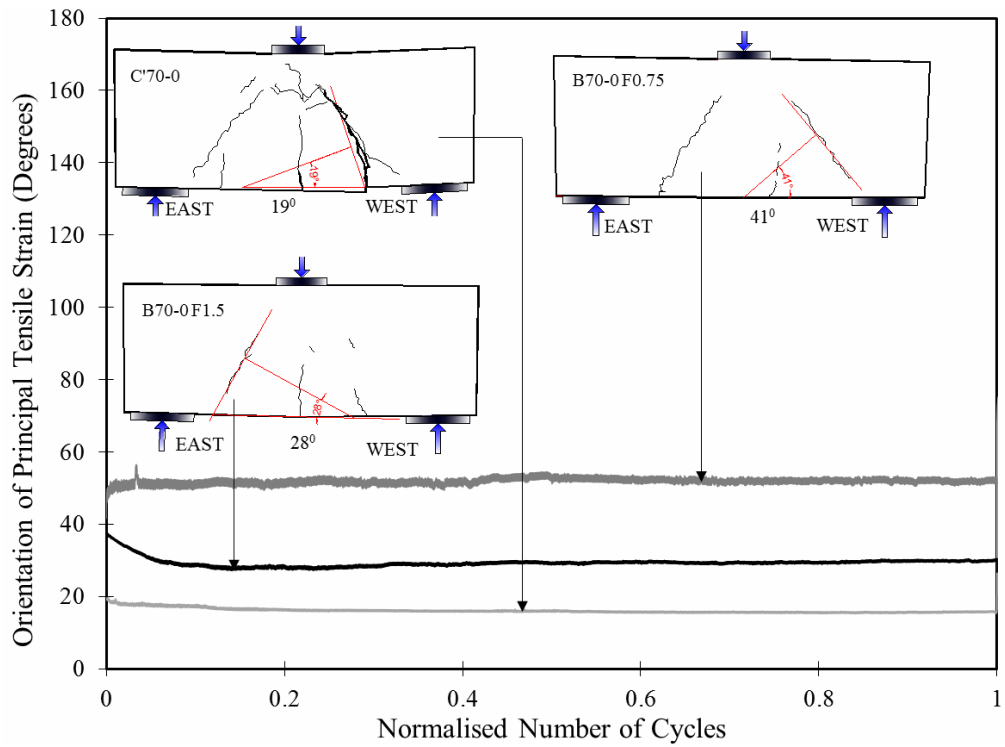


Fig. 5.6 - Crack pattern and inclination of principal tensile strain (15M-70%Pu).

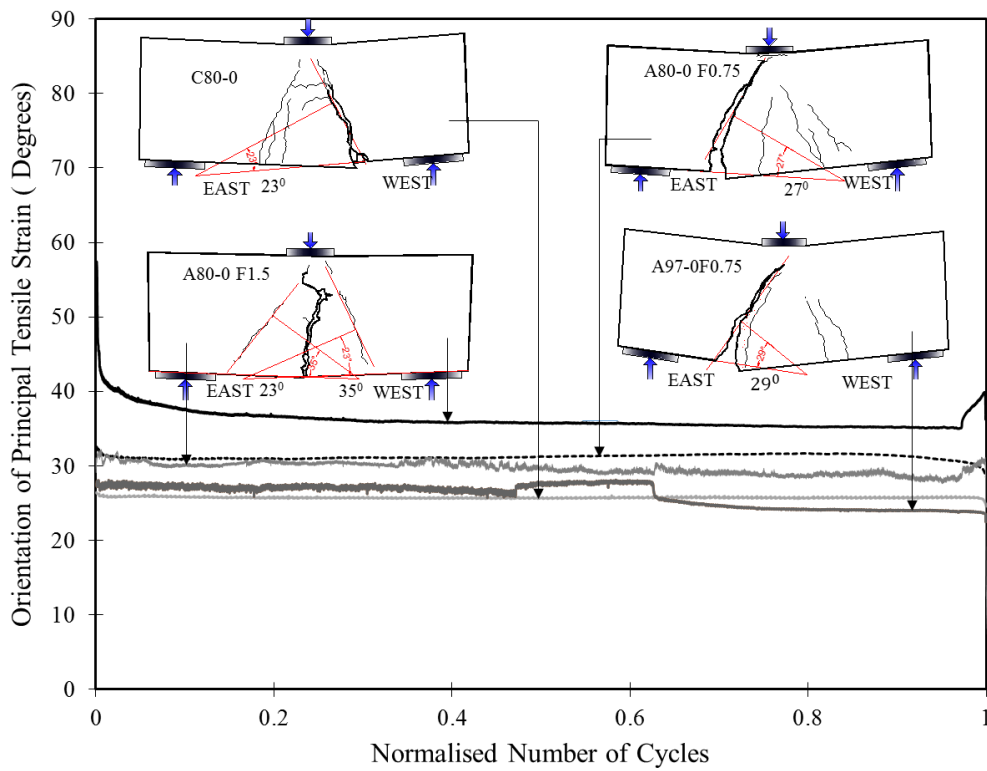


Fig. 5.7 - Crack pattern and inclination of principal tensile strain (10M-80% Pu).

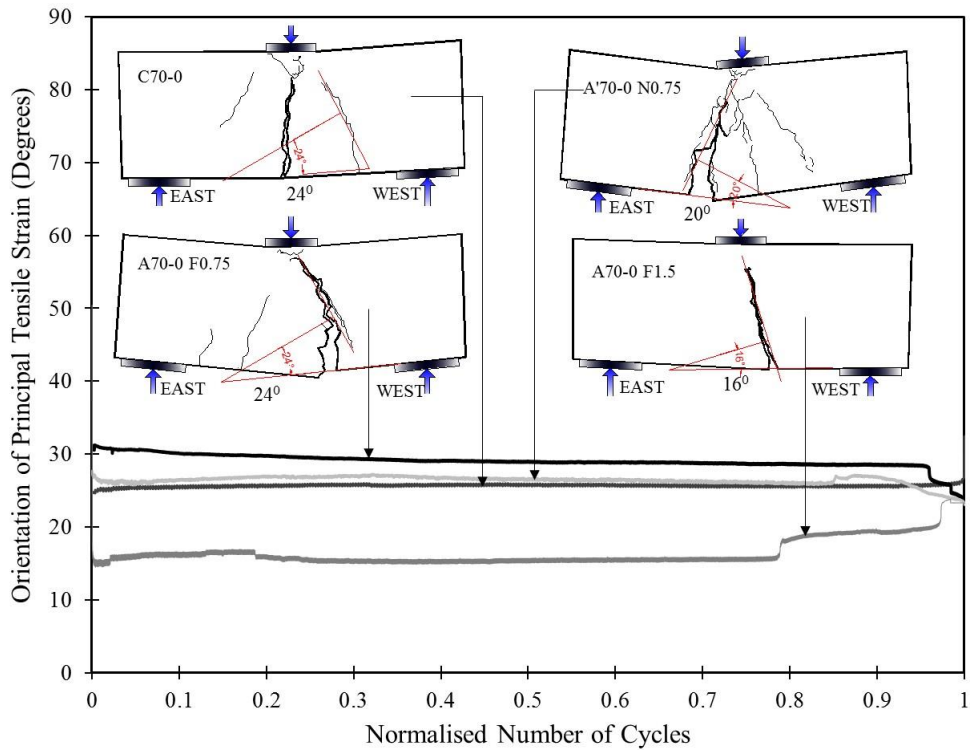


Fig. 5.8 - Crack pattern and inclination of principal tensile strain (10M-70%Pu).

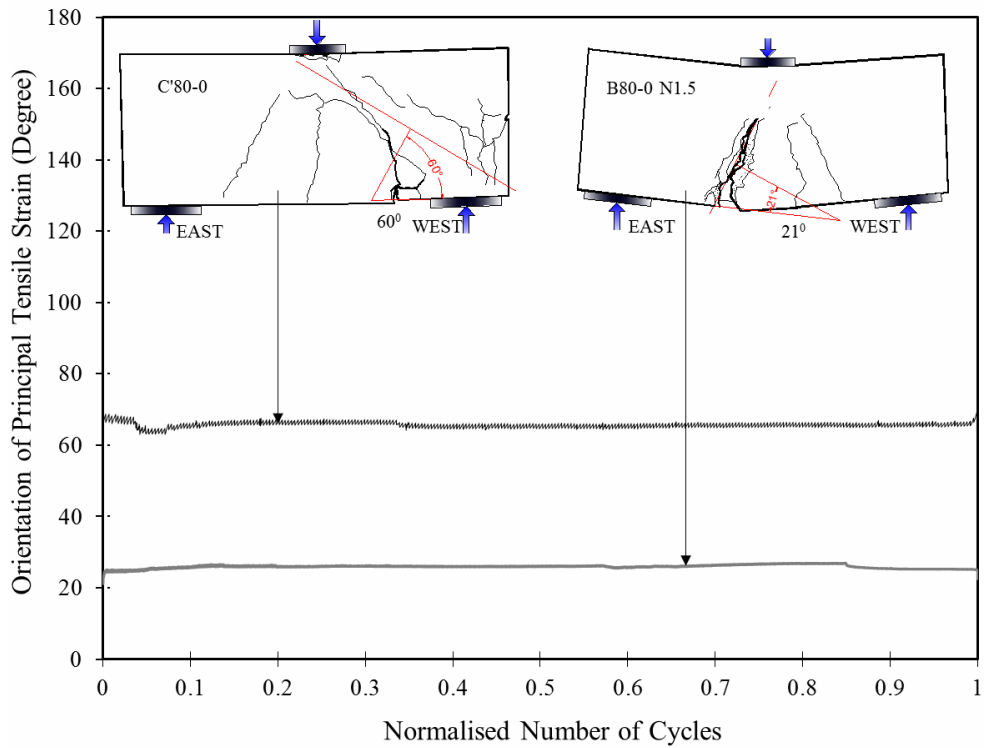


Fig. 5.9 - Crack pattern and inclination of principal tensile strain (15M-80%Pu).

As shown in the deformation evolution plots (Figures 5.10 to 5.15, and Appendix G) for conventional and steel-fibre reinforced concrete beams, after significant fracture of the longitudinal reinforcement, collapse of the steel-fibre reinforced concrete beams did not occur immediately thereafter. The presence of steel fibres resulted in the beams resisting more cycles under high deformation before final fracture. This is attributed to the crack-bridging ability of steel fibres.

Since specimens B70-0 F0.75 and B70-0 F1.5 did not fail after 3,000,000 cycles, the beams were further subjected to monotonic loading (Figure 5.5). The observed residual strength for the two beams were higher than the capacity of the conventional reinforced concrete beam without fatigue damage. This further shows that reduced section sizes obtainable in steel-fibre reinforced concrete beams can be used to achieve the same fatigue life as in larger conventional reinforced concrete beams.

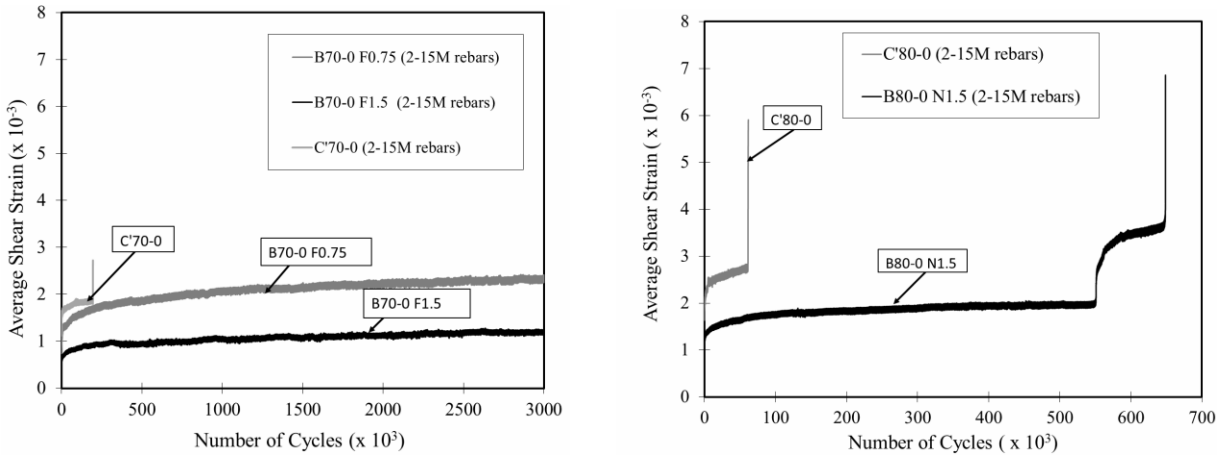


Fig. 5.10 - Average shear strain evolution (2-15M).

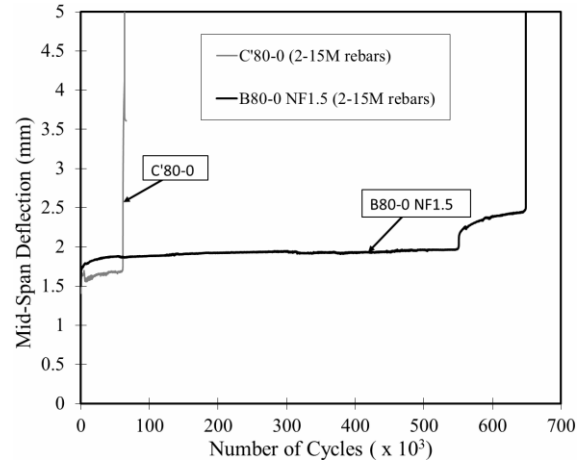
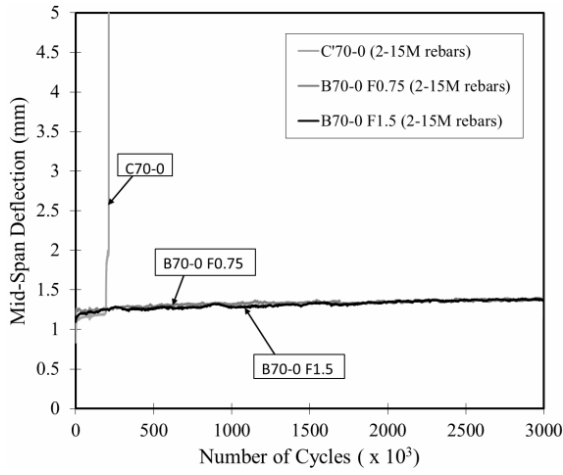


Fig. 5.11 - Mid-span deflection (2-15M).

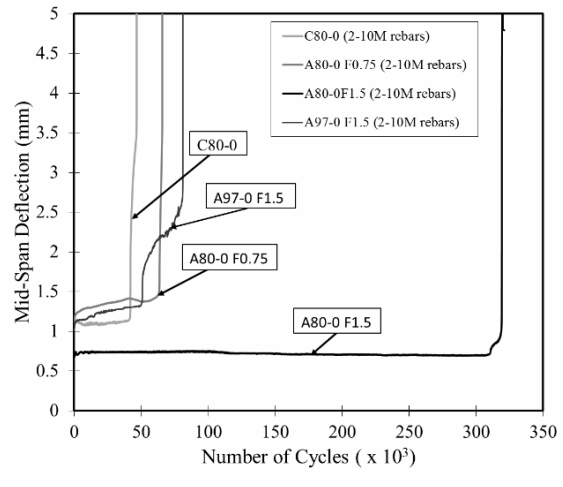
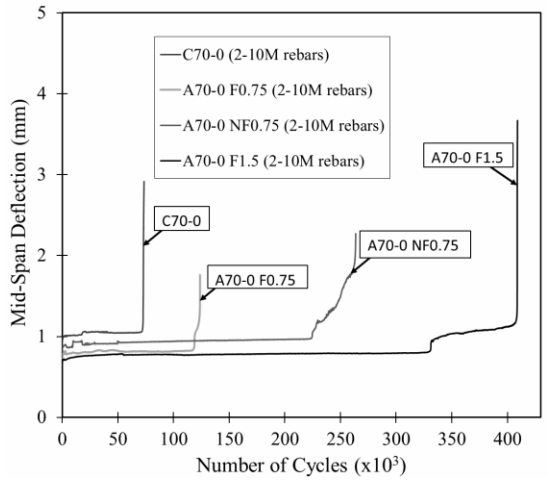


Fig. 5.12 - Mid-span deflection (2-10M).

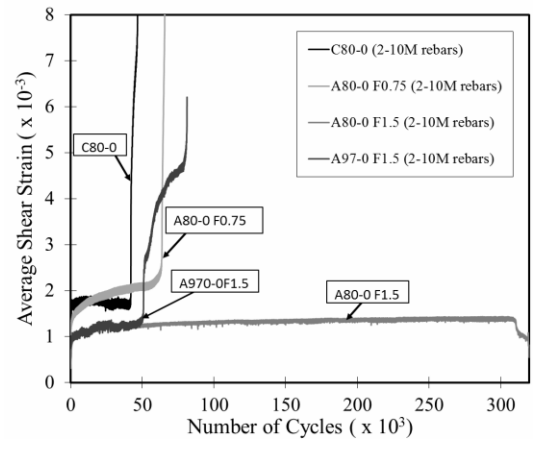
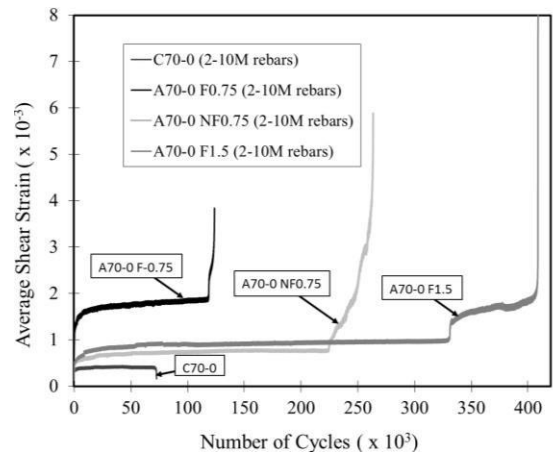


Fig. 5.13 - Average shear strain evolution (2-10M).

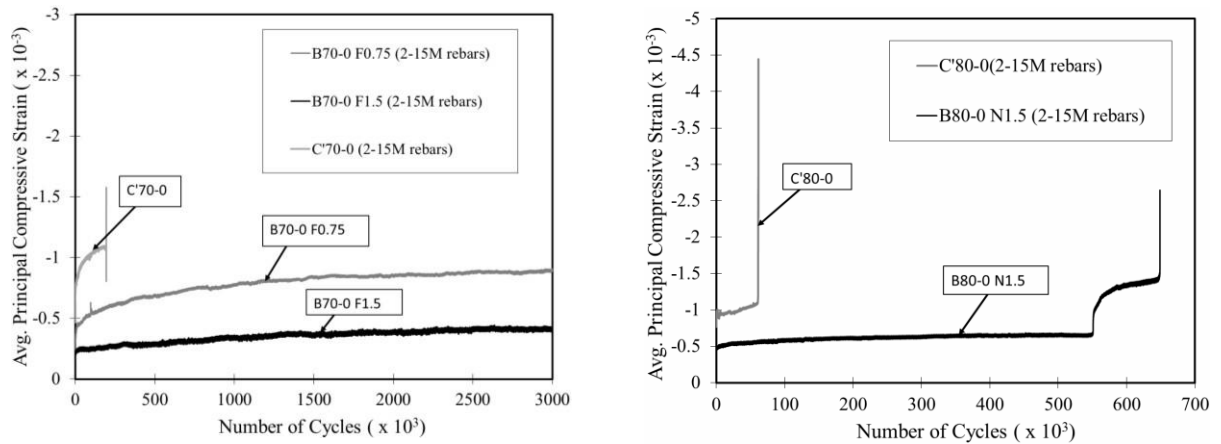


Fig. 5.14 - Average principal compressive strain evolution (2-15M).

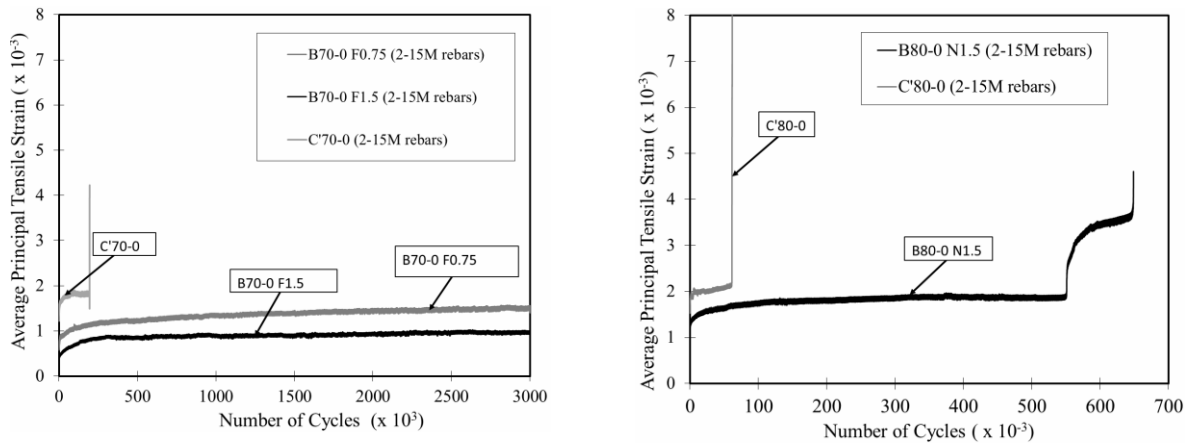


Fig. 5.15 - Average principal tensile strain evolution (2-15M).

### 5.5.2 Crack Pattern

During fatigue loading, flexural and shear-flexural cracks were initially observed on the surfaces of the beams reinforced with 2-10M reinforcing bars (under-reinforced beams). Inclined and diagonal cracks accompanied such cracks in a few of the 2-10M reinforced beams and in beams reinforced with 2-15M reinforcing bars. Final fatigue failure observed in each specimen occurred at a major crack plane that developed from the onset of the fatigue tests. The failure regions are shown in Figures 5.6 to 5.9 with thick crack patterns.

After fracture of the longitudinal reinforcement, sudden collapse of the steel-fibre reinforced

concrete beams did not occur immediately thereafter. The presence of steel fibres resulted in the beams resisting more cycles under high deformation before final fracture.

Specimen A70-0NF0.75 failed after about 260,000 cycles (more than twice the number of cycles to failure for specimen A70-0F0.75 with shear reinforcement). As observed in Figure 5.4, the two specimens started approximately at similar longitudinal reinforcement strain values. The increase in fatigue life of the specimen without shear reinforcement may be attributed to stress redistribution (leading to reduced strain in the reinforcement) as a result of more fatigue cracks on the surface of specimen A70- 0NF0.75 (see Figure 5.8 and Appendix E). Active bridging contribution of the fibres intersecting the cracks occurred while the stresses in the reinforcement intersecting the initial governing concrete crack reduced. The initial cracked concrete plane traversing reinforcing bars in A70-0NF0.75 closed up after a considerable number of cycles as a result of the subsequent significant cracks at other regions. This redistribution halted the crack propagation of the reinforcing bars at the intersection with the initial cracked concrete plane. On the other hand, a discrete crack was observed from the onset of the fatigue loading of beam A70-0F0.75. The behaviour of the beam (reinforcement crack propagation) was governed by this plane because significant concrete cracks were not observed afterwards.

The approximate orientations of the fatigue failure planes were estimated from strain transformations of the LVDT data obtained from the experiments. The obtained evolutions further show that the accuracy of the instrumentation used was acceptable. From Figures 5.6 to 5.9, no significant change in the orientation of the principal strain evolution was observed except at the initial stage of loading, at the point of reinforcement fracture, and at failure.

### 5.5.3 Shear Strain Evolution/Mid-Span Deflection

Under fatigue loading of the shear-critical beams (specimen C'S), shear forces are transferred through compression struts to the supports and irreversible compressive strain accumulates due to the induced compressive stress within the shear span. To maintain equilibrium, the horizontal tensile forces are resisted by the longitudinal reinforcement.

With the addition of steel fibres to the beams reinforced with 2-15M rebars, the shear span deformations (shear strains) were observed to reduce as the steel-fibre volume ratio increased from 0% to 1.5% ( see Figure 5.10). As well, insignificant increases in the mid-span deflections were observed (see Figure 5.11). This improvement was a result of crack-bridging of the inclined cracks within the shear span; hence, retarding the shear strains. However, the obvious increase in the deflection evolution of specimen B80-0NF1.5 was also attributed to the fact that there was no shear reinforcement and no top reinforcing bars (hanger bars).

After fatigue cracks develop at the mid-span in the conventional under-reinforced concrete deep beams with 2-10M rebars (specimen CS), the aforementioned mechanism in which shear force is transferred through compression strut to the support under fatigue loading no longer holds. This is attributed to the fact that the beams are subsequently governed by the reinforcement crack propagation at the intersection with the mid-span cracks, hence resulting in increased rotation.

Beams governed by flexure (beams reinforced with 2-10M rebars) were observed to exhibit reduced mid-span deflections under fatigue loading as the steel-fibre volume ratio increased from 0% to 1.5% (see Figure 5.12). On the other hand, the shear-span deformation (shear strain evolution) also increased, hence corresponding to an increase in the capacity for shear force

transfer through concrete struts (see Figure 5.13).

Under high fatigue loads (80% of static capacity of CS beam), a steel-fibre volume ratio of 1.5% reduced both the mid-span deflection and shear-span deformation of beam A80-0F1.5 compared to beams A80-0F0.75 and C80-0 (Figures 5.12 and 5.13). Although the use of 0.75% steel fibre volume ratio enhanced the fatigue life, it was ineffective in reducing the shear-span deformation and mid-span deflection under high fatigue loading when compared with the control beam C80-0. This was attributed to early pull-out and fracture of the steel fibres under high loads.

At a fatigue loading of 97% of the static capacity of the CS beam, the fatigue life of A97-0F1.5 was observed to be higher than the fatigue life obtained using 0.75% steel-fibre volume ratio and fatigue loading of 80% of the static capacity of beam CS. In addition, the shear-span deformation and mid-span deflection were observed to be lower when compared to those of beams A80-0F0.75 and C80-0. More steel fibres at the intersection with the concrete crack in beam A97-0F1.5 resulted in lower induced bond stresses between fibres and concrete and lower induced stresses in the fibres when compared with beams A80-0F0.75 and C80-0. These results further demonstrate the enhancing influence of steel-fibre volume ratio of 1.5% under high fatigue loading.

#### **5.5.4 Average Principal Strain Evolution**

As previously indicated, various tests have been conducted in order to observe the fatigue resistance properties of steel-fibre reinforced concrete. However, the majority of tests have been conducted on specimens in flexure and compression. Although tests in flexure indicated fatigue life enhancement with steel fibres, there have been conflicting observations on the behaviour in compression (RILEM Proceeding 31). Considering the beams governed by crushing of concrete

under static loading (using specimens reinforced with 2-15M rebars), the observed strain transformations of the LVDT data show substantial reduction in the values of the average compressive and tensile strain evolutions under fatigue loading as the steel-fibre volume ratio increased from 0% to 1.5% (see Figures 5.14 and 5.15). On the other hand, the increase in the tensile and compressive strain evolutions in beams reinforced with 2-10M rebars indicate that more stresses are transferred to the support through the compression strut, since lower deflections were observed.

### **5.5.5 Bond Behaviour**

In the literature, investigations conducted on the influence of bond deterioration under fatigue loading were based on beams with non-anchored reinforcing bars. Such specimens were deliberately allowed to fail by bond slip under fatigue loading (Hawkins, 1974). However, the beams tested in this investigation were provided with adequate anchorage based on code provisions.

Under fatigue loading, provided one of the following is observed, severe damage to the bond between concrete and steel reinforcement will not occur (Figure 5.16):

- The evolutions of the concrete and reinforcement strains (both in the direction of the reinforcement) are approximately parallel.
- The evolution of the difference between the concrete strain evolution and reinforcement strain evolution is approximately constant.

The average strain evolution of concrete in the horizontal direction and the strain gauge reading on the longitudinal reinforcing bars were obtained for the beams tested. Obtaining full evolution readings was not successful for all the beams since some connections of the strain gauges

malfunctioned when intersected by concrete cracks. However, results obtained from beams tested (with 2-15M rebars) at 70% of the static capacity are presented in Figure 5.16. From the figure, reasonable integrity of bond between concrete and steel reinforcement within the shear span can be inferred; however, the use of high strength concrete also contributed to the bond integrity.

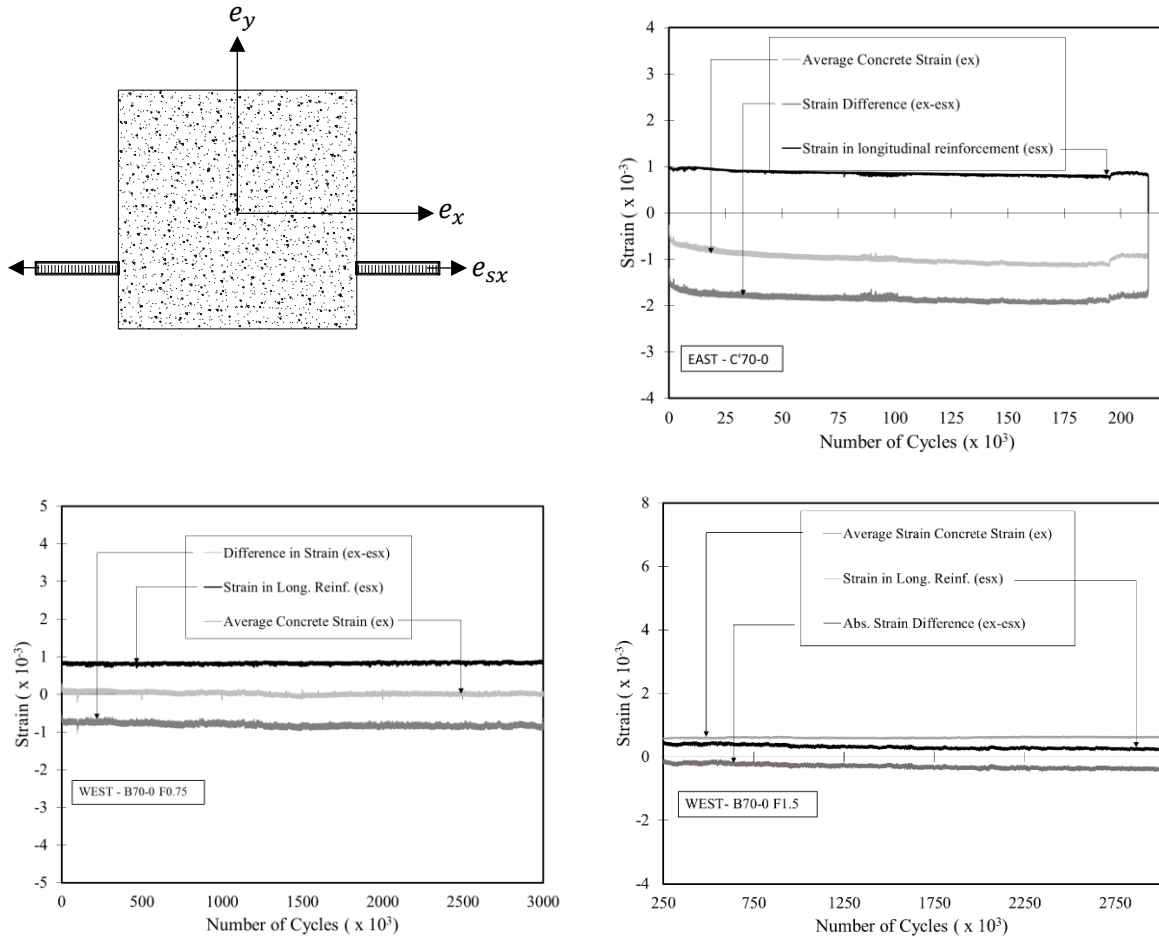


Fig. 5.16 - Evolution of concrete and reinforcement strain variation.

## 5.6 Conclusion

The influence of steel fibres in enhancing the fatigue life of deep beams was investigated by comparing conventional reinforced concrete deep beams with steel-fibre reinforced concrete deep beams. Shear reinforcement ratio, steel-fibre volume ratio, and longitudinal reinforcement ratio

were varied. A new approach was used in estimating the deformation evolution within the shear spans of each beam tested. Based on the results of the test program, the following conclusions are drawn:

1. Deep beams with a shear-span to effective-depth ratio below 1.5 (1.25 was used for this investigation) may fail by the fracture of the longitudinal reinforcement rather than of the shear reinforcement. This is attributed to the low magnitude of stresses induced in the shear reinforcement. These observations have also been previously reported in the literature for deep beams.
2. The fatigue life of reinforced concrete deep beams with shear reinforcement can be enhanced using steel fibres. In addition, depending on the reinforcement ratio, the corresponding deformations are reduced with the inclusion of steel fibres.
3. The use of steel fibres proved to be effective in enhancing the fatigue life and reducing the deformation of beams without shear reinforcement. However, it is recommended that larger beams be tested in order to confirm this observation.
4. Based on the observed results of the experiments conducted, the design of fatigue-critical structures can be optimised with reduced section sizes using steel-fibre reinforced concrete. The beneficial effect will be more substantial in large structures that are designed with reduced volumes of steel fibre concrete.

## **5.7 References**

1. ACI 318-14 to ACI 346-09. "Manual of Concrete Practice: Part 3 of 7." American Concrete Institute.

2. ACI Committee 544. (1999). "Design Considerations for Steel Fibre Reinforced Concrete." Report 544. 4R-88: American Concrete Institute.
3. ACI Committee 506. (1982). "State-of-the-Art Report on Fibre Reinforced Concrete, Report 544IR-82: Concrete International, Design and Construction." American Concrete Institute.
4. Chang D., and Chai W. (1995). "Flexural Fracture and Fatigue Behaviour of Steel-Fibre Reinforced Concrete Structures." Nuclear Engineering and Design, Vol. 156, pp. 201-207.
5. Chenkui H., and Guofan Z. (1995). "Properties of Steel Fibre Reinforced Concrete Containing Larger Coarse Aggregate." Cement & Concrete Composites, Vol. 17, 1995, pp.199-206.
6. CSA (Canadian Standards Association) (2004). "Design of Concrete Structures." CSA A23.3 Mississauga, ON, Canada.
7. EC2. Eurocode 2 (2004). "Design of Concrete Structures-Part 1-1: General Rules for Buildings." London, UK: British Standards Institution, BS EN 1992-1-1.
8. Goransson F., and Nordenmark A. (2011). "Fatigue Assessment of Concrete Foundations for Wind Power Plants." Department of Civil and Environmental Engineering (Master's Thesis), Chalmers University of Technology, Goteborg, Sweden.
9. Hawkins N.M. (1974). "Fatigue Characteristics in Bond and Shear of Reinforced Concrete Beams." Abeles Symposium, ACI Publication, SP-41-10.
10. Herwig A. (2008). "Reinforced Concrete Bridges under Increased Railway Traffic Loads-Fatigue Behaviour and Safety Measures." Ph. D. Thesis No. 4010, Ecole Polytechnique

Federale de Lausanne.

11. Isojeh M.B., and Vecchio F.J. (2016). "Parametric Damage of Concrete under High-Cycle Fatigue Loading in Compression." 9<sup>th</sup> International Conference on Fracture Mechanics of Concrete and Concrete Structures FraMCoS-9.
12. Komeling H.A., Reinhardt H.W., and Shah S.P. (1980). "Static and Fatigue Properties of Concrete Beams Reinforced with Continuous Bar and with Fibres." ACI J. Proc., Vol. 77, No. 1, pp. 36-43.
13. Kwak K., Suh J., and Hsu T. (1991). "Shear-Fatigue Behaviour of Steel Fibre Reinforced Concrete Beams." ACI Structural Journal, Vol. 88, No. 2, pp. 155-160.
14. Lee M.K., and Barr B.I.G. (2004). "An Overview of the Fatigue Behaviour of Plain and Fibre Reinforced Concrete." Cement & Concrete Composites, Vol. 26, pp. 299-305.
15. Naaman, A.E., Hammoud, H., "Fatigue Characteristics of High Performance Fibre-Reinforced Concrete." Cement and Concrete Composites, Vol. 20, 1998, pp. 353-363.
16. Nanni A. (1991). "Fatigue Behaviour of Steel Fibre Reinforced Concrete." Cement & Concrete Composites, Vol. 13, pp. 239-245.
17. Parvez A., and Foster S.J. (2013). "Fatigue Behaviour of Reinforced Concrete Beams with Addition of Steel Fibres." From Materials to Structures: Advancement through Innovation-Samali, Attard and Song (Eds).
18. Parvez A., and Foster S.J. (2015). "Fatigue Behaviour of Steel-Fibre-Reinforced Concrete Beams." Journal of Structural Engineering, ASCE, Vol. 141, No.4, pp. 04014117.

19. Ramakrishnan V., Wu Y.G., and Hossali G. (1989). "Flexural Fatigue Strength, Endurance Limit and Impact Strength of Fibre Reinforced Concretes." Transport Research Board, Washington, D.C.
20. RILEM Proceeding 31, "High Performance Fibre Reinforced Cement Composites 2 (HPFRCC2): Cyclic Behaviour, Fatigue Strength, Endurance Limit and Models for Fatigue Behaviour of FRC." Proceedings of the Second International RILEM, Workshop.
21. Rocha M., Bruhwiler E. (2012). "Prediction of Fatigue Life of Reinforced Concrete Bridges." In Biondini and Frangopol (Eds) Bridge Maintenance, Safety, Management, Resilience and Sustainability, pp. 3755-3760.
22. Teng S., Ma W., Tan K.H., and Kong F.K. (1998). "Fatigue Tests of Reinforced Concrete Deep Beams." Journal of the Structural Engineer, Vol. 76, No. 18, pp.347-352.
23. Teng S., Ma W., and Wang F. (2000). "Shear Strength of Concrete Deep Beams under Fatigue Loading." ACI Structural J., Vol. 97, pp. 572-580.

## CHAPTER 6

# HIGH-CYCLE FATIGUE LIFE PREDICTION OF REINFORCED CONCRETE DEEP BEAMS

*The material in this chapter was previously published as follows:*

*Isojeh B., El-Zeghayar M., Vecchio, F.J. (2017). "High-Cycle Fatigue Life Prediction of Reinforced Concrete Deep Beams." Engineering Structures Journal, Vol. 150, pp. 12-24.*

### 6.1 Abstract

Concrete elements deteriorate as a result of the continuous application of compressive fatigue loads. Irreversible deformation accumulates; hence, the effects on embedded steel reinforcing bar capacity and concrete resistance should be accounted for in the fatigue analysis of concrete structures. Experimental investigations were conducted to study the fatigue behaviour of eight small-scale reinforced concrete deep beams with a shear span to effective depth ratio of 1.25. Percentages of the diagonal cracking load from monotonic tests were used as fatigue loads. The deformation evolution within the shear spans of the deep beams were obtained by estimating the average principal strain and shear strain evolutions from the strain transformation analysis of LVDT (Linear Variable Displacement Transformer) data. Mid-span deflections and reinforcement strain evolutions with proximity to a major concrete crack location were obtained. In all beams, failure occurred with fracture of the longitudinal reinforcement at the intersection with the major concrete crack. Maximum strain evolutions for shear reinforcement measured at regions around the bends were observed to be lower than the strain evolutions observed in the longitudinal reinforcement. This was attributed to the governing arch mechanism common with deep beams.

The strut and tie method was modified to predict the fatigue life of the deep beams tested by

introducing fatigue damage parameters into the constitutive models for concrete. To achieve this, the irreversible compressive fatigue strain in concrete is considered as a pseudo-load. The crack initiation life and the progressive crack growth of steel reinforcement are accounted for using strain-life models and linear elastic fracture mechanics, respectively. Within the developed algorithm, failure will occur when one of the evolving forces in either the concrete strut or steel reinforcement approaches the corresponding residual resistance capacity.

Keywords: strut and tie, fatigue, fracture mechanics, strain-life, high-cycle, damage

## **6.2 Introduction**

Investigations of the behaviour of reinforced concrete elements subjected to fatigue loading began in the twentieth century. Due to complex observations in the performances of the constituent materials, further interest in this field of study has evolved. From previous studies (Okamura et al. (1981); Okamura and Ueda (1982); and Ueda (1982), failure of reinforced concrete elements due to the fracture of reinforcement at its intersection with concrete cracks, crushing of concrete, and excessive evolutions of diagonal tension cracks have been reported as modes of fatigue failure.

### **6.2.1 Mechanism of Fatigue Failure**

The failure mechanisms observed in previous tests conducted on reinforced concrete beams were reported to be significantly influenced by the shear span to effective depth ratio ( $a/d$ ), the stress ratio (ratio of the minimum stress to maximum stress), the reinforcement ratio, and the magnitude of fatigue load (Hawkins, 1974; Teng et al., 1998; Teng et al., 2000). Fracture of the tensile reinforcement was observed to occur in the region of maximum moment within the beams when subjected to smaller fatigue loads. On the other hand, shear failure due to diagonal cracking occurred under high fatigue loads (Chang and Kesler, 1958). The use of different

reinforcement ratios have also been reported to influence the failure mechanisms (Stelson and Cernica, 1958). For example, while beams with lower reinforcement ratios are governed by fracture of the reinforcement, heavily reinforced concrete members may fail due to crushing of concrete or diagonal tension cracks.

Reports on fatigue tests conducted on beams with shear reinforcement and having shear span to effective depth ratios greater than 2.0 showed increases in the shear reinforcement strains as diagonal or inclined cracks emanated (Okamura et al., 1981; Okamura and Ueda, 1982; Ueda, 1982). The fatigue load transfer was described as involving a truss mechanism in which shear forces were transmitted by the shear reinforcement from one surface of an inclined compression strut to an adjacent strut. Depending on the average induced strains or stresses in the reinforcement intersecting the diagonal cracks, localized crack growth in the shear reinforcement and widening of concrete cracks occurred. Fracture of the shear reinforcement typically occurred thereafter. However, beams with shear span to effective depth ratios lower than 2.0 were governed by arch mechanism and did not exhibit shear reinforcement fracture at failure (Higai, 1983).

Okamura et al. (1981), Okamura and Ueda (1982), and Ueda (1982) reported that the increase in the shear reinforcement strain was proportional to the logarithm of the number of cycles leading to fracture, especially at bends. As the shear reinforcement fractured, collapse of the beams occurred where the remaining stirrup legs intersecting the widened inclined cracks were insufficient to withstand the applied maximum fatigue load. As such, the fatigue behaviour of shear reinforcement in terms of its maximum strain evolution up to yield was considered as a fatigue limit state. Models developed and reported by Hawkins (1974), Ruhnau (1974), Okamura et al. (1981), and Higai (1983) for estimating the strain within a shear span at any

given cycle up to failure are used in the literature and codes of practice for this purpose.

Fatigue failure of deep beams with shear span to effective depth ratios of 1.0 and 1.5 were observed to fail under fatigue loading by crushing of concrete compressive struts, diagonal tension, or fracture of the longitudinal reinforcement. No fracture of the shear reinforcement was observed in any of the specimens (Teng et al., 1998; Teng et al., 2000). In the tests conducted by Teng et al. (2000), high-strength deformed steel bars and plain round steel bars were used as shear reinforcement in each shear span per beam. Deformations and crack patterns on both shear spans revealed no substantial difference. It was also observed that the shear reinforcement in the deep beams did not yield at failure.

An illustration of the behaviour of shear reinforcement in deep beams under fatigue loading can be observed from Higai's (1983) report on moving load tests. According to Higai (1983), as the distance between the moving load and the support reduced, the observed shear strength increased remarkably. Local compressive concrete stresses were also observed to develop in the vertical direction within the shear span, thus decreasing the principal tensile stress in the concrete. In addition, it was reported that strains in the stirrups decreased as the distance between the support region and loading point reduced. These observations are analogous to clamping or transverse compression stresses in deep beams under static loads (Bentz et al., 2006; Mau and Hsu, 1987). However, further investigation is still required in order to more fully understand the fatigue deformation of deep beams.

### **6.2.2 Design for Fatigue Resistance**

Deep beam can be designed appropriately and conservatively under static loads using the strut and tie modelling approach. Basically, the required concrete section sizes and amount of

reinforcement (dimensions of load transfer path) are obtained from the stresses estimated from the static loading conditions at failure (Ultimate Limit State) (Goransson and Nordenmark, 2011). Under fatigue loading, the stresses induced in the load transfer paths are estimated from the proposed or given fatigue load (usually lower than the expected load at failure). The stresses in these paths are further normalised with the material strengths in order to obtain stress levels needed in fatigue models. As a means of fatigue damage resistance verification, the normalized stresses from fatigue loads are implemented into their corresponding fatigue stress-life models to obtain the number of cycles that will result in local deformation by crushing (in the case of concrete) or fracture (in the case of steel). For an appropriate design, the number of cycles leading to failure obtained is ensured to be more than the number of cycles expected for service life. To achieve this, the volumes of the materials (section size and amount of reinforcement) are generally increased, if need be (Goransson and Nordenmark, 2011).

The use of S-N models does not account for damage evolution of the structural element (Zanuy et al., 2007; Tamulenas et al., 2014). The norm in fatigue design of structures using stress-life models neglects the influence of irreversible strain accumulation in concrete which may be significant in fatigue life prediction. Further, knowledge of the deformation evolution within the shear spans of deep beams in terms of shear strains, principal tensile strains, and principal compressive strains under fatigue loading is expedient in understanding the behaviour of deep beams under fatigue loading, since their resistance capacities may be governed by the behaviour within the shear spans.

In this chapter, the influence of load level, stress ratio, and longitudinal reinforcement ratio on the fatigue behaviour of deep beams with shear-span to effective depth ratio of 1.25 are investigated experimentally. An approach is developed using strut and tie analysis for predicting

the fatigue life of deep beams. The evolution of irreversible strain accumulation, concrete strength and stiffness degradation, and reinforcement crack growth are accounted for in this approach.

## **6.3 Experimental Program**

### **6.3.1 Test Specimens**

In this investigation, beams with dimensions of 175 x 250 x 700 mm and an a/d value of 1.25 were used for fatigue tests (Figure 6.1). The properties of the beams tested are given in Table 6.1 (columns 1 to 7). The reinforcement provisions used for the beams surpassed the minimum required in CSA (2006) A23.3-04 11.2.8.1 and 11.2.8.2 for shear, 10.5.1.2 for flexure, EC2-1-1(2004) 9.2.1.1 and 9.2.1.1 for shear and flexure respectively, and ACI(318-346) Section R9.6.3.1 and R9.6.1.2 for shear and flexure respectively.

Adequate anchorage was provided based on code requirements in CSA (2006)-N12.13.1, N12.13.2 (shear reinforcement anchorage), N12.5.2 (flexural reinforcement anchorage). The anchorage provisions also satisfied EC2-1-1 (2004) clause 8.5(1) and (2) for shear reinforcement and EC2-1-1 clause 8.4.1 (1) P for longitudinal reinforcement. ACI (318-346) Table 25-3-1 and Table 25.3.2 for longitudinal and shear reinforcement, respectively were also used as provision benchmarks. Longitudinal reinforcement ratios of 0.45%, 0.90%, and 1.40% were provided, while 0.20% was used as the shear reinforcement ratio.

From Table 6.1, the first three beams (CONT-1 to -3) having longitudinal reinforcement ratios of 0.45%, 0.90%, and 1.40%, respectively, were tested monotonically, in order to obtain the load corresponding to the diagonal cracking load. Once the cracking load was attained, results from further increases in loading were not required. Percentages of the maximum diagonal cracking

load were then used to define the fatigue loads for other beams with similar longitudinal reinforcement ratios.

The names attached to each beam tested under fatigue loading are indicative of the loading and reinforcement conditions; for example, C80-20-0 is assigned to a beam reinforced with 2-10M and subjected to fatigue maximum and minimum loads of 80% and 20% of diagonal cracking load. The last value, zero, signifies a 0.45% longitudinal reinforcement ratio. In the case of beams C75-0-1 and C75-0-2, C75-0 signifies maximum and minimum fatigue loads of 75% and approximately 0%, respectively. The last numeral (1 or 2) represents 0.9% or 1.40% longitudinal reinforcement ratio, respectively.

### **6.3.2 Materials**

A design compressive strength of 50 MPa (high strength concrete), having a mix design of 1:2:2 (cement: fine aggregate: coarse aggregate) and a water/cement ratio of 0.5 was selected. This comprised a maximum aggregate size of 10 mm and fine aggregate with a fineness modulus of 2.6. Slump readings between 80 and 150 mm were obtained during casting. At 28 days, the specimens were removed from the curing room and placed in a dry compartment afterwards. Canadian standard 15M, 10M, and D4 bars were used as reinforcement. The D4 reinforcing bars were used for the shear reinforcement, and 2-10M reinforcing bars were used for the hanger bars.

The average yield strength obtained based on coupon tests for the 15M, 10M, and D4 reinforcing bars were 430 MPa, 480 MPa, and 610 MPa respectively. The yield strength of the cold-worked D4 steel rebar corresponded to the 0.2% offset strain.

### 6.3.3 Test Setup

The setup for the fatigue tests consisted of a servo-hydraulic testing facility having a loading capacity of 350 kN. Each beam was simply supported and the load was applied symmetrically through the load cell (Figure 6.1). Strain gauges were attached to regions assumed to be cracking regions under fatigue loading. Hence, it was expected that under fatigue loading, provided diagonal inclined cracks occurred, the strain evolution in the shear and longitudinal reinforcing bars would be observed. The surfaces of the reinforcement were initially filed lightly and cleaned with acid and base solutions. Subsequently, the strain gauges (5 mm size) were glued to the reinforcement surfaces. In order to prevent damage when in contact with concrete, the surfaces of the strain gauges were protected using aluminum foil. The wires connecting the strain gauges in the concrete were labelled appropriately and connected to data acquisition system channels. As the tests resumed, strain readings were obtained progressively up to the instant of failure.

Table 6.1- Specimens Description.

| C1                | C2           | C3           | C4           | C5                   | C6             | C7                     | C8                                    |
|-------------------|--------------|--------------|--------------|----------------------|----------------|------------------------|---------------------------------------|
| Specimen name (#) | $f'_c$ (MPa) | $\rho_l$ (%) | $\rho_v$ (%) | Max. load (% Pcr) kN | Min. Load (kN) | Cracking load Pcr (kN) | Number of cycles to failure ( $N_f$ ) |
| CONT-1            | 52.8         | 0.45         | 0.20         | 100                  | -              | 156.70                 | -                                     |
| CONT-2            | 55.8         | 0.90         | 0.20         | 100                  | -              | 121.98                 | -                                     |
| CONT-3            | 54.3         | 1.40         | 0.20         | 100                  | -              | 139.39                 | -                                     |
| C80-0 (a)         | 46.6         | 0.45         | 0.20         | 80                   | 5.0            | -                      | 460,000                               |
| C80-0 (b)         | 54.8         | 0.45         | 0.20         | 80                   | 5.0            | -                      | 420,000                               |
| C75-0 (a)         | 57.1         | 0.45         | 0.20         | 75                   | 5.0            | -                      | 770,000                               |
| C75-0 (b)         | 53.3         | 0.45         | 0.20         | 75                   | 5.0            | -                      | 850,000                               |
| C70-0             | 52.2         | 0.45         | 0.20         | 70                   | 5.0            | -                      | 1,500,000*                            |
| C80-20-0          | 58.1         | 0.45         | 0.20         | 80                   | 31.3           | -                      | 2,550,000 <sup>b</sup>                |
| C75-0-1           | 52.4         | 0.90         | 0.20         | 75                   | 5.0            | -                      | 3 000 000 <sup>a</sup>                |
| C75-0-2           | 46.1         | 1.40         | 0.20         | 75                   | 5.0            | -                      | 3 000 000 <sup>a</sup>                |

<sup>a</sup> Test stopped without failure.

\*Number of cycles at first rebar fracture (final failure: 1,800,000).

<sup>b</sup> Number of cycles at first rebar fracture (final failure: 2,730,000)

\*\*No failure (Stresses lower than endurance limit value or stress intensity factor lower than the threshold value)

The mid-span deflection per cycle was obtained using an attached LVDT positioned under the beam. The LVDTs attached to the concrete surfaces were used to obtain deformations in their respective directions. The observed deformations were subsequently used to estimate the average principal strains and shear strains per fatigue loading cycle. As indicated in the fifth and sixth columns of Table 6.1, percentages of the diagonal cracking loads observed from the monotonic tests were used as maximum and minimum loads for the fatigue tests conducted, respectively. Each specimen was subjected to fatigue loading without prior application of monotonic loading.

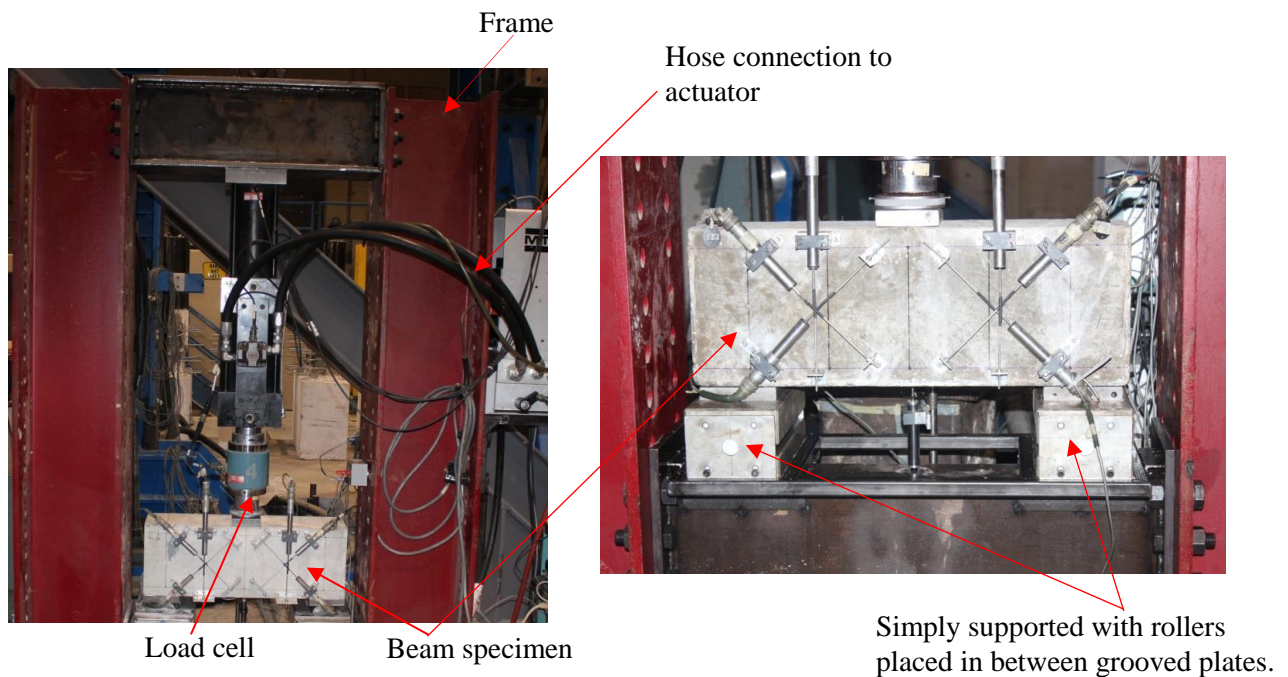


Fig. 6.1 - Beam specimen setup.

### 6.3.4 Test Procedure

Initially, the three control beams CONT-1, -2, and -3 as indicated in Table 6.1 and Figure 6.2, were tested under monotonic loading in order to obtain the diagonal cracking load (column 7). From Figure 6.3, it can be observed that the capacities of CONT-2 and CONT-3 were approaching the limit of the testing machine; hence, each test was stopped having achieved the

aim (obtaining the diagonal cracking load). Since the LVDTs attached to the surface of the beams could capture the cracking load, subsequent load values were not required. The diagonal cracking load for CONT-1 was observed to be higher than the values obtained for CONT-2 and CONT-3. This was attributed to the fact that heavily-reinforced deep beams are governed by shear deformations; hence, initial cracks under loading may be within the shear spans. On the other hand, lightly reinforced concrete deep beams are governed by flexural cracks within the mid-spans. Higher loads may be required for cracks to form within the shear spans of lightly reinforced beams.

For the fatigue loading, a pulsating load of a continuous sinusoidal waveform was generated from the loading equipment throughout the test duration. All fatigue tests were conducted at a frequency of 5 Hz and a minimum fatigue load of 5 kN was used, except for beam C80-20-0 where the minimum fatigue load was taken as 20% of the diagonal cracking load.

Although positive load ratios were considered in this investigation, structural components may be subjected to stress reversals (negative stress or load ratio) (Torrenti et al., 2010). Based on investigations conducted by Zhang et al. (1996), stress-life models obtained by plotting stress levels against the number of cycles to failure for different stress ratios, suggested a reduction in the fatigue life of concrete as the stress ratio reduced.

Further, the beams and the reinforcements used in this investigation were corrosion free. However, beams subjected to corrosion are significantly dependent on the frequency of loading (Veeman et al., 2015).

### **6.3.5 Instrumentation**

The LVDTs attached within the shear spans of each beam were used to measure the evolution

of the average deformation (Figures 6.1, 6.2, and 6.4). Average deformations in terms of the shear strains, the average principal strains, and the inclination of the principal tensile strain relative to the x- and y-directions within the shear spans of each beam were obtained from strain transformation of the LVDT data (Figure 6.4).

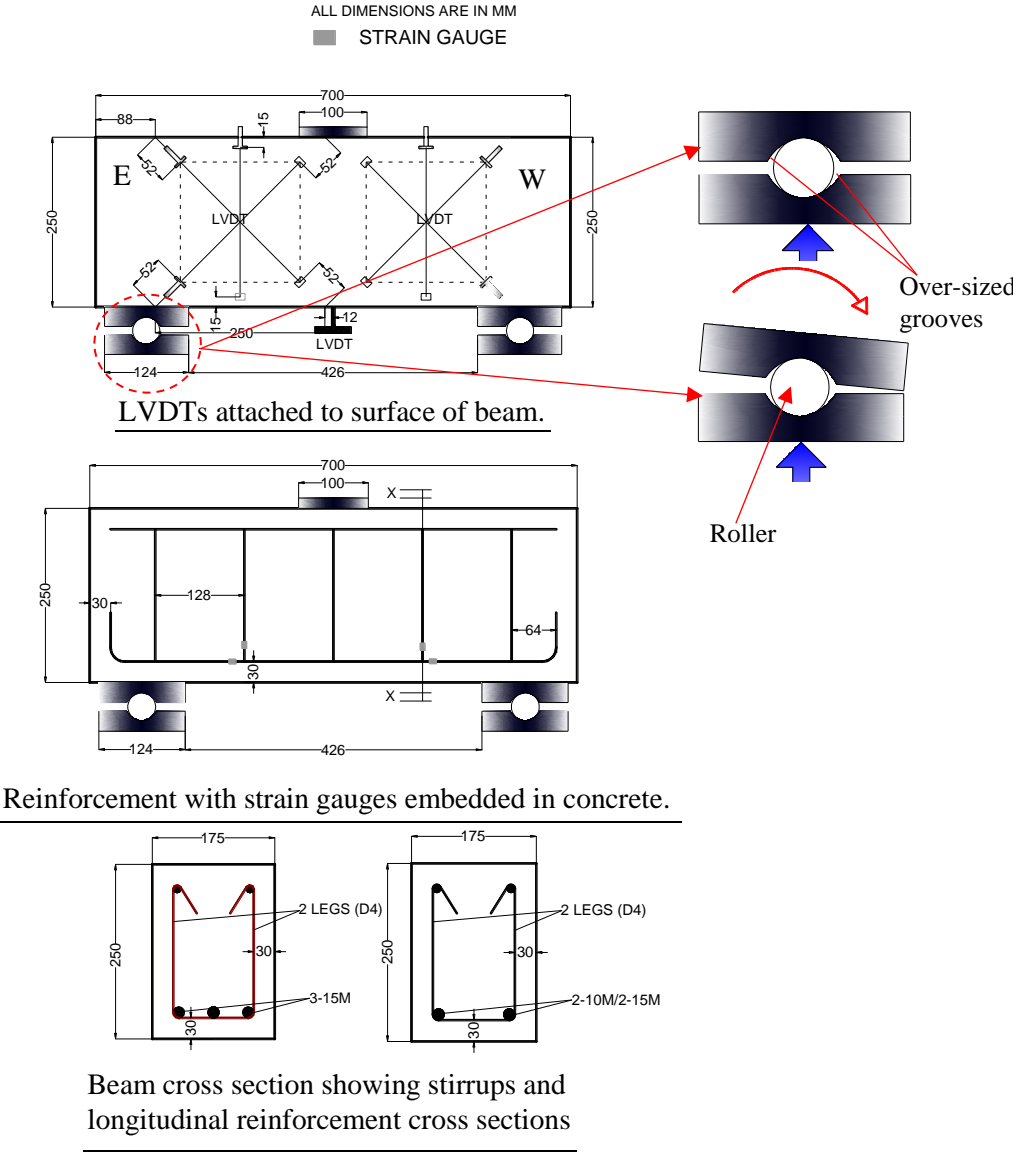


Fig. 6.2 - Details of deep beam specimen.

For the West LVDTs, (where  $\gamma_{xy}$  is positive, and  $\varepsilon_y = e_b$  )

$$\begin{aligned}\varepsilon_x &= e_c - e_b + e_a \\ \gamma_{xy} &= e_a - e_c\end{aligned}\tag{6.1}$$

For the East LVDTs, ( $\gamma_{xy}$  is negative, and  $\varepsilon_y = e_b$  )

$$\begin{aligned}\varepsilon_x &= e_c - e_b + e_a \\ \gamma_{xy} &= e_c - e_a\end{aligned}\tag{6.2}$$

The average principal concrete strains using Mohr circle of strains were obtained thus:

$$\varepsilon_{1,2} = \frac{1}{2}(\varepsilon_x + \varepsilon_y) \pm \frac{1}{2}\left(\sqrt{(\varepsilon_x - \varepsilon_y)^2 + \gamma_{xy}^2}\right)\tag{6.3}$$

The values for the evolution of  $\theta$ , the inclination of the principal tensile strain direction relative to horizontal, was estimated using  $\gamma_{xy}$  (shear strain),  $\varepsilon_x$  (average strain in the horizontal direction), and  $\varepsilon_y$  (average strain in the vertical direction).  $\varepsilon_1$  and  $\varepsilon_2$  are the average tensile and average compressive strain respectively. A program was developed to generate the deformation evolutions from the laboratory data.

In order to obtain the load corresponding to the diagonal cracking load, readings were obtained from LVDTs measuring tensile strains ( $e_a$ ) as shown in Figure 6.4. From each reading, the load corresponding to the diagonal cracking was taken as the load at which the slope of the deformation curve began to change significantly.

The results of the experiments conducted are presented subsequently. Figures 6.5 to 6.9 show mid-span deflections, the crack patterns, principal strain evolutions (tensile and compressive) and shear strain evolutions.

## 6.4 Test Results

The number of cycles leading to failure are given in Table 6.2. Specimens C75-0-1 and C75-0-2 were stopped at 3,000,000 cycles since no signs of failure were apparent. Although beam C75-0 failed at about 800,000 cycles, the fatigue load used was slightly higher compared to C75-0-1

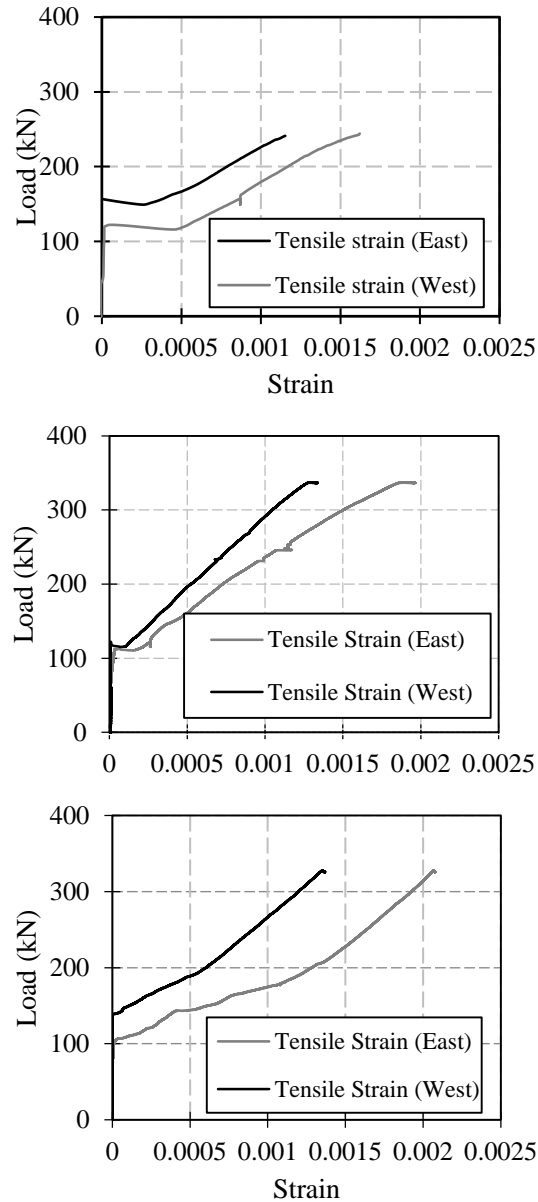


Fig. 6.3 – Load versus deformation (strain) plots.

and C75-0-2. It is well-known that fatigue life increases as the reinforcement ratio increases under a given load. However, the high fatigue load used for beam C75-0 may have resulted in

the large difference between observed fatigue cycles when compared with beams C75-0-1 and C75-0-2.

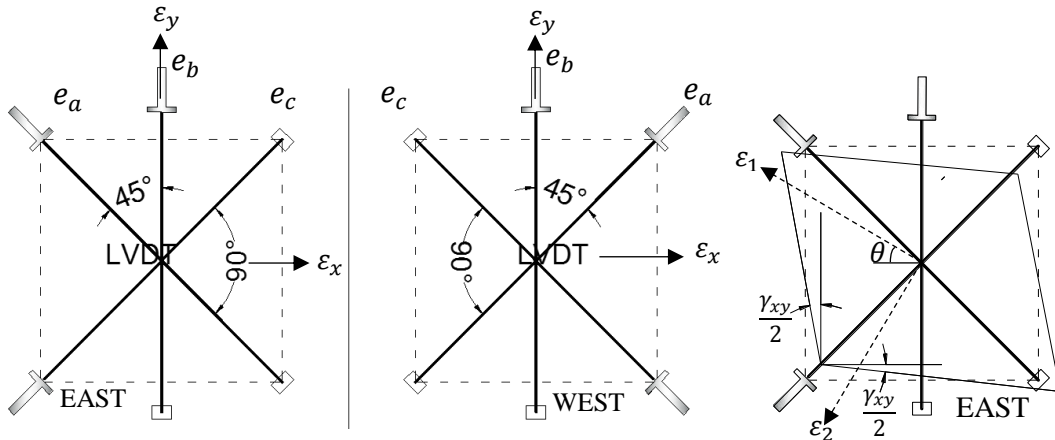


Fig. 6.4 - LVDTs strain transformation.

#### 6.4.1 Mid-Span Deflection/ Stiffness Degradation

The mid-span deflections of seven specimens are given in Figure 6.5. The applied fatigue load influenced the evolution of the mid-span deflection of the beams having the same reinforcement ratios (C70-0, C75-0 (A), C75-0 (B), and C80-0 (B)) (2-10M rebars). As the stress level increased, the deflection and the evolving rate increased. The specimens failed finally at 1,800,000, 770,000, 850,000, and 420,000 cycles, respectively.

Table 6.2 - Fatigue test results and predictions.

| C1                | C2   | C3   | C4  |
|-------------------|--|--|---|
| Specimen name (#) | Number of cycles to failure $N_f$ (Log $N_f$ ) | Predicted number of cycles to failure $N_f$ (Log $N_f$ ) | Helgason et al. [24] / AASHTO [25] predictions (Log $N_f$ ) |
| C80-0 (a)         | 460,000 (5.7)                                  | 466,000 (5.7)  | 350,000 (5.5)   |
| C80-0 (b)         | 420,000 (5.6)                                  | 466,000 (5.7)  | 350,000 (5.5)   |
| C75-0 (a)         | 770,000 (5.9)                                  | 842,000 (5.9)  | 450,000 (5.7)   |
| C75-0 (b)         | 850,000 (5.9)                                  | 842,000 (5.9)  | 450,000 (5.7)   |
| C70-0             | 1,500,000 <sup>a</sup> (6.2)                   | 1,060,000 (6.0)  | 530,000 (5.7)   |
| C80-20-0          | 2,550,000 <sup>b</sup> (6.4)                   | 1,640,000 (6.2)  | **  |
| C75-0-1           | 3 000 000 <sup>a</sup>                         | **   | **  |
| C75-0-2           | 3 000 000 <sup>a</sup>                         | **   | **  |

<sup>a</sup> Test stopped without failure.

<sup>\*</sup>Number of cycles at first rebar fracture (final failure: 1,800,000).

<sup>b</sup> Number of cycles at first rebar fracture (final failure: 2,730,000)

\*\*No failure (Stresses lower than endurance limit value or stress intensity factor lower than the threshold value)

For similar maximum load levels (C80-0 and C80-20), an increase in the minimum load level (20% of diagonal cracking load) resulted in the reduction of the mid-span deflection and its rate of evolution, and an increase in fatigue life. The failure of specimen C80-20 occurred after 2,730,000 cycles. By comparing beams reinforced with 10M and 15M rebars, it can be deduced that beams with higher longitudinal reinforcement ratios exhibited lower deflection. Although beam C75-0-2 with 3-15M rebars exhibited a higher initial deflection (due to stochastic behaviour of concrete) compared to C75-0-1, the rate of increase of deflection with fatigue cycles was observed to be lower in C75-0-2 (see Figure 6.5).

The crack patterns of beams C70-0, C80-20-0, C80-0, and C75-0(b) are shown in Figure 6.6. Inclined or shear-flexural cracks formed within the shear spans of C80-0 and C80-20-0 at the initial stage of fatigue loading. For beam C80-0, a flexural crack at the mid-span region was initially observed; however, the propagation of the inclined crack due to a high fatigue load range prevailed, while no progressive opening of the flexural crack at the mid-span occurred.

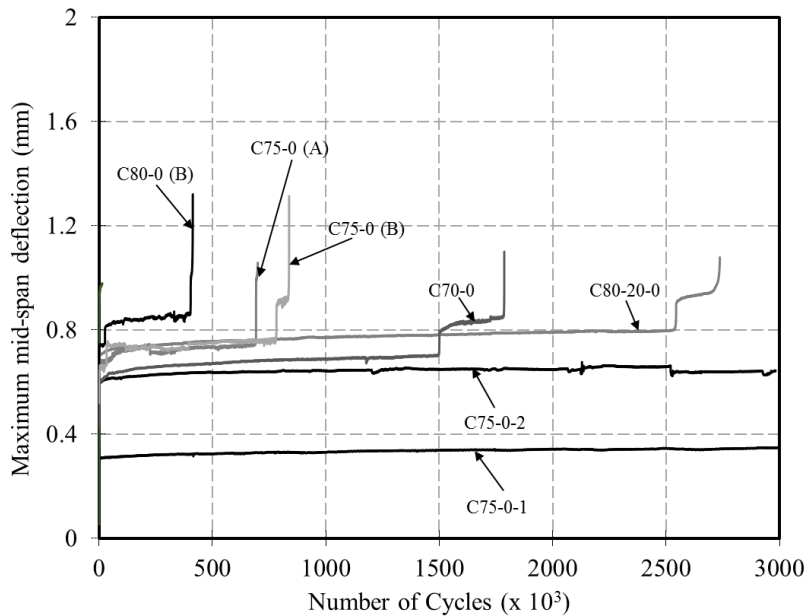


Fig. 6.5 – Evolution of mid-span deflection.

In other beams (C75-0, C70-0), flexural cracks occurred at the initial stage of fatigue loading. The applied fatigue load range was insufficient (low) to result in a shear-flexural crack at the initial stage. Although the development of inclined cracks away from the mid-span regions occurred afterwards due to the degradation of the tensile strength of concrete to a value corresponding to the induced tensile stress within the plane, the reinforcement fatigue damage within the mid-span region had increased substantially before the emergence of inclined cracks and initiation of rebar damage growth (crack propagation); hence, the observed failure occurred within the mid-span region. In beam C80-20-0, the maximum fatigue load resulted in a diagonal crack at

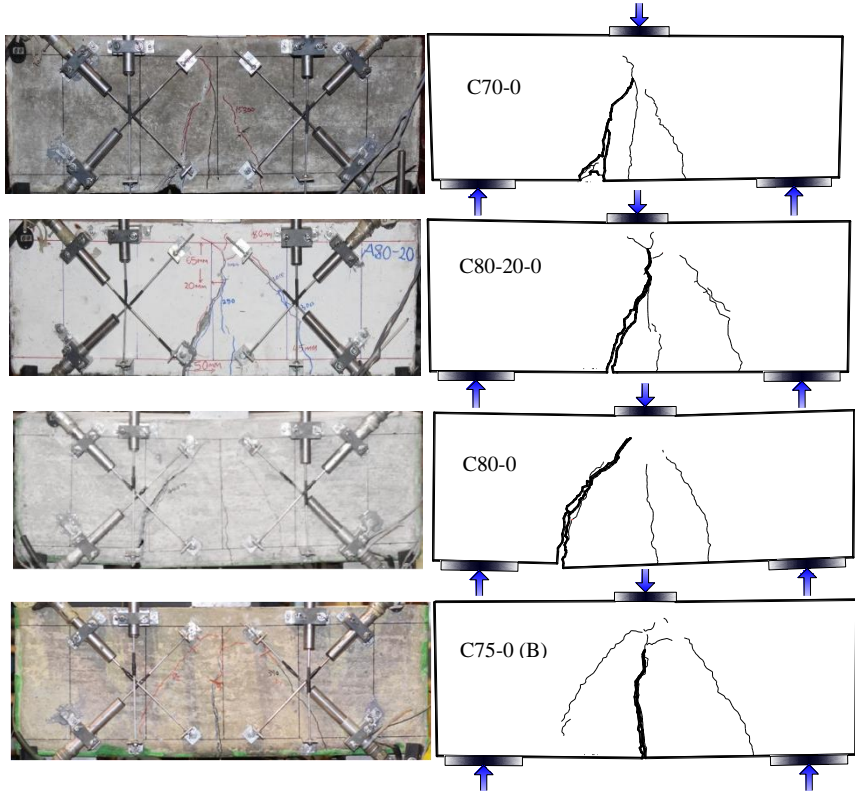


Fig. 6.6 - Crack pattern and shear-span fatigue degradation.

the initial stage of fatigue loading; however, the damage concentration within the mid-span region was also attributed to the increased minimum fatigue load which resulted in a low fatigue load range. This behaviour supports the observation by Chang and Kesler (1958) regarding the

influence of fatigue load on failure regions.

The degradation of the beams under fatigue loading can also be observed from the hysteresis loops obtained from each tested specimen (Figure 6.7). As the minimum fatigue load increased, the degradation or inclination of each hysteresis loop towards the abscissa tended to decrease (C80-0 and C80-20-0). As the fatigue load range increased, a corresponding increase in the degradation of the hysteresis loops was also observed. The large increase in mid-span deflection between hysteresis loops as indicated in C75-0, C70-0, and C80-20-0 indicates reinforcement fracture or substantial cracking.

#### **6.4.2 Shear-Span Deformation**

Within the shear span, the average shear strain, the average principal compressive strain evolution, and the average tensile strain evolution were monitored. In addition, the strain evolution on the reinforcing bars (shear and longitudinal) at regions within the shear spans were observed. As shown in Figure 6.8, the strain evolutions in the longitudinal reinforcing bars in beams C75-0-1 and C75-0-2 were higher than the strain evolutions in the shear reinforcement. This further supports the predominance of the arch mechanism (load transfer path) behaviour and the obvious reason for fracture of the longitudinal reinforcing bars instead of the shear reinforcement. The analysis involved in the prediction of the strain evolutions will be discussed in a subsequent section (including beam C80-0).

From Figure 6.9, it can be observed that for beams with similar reinforcement ratios (C80-0, C75-0, and C70-0), the shear span deformations in terms of the average shear strain, and average principal compressive and tensile strain evolutions, increased as the fatigue load level increased. Since the fatigue behaviour of beams C75-0 and C70-0 was governed by reinforcement crack

growth at the mid-span after concrete cracking, the mechanism which involved the transfer of forces through the compression strut to the support was altered due to localised behaviour at the mid-span as the reinforcement crack propagated. As such, the compressive strain within the shear span and its corresponding evolution, along with the average shear and average principal tensile strains, for beams C75-0 and C70-0 were almost constant except towards failure (see Figure 6.9).

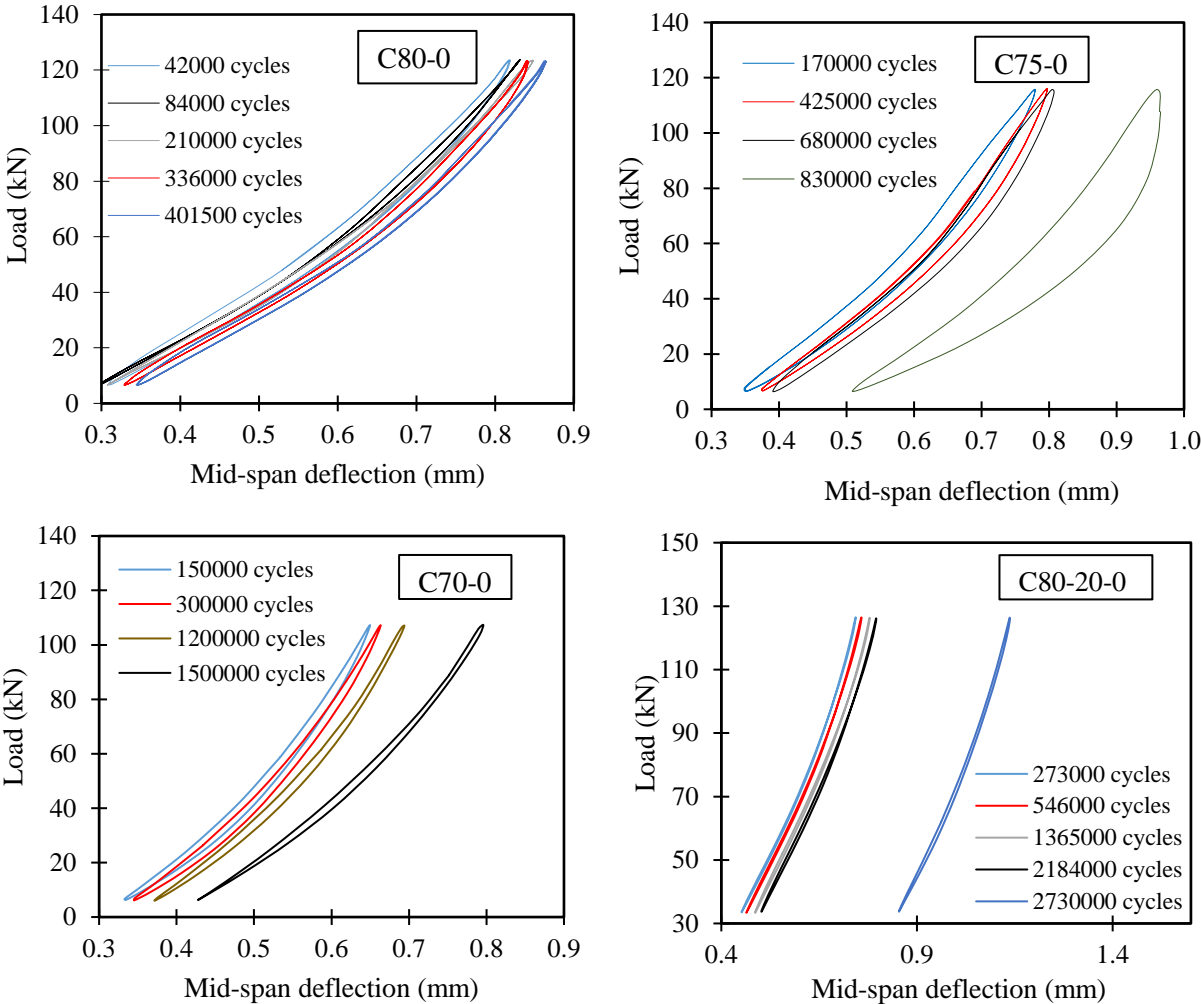


Fig. 6.7 – Fatigue hysteresis loops

**6.5 Fatigue Life Verification using Strut and Tie Model**

Under monotonic loading, an insight into the flow of forces in a deep beam can be obtained using

strut and tie models. The internal flow of forces is represented using concrete compression struts

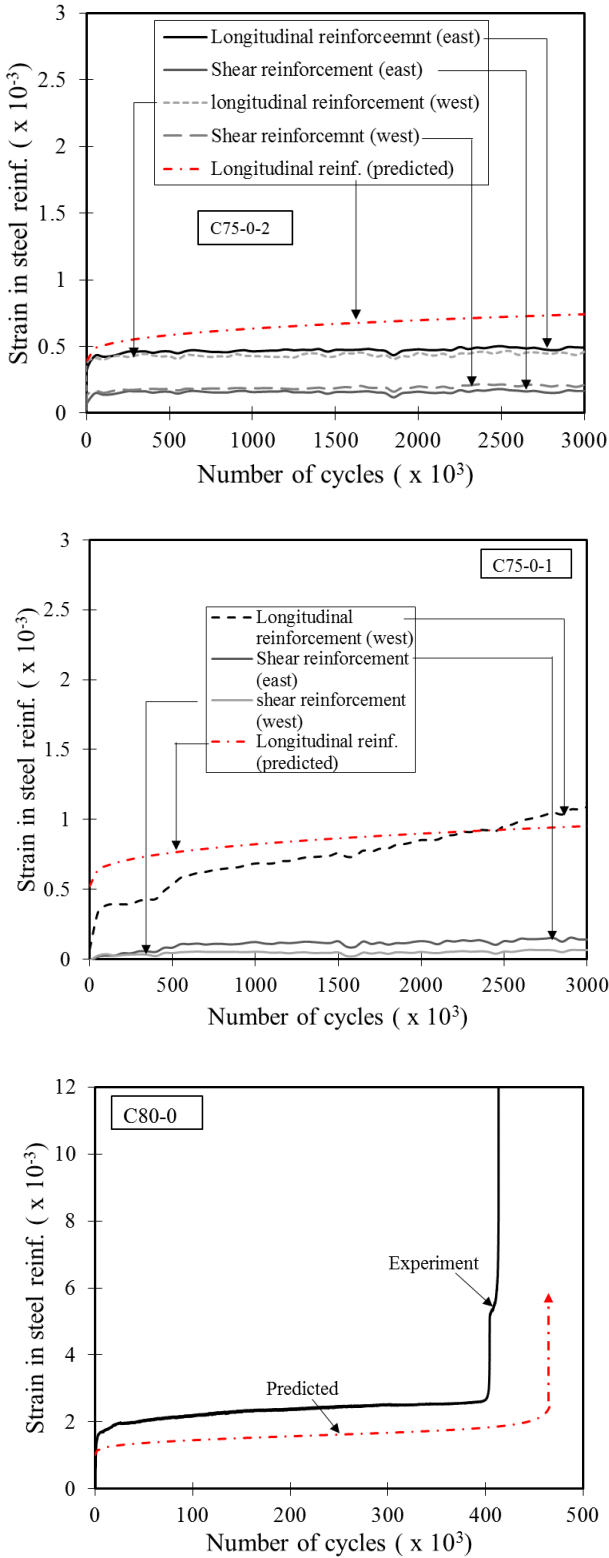


Fig. 6.8 –Strain evolution in reinforcing bars

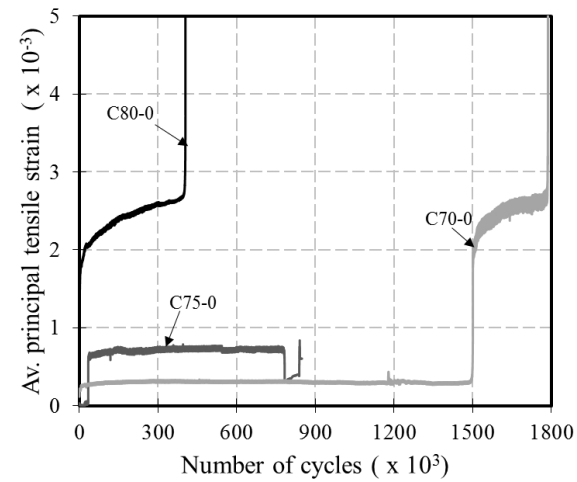
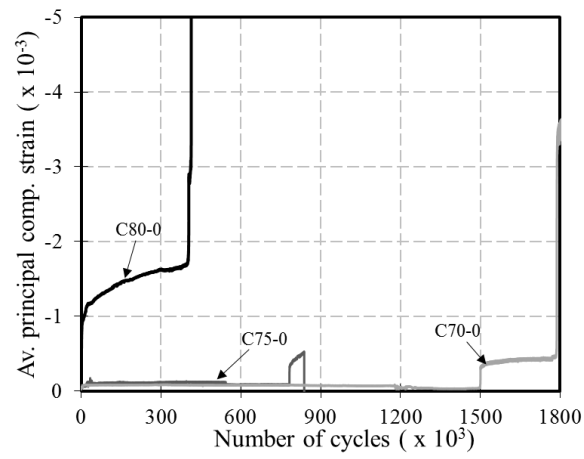
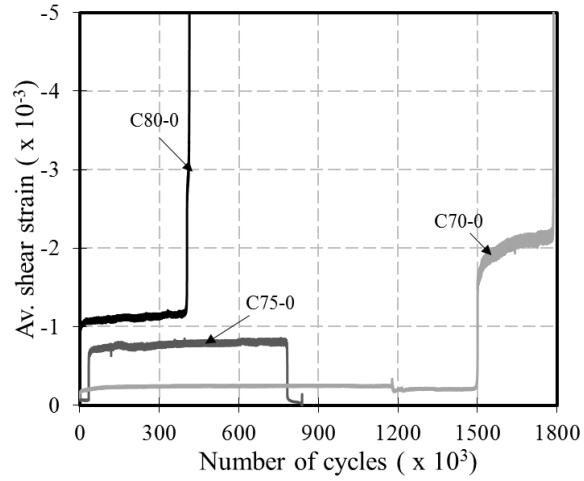


Fig. 6.9 – Average principal strain and shear strain evolutions.

and reinforcement ties, meeting at nodes. Since this concept is based on the lower bound theorem, equilibrium conditions must be fulfilled and the yield condition is not violated. A mechanism occurs once plasticity develops. Stresses in concrete are limited to the crushing strength, while steel reinforcement is governed by the yield value (Muttoni et al., 1996; Collins and Mitchell, 1997).

Under fatigue loading, the initial stresses in the steel and concrete are lower than the limiting capacity along the stress trajectory (see Figure 6.10). As the number of cycles increases, the induced stress in concrete increases, irreversible strain accumulates, and the limit strength decreases. Further, an increase in steel stress due to crack growth occurs. Provided models can be developed to account for the occurrence of a mechanism due to progressive deterioration, then the fatigue life of the structure can be predicted.

From the experimental results reported herein, the collapse due to fatigue failure of each beam was governed by fracture of the longitudinal reinforcing bars under fatigue loading. It was postulated previously that this behaviour is attributable to the fact that load is transferred to the support from the loading point through arch mechanism and not by truss action common with beams having shear span to effective depth ratios greater than 2.0.

In the analysis of fatigue loading, the deterioration of material properties such as concrete strength, steel residual area after crack growth, and the irreversible compressive strain accumulation can be accounted for in the constitutive, compatibility, and equilibrium equations of an analysis algorithm such as used with strut and tie models. As such, a reinforced concrete beam damaged due to fatigue may fail when reloaded statically up to the same fatigue load after a given number of cycles. At the point of failure, crushing of the concrete struts or fracture of

the reinforcing bars (shear or longitudinal, depending on the  $a/d$  value) may govern when the acting force in either the concrete or steel reinforcing bars becomes equal to the corresponding resistance capacity. The number of cycles at which this occurs is termed the fatigue life of the structural element.

To further illustrate this concept, the number of cycles leading to failure for each beam tested in this investigation were predicted. The predicted number of cycles were compared with those obtained using Helgason et al. (1976) (used by AASHTO (2007)). The fatigue load used for the prediction was taken as the average load from the two curves for the CONT-1, CONT-2 and CONT-3 beams (Figure 6.2).

### 6.5.1 Fatigue equilibrium equation

From Figure 6.10,

$$F_o = A(i) E_s \varepsilon_x \quad (6.4)$$

$$T_o = A_v E_s \varepsilon_v \quad (6.5)$$

$$D_i = f_{c2} w (p_u \sin \theta + d_a \cos \theta) \quad (6.6)$$

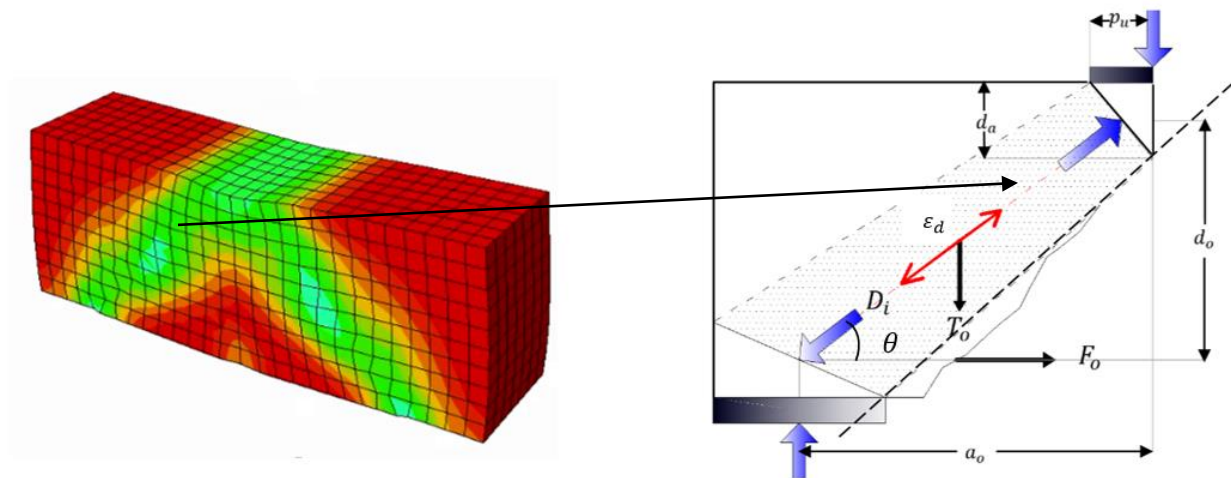


Fig. 6.10 - Strut and tie model for a deep beam under fatigue loading.

Under fatigue loading, the irreversible strain ( $\varepsilon_d$ ) is considered as a pseudo-load. The value is assumed to be zero at the first cycle (Isojeh and Vecchio, 2016). For subsequent cycles,

$$F_{ed} = E_{cfat} \varepsilon_d w (p_u \sin \theta + d_a \cos \theta) \quad (6.7)$$

In Figure 6.10 and Equations. 6.4 to 6.7,  $F_o$  is the force in the longitudinal reinforcement,  $A(i)$  is the residual longitudinal reinforcement area (function of reinforcement crack growth),  $E_s$  is the elastic modulus of the steel reinforcement,  $\varepsilon_x$  is the strain in the longitudinal reinforcement,  $T_o$  is the force in the shear reinforcement within the shear span,  $A_v$  is the area of shear reinforcement within the shear span,  $\varepsilon_v$  is the assumed strain in the shear reinforcement,  $D_i$  is the compressive force in the concrete strut,  $f_{c2}$  is the compressive stress in the concrete strut (function of concrete damage evolution),  $w$  is the width of the beam,  $p_u$  is taken as half of the loading plate length,  $\theta$  is the inclination of the compressive strut to the horizontal,  $d_a$  is the depth of the nodal zone under the loading plate,  $F_{ed}$  is the pseudo-load due to irreversible strain accumulation,  $E_{cfat}$  is the residual stiffness of concrete strut, and  $\varepsilon_d$  is the irreversible fatigue strain.

## 6.5.2 Fatigue Constitutive Models

The fatigue constitutive models used for concrete under compression fatigue loading and the corresponding irreversible strain ( $\varepsilon_d$ ) model have been previously developed by Isojeh et al., (2017a and b) and reported in Chapters 2 and 3. These models were used in this investigation for the fatigue damage analysis of concrete. Equations 6.8 and 6.9 are constitutive models for normal strength concrete using Hognestad's equation. Using the Hognestad (1954) equation for concrete compressive stress –strain model, the stress in a fatigue-damaged strut is expressed as

$$\left(\frac{\varepsilon_{c2}}{\varepsilon_c^*}\right)^2 - \frac{2\varepsilon_{c2}}{\varepsilon_c^*} + \frac{f_{c2}}{f_p(1-D_{fc})} = 0 \quad (6.8)$$

$$\varepsilon_c^* = \varepsilon_p (1 + \sqrt{D_{fc}}) - \varepsilon_d \quad (6.9)$$

$f_{c2}$  is the principal compressive stress,  $f_p$  is the peak concrete compressive stress (equal to  $f'_c$ ),  $\varepsilon_p$  is the compressive strain corresponding to  $f_p$ ,  $\varepsilon_{c2}$  is the average net strain in the principal compressive direction, and  $\varepsilon_c^*$  is the strain corresponding to the peak stress of the degraded concrete. Models for  $D_{fc}$  and  $\varepsilon_d$  can be obtained from Isojeh et al. (2017a) and (2017b), respectively.

The total fatigue life of the steel reinforcement can be assumed to constitute the crack initiation life (controlled by localised plasticity-crack nucleation) and the crack propagation life. For ductile materials, the crack initiation life is usually lower than the crack propagation life. However, the reverse is true for brittle materials. The strain-life approach which considers localised plasticity was used to obtain the crack initiation life, while fracture mechanics was used to estimate the crack propagation life from an initial crack length (Socie et al., 1984). The localised stress and strain on the reinforcement at the intersection with a concrete crack can be obtained using finite element analysis modelling or simply by Neuber's rule (Equation 6.10). Neuber's rule is often used to extrapolate elastic analysis so that stresses and strains associated with the effects of local yielding can be obtained.

$$\sigma \varepsilon = \frac{(K_t S)^2}{E} \quad (6.10)$$

$K_t$  is the stress concentration factor, and  $S$  is the nominal stress.  $\sigma$  and  $\varepsilon$  are the localised stress and strain, respectively. The mean value of  $K_t$  (depending on the reinforcement geometries) was obtained as 1.9 from a table and chart given by Jhamb and MacGregor (1974) on stress concentration factors for reinforcing bars. In order to express the material properties of steel in the form of a cyclic stress-strain and strain-life curve, Masing's (1926) model and the Smith-Watson-Topper (SWT) approach expressed in Equations 6.11 and 6.12, respectively, were used (Smith et

al., 1970; Dowling and Thangjitham, 2000). The SWT model is empirically based and accounts for the effect of mean stresses on fatigue behaviour. The SWT model relates the product of the maximum stress and total strain amplitude ( $\sigma_{max}\varepsilon_a$ ) to the fatigue life. The total strain consists of the summation of the elastic and plastic terms. According to the model, the product of the stress amplitude and strain amplitude for a fully reversed test is equal to  $\sigma_{max}\varepsilon_a$  for a mean stress test (Lee et al., 2005). The parameters (mean test values) in the model  $\sigma'_f$ ,  $b$ ,  $c$ ,  $\varepsilon'_f$  are fitting constants which are essentially material properties.

$$\varepsilon_a = \frac{\sigma_a}{E} + \left(\frac{\sigma_a}{H'}\right)^{\frac{1}{n'}} \quad (6.11)$$

$$\sigma_{max}\varepsilon_a = \frac{(\sigma'_f)^2}{E} (2N_f)^{2b} + \sigma'_f\varepsilon'_f (2N_f)^{b+c} \quad (6.12)$$

The approach for estimating  $\sigma_{max}$ ,  $\varepsilon_{max}$  (maximum stress and strain at a notch) and  $\sigma_a$  (stress amplitude and corresponding strain) are illustrated in Boller and Seeger (1987) and Dowling and Thangjitham (2000). From Boller and Seeger (1987), the parameters in Equations 6.11 and 6.12 common to the tests conducted in this investigation (mean test values) are given as

$$b = -0.087, c = -0.58, \varepsilon'_f = 0.59, \sigma'_f = 720 \text{ MPa}, n' = b/c = 0.15, H' = \frac{\sigma'_f}{\varepsilon'_f n'} = 779.3 \text{ MPa}.$$

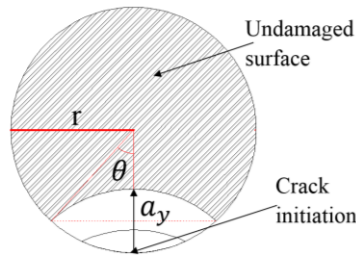


Fig. 6.11 - Crack growth on a reinforcing bar surface.

For the crack propagation life prediction, the residual area of the cracked reinforcement was estimated using the approach and formulas reported in Isojeh and Vecchio (2016), reproduced in Figure 6.11 and Equations 6.13 and 6.14:

$$A(a_y) = \frac{\theta}{90} \pi r^2 - r \sin \theta (2r - a_y) \quad (6.13)$$

$$\theta = \cos^{-1} \left( \frac{r - 0.5a_y}{r} \right) \quad (6.14)$$

$A(a_y)$  is the area of the fractured surface of a steel reinforcing bar,  $\theta$  is shown in Figure 6.11,  $a_y$  is the crack depth, and  $r$  is the radius of the reinforcing bar. The fracture mechanics models for estimating  $a_y$ , the initial crack, and the shape factor are considered subsequently.

### 6.5.3 Reinforcement Crack Growth

From the Paris crack growth law (Equation 6.15), the propagation of a reinforcing bar crack can be expressed as a function of the stress intensity factor range ( $\Delta K$ ) (Equation 6.16). The parameter  $\Delta K$  is generally expressed as a function of the fatigue stress range ( $\Delta\sigma$ ), crack size ( $a$ ) and a shape factor ( $Y$ ) for the reinforcing bar (Paris et al., 1960; Lee et al., 2005; Rocha and Bruhwiler, 2012, Herwig et al., 2008).

$$\frac{da}{dN} = C \cdot \Delta K^n \quad (6.15)$$

$$\Delta K = Y \cdot \Delta\sigma \cdot \sqrt{\pi a} \quad (6.16)$$

The crack depth ( $a_j$ ) for a given number of cycles is estimated from Equations 6.15 and 6.16 thus:

$$a_j = \left( \frac{a_i^\alpha}{1 - [N_{ij} (C \cdot \alpha \cdot \pi^{\frac{n}{2}} \cdot Y^n \cdot \Delta\sigma^n \cdot a_i^\alpha)]} \right)^{\frac{1}{\alpha}} \quad (6.17)$$

where  $\alpha = (n/2) - 1$ .

$a_i$  and  $a_j$  are the smallest and largest crack depth for the interval of cycles considered ( $N_{ij}$ ).

However, the estimation of  $a_j$  requires the value of  $a_i$ , which is the previous crack depth.  $Y$  is the shape factor. The initial minimum crack can be obtained iteratively from Equation 6.18 (Herwig, 2008):

$$a_o = \frac{1}{\pi} \left( \frac{\Delta K_{th}}{Y \Delta\sigma_{lim}} \right)^2 \quad (6.18)$$

where  $\Delta\sigma_{lim}$  corresponds to the fatigue limit stress at which fatigue damage will not initiate, and  $\Delta K_{th}$  is the threshold stress intensity factor. The crack does not propagate for stress intensity values lower than  $\Delta K_{th}$ . However, the threshold intensity factor was taken as  $5 \text{ MPa} \sqrt{m}$  (Farahmand and Nikbin, 2005) (m is in metres). An equation for the shape factor, recommended in BS 7910 (2005) as a function of the crack depth, is given in Equation 6.19.

$$Y = \frac{\frac{1.84}{\pi} \left\{ \tan\left(\frac{\pi a}{4r}\right) / \left(\frac{\pi a}{4r}\right) \right\}^{0.5}}{\cos\left(\frac{\pi a}{4r}\right)} \cdot \left[ 0.75 + 2.02 \cdot \left(\frac{a}{2r}\right) + 0.37 \cdot \left\{ 1 - \sin\left(\frac{\pi a}{4r}\right) \right\}^3 \right] \quad (6.19)$$

where r is the radius of the reinforcing bar and a is the crack depth.

The residual area of reinforcement A(i) required in Equation 6.4 was obtained by subtracting the area of the fractured surface from the initial reinforcing bar area. It was assumed that the stresses induced in the reinforcing bars on the same layer in a beam cross section are equal. As such, the progressive reduced area can be obtained by multiplying the initial area of reinforcement or reinforcement ratio by the ratio of a rebar's residual area to its uncracked area.

#### 6.5.4 Compatibility Equation

From a Mohr's circle of strain, the relationship between the strain in the horizontal direction, the principal tensile strain and the principal compressive strain can be estimated from:

$$\varepsilon_{c1} = \varepsilon_x + (\varepsilon_x - \varepsilon_{c2}) \cot^2 \theta \quad (6.20)$$

where  $\varepsilon_{c1}$  is the average effective principal tensile strain,  $\varepsilon_x$  is the average strain the horizontal direction,  $\varepsilon_{c2}$  is the average effective principal compressive strain, and  $\theta$  is the inclination of the compression strut. The average strain in the vertical direction (required in Equation 5) within the shear span is estimated as:

$$\varepsilon_v = 0.5 \varepsilon_{c1}(1 - \cos 2\theta) + 0.5 \varepsilon_{c2}(1 + \cos 2\theta) \quad (6.21)$$

Since appropriate anchorage was ensured based on design specification, perfect bond was assumed in this investigation. Hence, the horizontal strain  $\varepsilon_x$  is taken as the strain in the longitudinal reinforcement, while the vertical strain  $\varepsilon_v$  is the strain in the shear reinforcement within the shear-span. In this approach, it was also assumed that cracks do not propagate on the shear reinforcement as the number of cycles increases. This is attributed to the fact that the estimated forces in shear reinforcement are overly conservative since the contributions of other mechanisms such as aggregate interlock and clamping effects were neglected. This approach was used to estimate the number of cycles at which the fracture of the longitudinal reinforcing bars at the intersection with

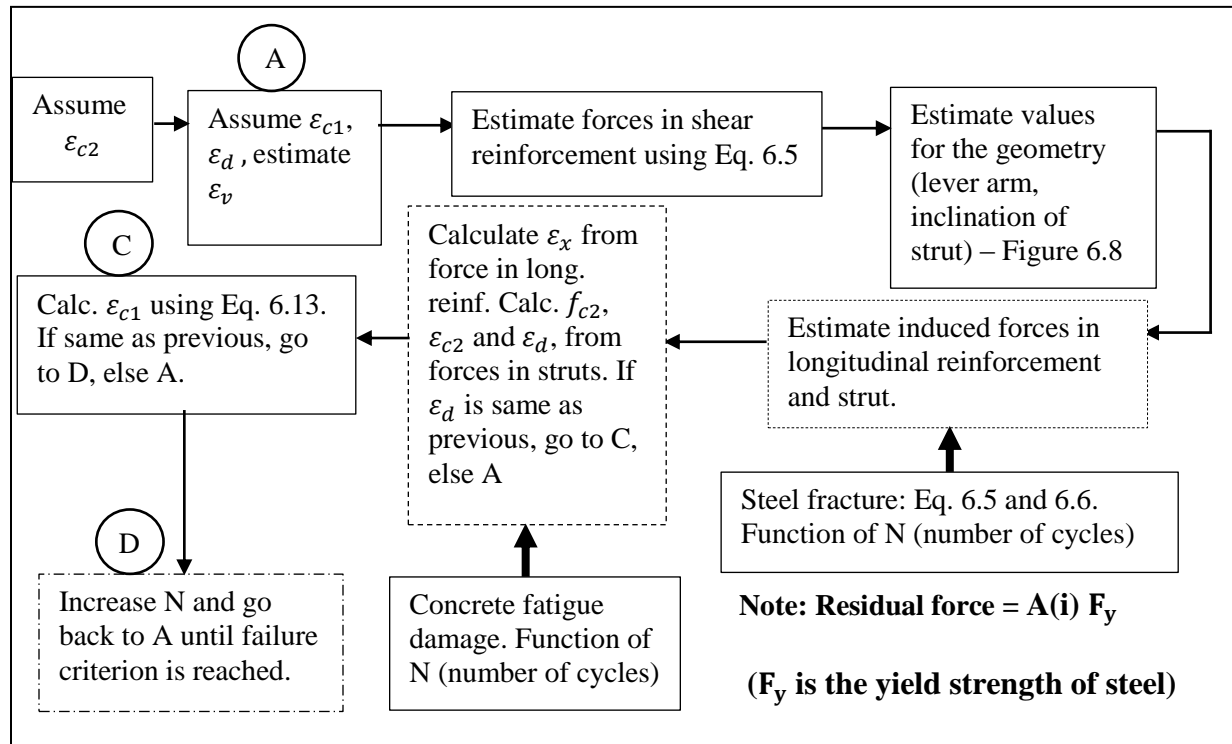


Fig. 6.12 - Algorithm for predicting the fatigue life of a deep beam.

a concrete crack will occur. The algorithm used is shown in Figure 6.12. Basically, the equilibrium, compatibility, and constitutive equations are satisfied for each cycle of fatigue loading

considered while accounting for the progressive damage and area reduction of the strut and tie, respectively, until the governing failure criterion is reached.

The fatigue life predictions for beams C80-0, C75-0, C70-0, and C80-20-0 are shown in Figures 6.13 and 6.14 in addition to the predictions obtained using Helgason et al. (1976). The predictions using Helgason et al.'s model tend to be overly conservative compared to the predictions using the proposed approach. The numbers of cycles predicted in both cases are given in Table 6.2. From the models proposed by Helgason et al. (1976), an endurance limit is assumed below which failure will not occur. This simply means beam C80-20 will not fail under fatigue loading, hence leading to an unsafe fatigue life prediction.

One of the motives of the proposed approach in this chapter was to develop a conservative means for fatigue life prediction. However, as the fatigue load range begins to reduce as in the cases of C70-0 and C80-20 in Figure 6.14, the range for acceptable predictions is expected to be wider since variations in the number of cycles to failure corresponding to small or insignificant changes in loading are significantly large due to the low induced stresses (as revealed in fatigue tests and in developed S-N curves for high and low stresses in the literature). This is attributed to the lower fatigue life prediction shown in Figure 6.14. In addition, for low fatigue loads and under-reinforced beams, fatigue damage tends to concentrate within the mid-span region; hence the effect of the irreversible strain in the compressive strut on the longitudinal reinforcing bars reduces. Conservatively, the influence of irreversible strains were fully considered in the predictions for the fatigue lives of beams C70-0 and C80-20; hence the lower fatigue life predictions.

The strain in the longitudinal reinforcing bars ( $\epsilon_x$ ) per interval of cycles up to failure were also plotted and shown in Figure 6.8. As observed, the three phases of fatigue damage evolution are

well-defined within the fatigue life for beam C80-0.

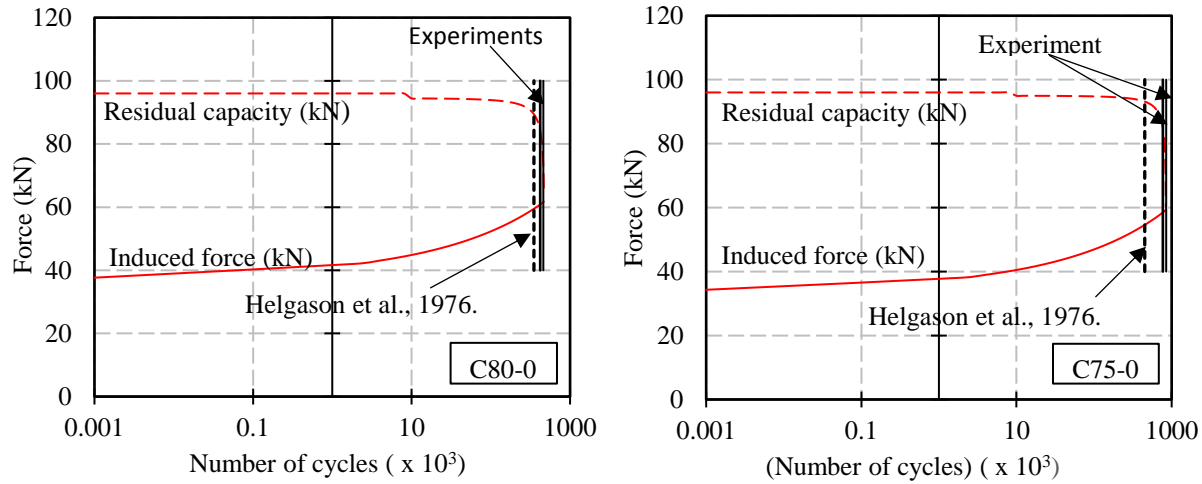


Fig. 6.13 - Fatigue life prediction from strut and tie model (C80-0 and C75-0).

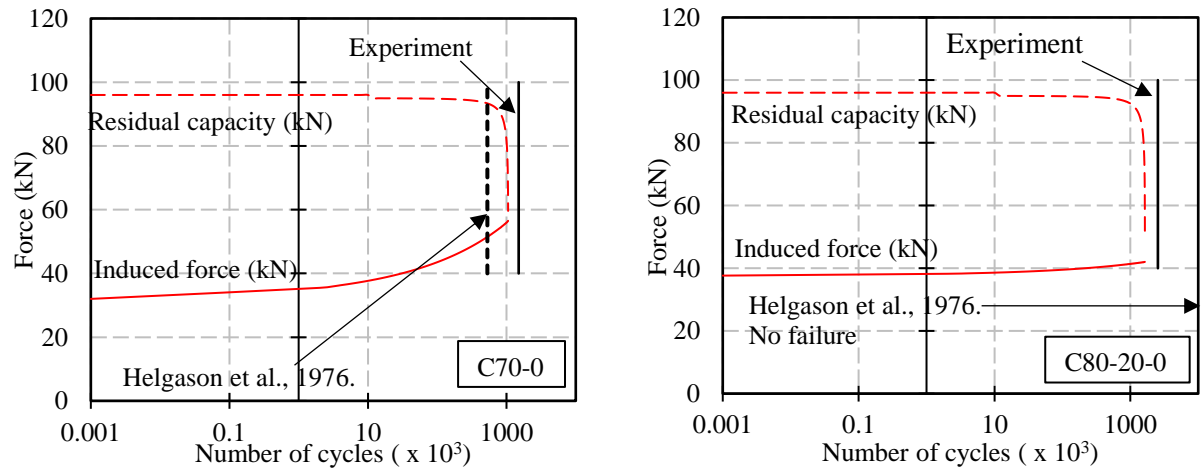


Fig. 6.14 - Fatigue life prediction from strut and tie model (C70-0 and C80-20).

The first phase entails a nonlinear deformation. The second phase is characterized by a constant rate of deformation, and the last stage is characterized by an increasing rate of damage leading to failure. The induced force in the steel reinforcement is estimated using Equation 6.4, while the residual capacity of the reinforcement is obtained from the product of the residual area and the yield strength. Failure becomes imminent when both evolutions converge (Figures 6.13 and 6.14).

The predicted results using the proposed approach are conservative and reasonably close to the experimental values; hence, the approach can be implemented in the prediction of the fatigue life of deep beams.

The simple strut-tie model used in this investigation was based on the low value of the shear span to effective depth ratio and the actual load path of force transfer from the load point to the support of the tested specimens (see Figure 6.10). For larger spans which involve more struts and ties, the same concept of constitutive, compatibility, and equilibrium equation modification can be employed. In these cases, failure will occur in the region with the highest stress.

The significance of this approach stems from the fact that the fatigue failure of beams with large shear span to effective depth ratios (governed by truss action) can also be predicted. In essence, the approach accounts for progressive crack development in reinforcement (shear or longitudinal) and concrete damage; hence, it represents an advantage over previous models which consider fracture of the shear reinforcement as the only fatigue limit state.

Although a point load was considered in this investigation, in the case of distributed loading, the fanning concept of struts is used (Muttoni et al., 1996; Collins and Mitchell, 1997). In the same manner as described for the point load, the governing equations for equilibrium, compatibility, and stress-strain response can be modified using the referred damage evolution models; however, experimental verification of these is required.

Small-scale beams have been considered in this investigation. The size effect on plain concrete under monotonic and fatigue loading is well known. The crack growth rate per fatigue loading cycle of plain concrete is higher for larger sizes (Bazant and Xu, 1991; Sain and Chandra, 2007). It is considered expedient that more tests be conducted on lightly-reinforced and sufficiently

reinforced large scale beams, and that the proposed approach be further scrutinized to ascertain its validity.

## **6.6 Conclusions**

The behaviour of deep beams under fatigue loading has been investigated by conducting tests on small-scale deep beams. The progressive deformations within the shear spans and mid-spans were measured. In all, the rate of deformation was observed to increase as the stress level or stress range increased. It was observed that beams with increased longitudinal reinforcement ratios exhibited a higher fatigue life, hence supporting our current understanding of the fatigue behaviour of reinforced concrete structures.

The fatigue behaviour observed was governed by the load transfer mechanism and the induced stresses within the load path. The specimens tested failed by fracture of the longitudinal reinforcement either within the shear span or in the mid-span region. The results obtained using the modified strut and tie analysis approach described in this chapter gave appropriate fatigue life prediction; hence, the approach provides a reliable means for the fatigue analysis of deep beams.

Within the range of failure, the predicted results obtained for the specimens using the proposed approach were found to be conservative. An additional advantage of the proposed fatigue analysis approach stems from the fact that the progressive deformation and the actual mechanism of failure (crushing of concrete or fracture of steel), depending on the governing criterion, can be observed.

## **6.7 References**

1. AASHTO. AASHTO LRFD Bridge Design Specifications, 4<sup>th</sup> Edition, 2008 and 2009

- Interim, American Association of State Highway and Transportation Officials, Washington DC 2007.
2. ACI 318-14 to ACI 346-09. Manual of Concrete Practice: Part 3 of 7. American Concrete Institute.
  3. Bazant Z., and Xu K. (1991). "Size Effects in Fatigue Fracture of Concrete." *ACI Materials Journal*, Vol.88, No. 4, pp. 390-9.
  4. Bentz E., Vecchio F.J., and Collins M.P. (2006). "Simplified Modified Compression Field Theory for Calculating Shear Strength of Reinforced Concrete Elements." *ACI Structural J.*, Vol.103, No. 4, pp. 614-24.
  5. Boller C., and Seeger T. (1987). "Materials Data for Cyclic Loading." Elsevier Science Pubs., Amsterdam, 1987.
  6. British Standard (2005). "Guide to Methods for Assessing the Acceptability of Flaws in Metallic Structures." BS 7510.
  7. Cement Association of Canada (2006). "Concrete Design Handbook. 3<sup>rd</sup> Edition." CAC.; Ottawa, Ontario.
  8. Chang T.S., and Kesler C.E. (1958). "Static and Fatigue Behaviour in Shear of Beams with Tensile Reinforcement." *ACI Journal*, Vol. 54, pp. 1033-1058.
  9. Collins M.P, and Mitchell D. (1997). "Prestressed Concrete Structures." Response Publication, Canada.
  10. Dowling N.E., and Thangjitham N.E. (2000). "An Overview and Discussion of Basic

- Methodology for Fatigue.” Fatigue and Fracture mechanics: ASTM STP 1389, Vol. 31:3-36.
11. EC2. Eurocode 2 (2004): Design of Concrete Structures-Part 1-1: General Rules for Buildings. London, UK: British Standards Institution, BS EN 1992-1-1.
  12. Farahmand B., and Nikbin K. (2008). “Predicting Fracture and Fatigue Crack Growth Properties using Tensile Properties.” Engineering Fracture Mechanics, Vol.75, pp. 2144-2155.
  13. Goransson F., and Nordenmark A. (2011). “Fatigue Assessment of Concrete Foundations for Wind Power Plants.” Department of Civil and Environmental Engineering (Master’s Thesis), Chalmers University of Technology, Goteborg, Sweden.
  14. Hawkins N.M. (1974). “Fatigue Characteristics in Bond and Shear of Reinforced Concrete Beams.” Abeles Symposium, ACI Pub. SP41-10, pp. 203-36.
  15. Herwig A. (2008). “Reinforced Concrete Bridges under Increased Railway Traffic Loads- Fatigue Behaviour and Safety Measures.” Ph. D Thesis No. 4010, Ecole Polytechnique Federale de Lausanne.
  16. Higai T. (1983). “Fundamental Study on Shear Failure of Reinforced Concrete Beams.” JSCE, Vol.1, pp. 25-39.
  17. Helgason T., Hanson J.M., Somes NF, Corley WG, and Hognestad E. (1976). “Fatigue Strength of High-Yield Reinforcing Bars.” National Cooperative Highway Research Program Report, Vol.161, pp.1-90.
  18. Hognestad, E. (1954). “Confirmation of Inelastic Stress Distribution in Concrete.”

- Proceedings, ASCE 1954; Vol. 83, No. 2, pp.1-17.
19. Isojeh B., El-Zeghayar M., and Vecchio F.J. (2017a). “Concrete Damage under Fatigue Loading in Uniaxial Compression.” *ACI Materials Journal*, Vol. 114, No. 2, pp. 225-235.
  20. Isojeh B., El-Zeghayar M., and Vecchio, F.J. (2017b). “Simplified Constitutive Model for Fatigue Behaviour of Concrete in Compression.” *ASCE Journal of Materials*, 10.1061/(ASCE)MT.1943-5533.0001863.
  21. Isojeh, M.B., and Vecchio, F.J. (2016). “Parametric Damage of Concrete under High-Cycle Fatigue Loading in Compression.” *Proc., 9<sup>th</sup> International Conference on Fracture mechanics of Concrete and Concrete Structures. FraMCoS-9*, 10.21012/FC9.009.
  22. Jhamb I.C., and MacGregor J.G. (1974). “Stress Concentration Caused by Reinforcing Bar Deformations.” *ACI SP J. Vol. 41*, pp. 169-182.
  23. Lee Y., Pan J., Hathaway R., and Barkey M. (2005). “Fatigue Testing and Analysis: Theory and Practice.” Elsevier Butterworth-Heinemann.
  24. Masin G. (1926). “Internal Stresses and Hardening of Brass.” *Proc. 2<sup>nd</sup> Int. Congress for Appl. Mech., Zurich*.
  25. Mau S.T., and Hsu T.T.C. (1987). “Shear Strength Prediction for Deep Beams with Web Reinforcement.” *ACI Structural J.*, Vol. 84, pp. 513-523.
  26. Muttoni A., Schwartz J., and Thurlimann B. (1996). “Design of Concrete Structures with Stress Fields.” Birkhauser Basel Boston Berlin.

27. Okamura H., Farghaly S.A., and Ueda T. (1981). "Behaviour of Reinforced Concrete Beams with Stirrups Failing in Shear under Fatigue loading." Proc. of JSCE, Vol. 308, pp. 109-123.
28. Okamura H., and Ueda T. (1982). "Fatigue Behaviour of Reinforced Concrete Beams under Shear Force." IABSE Reports, Vol. 37, pp. 416-422.
29. Paris, P., Gomez, M.P., and Anderson W.E. (1961). "A Rational Analytical Theory of Fatigue." The Trend in Engineering, Vol. 13, pp. 9-14.
30. Rocha M., and Bruhwiler E. (2012). "Prediction of Fatigue Life of Reinforced Concrete Bridges." In Biondini and Frangopol (Eds) Bridge Maintenance, Safety, Management, Resilience and Sustainability, pp. 3755-3760.
31. Ruhnau J. (1974). "Influence of Repeated Loading on the Stirrup Stress of Reinforced Concrete Beams." ACI Pub. SP42-1, pp. 169-181.
32. Sain T., and Chandra Kishen J. (2007). "Prediction of Fatigue Strength in Plain and Reinforced Concrete Beams." ACI Materials Journal, Vol. 1, No. 5, pp. 621-628.
33. Smith K. N., Watson P., and Topper T. H. (1970). "A Stress-Strain Function for the Fatigue of Metals." Journal of Material Vol. 5, pp. 767-778.
34. Socie D., Dowling N.E., and Kurath P. (1984). "Fatigue Life Estimation of Notched Members." Fracture Mechanics: Fifteenth Symposium. ASTM STP 833, pp. 284-299.
35. Stelson T.E., and Cernica J.N. (1958). "Fatigue Properties of Concrete Beams." ACI Journal, Vol. 55, pp. 255-259.
36. Tamulenas V, Gelazius V, and Ramanauskas R. (2014). "Calculation Technique for Stress-

- Strain Analysis of RC Elements Subjected to High-Cycle Compression.” *Mokslas: Lietuvos Ateitis*. Vol. 6, No. 5, pp. 468–473.
37. Teng S., Ma W., Tan K.H., and Kong F.K. (1998). “Fatigue Tests of Reinforced Concrete Deep Beams.” *The Structural Engineer*, Vol. 76, pp. 347-352.
38. Teng S., Ma W., Wang F. “Shear Strength of Concrete Deep Beams under Fatigue Loading.” *ACI Structural J*. Vol. 97, pp. 572-580.
39. Ueda T. (1982). “Behaviour in Shear of Reinforced Concrete Deep Beams under Fatigue Loading.” Dissertation for the degree of Doctor of Engineering, University of Tokyo.
40. Veeman R., Van Breugel K., and koenders E. (2015). “Effects of Corrosion on the Fatigue Service-Life on Steel and Reinforced Concrete Beams.” *Concrete-Innovation and Design*, FIB Symposium, Copenhagen.
41. Zanuy C., Fuente P., and Albajar L. (2007). “Effect of Fatigue Degradation of the Compression Zone of Concrete in Reinforced Concrete Sections.” *Engineering Structures*. Vol. 29, pp. 2908-2920.
42. Zhang B., Phillips D.V., Wu K. (1996). “Effects of Loading Frequency and Stress Reversal on Fatigue Life of Plain Concrete.” *Magazine of Concrete Research*, Vol. 48, pp. 361-375.

## CHAPTER 7

### REINFORCED CONCRETE AND STEEL-FIBRE CONCRETE ELEMENTS UNDER FATIGUE LOADING: MODEL FORMULATION

*This material was submitted to ASCE Structural Journal, and is in review for publication as a technical paper.*

*Isojeh B., El-Zeghayar M., Vecchio F.J. "Reinforced Concrete and Steel Fibre Concrete Elements under Fatigue Loading: Model Formulation."*

#### 7.1 Abstract

The implementation of fatigue damage models into the governing equations of the Disturbed Stress Field Model algorithm for the fatigue analysis of reinforced concrete structures, within the context of nonlinear finite element analysis, is presented in this paper. The models account for concrete deterioration, localised reinforcement crack growth, and accumulation of irreversible compressive strain in conventional reinforced concrete or steel fibre reinforced concrete due to fatigue loading. As such, analyses involving fatigue damage can be expressed in terms of the deformation evolution and residual capacity. These concepts overcome the well-known limitations of stress-life models for fatigue analysis of reinforced concrete structures. The implementation using robust models previously proposed by the authors are described in this report. As a means of further illustration, the solution to the deformation of a shear element under pure shear fatigue loading is presented. The corroboration of the modified algorithm with experimental results for fatigue life and residual strength prediction are presented in Chapter 8.

#### 7.2 Introduction

A majority of collapsed dynamics-susceptible structures are linked to fatigue damage. Hence,

fatigue limit state verification is required to complement ultimate and serviceability limit states in the structural design of these structures. As a norm, the fatigue resistance capacity of a reinforced concrete structure is typically verified from the stresses induced in the constituent materials, obtained from static analyses of the maximum and minimum fatigue loads that the structure may resist. The highest stress values at critical sections are normalised with the ultimate strengths of the materials and are substituted into corresponding fatigue stress-life models (S-N curves) in order to obtain the number of cycles leading to failure (Aas-Jakobsen, 1970).

Experiments conducted and reported in the literature on the fatigue behaviour of concrete composites depict progressive parametric deterioration and accumulation of irreversible strains as governing mechanisms. In addition, cracks have been observed on reinforcing bars which evolve to final fracture (Salah El Din and Lovegrove, 1980; Okamura and Farghaly, 1981; Schlafli and Bruhwiler, 1998; Zanuy et al., 2009).

The inability of S-N models to account for progressive deformation became evident as the need arose for the damage evolution of concrete after some given number of cycles and load history (Holmen, 1982). Further, the significant influence of accumulated irreversible strains on structural components has typically been neglected.

In order to account for the progressive deformation under fatigue loading, constitutive models were developed for concrete composites and steel reinforcement by various researchers (Otter and Naaman, 1986; Otter and Naaman, 1988; Oh, 1991; Eligehausen et al., 1992; Park, 1990; Gao and Hsu, 1998; Teng et al., 2001; Petryna et al., 2002; Maekawa et al., 2006; Xiang and Zhao, 2007; Gebreyouhannes et al., 2008; Vega et al. 1995; Zanuy et al., 2009; Tamulenas et al., 2014). These simplified the prediction of the damage evolution of a structural component up to the instant of

collapse due to instability arising from concrete composite degradation and steel reinforcement fracture. However, a majority of the constitutive models developed for concrete are based on assumptions not adequately verified experimentally. In addition, significant fatigue-influencing parameters that were neglected limit the use of such models to structures having similar loading parameters as those used for developing such models (Isojeh et al., 2017a).

Although stress-life models (Tilly and Moss, 1982; Hanson, 1983; JSCE, 1986; Petryna et al., 2002) and the Palmgren-Miner rule (linear rule) (Palmgren, 1924; Miner, 1945) are used in modelling the progressive fatigue degradation of steel reinforcement, it is well-known that crack propagation in steel reinforcement is nonlinear. Since the main region of fatigue failure in reinforced concrete structures typically coincides with the location of concrete cracks intersecting the reinforcing bars, the progressive crack-growth of the reinforcement traversing the concrete crack plane should be well accounted for in order to appropriately predict the deformation within the concrete plane. Available models in the literature which incorporate the stress-life models and the Palmgren-Miner rule for steel reinforcement fatigue fracture do not capture this governing fatigue-damage mechanism and its corresponding evolution.

In this paper, robust modified damage models, an irreversible strain model, and constitutive models which have been proposed by the authors are used (Isojeh et al., 2017a; Isojeh et al., 2017b; Isojeh et al., 2017c). In addition, the governing fatigue damage mechanism and local stress conditions at crack locations are adequately accounted for by implementing reinforcement crack-growth models developed from fracture mechanics. These models are incorporated into the monotonic models of the well-known Disturbed Stress Field Model (DSFM) as functions of fatigue loading cycles and other salient fatigue loading parameters; hence, as fatigue loading cycles increase, the residual capacity of a structural element and its progressive deformation can

be obtained from load-deformation plots and deflection evolutions.

### **7.3 Disturbed Stress Field Model**

Solutions to engineering mechanics problems are obtainable provided associated equilibrium, compatibility and constitutive equations are satisfied. The capability of the Disturbed Stress Field Model (Vecchio, 2000; Vecchio, 2001) in predicting the behaviour of reinforced concrete structures subjected to different loading conditions, based on the aforementioned concept, is well documented (Vecchio, 2001; Vecchio et al., 2001; Facconi et al., 2014; Lee et al., 2016). As an extension of the Modified Compression Field Theory (Vecchio and Collins, 1986), the DSFM, founded on a smeared-rotating crack model, includes the consideration of deformation within concrete crack planes. The formulations of the DSFM can be adapted to allow for the consideration of the damage of concrete and the corresponding crack growth on steel reinforcement (longitudinal and transverse) intersecting a concrete crack under fatigue loading. The modification of these models are considered subsequently.

#### **7.3.1 Equilibrium Condition**

An orthogonally reinforced element under external forces (Figure 7.1) is in equilibrium as a result of the resistance from the induced average material stresses in the concrete composite and steel reinforcement. In the cracked state, the verification of equilibrium at the crack locations is required to ensure stresses are adequately transferred between cracks (Figure 7.2).

#### **7.3.2 Equilibrium of Average Stresses**

In Figure 7.1, the normal stresses are denoted by  $\sigma_x$  and  $\sigma_y$  and the shear stress as  $\tau_{xy}$ . Considering the average stresses in the element under static loading condition, the equilibrium condition based on the superposition of concrete and steel reinforcement stresses can be

expressed as shown in Equations 7.1 to 7.3.

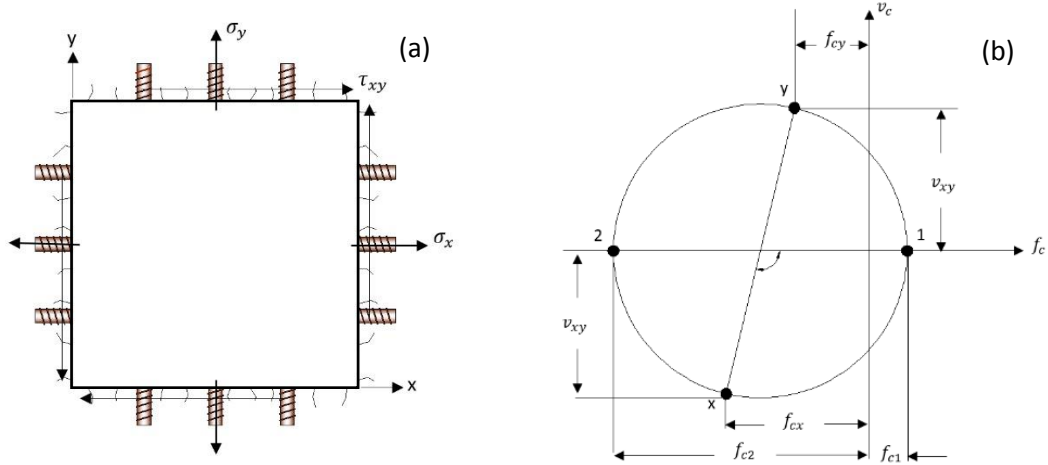


Fig. 7.1 - Steel fibre reinforced concrete element (a) Loading conditions; (b) Mohr's circle for average stresses in concrete.

$$\sigma_x = f_{cx} + \rho_x f_{sx} \quad (7.1)$$

$$\sigma_y = f_{cy} + \rho_y f_{sy} \quad (7.2)$$

$$\tau_{xy} = v_{cxy} \quad (7.3)$$

where  $\rho_x$  and  $\rho_y$  are the reinforcement ratios in the x- and y- directions, respectively.

The stresses in the concrete or steel fibre concrete ( $f_{cx}$ ,  $f_{cy}$ , and  $v_{cxy}$ ) can be obtained using Mohr's stress circle (Figure 1(b)) with known principal stresses ( $f_{c1}$ ,  $f_{c2}$ ). The principal stresses are obtained from constitutive models which are functions of concrete parameters such as strength, stiffness, and induced strains. Since these parameters (strength and stiffness) degrade and strains accumulate under fatigue loading, the material stresses change correspondingly. Constitutive models which account for fatigue degradation will be considered in a subsequent section.

### 7.3.3 Equilibrium of Stresses at a Crack

Under static loading, stresses in the reinforcement at crack locations are higher than the values between cracks (average values) since the concrete tensile stress is zero at such locations. As a result, shear stresses also develop on the crack surfaces at crack locations.

Since fatigue crack propagation is a function of the stress values, its initiation tends to occur at a reinforcement region traversing the concrete cracks where the stresses are high. From Figures 7.2(a) and 7.2(b), the general static equilibrium equations which involves steel fibre are given thus (Lee et al., 2016):

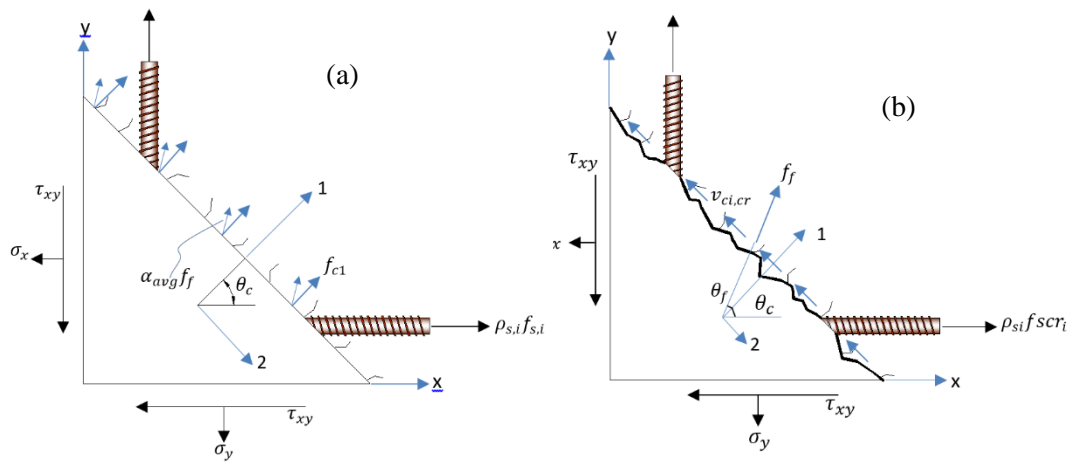


Fig. 7.2 - Equilibrium conditions: (a) Parallel to crack direction; (b) Along crack surface.

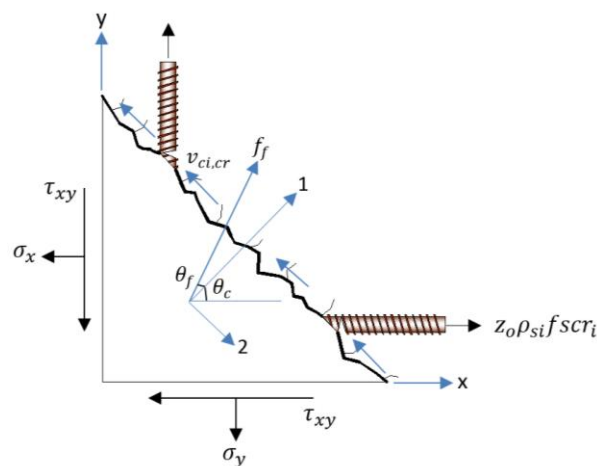


Fig. 7.3 - Equilibrium conditions along crack surface after reinforcement crack propagation.

$$f_{c1} = \sum_i^n \rho_{si} (f_{scri} - f_{si}) \cdot \cos^2 \theta_{ni} + (1 - \alpha_{avg}) f_f \cos \theta_f \quad (7.4)$$

$$v_{ci,cr} = \sum_i^n \rho_{si} (f_{scri} - f_{si}) \cdot \cos \theta_{ni} \sin \theta_{ni} - (1 - \alpha_{avg}) f_f \sin \theta_f \quad (7.5)$$

In Equations 7.4 and 7.5,  $(1 - \alpha_{avg}) f_f$  represents the contribution from steel fibre bridging a crack.  $\alpha_{avg}$  relates the tensile stress in steel fibre to the average principal tensile stress, while  $f_f$  is a function of the equivalent bond strength due to the mechanical anchorage of the steel fibre and the friction bond strength of steel fibre (Lee et al., 2016).

As cracks propagate in the reinforcement traversing a concrete crack, the area of reinforcement intersecting the crack reduces, hence resulting in lower reinforcement ratio at the crack. To account for the progressive reinforcement ratio reduction due to fatigue loading, Equations 7.4 and 7.5 are modified thus (Figure 7.3):

$$f_{c1} = \sum_i^n \rho_{si} (Z_0 f_{scri} - f_{si}) \cdot \cos^2 \theta_{ni} + (1 - \alpha_{avg}) f_f \sqrt{1 - D_{fc}} \cos \theta_f \quad (7.6)$$

$$v_{ci,cr} = \sum_i^n \rho_{si} (Z_0 f_{scri} - f_{si}) \cdot \cos \theta_{ni} \sin \theta_{ni} - (1 - \alpha_{avg}) f_f \sqrt{1 - D_{fc}} \sin \theta_f \quad (7.7)$$

$Z_0$  and  $D_{fc}$  are parameters representing reinforcement crack growth and plain or steel fibre concrete strength degradation, respectively.

### 7.3.4 Reinforcement Crack Growth Factor ( $Z_0$ )

From the Paris crack growth law (Equation 7.8), the propagation of a reinforcing bar crack, up to a depth resulting in fatigue fracture, can be predicted using a parameter representing the stress intensity factor range ( $\Delta K$ ) (Equation 7.9). This parameter is generally expressed as a function of the stress range ( $\Delta \sigma$ ), crack size ( $a$ ) and a shape factor ( $Y$ ) for the reinforcing bar (Paris et al., 1961; Rocha and Bruhwiler, 2012; Herwig et al., 2008).

$$\frac{da}{dN} = C.\Delta K^n \quad (7.8)$$

$$\Delta K = Y.\Delta\sigma.\sqrt{\pi a} \quad (7.9)$$

Equation 7.10 can be obtained from the integration of Equation 7.8 with respect to fatigue loading cycles, after substituting Equation 7.9 into Equation 7.8. Hence, the crack depth ( $a_y$ ) after a given number of cycles can be estimated.

$$a_y = \left( \frac{a_i^\alpha}{1 - [N_{ij} (C.\alpha.\pi^{\frac{n}{2}}.Y^n.\Delta\sigma^n.a_i^\alpha)]} \right)^{\frac{1}{\alpha}} \quad (7.10)$$

where  $\alpha = (n/2)-1$ ;  $C = 2 \times 10^{-13}$ ; and  $n = 3.0$ .

$a_i$  and  $a_y$  are the previous and current crack depth for the interval of cycles considered ( $N_{ij}$ ), respectively. In order to estimate  $a_y$  using Equation 7.10, the value of  $a_i$  must be known, which is the previous crack depth (Paris et al., 1961).

An equation for the shape factor (Y), proposed in BS 7910 (1999) as a function of the crack depth, is given in Equation 7.11. The crack depth ( $a_y$ ) can be obtained iteratively by substituting the equation for the shape factor (Equation 7.11) into Equation 7.10.

$$Y = \frac{\frac{1.84}{\pi} \left\{ \tan\left(\frac{\pi a}{4r}\right) / \left(\frac{\pi a}{4r}\right) \right\}^{0.5}}{\cos\left(\frac{\pi a}{4r}\right)} \cdot \left[ 0.75 + 2.02 \cdot \left(\frac{a}{2r}\right) + 0.37 \cdot \left\{ 1 - \sin\left(\frac{\pi a}{4r}\right) \right\}^3 \right] \quad (7.11)$$

The initial crack depth ( $a_i$ ) expressed as  $a_o$  at the onset of fatigue loading is obtained iteratively using Equation 7.12:

$$a_o = \frac{1}{\pi} \left( \frac{\Delta K_{th}}{Y\Delta\sigma_{lim}} \right)^2 \quad (7.12)$$

$r$  is the radius of the reinforcing bar and  $a$  is the crack depth,  $\Delta\sigma_{lim}$  corresponds to the fatigue limit stress at which fatigue damage will not initiate, and  $\Delta K_{th}$  is the threshold stress intensity factor.

The crack does not propagate for stress intensity values lower than  $\Delta K_{th}$ . The  $\Delta K_{th}$  value is taken as  $158 \text{ Nmm}^2$  (Farahmand and Nikbin, 2008).

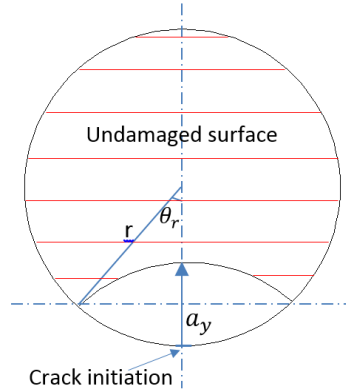


Fig. 7.4 - Crack growth on a reinforcing bar cross section.

The fractured surface area of a reinforcing bar can be assumed as shown in Figure 7.4. The crack depth ( $a_y$ ) evolves from an initiation point up to the instant when the reserve capacity of the reinforcement at the crack is no longer sufficient for tensile stress transfer.

From Figure 7.4, the fractured area ( $A(a_y)$ ) is estimated as:

$$A(a_y) = \frac{\theta_r}{90} \pi r^2 - r \sin \theta_r (2r - a_y) \quad (7.13)$$

$$\theta_r = \cos^{-1} \left( \frac{r - 0.5a_y}{r} \right) \quad (7.14)$$

The residual area ( $A_{res}$ ) of a reinforcing bar after crack propagation to a given number of cycles is obtained as:

$$A_{res} = A_o - A(a_y) \quad (7.15)$$

From Equation 7.15, the reinforcement crack growth factor ( $Z_o$ ) required in Equations 7.6 and 7.7 is obtained thus:

$$Z_o = \frac{A_{res}}{A_o} \quad (7.16)$$

where  $A_o$  is the cross-sectional area of the uncracked rebar. This is estimated for all reinforcing bars traversing the concrete crack, provided the induced stresses are higher than the threshold value

for crack initiation.

Prior to reinforcement crack propagation, the number of cycles resulting in a localised plasticity-crack nucleation or crack initiation may also be included using Masing's model and the SWT approach (Socie et al., 1984; Dowling and Thangjitham, 2000). To account for this, the value of the reinforcement crack growth factor is assumed to be a value of 1.0 in Equations 7.6 and 7.7 until the estimated crack initiation cycles is reached.

#### 7.4 Compatibility Condition

In the Disturbed Stress Field Model, the total strain  $[\varepsilon]$  in an element consists of the net strain  $[\varepsilon_c]$ , plastic offset strain  $[\varepsilon_c^p]$ , elastic offset strain  $[\varepsilon_c^o]$ , and strain effect due to slip at crack  $[\varepsilon_c^s]$ . The net strain, obtained from the difference between the total strain and the other aforementioned strains (generally called prestrains), is required in constitutive models for obtaining average stresses.

As reported in the literature, irreversible strain accumulates under fatigue loading; hence, it can be considered as a prestrain at any given fatigue loading instant. An irreversible fatigue strain model developed by the authors (Isojeh et al., 2017b) in the literature, reported herein, is used for the fatigue prestrain  $[\varepsilon_{c,2}^{fat}]$  in the principal compressive strain direction for conventional and steel fibre reinforced concrete. The model was developed as a function of residual strength and stiffness damage. These parameters in turn are functions of salient factors such as frequency, stress ratio, and fatigue loading cycles. As such, the model is capable of accounting for variations in the loading parameters.

In the x-y direction, the total strain  $[\varepsilon]$  is

$$[\varepsilon] = [\varepsilon_c] + [\varepsilon_c^p] + [\varepsilon_c^o] + [\varepsilon_c^s] + [\varepsilon_c^{fat}] \quad (7.17)$$

Total strains are used in the constitutive equations for obtaining the steel reinforcement stresses; however, net strains  $[\varepsilon_c]$  are required in the constitutive models for obtaining average stresses in concrete or steel fibre concrete. Considering the x-y direction,

$$[\varepsilon] = [\varepsilon_x, \varepsilon_y, \gamma_x] \quad (7.18)$$

$$[\varepsilon_c] = [\varepsilon_{cx}, \varepsilon_{cy}, \gamma_{cx}] \quad (7.19)$$

$$[\varepsilon_c^{fat}] = [\varepsilon_{cx}^{fat}, \varepsilon_{cy}^{fat}, \gamma_{cxy}^{fat}] \quad (7.20)$$

From a strain transformation of the fatigue prestrain,

$$\varepsilon_{cx}^{fat} = \frac{1}{2} \varepsilon_{c,2}^{fat} (1 - \cos 2\theta) \quad (7.21)$$

$$\varepsilon_{cy}^{fat} = \frac{1}{2} \varepsilon_{c,2}^{fat} (1 + \cos 2\theta) \quad (7.22)$$

$$\gamma_{cxy}^{fat} = \varepsilon_{c,2}^{fat} \sin 2\theta \quad (7.23)$$

From Mohr's circle of strain, the principal strains from the net strains can be estimated as:

$$\varepsilon_{c1}, \varepsilon_{c2} = \frac{(\varepsilon_{cx} + \varepsilon_{cy})}{2} \pm \frac{1}{2} [(\varepsilon_{cx} - \varepsilon_{cy})^2 + \gamma_{cx}^2]^{1/2} \quad (7.24)$$

The inclination of the principal strains in the concrete,  $\theta$ , is given by:

$$\theta = \frac{1}{2} \tan^{-1} \left[ \frac{\gamma_{cx}}{\varepsilon_{cx} - \varepsilon_{cy}} \right] \quad (7.25)$$

From Isojeh et al. (2017b):

$$[\varepsilon_{c,2}^{fat}] = \varepsilon_{do} + \varepsilon_{d1} + \varepsilon_{d2} \quad (7.26)$$

$$\varepsilon_{do} = - \left( \frac{f_c' + (\sigma_{max R})}{E} \right) - 0.3 \varepsilon_c' \quad (7.27)$$

$$\varepsilon_{d1} = k_2 q \left( \frac{D_{fc}}{\sqrt{D_{ce}}} \right) \quad (7.28)$$

$$\varepsilon_{d2} = \frac{(\sigma_{max R})}{E_{sec}} \quad (7.29)$$

E is the fatigue secant modulus,  $k_2$  is 1.0 for high strength concrete and 2.0 for normal strength concrete, q in Equations 7.27 and 7.28 is equal to  $-0.3 \varepsilon'_c$ , R is the stress ratio,  $\sigma_{max}$  is the maximum stress level, and  $E_{sec}$  is the residual static secant modulus. The models for  $D_{fc}$  (concrete strength damage) and  $D_{ce}$  (fatigue secant modulus damage) are given in a subsequent section.

## 7.5 Constitutive Relation

The behaviour of cracked concrete in compression and the corresponding influences of transverse stresses and shear slip effects under static loading are well illustrated in Vecchio (2000). Constitutive models for plain and steel fibre reinforced concrete are usually given in terms of peak stresses and the corresponding strains at peak stresses. Models proposed by Hognestad and Popovics for normal and high strength concrete, respectively, were modified by Isojeh et al. (2017b and c) to account for concrete deterioration, and are presented herein for fatigue constitutive relation.

For normal strength concrete ( $f_p < 40$  MPa) (Hognestad equation), the residual peak stress and the corresponding strain can be expressed as given in Equations 7.30 and 7.31, respectively, after a given number of fatigue loading cycles.

The Hognestad model for fatigue damage is expressed in Equations 7.30 to 7.32 and the residual strength damage ( $D_{fc}$ ) in the equations will be considered shortly.

$$f_c^* = (1 - D_{fc}) f_p \quad (7.30)$$

$$\varepsilon_c^* = \varepsilon_p (1 + \sqrt{D_{fc}}) - \varepsilon_d \quad (7.31)$$

The effective stress in fatigue damaged concrete is:

$$f_{c2} = f_c^* \left( \frac{2\varepsilon_{c2}}{\varepsilon_c^*} - \left( \frac{\varepsilon_{c2}}{\varepsilon_c^*} \right)^2 \right) \quad (7.32)$$

For high strength plain concrete ( $f_p \geq 40$  MPa) (using Popovics' equation), the fatigue constitutive equation is given in a simplified form as:

$$f_{c2} = f_p (1 - D_{fc}) \frac{n(\varepsilon_{c2}/\varepsilon_p)}{(n-1) + (\varepsilon_{c2}/\varepsilon_p)^{nk}} \quad (7.33)$$

where according to Collins et al. (1997):

$$n = 0.80 - f_p/17 \text{ (in MPa)} \quad (7.34)$$

$$k = 0.6 - \frac{f_p}{62} \quad \text{for } \varepsilon_{c2} < \varepsilon_p < 0 \quad (7.35)$$

$$k = 1 \quad \text{for } \varepsilon_{c2} < \varepsilon_p < 0 \quad (7.36)$$

For steel fibre concrete, the monotonic constitutive model proposed by Lee et al. (2016) was modified to account for fatigue damage; thus:

$$f_{c2} = f_{c2max} (1 - D_{fc}) \left[ \frac{A(\varepsilon_{c2}/\varepsilon_p)}{A-1 + (\varepsilon_{c2}/\varepsilon_p)^B} \right] \quad (7.37)$$

where:

$$f_{c2max} = \frac{f'_c}{1 + 0.19(-\varepsilon_{c1}/\varepsilon_{c2} - 0.28)^{0.8}} \not\geq f'_c \quad (7.38)$$

The values for A and B differ for the hardening and softening portion of the stress-strain envelope.

From Lee et al. (2016), the values are given thus:

For the pre-peak ascending branch,

$$A = B = 1/[1 - (f'_c/\varepsilon'_c E_c)] \quad (7.39)$$

For the post-peak descending branch,

$$A = 1 + 0.723(V_f l_f/d_f)^{-0.957}; B = (f'_c/50)^{0.064}[1 + 0.882(V_f l_f/d_f)^{-0.882}] \quad (7.40)$$

From the equations given,  $f'_c$  is the degraded compressive strength,  $f_p$  is the compressive strength of concrete,  $D_{fc}$  is the residual strength damage,  $\varepsilon'_c$  is the strain corresponding to the degraded concrete compressive strength, and  $\varepsilon_d$  is the irreversible fatigue strain.

The residual strength damage evolution model is given in Equation 7.39 (Isojeh et al., 2017a). The damage parameter  $s$  in the equation depends on the steel fibre volume and can be obtained from Figure 7.5.  $D_{cr}$  in Equation 7.41 is the critical damage value which is taken as 0.35 and 0.40 for strength and elastic modulus, respectively.

$$D_{fc} = D_{cr} \text{Exp} \left[ s \left( \frac{\Delta f}{f'_c} - u \right) \right] N^v \quad (7.41)$$

$$u = C_f \left( 1 - \gamma_2 \log(\zeta N_f T) \right) \quad (7.42)$$

$$v = 0.434 s C_f (\beta_2 (1 - R)) \quad (7.43)$$

$C_f$  (frequency factor), and  $\gamma_2$  and  $\beta_2$  (material constants) are given respectively as (Zhang et al., 1996):

$$C_f = ab^{-\log f} + c \quad (7.44)$$

$$\gamma_2 = 2.47 \times 10^{-2}, \quad \gamma_2 = 0 \text{ (for steel fibre)}$$

$$\beta_2 = 0.0661 - 0.0226R \quad (7.45)$$

For steel fibre concrete,  $\beta_2$  is equal to 0.0588 and 0.0470 for steel fibre volume of 0.75% and 1.5%, respectively.  $a$ ,  $b$ , and  $c$  are 0.249, 0.920, and 0.796 for plain concrete (Zhang et al., 1996). For steel fibre concrete,  $a$ ,  $b$ ,  $c$  are taken as 0.283, 0.941, and 0.715, respectively (Isojeh et al., 2017c).  $\zeta$  is a dimensionless coefficient which is taken as 0.15 for a sinusoidal cycle (Zhang et al., 1998; Torrenti et al., 2010).  $f$  is the fatigue loading frequency.

The behaviour of cracked concrete has been considered so far. In an uncracked element, a linear relation for concrete in tension is modified. Thus:

$$f_{c1} = E_c (1 - D_{te}) \varepsilon_{c1} \quad (7.46)$$

where  $E_c$  is the initial tangential modulus, and  $\varepsilon_{c1}$  is the principal tensile strain in the concrete. Compressive fatigue damage in an uncracked concrete element is generally considered insignificant, since the induced compressive stress is usually small.

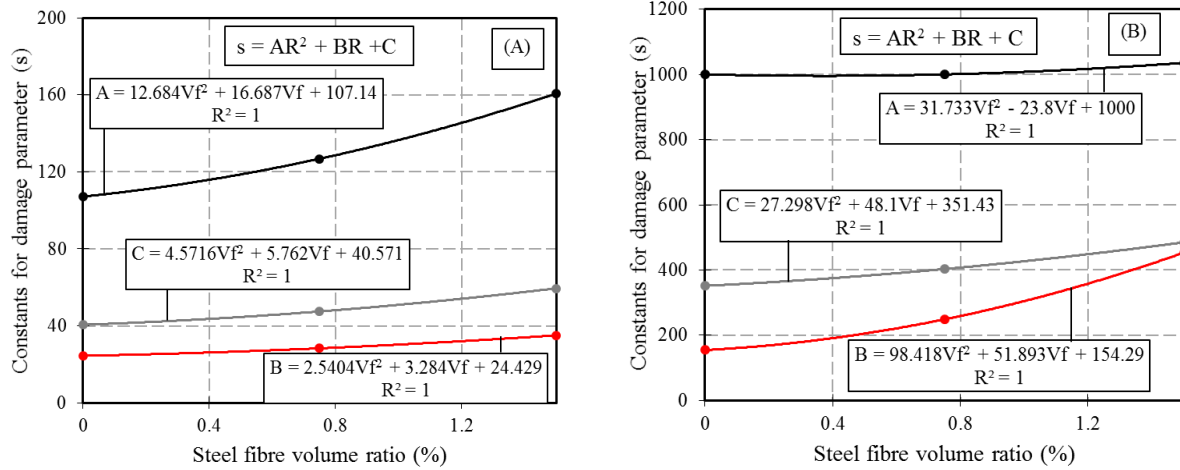


Fig. 7.5 - Damage parameter  $s$  for steel fibre secant modulus (A) and residual strength (B).

As a result of bonding between concrete and steel reinforcement, which results in load transfer between the concrete and the reinforcement, tension stiffening is usually considered under monotonic loading (Equation 7.47). Under fatigue loading however, the effect reduces progressively due to the evolving tensile strain in cracked concrete and reinforcement crack propagation.

The coefficient  $c_f$  accounts for the influence of steel fibre (end-hooked),

$$f_{c,TS} = \frac{f_{tp}}{1 + \sqrt{3.6c_f \cdot \varepsilon_{c1}}} \quad (7.47)$$

$c_f = 0.6 + (1/0.034) (l_f/d_f)[(100V_f)^{1.5}/M^{0.8}]$ ;  $M$  (bond parameter) =  $A_c / (\sum d_{bs}\pi)$ , in millimeters.

For plain concrete, the value of  $c_f$  reduces to 0.6. The tensile stress in steel fibre concrete is estimated as the sum of the tension stiffening effect and the stresses transmitted by steel fibre across cracks; hence,

$$f_{c1} = f_{c,TS} + (1 - \alpha_{avg}) f_f \cos \theta_f \quad (7.48)$$

where  $f_{c1}$  is the effective tensile stress in the concrete,  $\varepsilon_{c1}$  is the tensile strain of the concrete,  $d_{bi}$  is the rebar diameter,  $\theta$  is the inclination of principal strain direction,  $\alpha_i$  is the inclination of reinforcement, and  $n$  is the number of reinforcement directions. The second term in Equation 7.48 is null in the case of conventional reinforced concrete.

The tensile stress in Equation 7.48 is required to be less or equal to the right-side of Equation 7.6. Further, the crack spacing model proposed by Deluce et al. (2014) is used to relate crack width to average tensile strain, while the shear slip model proposed by Vecchio and Lai (2004) is used to estimate the slip prestrain and deviation of steel fibre tensile stress. The models are given subsequently:

For steel fibre concrete,

$$S_{cr} \text{ (average crack spacing)} = 2 \left( c_a + \frac{s_b}{10} \right) k_3 + \frac{k_1 k_2}{s_{mi}} \quad (7.49)$$

where  $c_a = 1.5 a_{gg}$ ;  $k_1 = 0.4$ ;  $k_2 = 0.25$ ;  $k_3 = 1 - [\min(V_f, 0.015)/0.015][1 - (1/k_f)]$ ;

$a_{gg}$  is the maximum aggregate size, given in millimeters.

$$s_b = \frac{1}{\sqrt{\sum_i \frac{4 \rho_{s,i}}{\pi d_{b,i}^2} \cos^4 \theta_i}} \quad (7.50)$$

$$s_{m,i} = \sum_i \frac{\rho_{s,i}}{d_{b,i}} \cos^2 \theta_i + k_f \frac{\alpha_f V_f}{d_f} \quad (7.51)$$

For conventional reinforced concrete,  $S_{cr} = \frac{1}{|\cos \theta|/s_{mx} + |\sin \theta|/s_{my}}$

$$\delta_s \text{ (crack slip)} = \delta_2 \sqrt{\frac{\psi}{1-\psi}} \quad (7.52)$$

$$\delta_2 = \frac{0.5v_{cmax} + v_{co}}{1.8w_{cr}^{-0.8} + (0.234w_{cr}^{-0.707} - 0.20)f_{cc}} \quad (7.53)$$

$\psi = v_{ci,cr}/v_{cmax}$ ;  $v_{cmax}$  (in MPa) =  $\sqrt{f'_c} / [0.31 + (24\frac{w_{cr}}{agg} + 16)]$ ;  $v_{co} = f_{cc}/30$ ;  $f_{cc}$  (in MPa), is taken

as the concrete cube strength;  $w_{cr} = S_{cr}\epsilon_{c1}$ . For conventional reinforced concrete,  $\delta_s$  is taken as  $\delta_2$ , but the numerator is replaced with the shear stress  $v_{ci}$  (Equation 7.7).

The shear strain resulting from the crack slip is estimated as  $\gamma_s = \delta_s/s$ ; and resolving into x and y components,

$$\epsilon_x^s = -\gamma_s/2. \sin 2\theta \quad (7.54)$$

$$\epsilon_y^s = \gamma_s/2. \sin 2\theta \quad (7.55)$$

$$\gamma_{xy}^s = -\gamma_s/2. \cos 2\theta \quad (7.56)$$

Since the shear stresses and slip are functions of the reinforcement ratio or progressing principal stresses, their values also evolve. The tensile stress resulting from steel fibre bridging deviates by an angle  $\theta_f$  from the direction of the principal tensile stress ( $f_{c1}$ ). This deviation angle, according to Lee et al. (2016), is estimated thus:

$$\theta_f = \tan^{-1} \frac{\delta_s}{w_{cr}} \quad (7.57)$$

### 7.5.1 Conventional Reinforcement

Although a trilinear stress-strain relation is used to model the response of reinforcement in the Disturbed Stress Field Model, a bilinear stress-strain relation (elastic-perfectly plastic) is used for fatigue analysis. This is attributed to the fact that the behaviour of reinforcement under high cycle fatigue loading is usually brittle; hence increased strength due to strain hardening is avoided.

## 7.6 Finite Element Implementation

After each fatigue loading cycle, a structural element may exhibit some level of damage. The response of the structural element per fatigue loading cycle can be obtained. The general formulation of material stiffness matrix is expressed thus:

$$[\sigma] = [D] [\varepsilon] - [\sigma^o] \quad (7.58)$$

$\{\sigma\}$  and  $\{\varepsilon\}$  are the total stress and total strain vectors due to the applied maximum fatigue load. (The ratio of the minimum to maximum fatigue loading is a parameter required in a subsequent section.)  $[D]$  is the transformed composite stiffness matrix in which the concrete composite degrades progressively due to fatigue loading.

$$\{\sigma\} = \begin{bmatrix} \sigma_x \\ \sigma_y \\ \tau_{xy} \end{bmatrix} \text{ (normal and shear stresses on an element)} \quad (7.59)$$

$$\{\varepsilon\} = \begin{bmatrix} \varepsilon_x \\ \varepsilon_y \\ \gamma_{xy} \end{bmatrix} \text{ (corresponding strain values)} \quad (7.60)$$

$$[D] = [D_c] + \sum_{i=1}^n [D_s]_i + [D_f] \quad (7.61)$$

Prior to cracking,

$$[D_c] = \frac{E_c (1-D_{te})}{1-\nu^2} \begin{bmatrix} 1 & \frac{\nu}{(1-D_{te})} & 0 \\ \nu & \frac{1}{(1-D_{te})} & 0 \\ 0 & 0 & \frac{1-\nu}{2(1-D_{te})} \end{bmatrix} \quad (7.62)$$

$D_{te}$  is obtained using Equations 7.41 to 7.45. However,  $\Delta f$  and  $f'_c$  are replaced with the induced tensile stress and the concrete tensile strength of concrete, respectively. For a given element strain condition, normal stresses in the concrete can be found and subsequently, the principal tensile and compressive stresses and the principal strain direction can be obtained.

For a two-dimensional cracked state, the stiffness of the concrete with respect to the axes of orthotropy, the stiffness of the steel reinforcement with respect to its direction, and the stiffness of the steel fibre with respect to the inclination of tensile stress due to steel fibre are all required (Equations 7.63 to 7.65). Subsequently, the stiffnesses are transformed back to the reference x, y axes (Equations 7.66 and 7.67).

$$[D_c]' = \begin{bmatrix} \overline{E_{c1}} & 0 & 0 \\ 0 & \overline{E_{c2}} & 0 \\ 0 & 0 & \overline{G_c} \end{bmatrix} \text{ for concrete} \quad (7.63)$$

$$\overline{E_{c1}} = f_{c1}/\varepsilon_{c1}; \overline{E_{c2}} = f_{c2}/\varepsilon_{c2}; \text{ and } \overline{G_c} = \overline{E_{c1}} \cdot \overline{E_{c2}} / (\overline{E_{c1}} + \overline{E_{c2}})$$

$$[D_s]'_i = \begin{bmatrix} \rho_i \overline{E_{s1}} & 0 & 0 \\ 0 & 0 & 0 \\ 0 & 0 & 0 \end{bmatrix} \text{ for steel reinforcement} \quad (7.64)$$

$$\overline{E_{s1}} = f_{s,i}/\varepsilon_{s,i}$$

$$[D_f]' = \begin{bmatrix} \rho_i \overline{E_{f1}} & 0 & 0 \\ 0 & 0 & 0 \\ 0 & 0 & 0 \end{bmatrix} \text{ for steel fibre} \quad (7.65)$$

$$\overline{E_{f1}} = \alpha_{avg} f_f / \varepsilon_{cf}; \varepsilon_{cf} = (\varepsilon_{c1} + \varepsilon_{c2})/2 + [(\varepsilon_{c1} - \varepsilon_{c2})/2] \cos 2\theta_f$$

$$[D_c] = [T_c]^T [D_c]' [T_c]; [D_f] = [T_f]^T [D_f]' [T_f];$$

$$[D_{s,i}] = [T_{s,i}]^T [D_{s,i}]' [T_{s,i}] \quad (7.66)$$

$$[T] = \begin{bmatrix} \cos^2 \psi & \sin^2 \psi & \cos \psi \sin \psi \\ \sin^2 \psi & \cos^2 \psi & -\cos \psi \sin \psi \\ -2 \cos \psi \sin \psi & 2 \cos \psi \sin \psi & (\cos^2 \psi - \sin^2 \psi) \end{bmatrix} \quad (7.67)$$

For concrete,  $\psi = \theta_c$ , for steel fibre,  $\psi = \theta_c + \theta_f$ , and for a steel reinforcing bar,  $\psi = \alpha_i$ .

$\sigma^o$  is estimated as a pseudo-load using Equations 7.17 to 7.29 (in this case, it is assumed that there are no prestrains in the steel reinforcement). For a given stress condition and loading cycle (due to

applied fatigue load), the total strain in the element can be obtained. The solution approach is iterative since the secant moduli of materials are needed to find the strain condition  $\{\varepsilon\}$  and vice versa.

$$[\sigma^o] = [D_c] ([\varepsilon_c^p] + [\varepsilon_c^o] + [\varepsilon_c^s] + [\varepsilon_c^{fat}]) \quad (7.68)$$

In the iterative process for an element at the first fatigue loading cycle, strain values are initially assumed. Subsequently, the principal strain values and the corresponding inclination of the principal tensile strain are estimated. Using the modified compatibility and constitutive equations illustrated previously, the net strains are estimated and subsequently, the average principal stresses in the concrete and the average stresses in the reinforcement are estimated with the assumption that fatigue damage is zero.

Stresses at the crack are also checked and shear stress and crack slip are estimated using the modified equilibrium equation; however,  $Z_o$  is assumed to be zero for the first cycle. From the crack slip, prestrains are estimated and are subtracted from the total strains in order to obtain net strains. Further, secant moduli for the constituent materials are estimated and the material stiffness matrices are obtained using Equations 7.63 to 7.67. Subsequently, the total strains are estimated and compared with the previous values assumed (Equation 7.69). The iterative process continues until the errors become minimal. The element stresses estimated are saved for subsequent loading cycles.

$$[\varepsilon] = [D]^{-1} ([\sigma] + [\sigma^o]) \quad (7.69)$$

For subsequent fatigue loading cycles, the saved stresses and the number of fatigue loading cycles considered are substituted into the corresponding fatigue damage model in order to estimate the required damage for the irreversible strain, the modified constitutive models and the modified

equilibrium equations. The described iterative process is also repeated as the fatigue loading cycles are increased. Failure becomes imminent when instability due to fractured reinforcement or significant crushing of concrete occurs. Deformation evolution plots can be obtained from the material parameter values as the fatigue loading cycles are increased up to the point of failure.

The modified algorithm for the Disturbed Stress Field Model which accounts for fatigue damage in an element is shown in the flow chart in Figure 7.6. The original algorithm is void of the damage models (A, B, and C). In all, the analyses involve modelling the monotonic loading responses of structural components which exhibit some level of damage due to fatigue loading cycles.

### **7.7 Failure Criterion for Reinforced Concrete and Steel-Fibre Concrete under Fatigue Loading**

The evolution of deformation is attributed to plain or steel fibre concrete strength and stiffness deterioration, irreversible strain accumulation, and steel reinforcement crack growth (A, B, and C in Figure 7.6). Monotonic tests of structural elements subjected to different fatigue loading cycles will exhibit decreasing resistance capacity as the loading cycles increase. The number of cycles at which the residual capacity of the element becomes equal to the fatigue load is termed the fatigue life of the structural element. At this instant, severe crushing of concrete or fracture of reinforcing bars may occur, leading to structural collapse.

For further exemplification, the solution to the fatigue analysis of a shear panel is illustrated using the flow chart given in Figure 7.6 in a stepwise manner. The properties and loading parameters are also given. Three different pure shear fatigue loads (Figure 7.7) (3.5 MPa, 3.0 MPa, and 2.7 MPa) were used and the corresponding deformation evolution of the material parameters were obtained. The significance of the proposed analysis approach can be observed from the predicted three-

staged deformation evolution plots. In addition, the effect of fatigue loading is explicitly shown in all plots given in Figures 7.8 to 7.13.

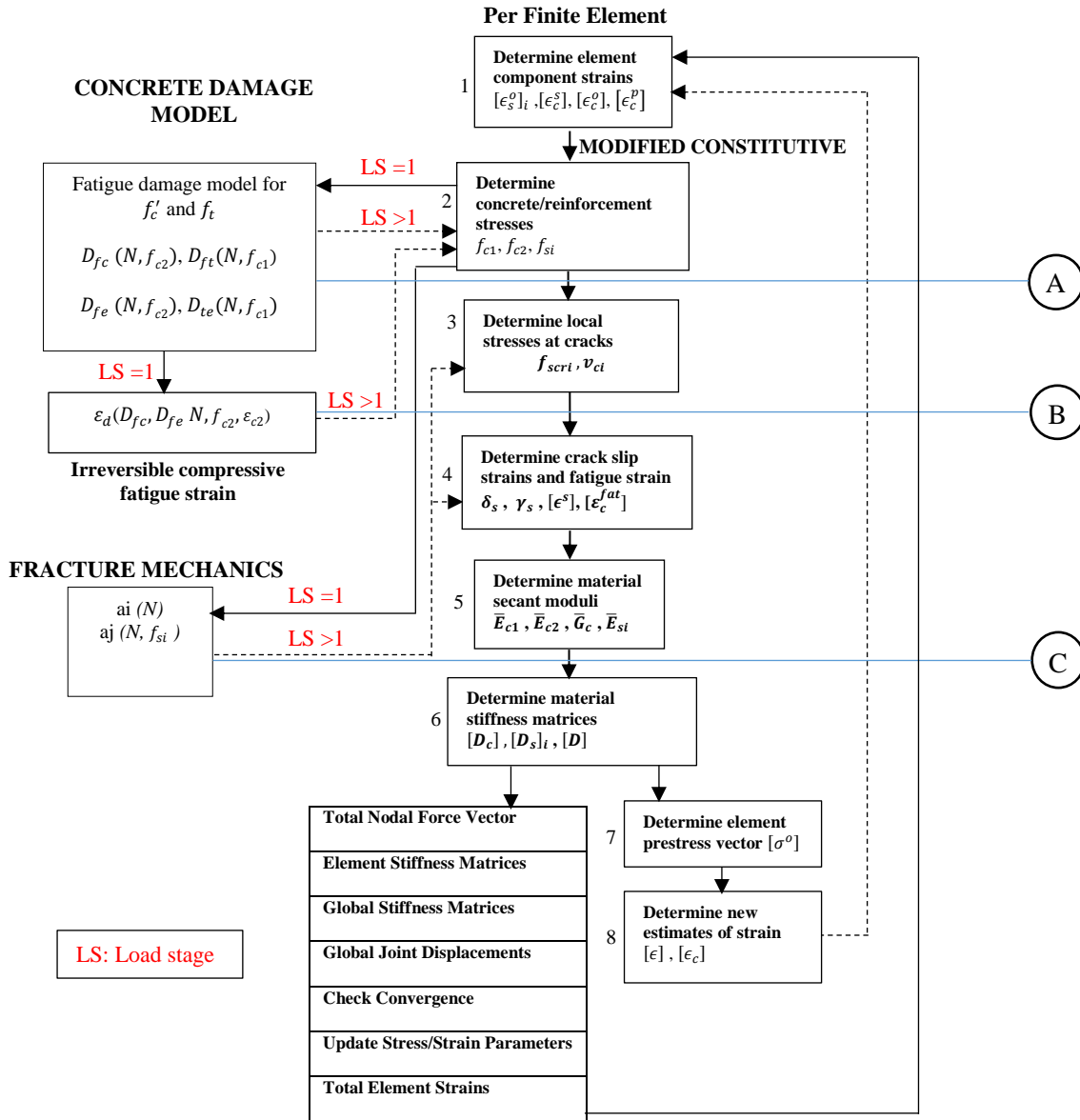


Fig. 7.6 - Flow chart for the modified solution algorithm for DSFM.

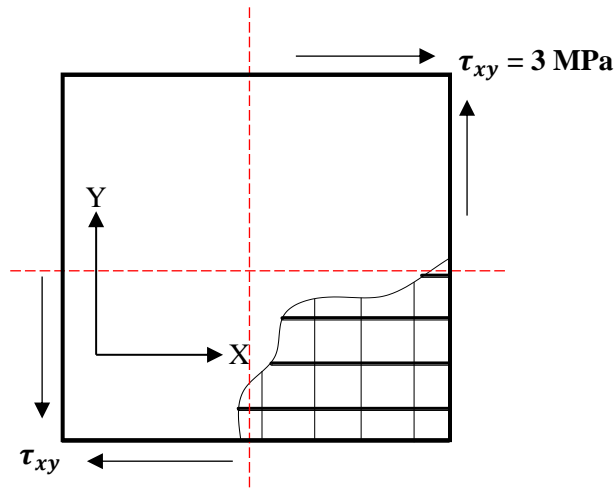


Fig. 7.7 - Shear panel (PV19).

$$\begin{aligned}
 f'_c &= 19.0 \text{ MPa}; & \rho_x &= 1.785\% \\
 f'_t &= 1.72 \text{ MPa}; & \rho_y &= 0.713\% \\
 \varepsilon'_c &= -2.15 \times 10^{-3}; & f_{yx} &= 458 \text{ MPa} \\
 & & f_{yy} &= 300 \text{ MPa} \\
 & & E_s &= 200000 \text{ MPa}
 \end{aligned}$$

$$a = 10 \text{ mm}$$

$$s_x \approx 50 \text{ mm} \quad d_{bx} \approx 6.35 \text{ mm}$$

$$s_y \approx 50 \text{ mm} \quad d_{by} \approx 4.01 \text{ mm}$$

Fatigue frequency = 5 Hz waveform = sinusoidal

Load ratio (R) = 0

$$[\sigma] = \begin{bmatrix} 0 \\ 0 \\ 3.0 \end{bmatrix} \text{ MPa}$$

Solution:

The assumed initial total and net strains (from previous calculations) for an applied shear stress of 3.0 MPa on the shear element in Figure 7.7, are:

$$\{\varepsilon\} = \begin{bmatrix} 0.431 \\ 0.792 \\ 1.725 \end{bmatrix} \times 10^{-3} \qquad \{\varepsilon_c\} = \begin{bmatrix} 0.566 \\ 0.659 \\ 1.716 \end{bmatrix} \times 10^{-3}$$

Using the iterative process described previously, the monotonic response of the shear panel which includes induced stress and strain values due to the applied fatigue load (3.0 MPa) is obtained (without considering fatigue damage). The obtained and saved element stresses due to the monotonic response or at the first cycle, required in calculating damage values in subsequent cycles, are given thus:

$f_{sx} = 111$  MPa;  $f_{sy} = 241$  MPa (both stresses are required in the fracture mechanics model)

$f_{c2} = -5.35$  MPa;  $f_{c1} = 1.08$  MPa (required in concrete damage model and irreversible strain model).

These values are substituted into A, B, and C in Figure 7.6 in order to estimate the corresponding damage at any given fatigue loading cycle. Having accounted for the corresponding damage, the monotonic response is again obtained iteratively. This is repeated for given cycles until instability is reached.

### **Solution for fatigue loading at 10000 cycles**

Figure 7.6 (Box 1) - Strain components after iterations are:

$$\{\varepsilon\} = \begin{bmatrix} 0.584 \\ 1.278 \\ 2.604 \end{bmatrix} \times 10^{-3} \qquad \{\varepsilon_c\} = \begin{bmatrix} 0.804 \\ 1.072 \\ 2.569 \end{bmatrix} \times 10^{-3}$$

The principal strains are estimated from  $\{\varepsilon_c\}$  (Equations 7.24 and 7.25) as:

$$\varepsilon_{c1} = 2.23 \times 10^{-3} \qquad \varepsilon_{c2} = -0.353 \times 10^{-3} \qquad \theta_\sigma = 42.02^\circ$$

Figure 7.6 (Box 2) - Average Stresses in Concrete and Reinforcement:

Since the concrete is in a cracked state, Equations 7.30 to 7.32 are used for concrete compressive stress, and Equation 7.45 is used for concrete tensile stress (neglecting the influence of steel fibre).

The damage parameter required in the equation is obtained from Equations 7.39 to 7.43. The fatigue prestrain value (Equation 7.26 to 7.29) is also required in estimating the concrete compressive stress.

$$f_{c2} = 5.34 \text{ MPa}$$

$$f_{c1} = 1.07 \text{ MPa}$$

Assuming perfect bond between the concrete and the steel reinforcement, the average strain in the concrete is equal to the average strain in the steel reinforcing bars. Hence:

$$E_s = 200000 \text{ MPa}$$

$$\varepsilon_{sx} = 0.584 \times 10^{-3}$$

$$\varepsilon_{sy} = 1.278 \times 10^{-3}$$

$$f_{sx} = E_s \varepsilon_{sx} = 117 \text{ MPa (x-direction)}$$

$$f_{sy} = E_s \varepsilon_{sy} = 256 \text{ MPa (Y-direction)}$$

Figure 7.6 (Box 3) - Local stresses at crack:

The local stresses are estimated from Equations 7.6 and 7.7 (neglecting the influence of steel fibre). In Equations 7.6 and 7.7, the reinforcement crack growth factor ( $Z_o$ ) is estimated from Equations 7.10 to 7.16 (shown as C in Figure 7.6). The average reinforcement stresses are required in C in order to estimate the progressive crack depth; Thus:

$$\varepsilon_{scrx} = 1.033 \times 10^{-3} \quad , \quad f_{scrx} = 207 \text{ MPa}$$

$$\varepsilon_{scry} = 1.642 \times 10^{-3} \quad , \quad f_{scry} = 300 \text{ MPa}$$

$$v_{ci} = 0.621 \text{ MPa}$$

Figure 7.6 (Box 4) - Crack slip strains:

The slip at a given fatigue loading cycle can be estimated using Equation 7.50. Subsequently, the shear strains (in x-y directions) resulting from slip at the crack are estimated. Fatigue irreversible compressive strain values are also estimated in the x-y direction (Equations 7.21 to 7.23). The prestrain is equal to the summation of the shear strains. The pseudo-load [ $\sigma^o$ ] is estimated from the obtained values of prestrain.

The shear strain resulting from the crack slip is estimated as:  $\gamma_s = \delta_s/s = 0.429 \times 10^{-3}$ ; resolving into x and y components,

$$\varepsilon_x^s = -\gamma_s/2. \sin 2\theta = -0.213 \times 10^{-3}$$

$$\varepsilon_y^s = \gamma_s/2. \sin 2\theta = 0.213 \times 10^{-3}$$

$$\gamma_{xy}^s = -\gamma_s/2. \cos 2\theta = 0.022 \times 10^{-3}$$

Inclusion of the irreversible fatigue strain is done in the manner of an offset strain:

$$\varepsilon_x^{fat} = \varepsilon_{c,2}^{fat}/2. (1 - \cos 2\theta) = -6.09 \times 10^{-6}$$

$$\varepsilon_y^{fat} = \varepsilon_{c,2}^{fat}/2. (1 + \cos 2\theta) = -7.50 \times 10^{-6}$$

$$\gamma_{xy}^{fat} = -\varepsilon_{c,2}^{fat}/2. \sin 2\theta = 13.5 \times 10^{-6}$$

Figure 7.6 (Box 5) - Material secant moduli:

The net strain values are estimated from Equation 7.17 (for concrete). The ratio of the average stress to the net strain gives the secant modulus for concrete. In the case of steel reinforcement, the ratio of the average stress in steel reinforcement to the induced strain gives the secant modulus.

$$E_{c1} = 480 \text{ MPa}$$

$$E_{c2} = 15124 \text{ MPa}$$

$$G_c = 466 \text{ MPa}$$

$$E_{sx} = 200000 \text{ MPa}$$

$$E_{sy} = 200000 \text{ MPa}$$

Figure 7.6 (Box 6) - Material stiffness matrices  $[D_c]$ ,  $[D_s]$ ,  $[D]$ :

The stiffness matrices are estimated from Equations 7.61 to 7.65. The transformed composite stiffness matrix is obtained using Equation 7.59. The transformed composite stiffness matrix at 10000 cycles was obtained thus:

$$[D] = \begin{bmatrix} 7213 & 3367 & -3256 \\ 3367 & 6653 & -3992 \\ -3256 & -3992 & 3861 \end{bmatrix} \text{ (MPa)}$$

Figure 7.6 (Box 7) - Determine element prestress vector  $[\sigma^o]$ :

The element prestress vector was estimated from Equation 7.66. Herein, two prestrain values were considered: the shear strain at crack and the fatigue irreversible strain. The summation of the

prestrains is equal to:

$$[\varepsilon_{ps}^o] = \begin{bmatrix} -0.22 \\ 0.21 \\ 3.58 \end{bmatrix} \times 10^{-3} \text{ and,}$$

$$[\sigma^o] = \begin{bmatrix} -0.13 \\ 0.26 \\ -5.35 \end{bmatrix} \text{ MPa}$$

Figure 7.6 (Box 8) - Determine new estimates of strain  $\{\varepsilon\}$ ,  $\{\varepsilon_c\}$ :

The total and net strain values are estimated using Equation 7.67. Since the results presented herein were obtained after convergence, the final values were also equal to the initial values. However, where significant variations are observed, the iteration continues as illustrated using the given steps. This procedure was repeated as the number of fatigue loading cycles was increased.

At the final collapse or failure of a structural element (in this case, the shear reinforcement in the vertical direction failed first), instability is observed and significant deformation persists. The results for the three different loads used are given in Figures 7.8 to 7.13. They are presented in terms of the crack slip evolution, shear stress evolution, reinforcement crack depth propagation (in the Y-direction where failure occurred), reinforcement strain, and stress evolutions.

From the results, the influence of fatigue load on the fatigue life is well-captured as observed in all deformation evolution plots (Figures 7.8 to 7.13). As the fatigue load increased, the corresponding fatigue life reduced, and the rates of deformation were observed to increase. In addition, the significance of the proposed approach stems from the fact that the profiles obtained

in each case resemble the well-known fatigue deformation profile for reinforced concrete. Based on these observations, the deformation evolution within the cracked plane in reinforced concrete or steel fibre concrete can be obtained using the proposed approach.

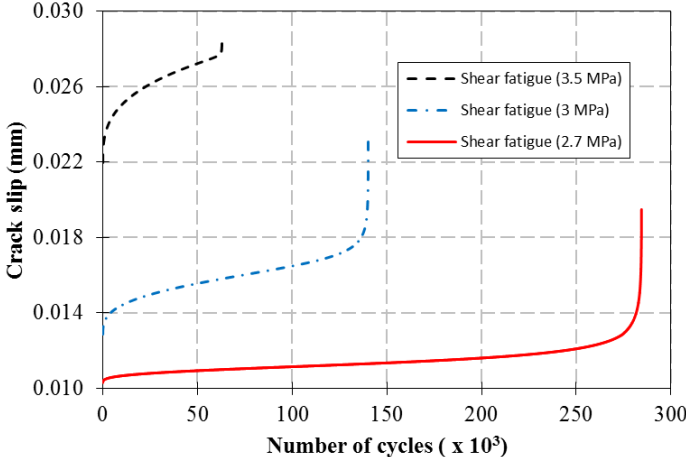


Fig. 7.8 - Crack slip evolution.

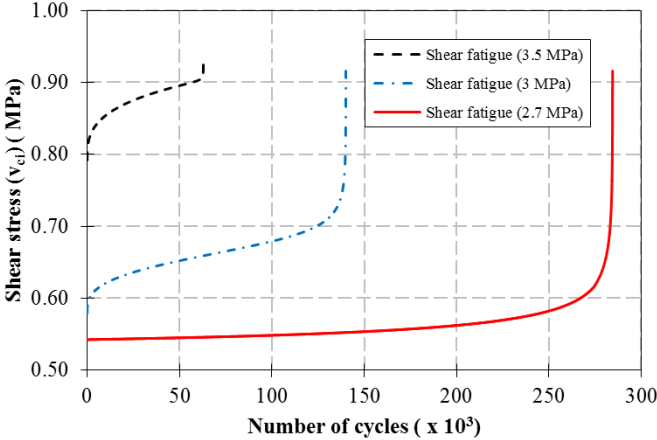


Fig. 7.9 - Shear stress evolution at crack.

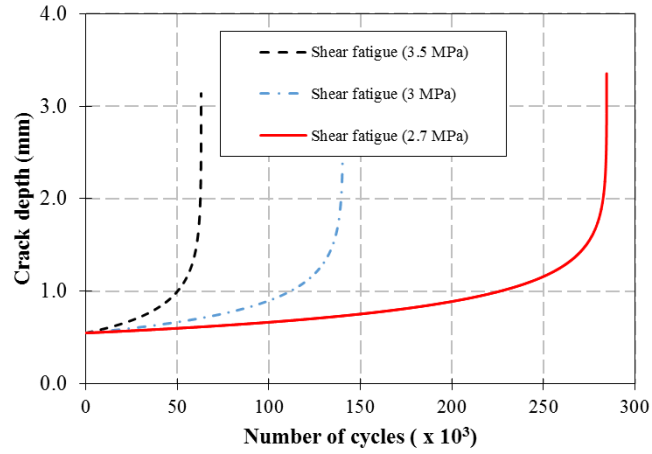


Fig. 7.10 - Reinforcement (Y-direction) crack growth depth.

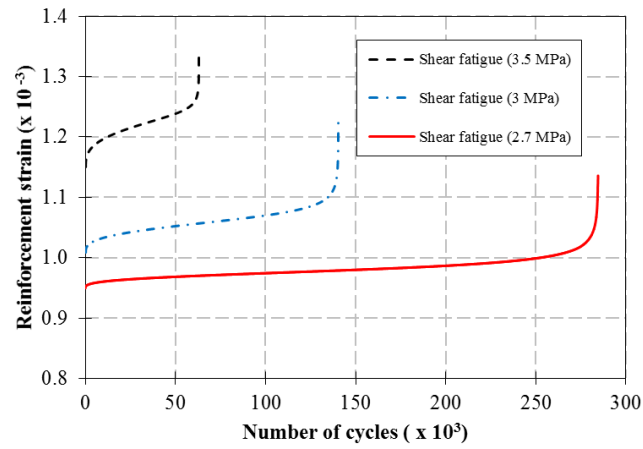


Fig. 7.11 - Reinforcement (X-direction) strain evolution at crack location.

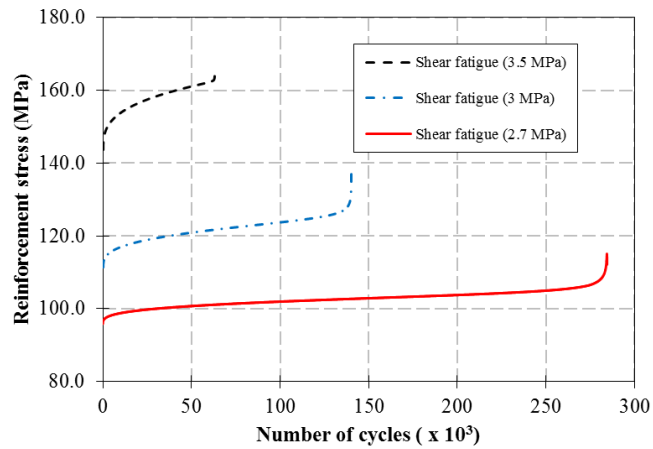


Fig. 7.12 - Reinforcement (X-direction) average stress evolution.

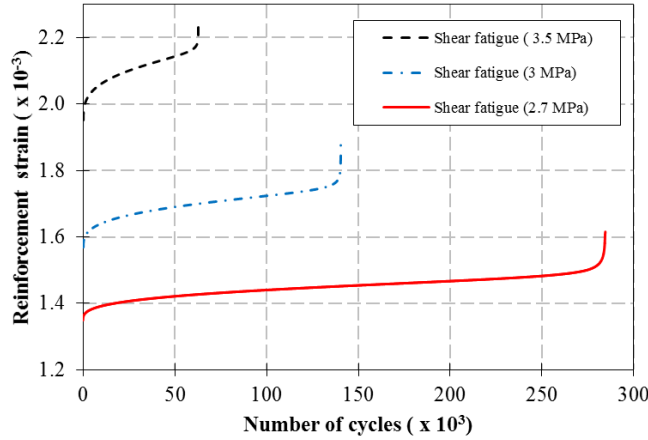


Fig. 7.13 - Localised reinforcement strain evolution (Y-direction).

## 7.8 Conclusions

An algorithm was described for implementing damage models for concrete strength and stiffness, irreversible strain accumulation, and steel reinforcement crack growth in a finite element analysis framework. This procedure was implemented within the Disturbed Stress Field Model for fatigue analysis of reinforced concrete and steel fibre structures. Fatigue damage models which account for salient loading parameters and appropriate evolution models for concrete parameters were introduced. As an improvement to reported models, the implementation of the reinforcement crack growth model and concrete damage models account for the progressive deformation and shear transfer at a crack under fatigue loading for reinforced concrete and steel fibre reinforced concrete. It is proposed that the fatigue life of a structural component corresponds to the number of fatigue loading cycles at which the resistance capacity degrades to a value equal to the fatigue load. Verification of the proposed algorithm and fatigue failure criterion with conducted experimental results is required to ascertain its validity. Accordingly, corroborated results using nonlinear finite element analysis are presented in the next chapter.

## 7.9 Notation

*The following symbols are used in this chapter:*

a,b,c : material parameters

C: material constant =  $2 \times 10^{-13}$

$C_f$  : frequency factor

$D$  : damage

$d_{bi}$ : rebar diameter

$D_c$ : concrete stiffness matrix

$D_{cr}$  : critical damage

$D_{ft}$  : concrete tensile strength damage

$D_c$ : reinforcement stiffness matrix

$D_{te}$  : concrete tensile secant modulus damage

$E_c$ : elastic modulus of concrete

$E_{c1}$ : secant modulus in tension

$E_{c2}$ : secant modulus in compression

$E_s$ : elastic modulus of steel reinforcement

$G_c$ : shear modulus

f : frequency

$f_{c1}$ : effective tensile stress of concrete

$f_{c2}$ : effective compressive stress of concrete

$f_{c,TS}$ : average tensile stress in concrete due to tension stiffening effect

$f_{cx}$ : normal stress in concrete in horizontal direction

$f_{cy}$ : normal stress in concrete in vertical direction

$v_{cxy}$ : shear stress in concrete in horizontal direction

$f_{c2max}$ : peak compressive stress in concrete considering compression softening effect

$f_{eh}$ : tensile stress due to mechanical anchorage effect of end-hooked steel-fibre

$f_f$ : tensile stress at crack due to steel fibre

$f_p$ : initial compressive strength

$f_{st}$ : tensile stress due to frictional bond behaviour of steel fibre

$f_{tp}$ : initial concrete tensile strength

$f'_c$ : compressive strength of concrete

$f_c^*$ : degraded compressive strength

$f_{scri}$ : local stress in reinforcement at crack

$f_{si}$ : average stress in steel reinforcement

$f_t$ : residual tensile strength of concrete

$f_t^*$ : degraded strength at which concrete cracks

$k$ : post-decay parameter for stress-strain response of concrete in compression

$N$ : number of cycles

$n$ : curve-fitting parameter for stress-strain response of concrete in compression

$n$ : material constant = 3

$N_f$ : numbers of cycles at failure

$N_{ij}$ : interval of cycles considered

$s_{cr}$ : crack spacing

$T$ : period of fatigue cycle

$t_d$ : direction coefficient (= 0.6 or 1.0)

$\nu$ : Poisson's ratio

$v_{ci}$ : shear stress

$v_{ci,cr}$ : shear stress at cracked concrete plane

$V_f$ : steel fibre volume ratio

$w_{cr}$ : crack width

$\alpha_{avg}$ : coefficient to relate tensile stress at a crack due to steel fibres with average tensile stress

$\alpha_i$ : inclination of reinforcement

$\beta$ : material constant

$\beta_2$ : material constant

$\Delta$ : deformation

$\Delta\varepsilon_{1cr}$ : change in strain at crack

$\delta_s$ : crack slip

$\varepsilon_{c1}$ : net tensile strain

$\varepsilon_{c2}$ : net compressive strain

$\varepsilon_c^*$ : strain corresponding to the degraded compressive strength

$\varepsilon_{scri}$ : local strain in the reinforcement

$\varepsilon_{si}$ : average strain in steel reinforcement

$\varepsilon_d$ : irreversible fatigue strain

$\varepsilon_p$ : initial strain corresponding to the initial compressive strength

$\varepsilon_{1cr}$ : local strain at crack

$\gamma_s$ : shear strain due to crack slip

$\theta, \theta_c$ : inclination of principal strain direction

$\theta_{ni}$ : angle between the reinforcement direction and the normal to the crack

$\rho_i$ : reinforcement ratio

## 7.10 References

1. Aas-Jacobsen, K. (1970). "Fatigue of Concrete Beams and Columns." Trondheim: Institutt for Betonkonstruksjoner, Bulletin No 70-1, 148 pp.
2. ACI 215R-74 (1997). "Considerations for Design of Concrete Structures Subjected to Fatigue Loading."
3. Bentz, C.E. (2005). "Explaining the Riddle of Tension Stiffening Models for Shear Panel Experiments." *Journal of Structural Engineering*, Vol. 13, No. 9, pp. 1422-1425.
4. Cornelissen, H.A.W., Reinhardt, H.W. (1984). "Uniaxial Tensile Fatigue of Concrete under Constant Amplitude and Programme Loading." *Magazine of Concrete Research*, Vol. 36, No. 129, pp. 216-227.
5. Dowling, N.E. (1993). "Mechanical Behaviour of Materials." Prentice Hall, New Jersey.
6. Dowling, N.E, Thangjitham, N.E. (2000). "An Overview and Discussion of Basic Methodology for Fatigue." *Fatigue and Fracture Mechanics: ASTM STP 1389*, Vol. 31, pp. 3-36.
7. Eligehausen, R., Kazic, M., and Sippel, T.M. (1992). "Creep and Fatigue Analysis of Reinforced Concrete Structures." *Proceedings, Riga, Latvia, International Conference on Bond in Concrete from Research to Practice. Bd. 3. Riga: Riga Technical University, S. 7-49-7-58.*
8. Facconi, L., Plizzari, G., Vecchio, F.J. (2014). "Disturbed Stress Field Model for Unreinforced Masonry." *Journal of Structural Engineering*, Vol. 140, No. 4, 11pp.

9. Farahmand, B. Nikbin, K.(2008). “Predicting Fracture and Fatigue Crack Growth Properties using Tensile Properties.” *Engineering Fracture Mechanics*, Vol. 75, pp. 2144-2155.
10. Gao, L., and Hsu, C.T.T. (1998). “Fatigue of Concrete under Uniaxial Compression Cyclic Loading.” *ACI Materials Journal*, Vol. 95, No. 5, pp. 575-581.
11. Grebreyouhannes, E., Kishi, T., Maekawa, K. (2008). “Shear Fatigue of Cracked Concrete Interface,” *Journal of Advanced Concrete Technology*, Vol. 6, No. 2, pp. 365-376.
12. Hanson, J.M. (1983). “Design for Fatigue.” F.K. Kong, et al., *Handbook of Structural Concrete*, Pitman, London (35 pp.)
13. Hirt, M.A., Nussbaumer, A. (2006). “Construction Metallique: Notions Fondamentales et Methods de Dimensionnement, Nouvelle Edition Revue et Adaptee aux Nouvelles Norms de Structures.” *Traite de Genie Civil de l’Ecole Polytechnique Federale*, Vol. 10. Lausanne, Switzerland.
14. Isojeh, M.B., Vecchio, F.J. (2016). “Parametric Damage of Concrete under High-Cycle Fatigue Loading in Compression.” *Proc., 9<sup>th</sup> International Conference on Fracture Mechanics of Concrete and Concrete Structures., FraMCoS-9.*
15. Isojeh B, El-Zeghayar M, Vecchio F.J (2017a). “Concrete Damage under Fatigue Loading in Uniaxial Compression.” *ACI Materials Journal*, Vol. 114, No. 2, pp. 225-235.
16. Isojeh B, El-Zeghayar M, Vecchio, F.J (2017b). “Simplified Constitutive Model for Fatigue Behaviour of Concrete in Compression.” *ASCE Journal of Materials* 2017;

DOI:10.1061/(ASCE)MT.1943-5533.0001863.

17. Isojeh, B., El-Zeghayar, M., Vecchio, F.J. (2016c). "Fatigue Behaviour of Steel Fibre Concrete in Direct Tension," ASCE Journal of Materials 2017; DOI: 10.1061/(ASCE)MT.1943-5533.0001949.
18. JSCE (1986). "Standard Specification for Design of Concrete Structures." Japan Society of Civil Engineers.
19. Lee, S.C., Cho, J.Y., Vecchio, F.J. (2016). "Analysis of Steel Fibre-Reinforced Concrete Elements Subjected to Shear." ACI Structural Journal, Vol. 113, No. 2, pp. 275-285.
20. Luong M.P. (2001). "Nondestructive Evaluation of Dissipative Behaviour of Reinforced Concrete Structure." International Conference on Nuclear Engineering, NICE Aeropolis (France).
21. Maekawa et al., (2006). "Direct Path-Integral Scheme for Fatigue Simulation of Reinforced Concrete in Shear." Journal of Advanced Concrete Technology, Vol. 4, No. 1, pp. 159-177.
22. Okamura H., Farghaly S.A., Ueda T. (1981). "Behaviour of Reinforced Concrete Beams with Stirrups Failing in Shear under Fatigue Loading." Proc. of JSCE, No. 308, pp. 109-122.
23. Otter, D.E.; Naaman, A.E. (1986). "Steel Fibre Reinforced Concrete under Static and Cyclic Compressive Loading." 3<sup>rd</sup> RILEM Symp. On Developments in Fibre Reinforced Cement and Concrete.

24. Otter, D.E.; Naaman, A.E. (1988). "Properties of Steel Fibre Reinforced Concrete under Cyclic Loading." *ACI Materials Journal*, Vol. 85, No. 4, pp. 254-261.
25. Paris, P., Gomez, M.P., Anderson W.E. 1961. "A Rational Analytical Theory of Fatigue." *The Trend in Engineering* 13:9-14.
26. Park, Y.J. (1990). "Fatigue of Concrete under Random Loadings." *Journal of Structural Engineering*, ASCE, Vol. 116, No. 11, pp. 3228-3235.
27. Petryna, Y.S., Pfanner, D., Stangenberg, F., and Kratzig, W.B. (2002). "Reliability of Reinforced Concrete Structures under Fatigue." *Reliability Engineering and System Safety*, Vol. 77, pp. 253-261.
28. Rocha, M., Bruhwiler, E. (2012). "Prediction of Fatigue Life of Reinforced Concrete Bridges." In Biondini and Frangopol (Eds) *Bridge Maintenance, Safety, Management, Resilience and Sustainability*, pp. 3755-3760.
29. Saito, M., Imai, S. (1983). "Direct Tensile Fatigue of Concrete by the Use of Friction Grips." *ACI Journal*, Vol. 80, pp. 431-438.
30. Schlafli, M. and Bruhwiler, E. (1998). "Shear Fatigue Failure of Reinforced Concrete Elements without Shear Reinforcement." *ECF 12-Fracture from Defects*, pp. 1527-1532.
31. Socie, D, Dowling N.E, Kurath P. (1984). "Fatigue Life Estimation of Notched Members." *Fracture Mechanics: Fifteenth Symposium*. ASTM STP 833, pp. 284-299.
32. Sparks, P.R., Menzies, J.B. (1973). "The Influence of Rate of Loading and Material Variability on the Fatigue Characteristics of Concrete." *Fatigue in Concrete Structures*, SP-

- 75, S.P Shah, ed., American Concrete Institute, Farmington Hills, Mich., pp. 331-343.
33. Tamulenas, V., Gelazius, V., and Ramanauskas R. (2014). "Calculation Technique for Stress-Strain Analysis of RC Elements Subjected to High-Cycle Compression." *Civil and Transport Engineering, Aviation Technologies*, Vol 6, No.5, pp. 468-473.
34. Teng, S., Wang, F. (2001). "Finite Element Analysis of Reinforced Concrete Deep Beams under Fatigue Loading." *ACI Structural Journal*, Vol. 98, No. 3, pp. 315-323.
35. Tilly, G.P., and Moss, D.S. (1982). "Long Endurance Fatigue of Steel Reinforcement." *Fatigue of Steel and Concrete Structures Colloquium, IABSE, Lausanne*, pp. 229-238.
36. Torrenti, J.M., Pijaudier-Cabot, G., and Reynouard J. (2010). "Mechanical Behaviour of Concrete: Cyclic and Dynamic Loading, Fatigue of Structural Concrete." ISTE Ltd and John Wiley & Sons, Inc. pp. 185-223.
37. Vecchio F.J., Collins M.P. (1986); *The Modified Compression Field Theory for Reinforced Concrete Elements Subjected to Shear*; *Journal of the American Concrete Institute*, Vol. 83, No. 2, pp. 219-231.
38. Vecchio F.J. (2000). "Disturbed Stress Field Model for Reinforced Concrete: Formulation." *Journal of Structural Engineering*, Vol. 127, No. 1, pp. 1070-1077
39. Vecchio F.J. (2001). "Disturbed Stress Field Model for Reinforced Concrete: Implementation." *Journal of Structural Engineering*, Vol. 127, No. 1, pp. 12- 20.
40. Vecchio, F.J., Lai, D., Shim, W., Ng, J. (2001). "Disturbed Stress Field Model for Reinforced Concrete: Validation." *Journal of Structural Engineering*, Vol. 127, No. 4, pp. 350-358.

41. Vega, I.M., Bhatti, M.A., Nixon, W.A. (1995). "A Nonlinear Fatigue Damage Model for Concrete in Tension." *International of Journal of Damage Mechanics*, Vol.4, No. 4, pp. 362-379.
42. Xiang, T., and Zhao. R. (2007). "Reliability Evaluation of Chloride Diffusion in Fatigue Damaged Concrete." *Engineering Structures*, Vol. 29, pp. 1539-1547.
43. Zanuy, C., Albajar L. and Fuente, P. (2007). "Sectional Analysis of Concrete Structures under Fatigue Loading." *ACI Structural Journal*, Vol. 106, No. 5, pp. 667-677.
44. Zhang, B. et al. (1996). "Effects of Loading Frequency and Stress Reversal on Fatigue Life of Plain Concrete." *Magazine of Concrete Research*, Vol. 48, pp. 361-375.
45. Zhang, B., and Wu, K. (1997). "Residual Fatigue Strength and Stiffness of Ordinary Concrete under Bending." *Cement and Concrete Research*, Vol. 27, No. 1, pp. 115-126.

## CHAPTER 8

### REINFORCED CONCRETE AND STEEL-FIBRE CONCRETE ELEMENTS UNDER FATIGUE LOADING: MODEL VERIFICATION

*This material was submitted to ASCE Structural Journal, and is in review for publication as a technical paper.*

*Isojeh B., El-Zeghayar M., Vecchio F.J. "Reinforced Concrete and Steel Fibre Concrete Elements under Fatigue Loading: Model Formulation."*

#### **8.1 Abstract**

The verification of finite element analysis results with experimental results from fatigue tests of small-scale deep beams are presented in this chapter. The VecTor2 nonlinear finite element analysis software, which incorporates the algorithm proposed in the previous chapter (Chapter 7), was used for this purpose. The results are given in terms of static load-deformation plots for each fatigue-damaged beam at successive intervals of loading cycles. Mid-span deflection evolution and embedded steel reinforcement stress progressions are also shown. In the results, the fatigue life corresponds to the number of cycles at which the residual capacity of each beam approaches a value equal to the applied maximum fatigue load, as previously hypothesised. The stresses in the reinforcement were observed to evolve up to the yield value at which point fracture became imminent. A comparison of the results with the experimental data suggests good correlation. Further, the results are significantly void of ambiguity in their interpretation; hence, the proposed formulation provides for a rational approach to the fatigue analysis of structural elements.

#### **8.2 Introduction**

The damaging effects of fatigue loading, such as strength and stiffness deterioration in materials

or structural components, are well-known and extensively reported in the literature (Schaff and Davidson, 1997; Zhang and Wu, 1997; Isojeh et al., 2017a; Isojeh et al., 2017b, Isojeh et al., 2017c). However, a major challenge has been the development of an explicit analysis approach which realistically predicts the damage evolution of materials and appropriately exemplifies complex analyses in an unambiguous and easy to comprehend manner.

The Disturbed Stress Field Model (Vecchio, 2000, Vecchio, 2001) was modified to account for fatigue damage of both conventional and steel fibre reinforced concrete structural components in Chapter 7. In the modified algorithm, fatigue damage mechanisms resulting from fatigue crack growth in reinforcement intersecting cracked concrete planes are accounted for using a fracture mechanics model. Residual strength, stiffness damage, and irreversible fatigue strain accumulation in concrete are also considered using appropriate models. The implementation of these damage mechanisms into equilibrium, constitutive, and compatibility relations of a monotonic analysis algorithm enables fatigue damage prediction in terms of deformation evolution (Isojeh et al., 2017a; Isojeh et al., 2017b; Isojeh et al., 2017c). In addition, the fatigue loading cycles at which the residual capacity approaches the maximum constant fatigue load corresponds to the fatigue life of the structural component.

To establish the accuracy and validity of the proposed approach, predictions of fatigue- damaged structural elements are required. As such, the results obtained from an experimental investigation which involved fatigue tests on conventional and steel fibre reinforced concrete beams were examined. The fatigue life and mid-span deflection evolution were obtained for each specimen. The predicted results based on finite element analyses are given in a subsequent section. Details of the experimental test procedures, material properties, and fatigue loading parameters used are given below.

### 8.3 Experiment Details

The experimental program, which involved fatigue tests on small-scale deep beams, has been reported previously in the literature. However, the details are succinctly reiterated in this section.

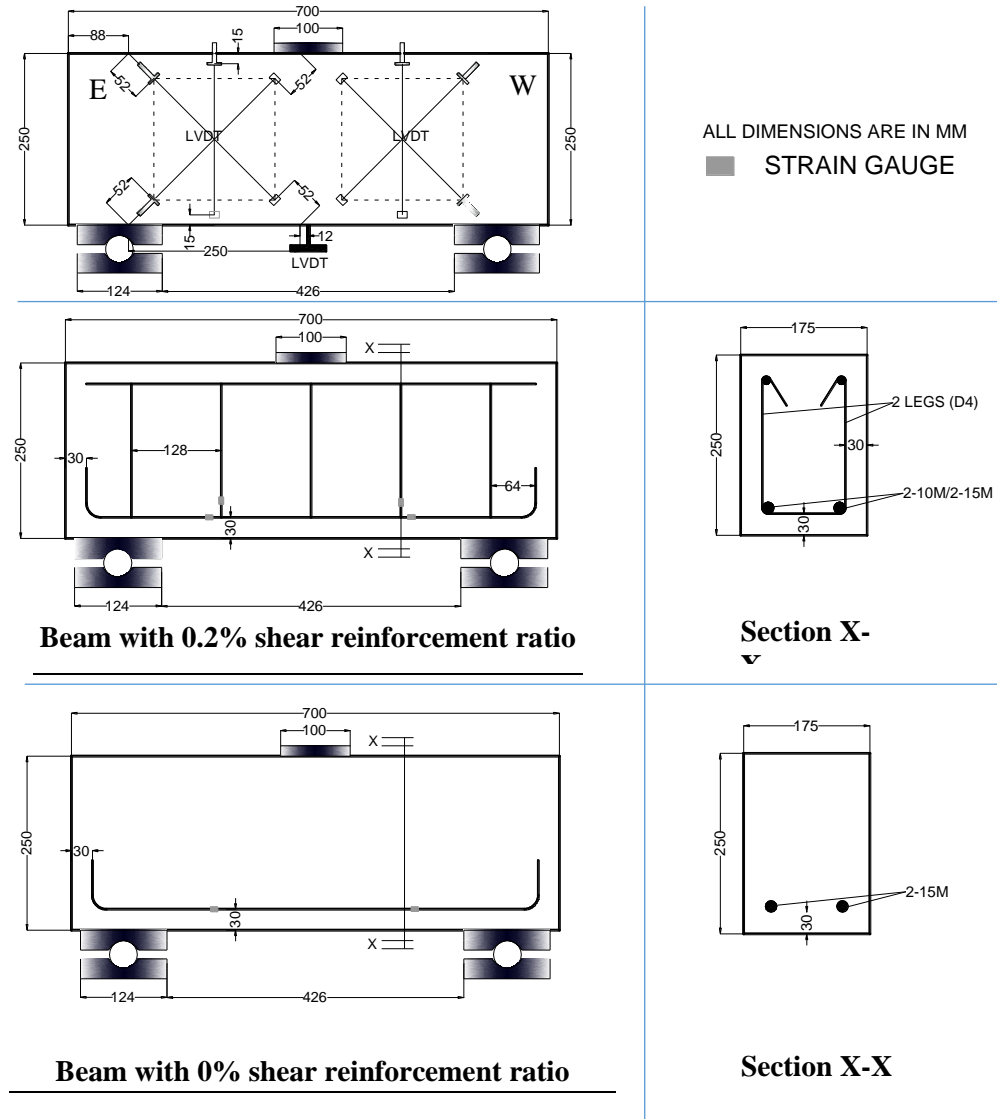


Fig. 8.1. Details of deep beam specimen.

The specimen dimensions are given in Figure 8.1 and test setup is shown in Figure 8.2. Steel fibre volume ratio, shear reinforcement, longitudinal reinforcement, and fatigue load were varied in order to study the corresponding damage effect on fatigue life and structural integrity.

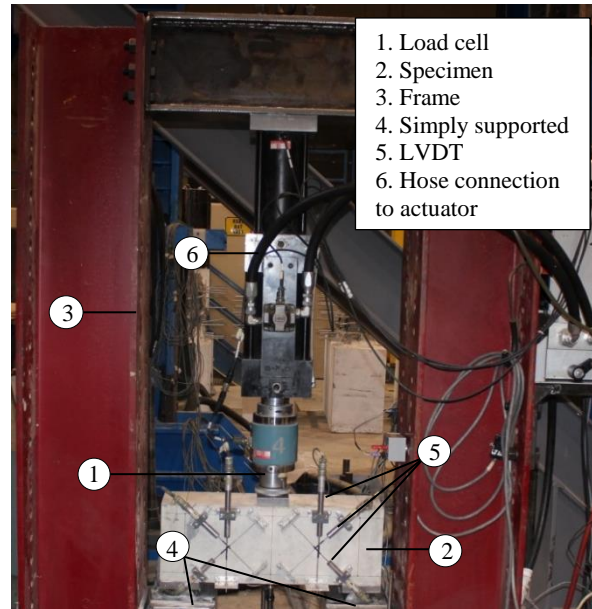


Fig. 8.2. Experimental setup.

Average compressive strengths of 59 MPa and 55 MPa at 28 days were measured for the conventional reinforced and steel-fibre reinforced concrete, respectively. The steel-fibre reinforced concrete specimens had steel fibre volume ratios of 0.75% and 1.5%, and all beams were reinforced longitudinally with either two 15M or two 10M Canadian standard rebars. Some beams contained Canadian standard D4 rebars as shear reinforcement. The average yield strength obtained for the 15M, 10M, and D4 bars were 430 MPa, 480 MPa, and 610 MPa, respectively.

High strength end-hooked steel fibre (Dramix RC80/30BP) with an ultimate tensile stress capacity of 3070 MPa was used for the steel-fibre reinforced concrete beams. Details of the beams tested in the reported experimental investigation are given in Table 8.1. The residual flexural tensile strength ( $FR_{1/FR,4}$ ) for steel fibre volume ratios of 0.75% and 1.5% from conducted experiments were obtained as 4.5/3.0 and 6.0/4.2, respectively (RILEM TC 162-TDF, 2003).

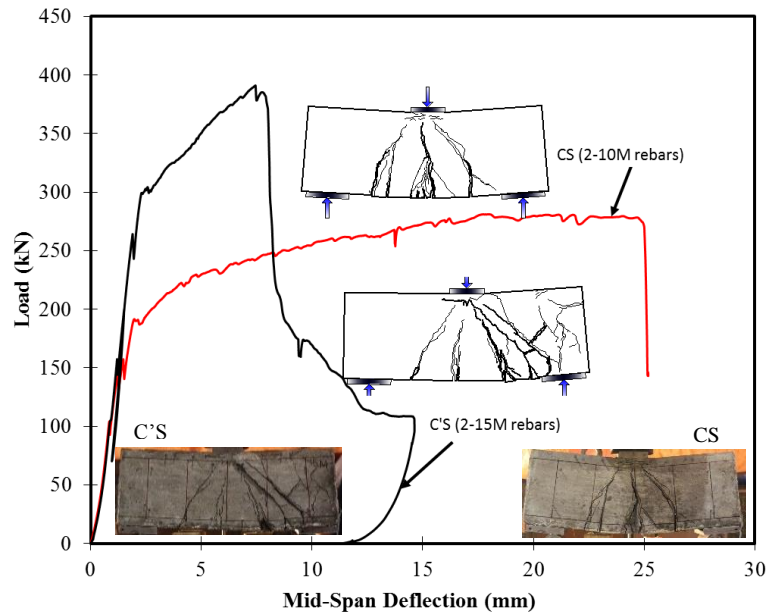


Fig. 8.3 - Load-deformation plot for beams CS and C'S.

Beams C'S and CS, reinforced longitudinally with two 15M and two 10M reinforcing bars, respectively, were initially subjected to monotonic loading in order to obtain their respective resistance capacities. Figure 8.3 shows the load-deformation plot for the beams; peak loads of 270 kN and 390 kN were obtained for beams CS and C'S, respectively.

As shown in Table 8.1, aside from beams CS and C'S which were subjected to monotonic loading, all other specimens were subjected to fatigue loading using 80% or 70% of the resistance capacity of beam CS or C'S. The fatigue loads used on the conventional reinforced concrete beams was also used on the steel-fibre reinforced concrete beams having similar longitudinal reinforcement provisions. A sinusoidal load waveform with a frequency of 5 Hz was used in all cases and the minimum fatigue load was 5 kN (expressed in percentage in column 8) for all specimens tested. The fatigue lives obtained during the experiments are given in Table 8.1, column 9.

Table 8.1 - Specimen description.

| 1              | 2                               | 3                              | 4                  | 5            | 6            | 7                           | 8                           | 9                                  |
|----------------|---------------------------------|--------------------------------|--------------------|--------------|--------------|-----------------------------|-----------------------------|------------------------------------|
| Concrete Batch | Volume of Steel Fibre $V_f$ (%) | Specimen Identification Number | Design $f_c^d$ MPa | $\rho_l$ (%) | $\rho_v$ (%) | Maximum Fatigue Load (% Pu) | Minimum Fatigue Load (% Pu) | No. of Cycles to Failure ( $N_f$ ) |
| 2              | 0                               | C'S                            | 50                 | 0.9          | 0.2          | Monotonic                   | -                           | -                                  |
| 2              | 0                               | CS                             | 50                 | 0.45         | 0.2          | Monotonic                   | -                           | -                                  |
| 1              | 0                               | C'-70-0                        | 50                 | 0.9          | 0.2          | 70                          | 1.3                         | 210,000                            |
| 1              | 0                               | C-80-0                         | 50                 | 0.45         | 0.2          | 80                          | 1.8                         | 47,000                             |
| 3              | 0.75                            | A80-0F0.75                     | 50                 | 0.45         | 0.2          | 80                          | 1.8                         | 66 000                             |
| 4              | 1.5                             | A80-0I.5                       | 50                 | 0.45         | 0.2          | 80                          | 1.8                         | 320 000                            |
| 1              | 0                               | C-70-0                         | 50                 | 0.45         | 0.2          | 70                          | 1.8                         | 72 000                             |
| 3              | 0.75                            | A70-0F0.75                     | 50                 | 0.45         | 0.2          | 70                          | 1.8                         | 123 000                            |
| 3              | 0                               | A70-0N0.75                     | 50                 | 0.45         | 0            | 70                          | 1.8                         | 260 000                            |
| 4              | 1.5                             | A70-0F1.5                      | 50                 | 0.45         | 0.2          | 70                          | 1.8                         | 410 000                            |
| 1              | 0                               | C'-80-0                        | 50                 | 0.9          | 0.2          | 80                          | 1.3                         | 62 000                             |
| 5              | 1.5                             | B80-0N1.5                      | 50                 | 0.9          | 0            | 80                          | 1.3                         | 650 000                            |

where:

$V_f$  (%) = steel fibre volume content (in percentage)

$f_c^d$  = design compressive strength of concrete

$\rho_l$  (%) = longitudinal reinforcement ratio (in percentage)

$\rho_v$  (%) = shear reinforcement ratio (in percentage)

<sup>a</sup> = specimen did not fail at the specified number of cycles

## 8.4 Finite Element Modelling

The beam specimen shown in Figure 8.4 was modelled with concrete or steel fibre concrete, discrete reinforcement, and steel plates at the loading point and at the supports. The labels in Figure 8.4 are described in Table 8.2. A roller and a pin support were used to portray a simply-supported beam.

### 8.4.1 Material Properties

The beam specimen was modelled using either concrete or steel-fibre reinforced concrete material.

The parameters used in the model include the beam dimensions as shown in Figure 8.1, cylinder compressive strength (59 MPa), cylinder strain corresponding to the compressive strength ( $2.1 \times 10^{-3}$ ), and aggregate size (10 mm). Default values were used for all other parameters.

For steel fibre concrete, a compressive strength of 55 MPa and a corresponding cylinder strain of approximately  $3.0 \times 10^{-3}$  were used (Lee et al., 2016). An initial tangent elastic modulus of 28000

MPa (as specified by Lee et al., 2016) was also included, while default values were used for the other properties. The tensile strength of the steel fibre concrete with volume ratios of 0.75% and 1.5% without shear reinforcement were taken as 3 MPa and 4 MPa, respectively, based on experimental results. Other steel fibre (Dramix RC80/30BP) properties include volume content (either 0.75% or 1.5%), length (30 mm), diameter (0.38 mm), and tensile strength (3070 MPa).

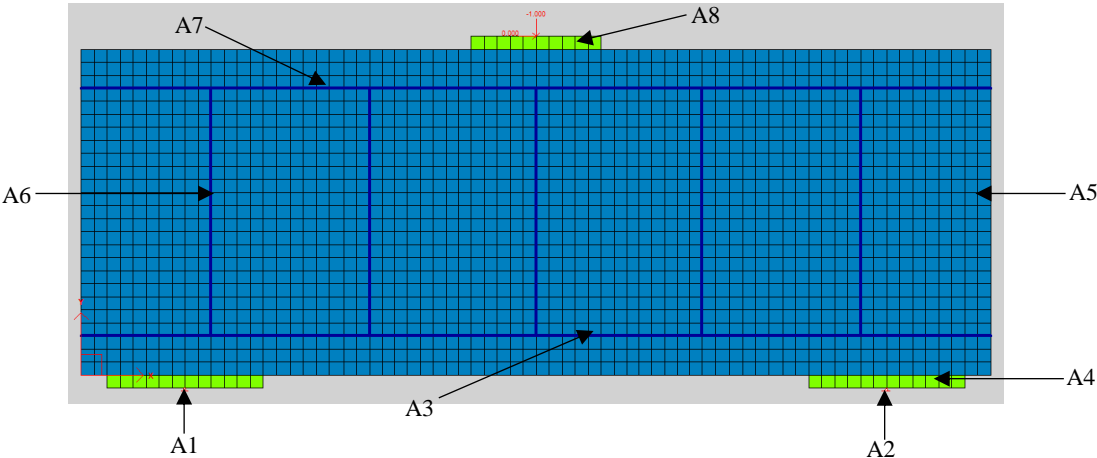


Fig. 8.4 - Beam specimen.

Table 8.2 – Finite element material description.

|    |  |
|----|--|
| A1 | Support condition ( Roller)                          |
| A2 | Support condition (pin)                              |
| A3 | Longitudinal reinforcing bars (2-10M or 2-15M)       |
| A4 | Structural steel plate on reaction                   |
| A5 | Concrete material or steel-fibre reinforced concrete |
| A6 | Shear reinforcement (D4)                             |
| A7 | Hanger bar (2-10M reinforcing bars)                  |
| A8 | Structural steel plate for load application          |

In the finite element model, perfect bond was assumed between the steel reinforcement and the concrete. The average yield strengths of the reinforcing bars, as measured, were used and the ultimate strength for the 15M, 10M, and D4 bars were taken as 700, 600, and 630, based on coupon test results. An elastic modulus of 200000 MPa was used for all reinforcement, while the values

for strain hardening and ultimate strain were taken as 10 millistrain and 100 millistrain. For fatigue loading, elasto-perfectly plastic models were used for the reinforcement.

### 8.4.2 Finite element mesh

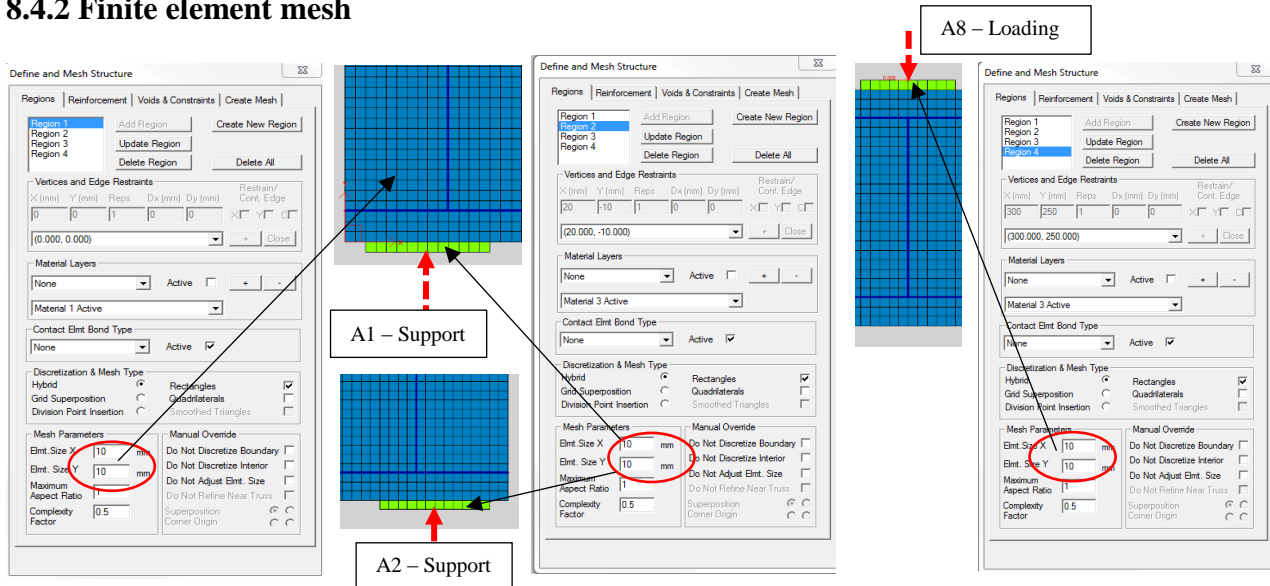


Fig. 8.5 - Mesh structure layout.

The modelled beam consisted of four regions: the concrete beam, the two support plates, and the loading plate as shown in Figure 8.5. In order to maximize the amount of elements that the model can be assigned, a reasonable element size of 10 mm x 10 mm, having an aspect ratio of 1.0, was used for all regions. As indicated previously, truss elements (discrete reinforcement) were used for modelling the steel reinforcing bars.

### 8.4.3 Constitutive Model

For plain concrete, the Popovics and Popovics/ Mander's models were implemented for compression pre-peak and post-peak, respectively for monotonic and fatigue loading. Default values were used for all other parameters. In the case of steel fibres, the models proposed by Lee et al. (2011) were used for compression pre-peak and post-peak. Under fatigue loading, an

advanced approach for crack stress calculation in VecTor2 for steel fibre reinforced concrete was implemented.

The loading cycles, frequency (5 Hz), loading ratio (0), fatigue waveform (0.15), and interval of loading cycles that characterise the fatigue load were included. For all fatigue loading cycles, it was ensured that the ratio between the loading cycles and the interval was at least 100.

#### **8.4.4 Loading Condition**

The resistance capacity of each beam tested (monotonic response) was obtained using displacement-controlled loading. However, under fatigue loading, load-control was used. The fatigue analysis results are expressed in terms of load-deformation curves (monotonic response of fatigue-damaged beams). The origin in the case of fatigue loading is taken to be equal to the fatigue load considered. The value is usually less than the capacity of the beam, except at the instant of failure where the fatigue damage reduces the capacity of the beam to a value equal to the fatigue load. Hence, monotonic loading begins from the actual maximum fatigue load.

#### **8.5 Finite Element Fatigue Damage Analysis Results**

The proposed concept for the fatigue damage analysis of conventional reinforced and steel-fibre reinforced concrete elements involves the estimation of the constituent material damage values in each element after a given number of fatigue loading cycles in the first load stage. The material parameters for plain concrete, steel fibre concrete, and steel reinforcement obtained from the experimental investigation were used in the finite element modelling at the initial load stage. Subsequently, the load-deformation response was obtained taking into account the damage effects on each element in subsequent load stages (incremental loads).

In the experiments conducted, the steel reinforcement fracture was significantly characterised by

a brittle nature, and the strains were less than the yield value prior to structural collapse. As reported in the literature, the results obtained from the experiments indicated that fatigue failure was a result of reinforcement crack propagation at the intersection with a cracked concrete plane. As the induced stresses in the steel reinforcement evolve to the yield value (due to progressive reduction of reinforcement area), fracture or structural collapse becomes imminent. In the proposed analysis approach, an elastic-perfectly plastic model was assumed for steel reinforcement constitutive model in all cases; hence, the influence of strain hardening was neglected.

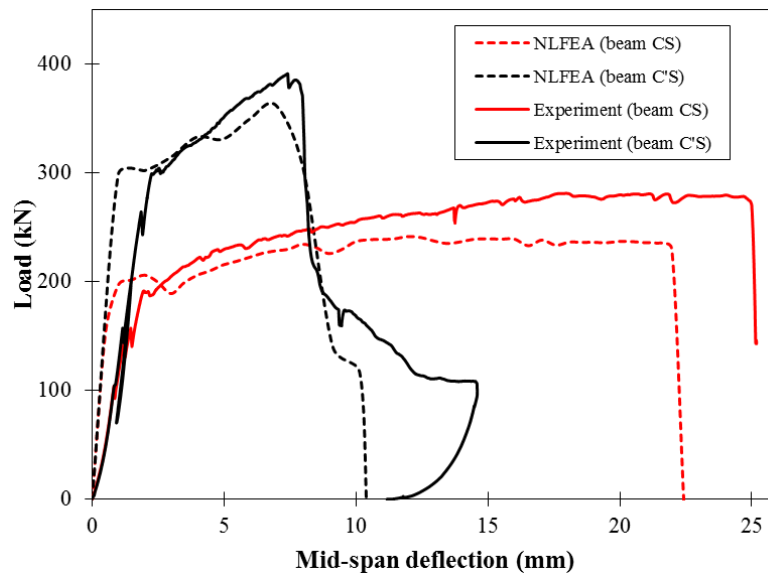


Fig. 8.6 - Load-deformation plot for beams CS and C'S.

The VecTor2 nonlinear finite element analysis (NLFEA) software was initially used to obtain the monotonic load-deformation responses (without fatigue damage) of beams CS and C'S. Figure 8.6 shows the load-deformation responses from VecTor2 alongside the load-deformation plots from the experiments conducted. The resistance capacities obtained for beams CS and C'S were 250 kN and 350 kN, respectively. Similar to the experimental test procedures and loading parameters, 80% and 70% of the resistance capacity of the modelled beams were used for fatigue loading responses. The analysis algorithm has been described in the previous chapter; herein, the validation results

from the NLFEA based on the aforementioned algorithm are given. The requirements for finite element modelling of fatigue-damaged elements using VecTor2 are described subsequently with brevity.

### **8.5.1 Fatigue Life and Deformation Evolution Predictions**

The fatigue life analysis protocol used involved the following major steps:

- The fatigue analysis results for structural components are expressed in terms of monotonic load-deformation plots corresponding to different fatigue loading cycles having accounted for the components' damage as the loading cycles increase.
- The monotonic load-deformation response, after a given regime of fatigue loading cycles in VecTor2, is obtained incrementally (in a load-controlled analysis). Initial and incremental load factors are required.
- The fatigue load parameters required include: fatigue loading cycles, fatigue loading frequency, fatigue load ratio, waveform, and interval of fatigue loading. The load ratio is taken as the ratio between the minimum and maximum applied fatigue load.
- The maximum fatigue load is used as the initial factor (first load stage). The material stresses in all elements corresponding to the first load stage under monotonic loading are substituted into damage models and estimated values are saved.
- Subsequent increments (load stages greater than 1) take into account these constant damage values. As the cycles are increased in each analysis conducted, the resistance capacity (based on load-deformation response) may reduce progressively depending on the extent of reinforcement fracture.

The predicted fatigue life corresponds to the number of cycles at which the resistance capacity of a beam reduces to a value approximately equal to the applied maximum fatigue load. Since fatigue

damage is accounted for from the second load stage onward and a small value of load increment is generally used, the deformation (mid-span deflection) at the second load stage is assumed to correspond to deformation resulting from the applied fatigue loading cycles.

The results of finite element analyses of the specimens in Table 8.1 are presented in terms of fatigue residual capacity, mid-span deflection evolution, and reinforcement stresses. The predicted fatigue life and fatigue loads are shown in Table 8.3.

### **8.5.2 Fatigue residual capacity**

Figures 8.7 and 8.8 are the load-deformation plots for conventional reinforced concrete beams at different numbers of cycles. Each load-deformation plot in Figures 8.7 and 8.8 indicated as A corresponds to a residual capacity approximately equal to the constant maximum fatigue load indicated at the load-deformation plot origin O. The other plots, after increasing the loading cycles, progressively exhibit substantial but depreciating resistance capacities to increasing load. A reduction in the stiffness of each beam was observed from the plots. Compared to the experimental results obtained for fatigue life, the fatigue life predictions obtained from the NLFEA are not only conservative, they portray good correlation.

In the case of the steel-fibre reinforced concrete beams, the approximate load that will result in the collapse of each modelled beam at the number of cycles corresponding to failure obtained from the experiment was first predicted. In Figure 8.9, as the load increased from 180 kN to 188 kN (at 400000 cycles for beam A70-0F1.5)), the residual capacity reduced. Subsequently, load-deformation plots for increments in the number of cycles at the predicted loads were obtained. The residual capacities are given in Figures 8.10 to 8.12. The predicted fatigue load for each steel-fibre reinforced concrete beam is reasonably close to the actual fatigue load of 80% and 70% of the monotonic resistance capacity of corresponding control beams from NLFEA; hence, the responses

from conventional reinforced and steel-fibre reinforced concrete can be compared for beams having similar loading parameters.

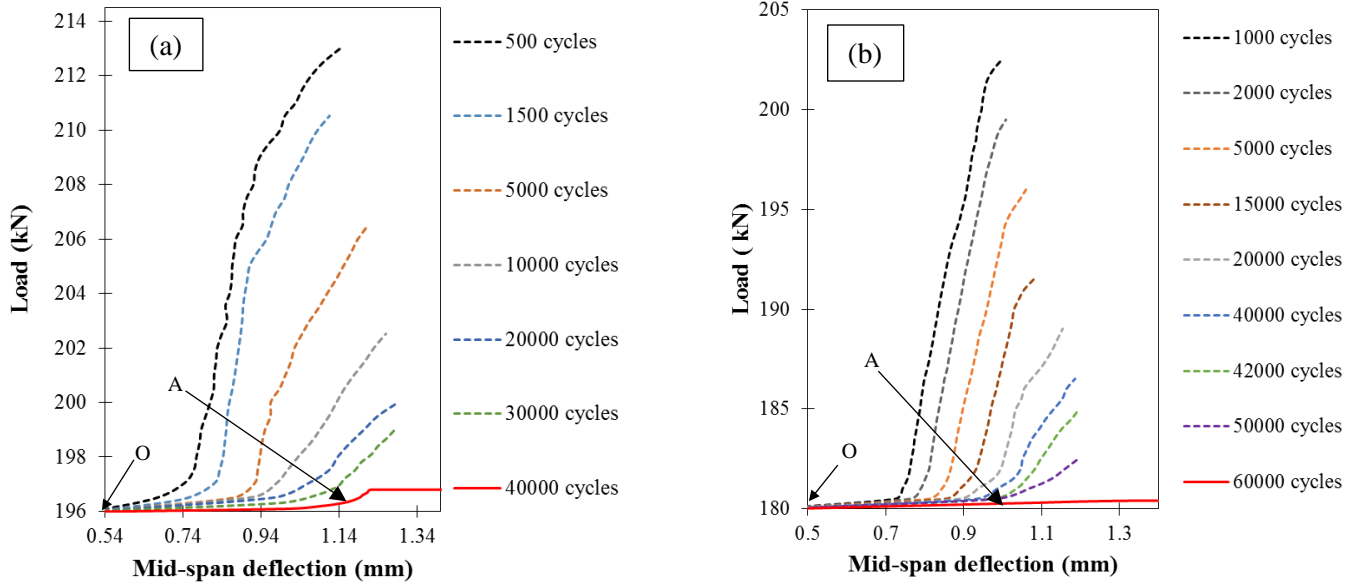


Fig. 8.7 - Calculated fatigue residual capacity for beam: (a) C-80-0 (b) C-70-0.

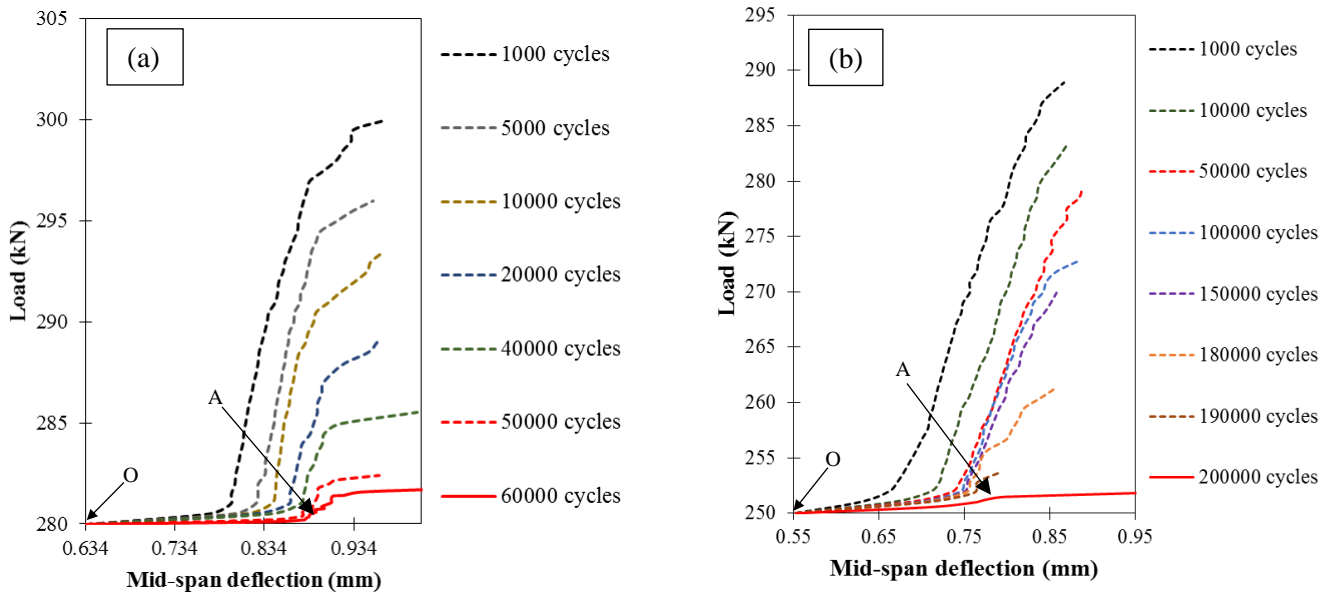


Fig. 8.8 - Calculated fatigue residual capacity for beam: (a) C'-80-0 (b) C'-70-0.

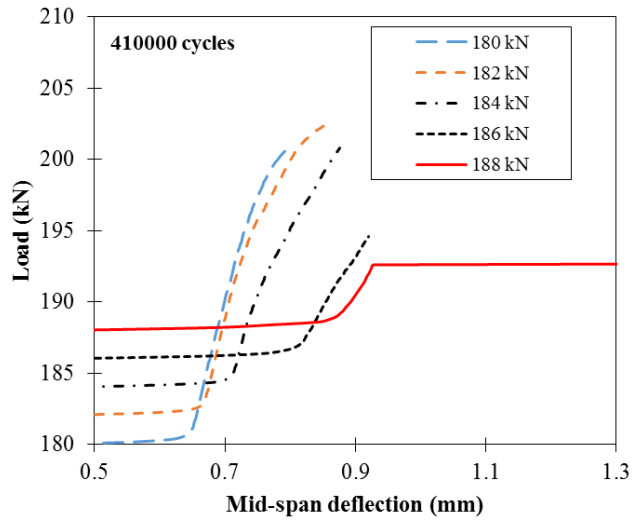


Fig. 8.9 - Calculated fatigue residual capacity evolution for beam A70-0F1.5.

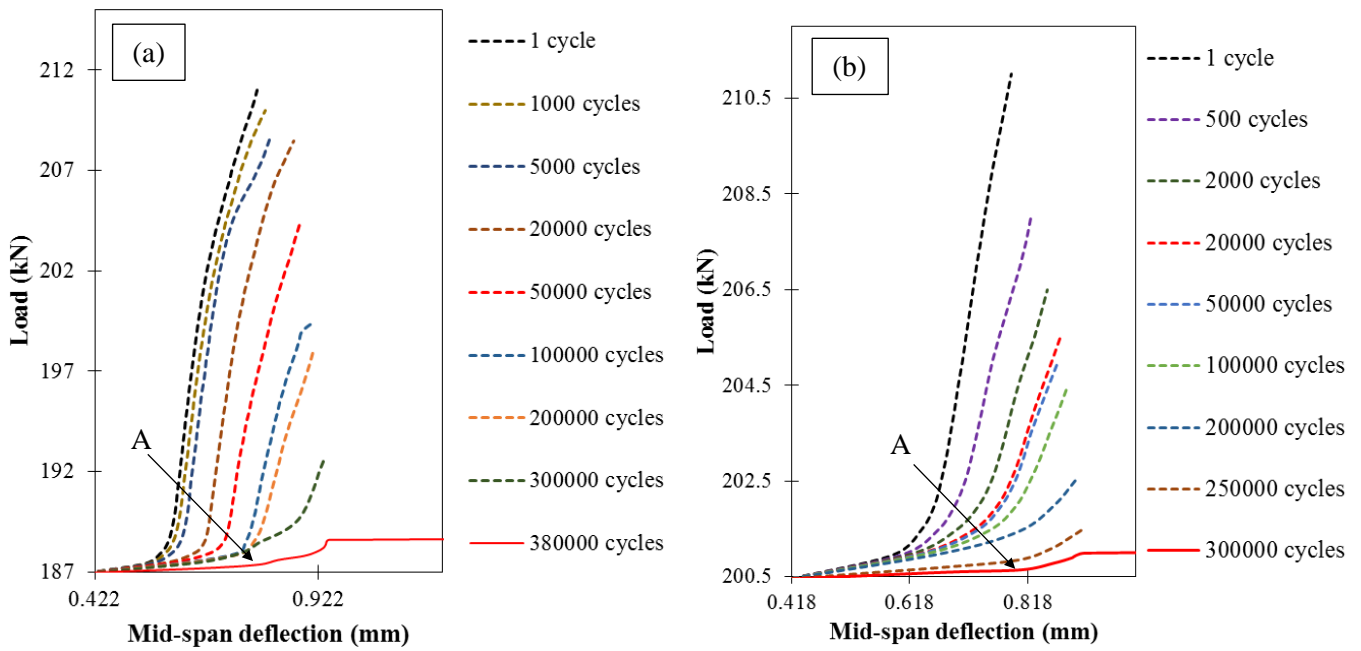


Fig. 8.10 - Calculated fatigue residual capacity for beam: (a) A70-0F1.5 (b) A80-0F1.5.

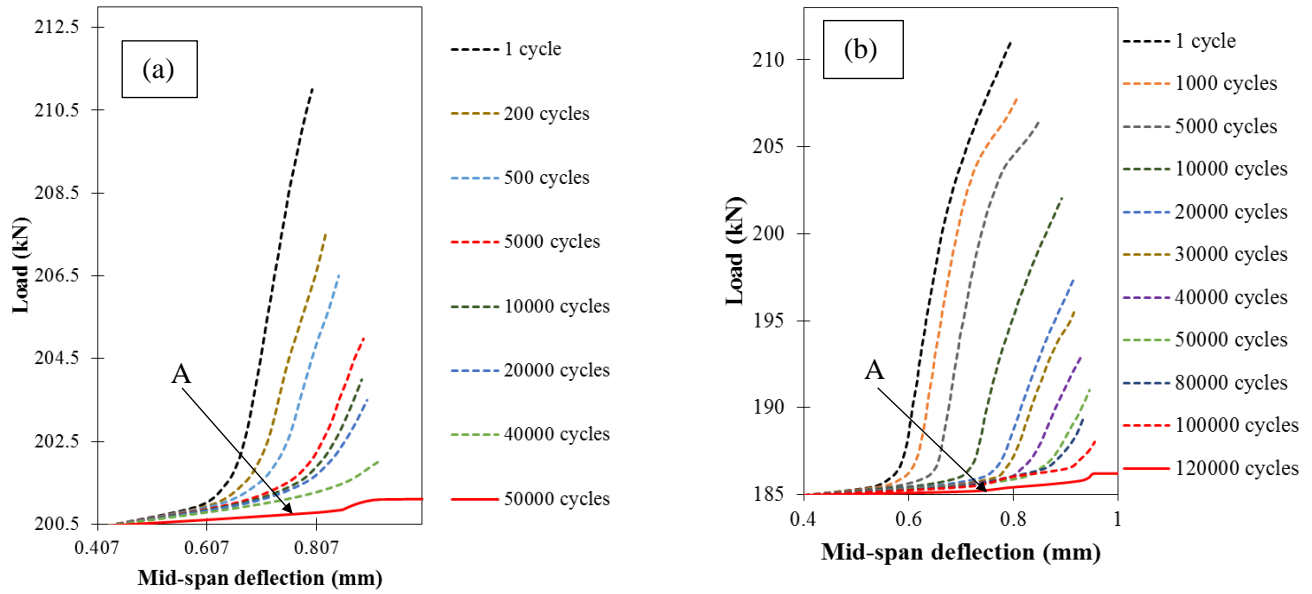


Fig. 8.11 - Calculated fatigue residual capacity for beam: (a) A80-0F0.75 (b) A70-0F0.75.

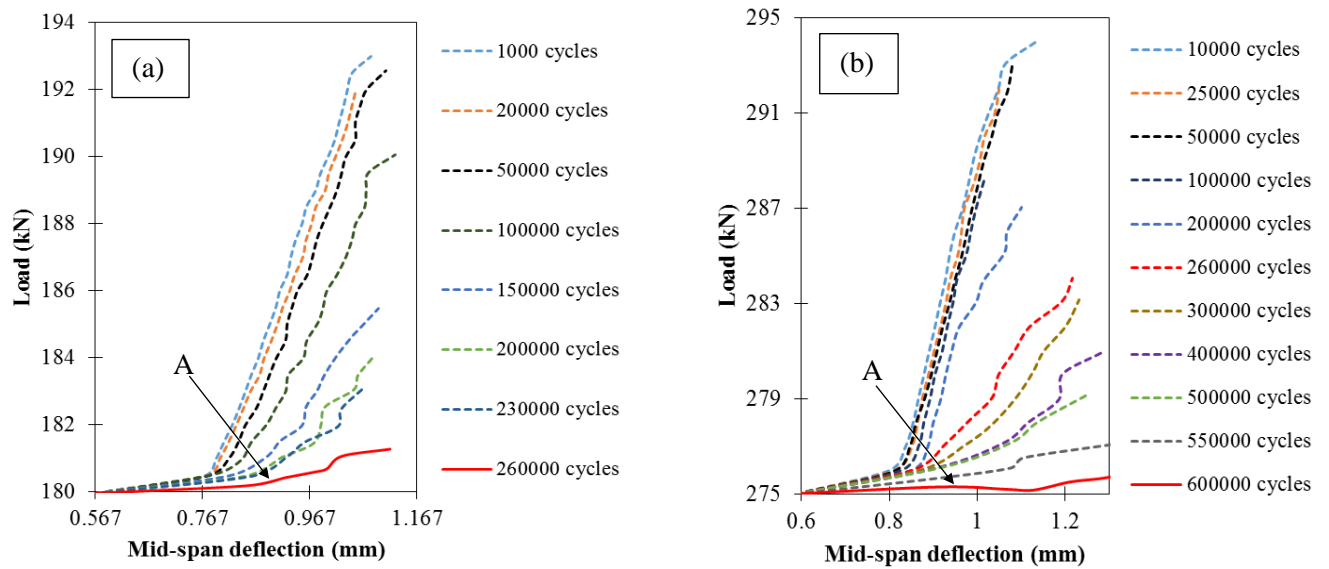


Fig. 8.12 - Calculated fatigue residual capacity for beam: (a) A70-0N0.75 (b) B80-0N1.5.

The results are also presented in Table 8.3. Column 7 in Table 8.3 shows the ratio of the calculated fatigue load to the actual fatigue loads corresponding to 70% or 80% of the undamaged beam resistance capacities obtained from the NLFEA. Column 8 shows the ratio of the logarithm of predicted fatigue life (using VecTor2) to the experimental fatigue life. As observed in both cases,

the predictions are of good accuracy; however, the predictions for steel fibre reinforced concrete beams fatigue load from NLFEA reveal a slight underestimation of the fatigue damage.

Table 8.3 - Fatigue life for beam specimens (experimental and predicted)

| 1          | 2              | 3   | 4                     | 5                                       | 6                                    | 7               | 8                          |
|------------|----------------|---|-----------------------|---|--------------------------------------|-----------------|----------------------------|
| Specimen   | Exp. load (kN) | Fatigue life (Experiment) Cycles $N_{fe}$ | NLFEA Load (kN) $H_l$ | Predicted Fatigue life (NLFEA) $N_{fv}$ | Predicted fatigue load (NLFEA) $H_p$ | NLFEA $H_p/H_l$ | Log $N_{fv}/$ Log $N_{fe}$ |
| C'-70-0    | 274            | 210000                                    | 250                   | 200000                                  | -                                    | -               | 1.00                       |
| C'-80-0    | 312            | 62000                                     | 275                   | 60000                                   | -                                    | -               | 0.98                       |
| C-70-0     | 192            | 72000                                     | 180                   | 60000                                   | -                                    | -               | 0.98                       |
| C-80-0     | 219            | 47000                                     | 196                   | 40000                                   | -                                    | -               | 0.99                       |
| A70-0F0.75 | 192            | 123000                                    | 180                   | -                                       | 185                                  | 1.03            | -                          |
| A80-0F0.75 | 219            | 66000                                     | 196                   | -                                       | 200                                  | 1.02            | -                          |
| A70-0F1.5  | 192            | 410000                                    | 180                   | -                                       | 187                                  | 1.04            | -                          |
| A80-0F1.5  | 219            | 320000                                    | 196                   | -                                       | 200                                  | 1.02            | -                          |
| A70-0N0.75 | 192            | 260000                                    | 180                   | -                                       | 180                                  | 1.00            | -                          |
| B80-0N1.5  | 312            | 650000                                    | 275                   | -                                       | 275                                  | 1.00            | -                          |

### 8.5.3 Mid-span deflection evolution

The mid-span deflection evolution for the beams modelled in VecTor2 are shown in Figures 8.13 to 8.17. The evolutions obtained from the experimental results are also included. Although the predicted evolving values from NLFEA tend to be slightly lower, overall, the correlation of the experimental results (mid-span deflection evolution) with the predicted results are of acceptable accuracy.

The significance of the deformation evolution predicted stems from the fact that each predicted point in Figures 8.13 to 8.17 is obtained from an independent analysis at different numbers of fatigue loading cycles and yet develop deformation evolution profiles which clearly depict the well-known fatigue deformation evolution profile from experiments on fatigue. The predicted evolution profiles are shown properly in a subsequent section for variations in loading and materials parameters.

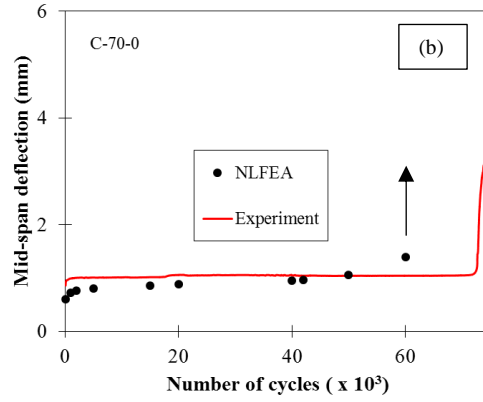
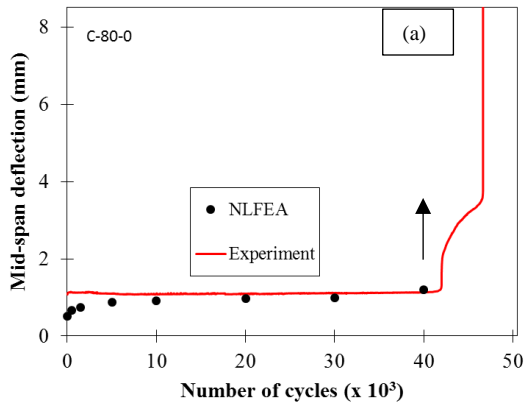


Fig. 8.13 - Mid-span deflection evolution for (a) C-80-0 and (b) C-70-0.

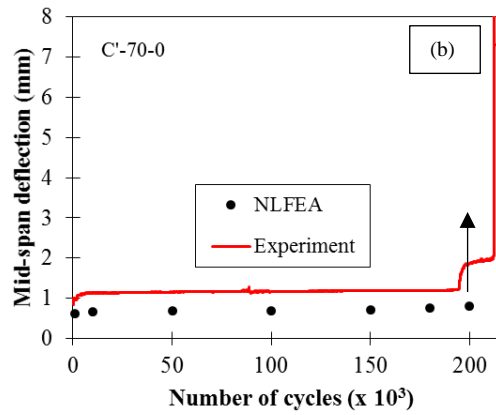
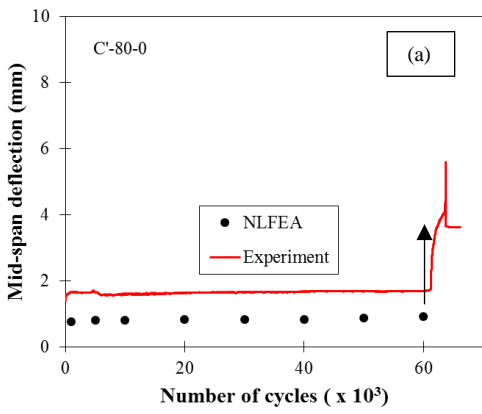


Fig. 8.14 - Mid-span deflection evolution for (a) C'-80-0 and (b) C'-70-0.

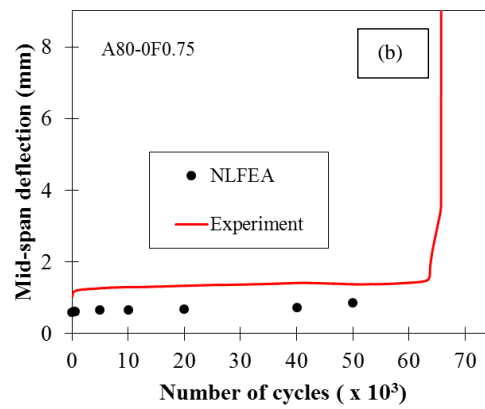
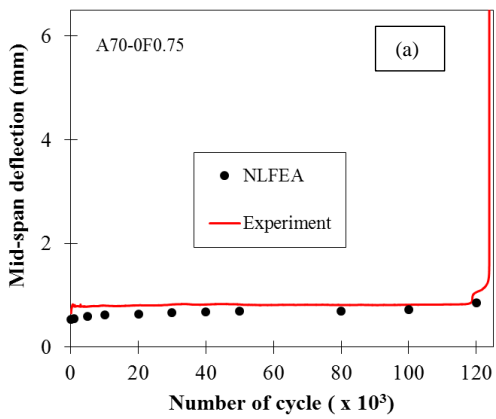


Fig. 8.15 - Mid-span deflection evolution for (a) A70-0.75 and (b) A80-0F0.75.

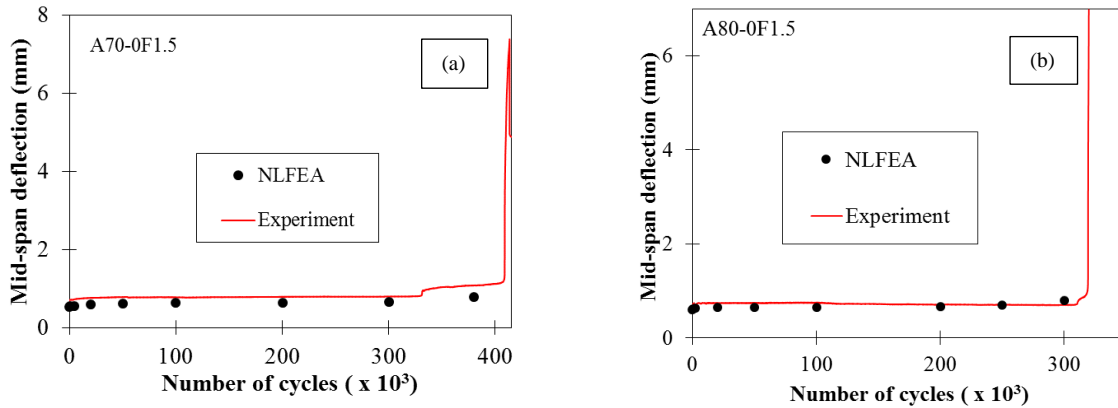


Fig. 8.16 - Mid-span deflection evolution for (a) A70-0F1.5 and (b) A80-0F1.5.

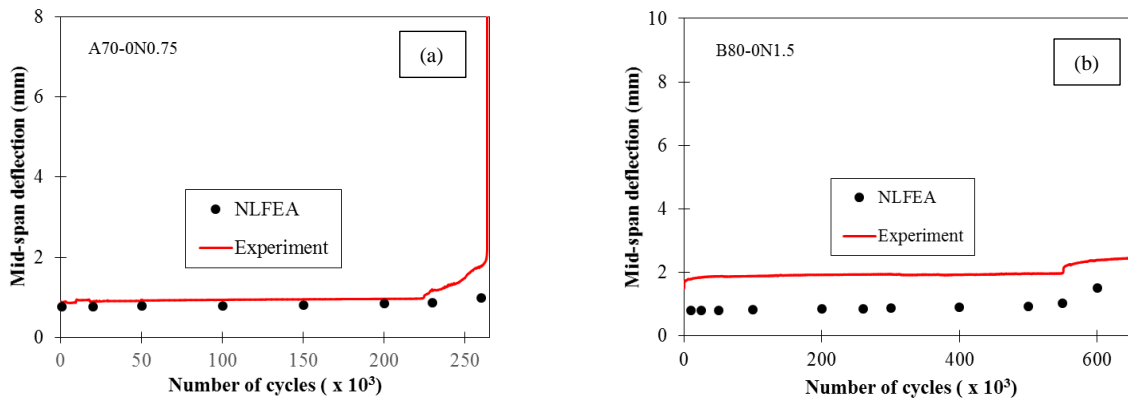


Fig. 8.17 - Mid-span deflection evolution for (a) A70-0N0.75 and (b) B80-0N1.5.

### 8.5.4 Variations in Loading and Material Parameters

The following findings from the numerical investigations are consistent with experimental observations well-established in the literature:

- The fatigue life of a structural component reduces as the applied fatigue load increases (Teng et al., 1998a, Teng et al., 1998b)
- The fatigue life increases as the steel-fibre volume ratio in a beam increases from 0% to 1.5% under the same fatigue loading.
- Steel fibre can be used to augment shear reinforcement in deep beams subjected to fatigue loading (Isojeh et al., Fatigue Resistance Behaviour of Steel-Fibre Reinforced Concrete Deep Beams,” in press, ACI Structural Journal).

As shown in Figures 8.18 and 8.19, as the fatigue load increased from 70% to 80% of the monotonic resistance capacity, the fatigue life was observed to reduce. In addition, the deformations (mid-span deflection) and the corresponding rate of evolution were also observed to increase.

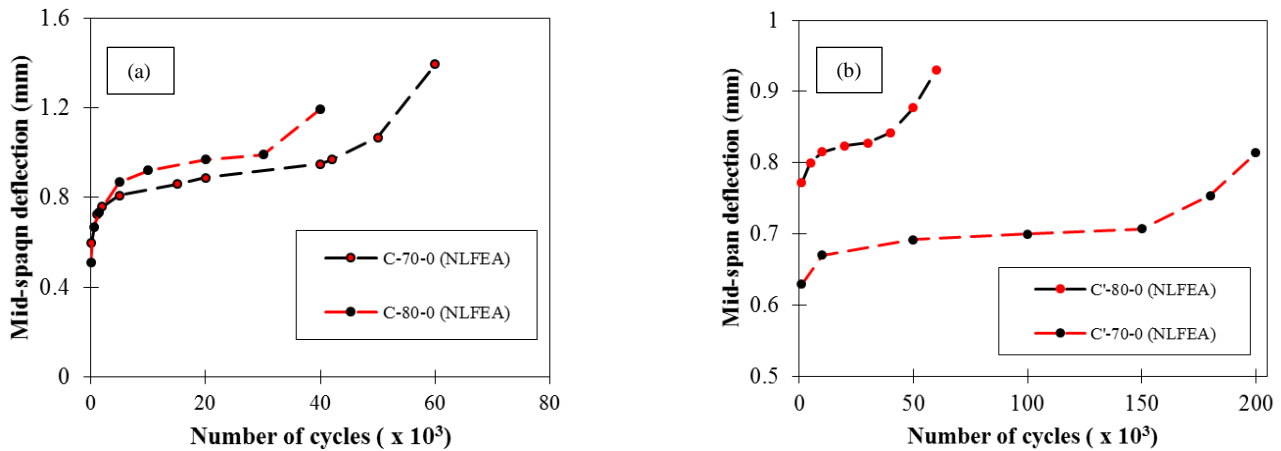


Fig. 8.18 - Mid-span deflection evolution (effect of stress level) (a) 10M bars (b) 15M bars.

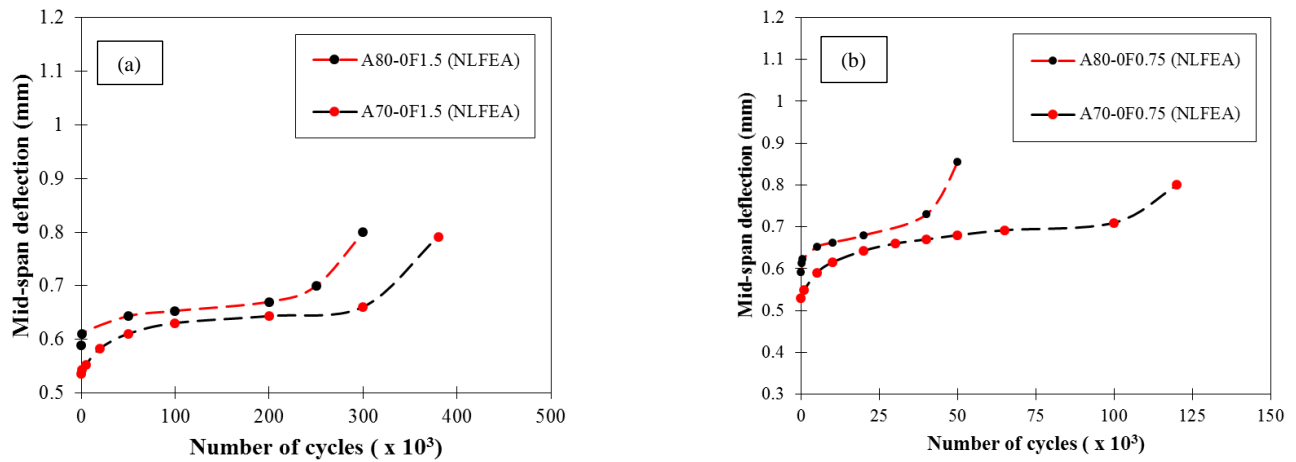


Fig. 8.19 - Mid-span deflection evolution (effect of stress level) (a) 1.5% V<sub>f</sub> (b) 0.75% V<sub>f</sub>.

From Figure 8.20, it can be seen that the increase in fatigue life as steel fibre volume ratio increases from 0% to 1.5% was well-captured using the VecTor2 NLFEA software (based on the proposed fatigue damage algorithm). In addition, from the NLFEA predictions (Figure 8.21), similar to the experimental results, steel-fibre reinforced concrete beams without shear reinforcement resulted

in enhanced fatigue life compared to conventional reinforced concrete beams. However, higher initial deflections were observed in the former.

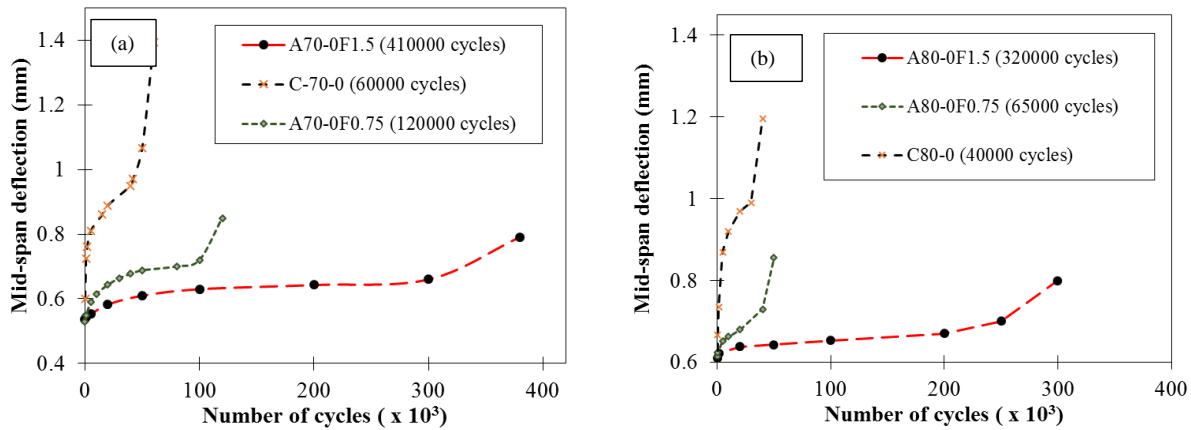


Fig. 8.20 - Mid-span deflection evolution (effect of steel fibres) (a) 70% (b) 80%.

### 8.5.5 Reinforcement Stresses under Fatigue Loading

As previously discussed, structural collapse under fatigue loading is most frequently attributable to crack initiation and growth on reinforcing bars traversing cracked concrete planes. The area of reinforcement at such regions reduces progressively as cracks evolve; hence, increases in the induced stress and strain in the steel reinforcement may be observed prior to the point of final fracture. In order to illustrate the steel reinforcement stress evolution, plots of the steel reinforcement stresses at given fatigue loading cycles were obtained as shown in Figure 8.22 and 8.23.

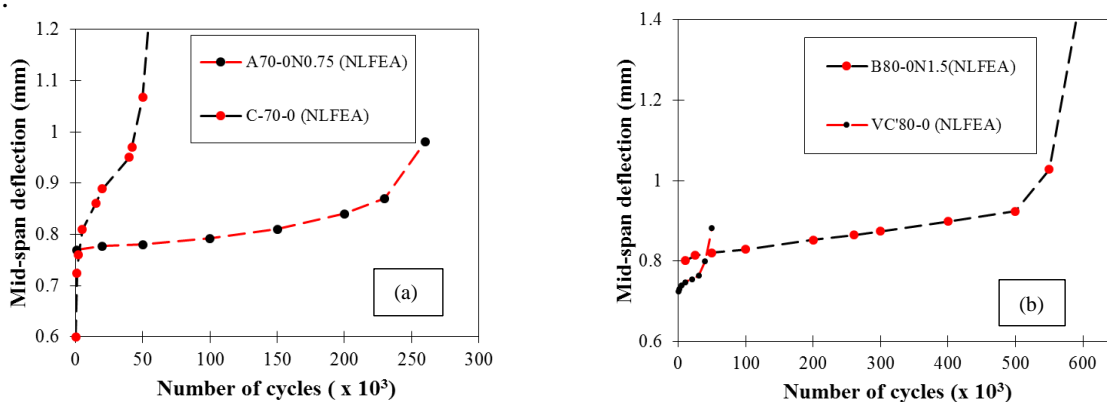


Fig. 8.21 - Mid-span deflection evolution (effect of steel fibres) (a) 70% (b) 80%.

As previously indicated, the yield stresses for the shear and longitudinal reinforcement were 610 MPa and 480 MPa, respectively. In Figure 8.22, the local stresses in the reinforcement at a concrete crack location after 500, 20000, and 40000 cycles are given (Figure 8.22(a) to (c)). The probable region of fracture (where the induced stress is equal to yield) is shown in Figure 8.22 (c) at 40000 cycles. Reinforcement stresses (shear and longitudinal) within the same region in Figure 8.22 (a) and (b) at 500 cycles and 20000 cycles are lower than the yield value. However, the stresses evolve progressively as the number of fatigue loading cycles increase. From the figures, failure was observed to be attributable to fracture of longitudinal reinforcement. Similar observations are shown in Figure 8.23.

## **8.6 Variable Fatigue Loading**

In practice, the fatigue loading of reinforced concrete structures is usually variable in nature and not constant. In the experimental investigation conducted and verified herein, constant fatigue loading was used. In addition, the approach described also considers constant fatigue loading. Two approaches for variable fatigue loading are discussed subsequently.

A majority of designers still prefer the use of the Palmgren-Miner damage rule based on its simplicity. Variable fatigue loads, and the corresponding number of cycles applied, are usually given in spectrums. The proposed approach (using NLFEA) can be used to estimate the number of cycles leading to failure ( $N_f$ ) for each fatigue load in the spectrum, and the ratio of  $N$  to  $N_f$  is obtained for each fatigue load in the spectrum. Hence, the Palmgren-Miner rule may be used to cumulate the expected damage.

The flaw of the negligence of loading sequence and the effect of previous damage consideration has reduced the reliability of this approach. Better still, an equivalent cycle concept may be used for the fatigue analysis of reinforced concrete structures under variable fatigue loading. Using

Figure 8.24, the approach is discussed as follows:

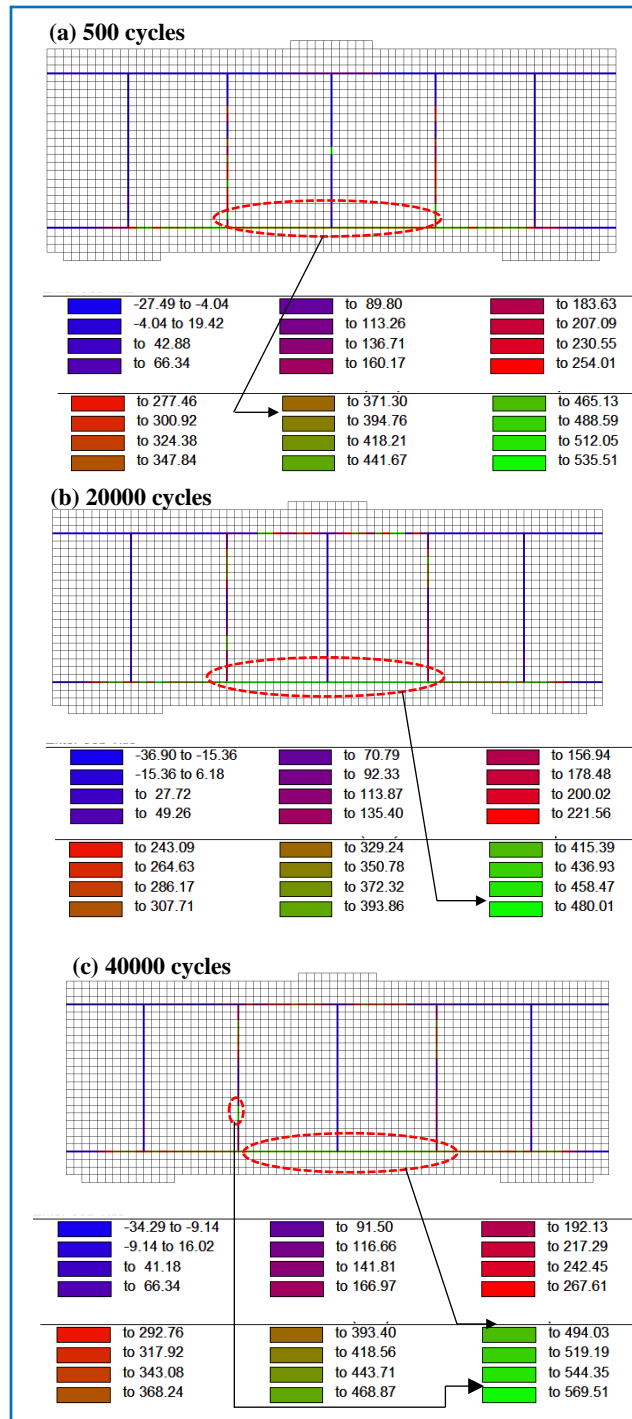


Fig. 8.22 - Evolution of stresses in reinforcing bars for beam C-80-0 (stresses shown in MPa).

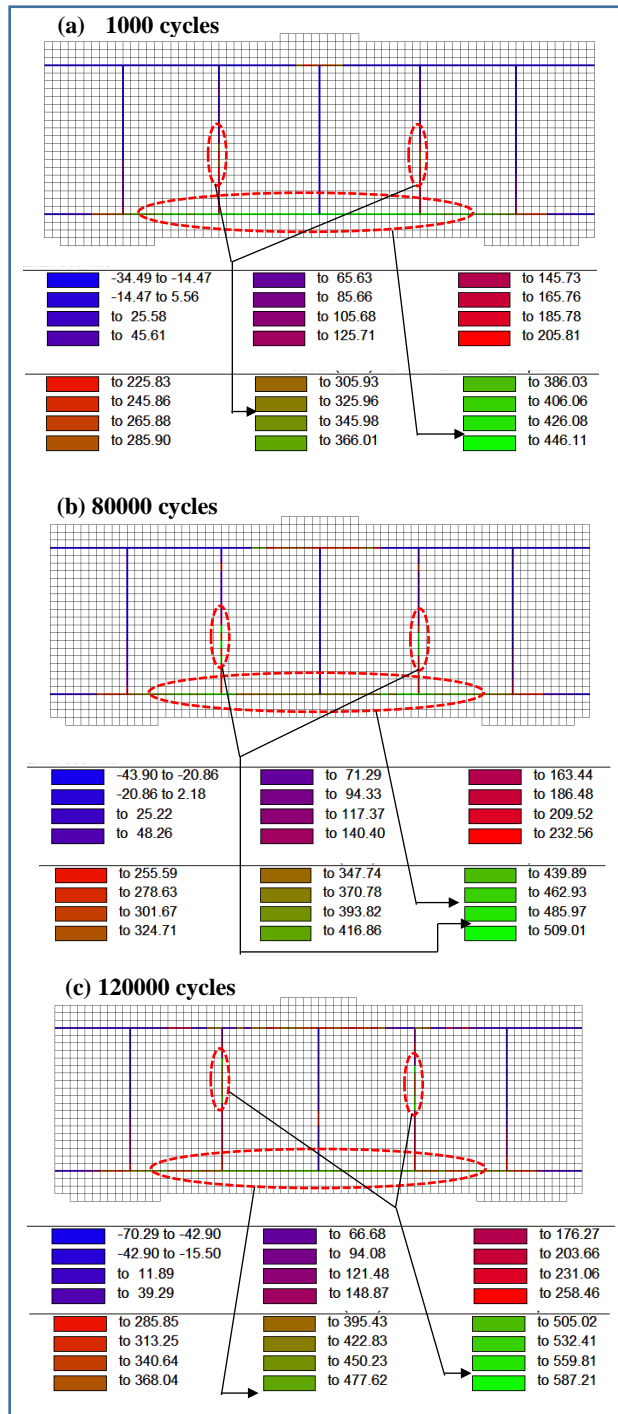


Fig. 8.23 - Evolution of stresses in reinforcing bars for beam A70-0F0.75 (stresses shown in MPa).

The load-deformation plots of all variable loads are obtained using the proposed approach and assuming constant fatigue load for each. For simplicity, the mid-span deflection evolution plots for beams C-70-0 and C-80-0 subjected to two different loads (70-0 and 80-0) are used for this illustration. Assuming a beam is subjected to  $N_1$  cycles (load 80-0), in Figure 8.24, the corresponding mid-span deflection is  $\delta_1$ . For a second variable load (70-0) subjected to  $N_2$  cycles, the effect of the first variable load must be accounted for. Hence,  $\delta_1$  is extended to the load-deformation plot for the second variable load, and the corresponding number of cycles is termed the equivalent cycles ( $N_{equiv}$ ) (Figure 8.24). In order to obtain the actual deflection ( $\delta_2$ ) due to  $N_2$  having considered the damage from the first load stage, the summation of  $N_{equiv}$  and  $N_2$  ( $N_{equiv} + N_2$ ) is extended to the load-deformation plot for the second variable load. This procedure is repeated for subsequent variable loads until the critical point on the last load-deformation plot is reached ( $Cr_i$ ). This approach accounts for previous loading damage; hence it overcomes the sequence and load history anomaly common with variable fatigue loading.

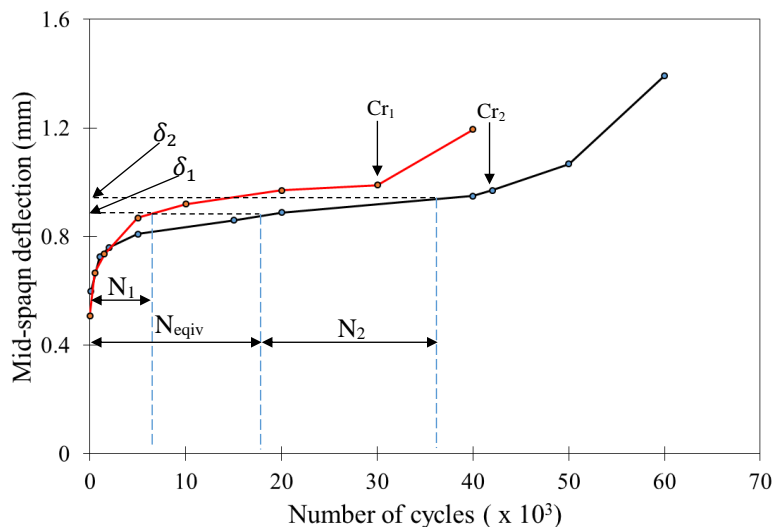


Fig. 8.24 - Variable fatigue loading of reinforced concrete.

## 8.7 Conclusions

The verification of finite element analysis models with experimental data from tests conducted by

the authors were presented. Finite element analysis for fatigue analysis was conducted using VecTor2 having implemented the proposed algorithm discussed in Chapter 7. From the analytical results obtained, the fatigue life predictions using the residual strength concept were found to be consistent with the results obtained from the experimental investigation. The acceptability of the proposed approach can also be attributed to its capability to predict variations in loading and materials parameters as in the case of the fatigue load and steel fibre volume ratios. In addition, conservative life predictions were observed. Further, the analysis of variable fatigue loading can be conducted appropriately using the proposed approach. Based on the observed results, the proposed approach can be incorporated for fatigue resistance verification of structural components prone to fatigue damage.

## 8.8 References

1. Isojeh, B., El-Zeghayar, M., and Vecchio, F.J. (2017a). “ Concrete Damage under Fatigue Loading in Uniaxial Compression.” *ACI Materials Journal*, Vol. 114, No. 2, pp. 225-235.
2. Isojeh, B., El-Zeghayar, M., and Vecchio, F.J. (2017b). “ Simplified Constitutive Model for Fatigue Behaviour of Concrete in Compression.” *Journal of Materials in Civil Engineering*, DOI: 10.1061/(ASCE)MT.1943-5533.0001863.
3. Isojeh, B., El-Zeghayar, M., and Vecchio, F.J. (2017c). “ Fatigue Behaviour of Steel Fibre Concrete in Direct Tension.” *Journal of Materials in Civil Engineering*, DOI: 10.1061/(ASCE)MT.1943-5533.0001949.
4. Isojeh, M.B., and Vecchio, F.J (2016). “Parametric Damage of Concrete under High-Cycle Fatigue Loading in Compression.” *Proc., 9<sup>th</sup> International Conference on Fracture mechanics of Concrete and Concrete Structures. FraMCoS-9 2016*; 10.21012/FC9.009.

5. RILEM TC 162-TDF (2003). "Test and Design Methods for Steel Fibre Reinforced Concrete." *Materials and Structures Journal*, Vol. 36, pp. 560-567.
6. Schaff, J.R., and Davidson, B.D. (1997). "Life Prediction Methodology for Composite Structures. Part 1- Constant Amplitude and Two-Stress Level Fatigue." *Journal of Composite Materials*, Vol. 31, No. 2, pp. 128-157.
7. Teng, S., Ma, W., Tan, K.H., and Kong, F.K. (1998). "Fatigue Tests of Reinforced Concrete Deep Beams," *Journal of the Structural Engineer*, Vol. 76, No. 18, pp. 347-352.
8. Teng, S., Ma, W., Tan, K.H., and Wang, F. (2000). "Shear Strength of Concrete Deep Beams under Fatigue Loading." *Journal of the American Concrete Institute*, No. 97-S60, pp. 572-580.
9. Vecchio, F.J. (2000). "Disturbed Dstress Field Model for Reinforced Concrete: Formulation." *Journal of Structural Engineering*, Vol. 126, No. 8, pp. 1070-1077.
10. Vecchio, F.J. (2001). "Disturbed Dstress Field Model for Reinforced Concrete: Verification." *Journal of Structural Engineering*, Vol. 127, No. 1, pp. 1070-1077.
11. Zhang, B., and Wu K. (1997). "Residual Fatigue Strength and Stiffness of Ordinary Concrete under Bending," *Cement and Concrete Research*, Vol. 27, No. 1, pp. 115-126.

## CHAPTER 9

### CONCLUSIONS AND RECOMMENDATIONS

#### 9.1 Summary

This thesis was written with the major goal of developing a robust approach for the fatigue analysis of wind turbine foundations and other similar fatigue-prone structural elements. Previously, the approach used for fatigue analysis of reinforced concrete structures was rudimentary owing to the fact that a majority of the fatigue damage models used do not account for salient factors influencing the fatigue behaviour of conventional reinforced concrete composites. In addition, a majority of the assumptions implemented into fatigue constitutive models were not experimentally proven to establish their prediction accuracy in ensuring that results are not overly conservative and are cost-effective. On the other hand, it was expedient to verify that predictions are utterly safe.

Flaws observed in previous fatigue resistance design approaches have been shown in this investigation. Previous assumptions have been verified and modified where necessary. New analysis concepts have been proposed for estimating the fatigue life of concrete and steel-fibre reinforced concrete. In addition, a new approach for the experimental investigation of deep beams under fatigue loading has been proposed. This involved the verification of the evolutions of the average principal strains and the evolution of the orientation of principal strain directions.

Because fatigue damage evolution becomes significant where cracks exist, a means of minimising or arresting crack propagation under fatigue loading of deep beams (such as wind turbine foundations) were investigated using steel-fibre reinforced concrete. In addition, a means of optimizing fatigue-prone structural components using smaller sections with sufficient ultimate limit state, serviceability limit state, and fatigue resistance capacity were verified using

steel-fibre reinforced concrete.

Previous approaches used in fatigue resistance verification neglected significant mechanisms that govern damage evolution. The influence of irreversible strain accumulation was ignored, and the crack propagation of reinforcing bars traversing cracked concrete planes were not appropriately accounted for.

In this thesis, the following objectives were addressed:

1. Developing a new fatigue data analysis method for obtaining a realistic damage model and proposing robust fatigue damage models that account for salient fatigue loading parameters.
2. Verifying previous assumptions used in fatigue constitutive models for concrete composites to ascertain their levels of safety and reliability in fatigue damage models.
3. Developing an irreversible strain model for concrete in compression that is required in the modified constitutive, compatibility, and equilibrium equations for fatigue analysis of concrete composite structural elements.
4. Verifying the performance of steel fibre reinforced concrete deep beams in fatigue resistance and also verifying the possibility of obtaining better optimised structural components using steel fibre concrete.
5. Developing a crack growth evolution model for steel reinforcement traversing cracked concrete planes. The model is required in equilibrium equations at concrete crack locations.
6. Verifying proposed models that involve the modification of the equilibrium, constitutive, and compatibility equations of the strut and tie model and the Disturbed Stress Field Model (DSFM) in order to account for fatigue damage evolution.
7. Verifying the analysis approach using nonlinear finite element analysis software.

The first four objectives were achieved by conducting experiments at the material and structural levels. A new approach was proposed for fatigue tests of structural components, and, as such, future tests can be conducted using the described procedures.

## 9.2 Conclusions

The main conclusions derived from the experimental and analytical results of the research conducted are presented in this section.

1. Fatigue models void of salient loading parameters such as frequency and stress ratio result in inappropriate fatigue life estimations, except when the loading parameters are similar to those used in developing the fatigue models.
2. Based on experimental verification, the secondary strain rate concept is an appropriate approach for fatigue life estimation because it is free from the stochastic variations prevalent with concrete.
3. From the experimental investigations conducted at the material level, the assumption implemented into the fatigue constitutive model for a concrete composite in compression in which the stress-strain curve of a fatigue-damaged concrete element intersects the stress-strain envelope was verified to be realistic.
4. From the experimental investigations conducted at the material level, the assumption that the fatigue hysteresis loop at failure intersects the stress-strain envelope was also verified to be realistic.
5. Although the assumption that the centrelines of fatigue hysteresis loops converge at a common point is realistic, the point of convergence was found to be approximately at the coordinate of  $(-0.3\varepsilon'_c, -f'_c)$ , resulting in a newly proposed model for irreversible strain accumulation.

6. Steel fibres can be used to extend the fatigue life of structural components (including deep beams) due to crack-bridging effects that subsequently reduce stresses in the reinforcing bars, hence inhibiting or minimising the rate of reinforcement crack propagation at the intersection with a concrete crack. The life enhancement was observed to increase as the fibre volume content increased from 0% to 1.5%.
7. Steel-fibre reinforced concrete beams without shear reinforcement exhibited a higher fatigue life compared to conventional reinforced concrete beams with shear reinforcement. This further shows the merit of partial replacement of shear reinforcement with steel fibres in fatigue-prone structures for enhanced fatigue life.
8. Optimised (smaller) cost-effective sizes using steel fibre concrete as replacement for larger conventional reinforced concrete structural elements are obtainable in the design of fatigue-prone structural element such as wind turbine foundations.
9. The modified approach using the strut and tie model for fatigue analysis of reinforced concrete deep beams was verified to be a realistic and conservative approach since the influence of irreversible deformation accumulation is accounted for.
10. Having accounted for fatigue damage of concrete, irreversible compressive strain accumulation, and reinforcement crack-growth in the equilibrium, constitutive, and compatibility equations of the Disturbed Stress Field Model (DSFM), comparisons of the analysis results of the fatigue life and deformation evolution with the experimental results gave good correlation. Thus, finite element analysis software modified accordingly can be used in the fatigue resistance verification of fatigue-prone structures such as wind turbine foundations.
11. Fatigue analysis results further show that the fatigue life of a structural component

corresponds to the number of cycles at which the residual capacity of the component becomes equal to the fatigue load.

### **9.3 Recommendations for Future Work**

Although the project objectives were largely accomplished, the current area of fatigue analysis of reinforced concrete can be extended. Recommendations are given subsequently.

1. The proposed approach for variable fatigue loading damage accumulation, both for plain concrete and reinforced concrete structural elements, requires further verification to support the validity of the approach, since tests using variable fatigue loading were not conducted.
2. Small-scale deep beams were tested in the investigation conducted; however, the results and findings should be supported with results from large-scale deep beams.
3. Strain gauges used in the experimental investigation were sometimes damaged once they were intersected by concrete cracks. An appropriate means of strain reading under fatigue loading should be developed.
4. The proposed secondary strain rate model was developed based on high-cycle fatigue results (less than ten million cycles); however, the application of the proposed model can be extended to very high-cycle fatigue loading using tests results greater than ten million cycles.
5. Although the analytical results for steel-fibre reinforced concrete elements gave good correlations in the estimation of fatigue life, fatigue deterioration of the beams were slightly under-estimated. However, more steel fibre models may be verified on this basis.
6. Lastly, the fatigue life estimation and deformation evolution of wind turbine foundations and similar elements are required using the proposed approaches (modified strut and tie

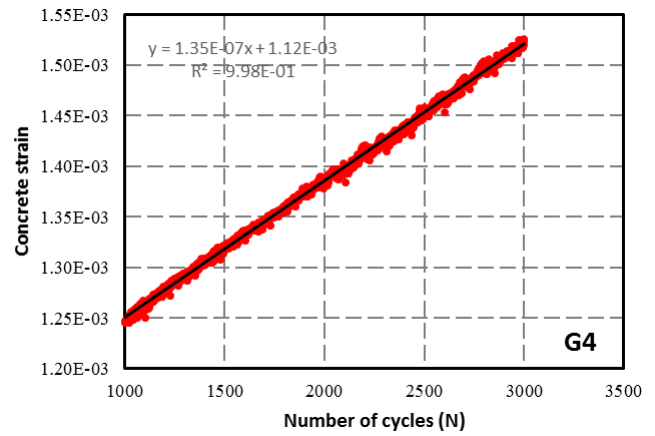
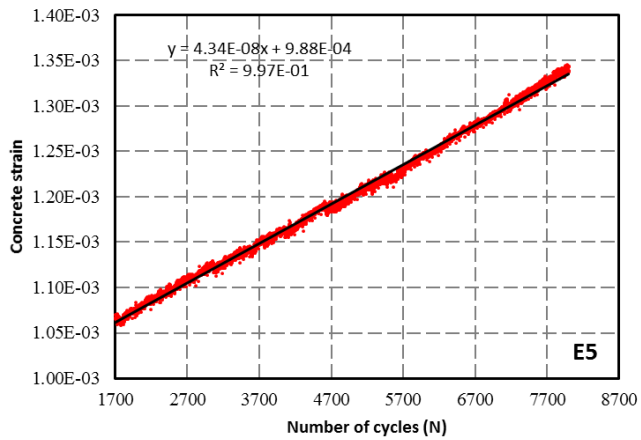
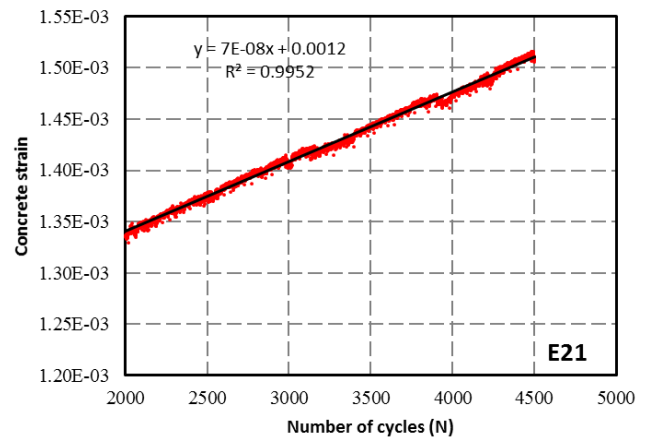
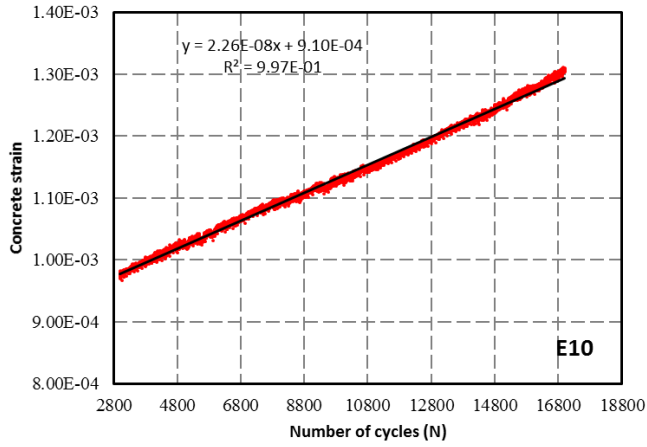
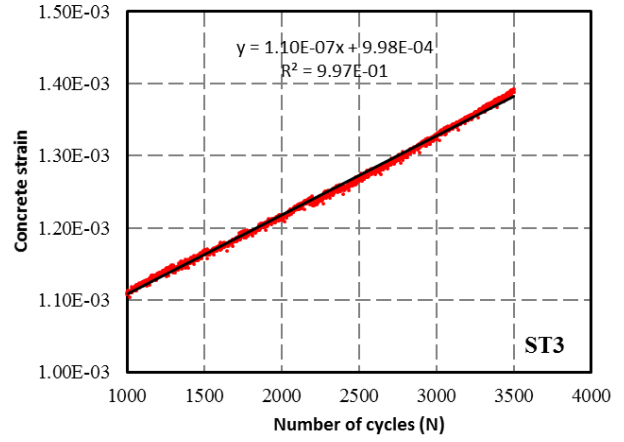
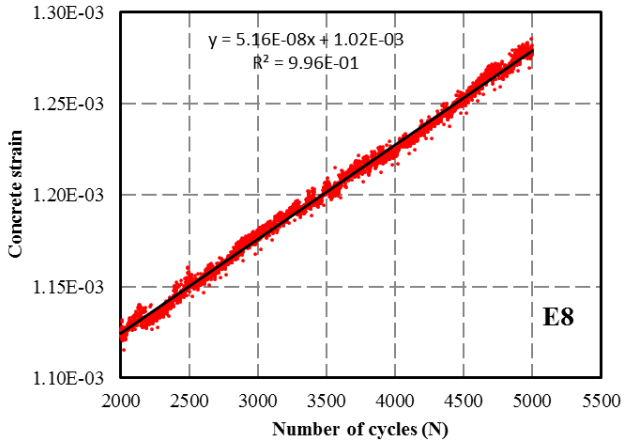
approach and nonlinear finite element analysis) in order to identify anomalies in current modelling procedures.

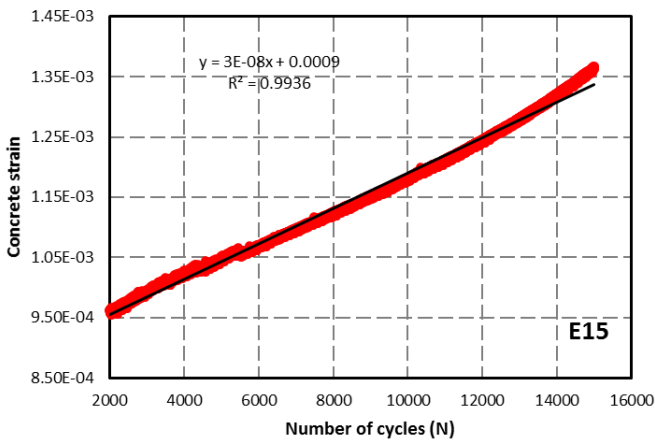
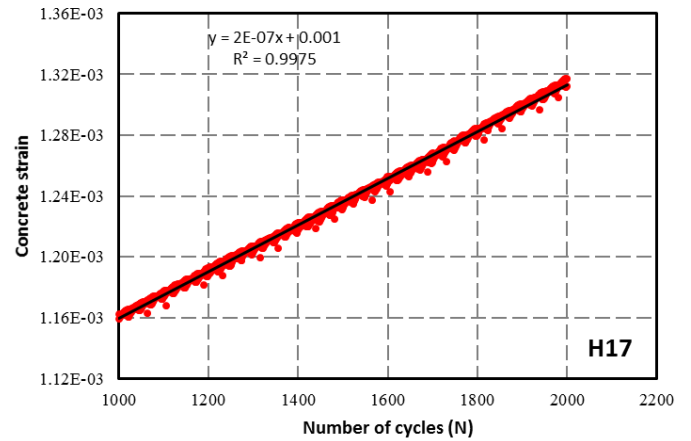
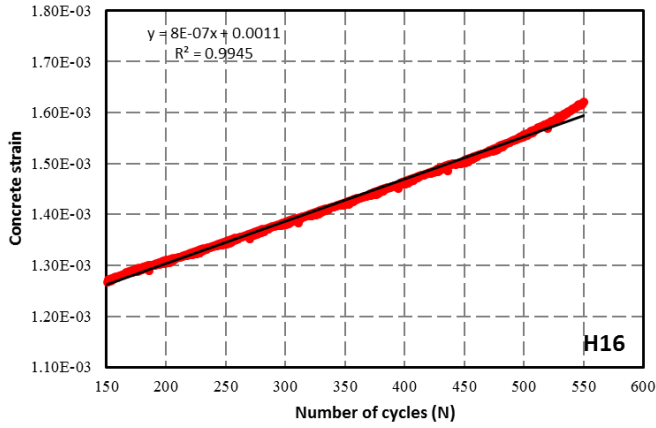
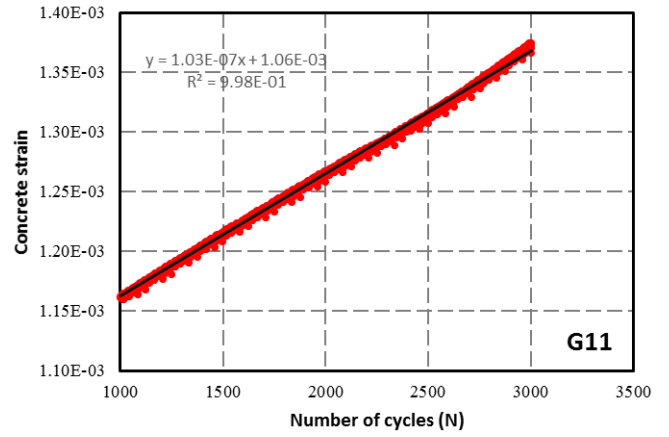
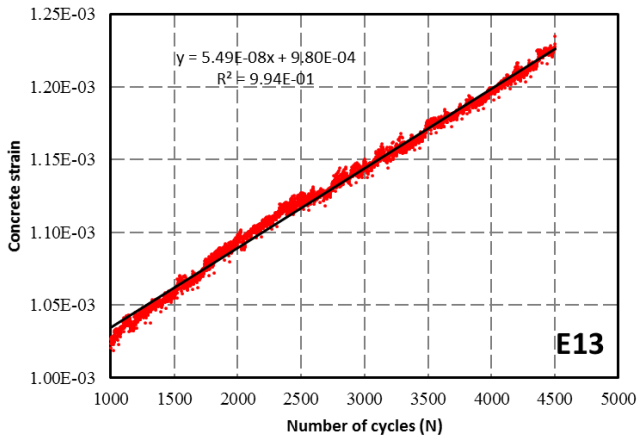
APPENDIX A- STRENGTH AND SECANT MODULUS DEGRADATION TEST DATA

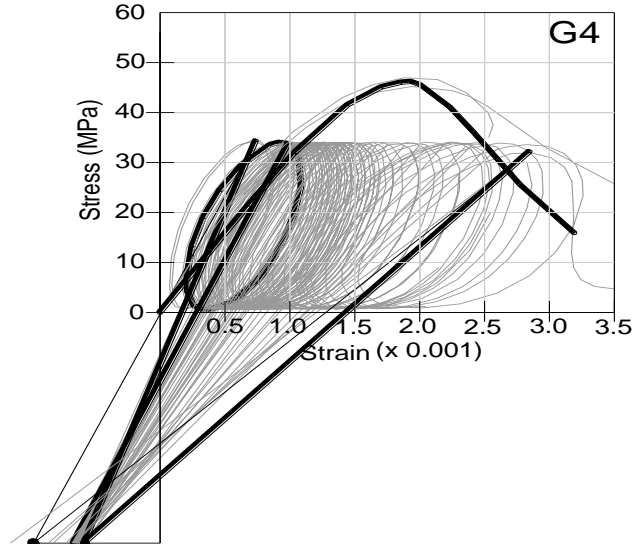
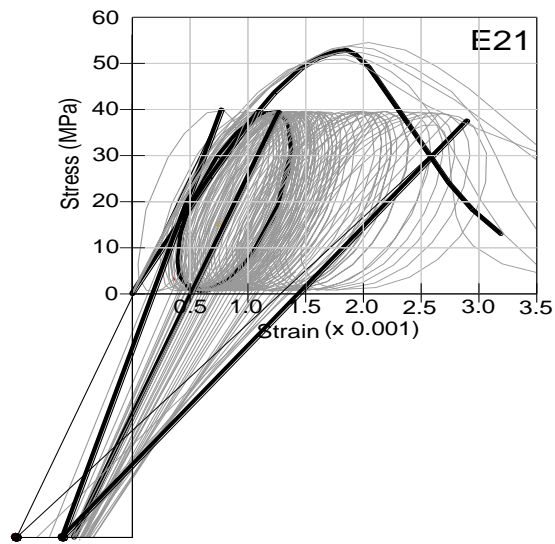
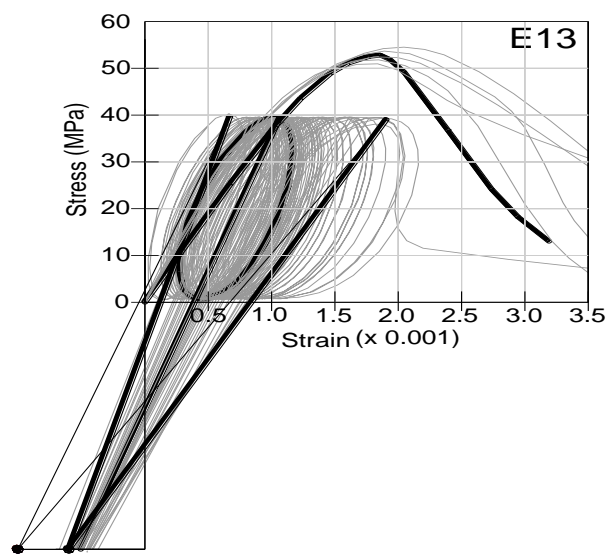
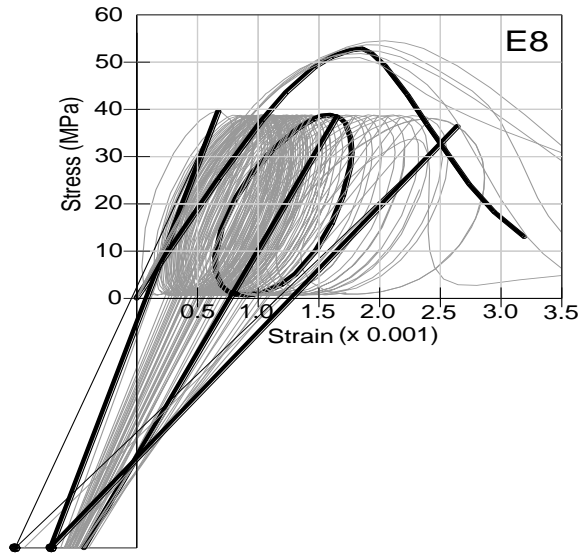
Table A-1

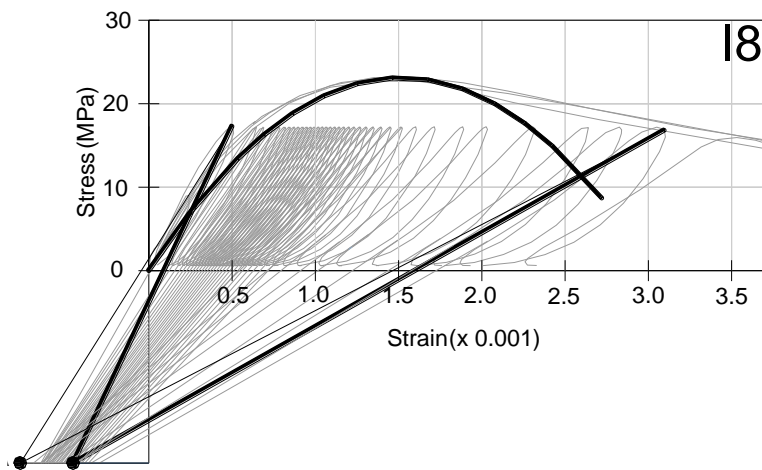
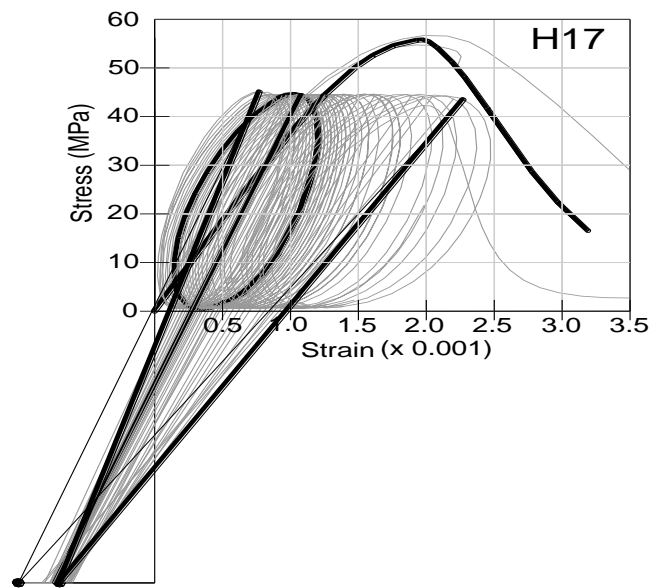
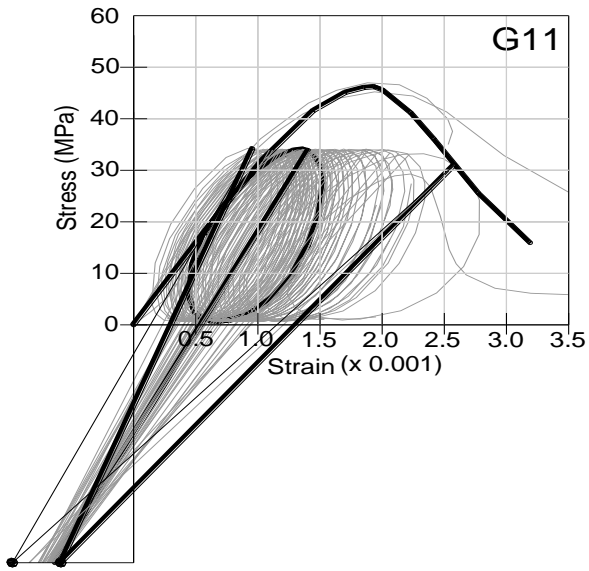
| Specimen | Initial compressive strength $f'_c$<br>MPa | Number of cycles before static loading | Residual strength after static loading<br>MPa | Residual fatigue modulus<br>MPa |
|----------|--|--|---|---------------------------------|
| E22      | 52.8                                       | 430                                    | 54.9  | 68900                           |
| E9       | 52.8                                       | 430                                    | 54.4  | 58100                           |
| E20      | 52.8                                       | 860                                    | 55.1  | 65100                           |
| E11      | 52.8                                       | 860                                    | 53.0  | 58800                           |
| E4       | 52.8                                       | 5150                                   | 55.3  | 62000                           |
| E17      | 52.8                                       | 7730                                   | 52.3  | 55200                           |
| E1       | 52.8                                       | 8160                                   | 53.4  | 53300                           |
| E2       | 52.8                                       | 3480                                   | 46.5  | 44200                           |
| G3       | 46.2                                       | 5550                                   | 41.7  | 33400                           |
| G7       | 46.2                                       | 5880                                   | 38.6  | 30100                           |
| G8       | 46.2                                       | 18080                                  | 36.3  | 31400                           |
| G9       | 46.2                                       | 6180                                   | 32.9  | 25800                           |
| H1       | 55.8                                       | 5000                                   | 51.4  | 50200                           |
| H3       | 55.8                                       | 1200                                   | 58.1  | 61800                           |
| H9       | 55.8                                       | 3000                                   | 56.2  | 57600                           |
| H4       | 55.8                                       | 6120                                   | 45.6  | 45100                           |
| H5       | 55.8                                       | 5840                                   | 49.2  | 43900                           |
| H6       | 55.8                                       | 7900                                   | 44.7  | 42800                           |
| H7       | 55.8                                       | 4680                                   | 36.1  | 37200                           |
| H11      | 55.8                                       | 6710                                   | 52.5  | 54300                           |
| H14      | 55.8                                       | 9870                                   | 46.8  | 38800                           |
| H15      | 55.8                                       | 8660                                   | 37.9  | 33300                           |

<sup>a</sup>Failed before reaching maximum fatigue load applied

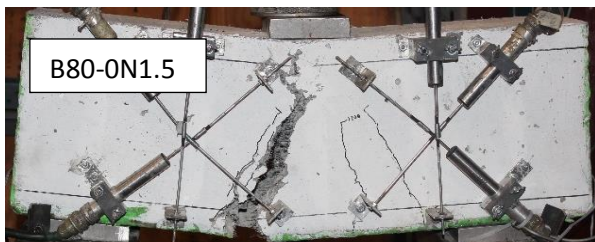
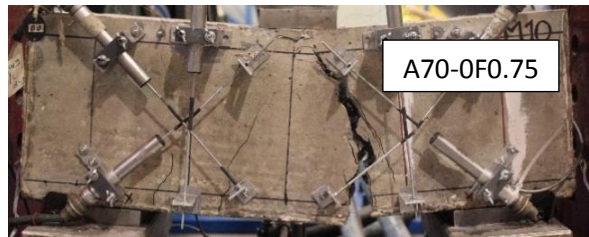
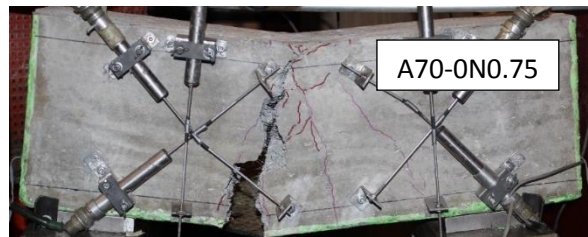
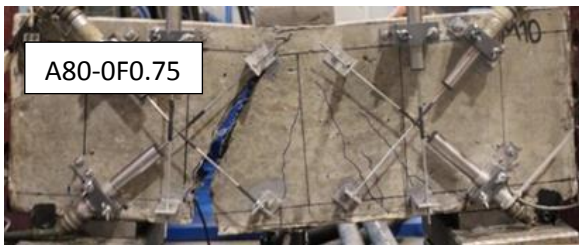
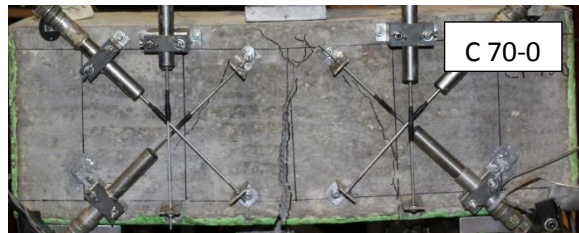
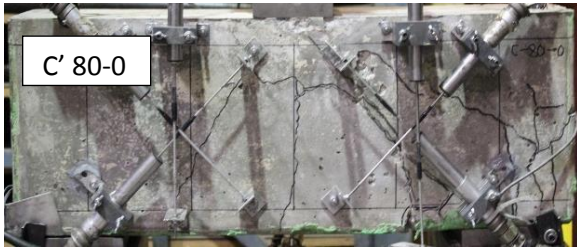
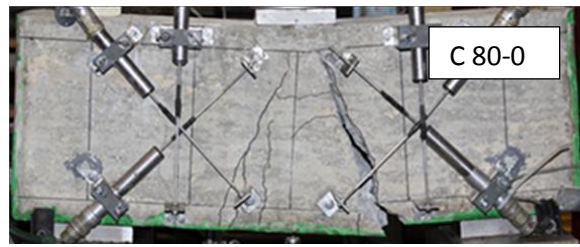
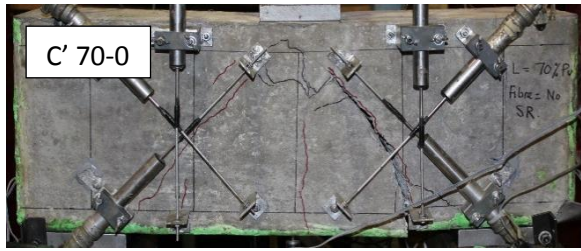


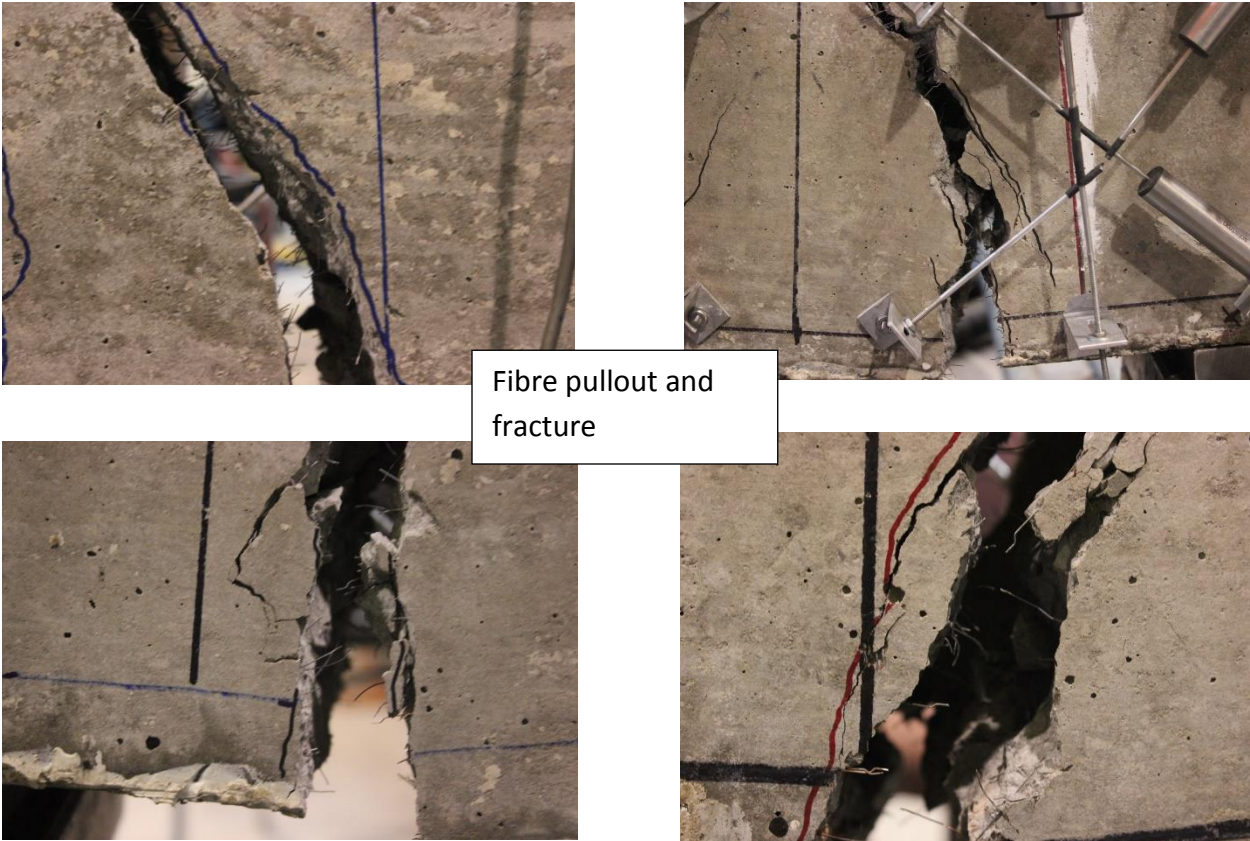












Fibre pullout and fracture



Oval-shaped rebar crack font.

